

# 博士論文

## 論文題目

Study of heavy quark pair production in high energy  
proton-nucleus collisions within the Color Glass  
Condensate framework

(カラーグラス凝縮の枠組みに基づく高エネルギー陽子原子核衝突における重クォーク対生成の研究)

東京大学大学院総合文化研究科

渡邊和宏

## Abstract

We investigate quarkonium and open heavy flavor meson productions in pA collisions at RHIC and LHC energies within the Color Glass Condensate (CGC) framework in order to study parton saturation effects in the target nucleus. The reason to focus on the heavy quark system is that the heavy quark pair is produced only in the initial gluon scattering. This means that the heavy quark is an ideal probe to investigate the QGP and heavy ion collision physics, while we can study the gluon structure in high energy hadron and the nucleus through the heavy quark productions. The heavy quark pair production cross section from the CGC in pA collisions is obtained by Blaizot, Gelis and Venugopalan [J.P. Blaizot, F. Gelis, R. Venugopalan, Nucl. Phys. **A 743**, 57 (2004).], where a pA collision is treated as a dilute-dense system and the cross section is evaluated at the leading order in strong coupling constant and color charge density of valence parton in the proton  $\rho_p$ , but in all orders in the color charge density of valence parton in the nucleus  $g^2\rho_A = O(1)$  because  $\rho_A$  should be proportional to approximately  $A^{1/3}$  with  $A$  being an atomic mass number. The CGC framework systematically includes multiple scattering of valence partons in the eikonal approximation and the resummation of large  $\alpha_s \ln(1/x)$  correction at small Bjorken's  $x$ , which is important in high energy hadronic interactions. Actually the quantum evolution equation resums the  $\alpha_s \ln(1/x)$  correction in the gluon distribution in the hadron. We use the unintegrated gluon distribution at small  $x$  in the proton obtained by solving the Balitsky-Kovchegov equation with running coupling correction (rcBK). In this study, the initial condition for the rcBK equation in the proton is constrained by global fitting of HERA data compared with McLerran-Venugopalan model which includes only multiple scattering effect of a dipole off the heavy nucleus. For the heavy nucleus, multi-parton functions are relevant to heavy quark pair production and given by solving the rcBK equation with use of appropriate initial condition in large- $N_c$  limit. When we focus on the minimum bias event, we replace the initial saturation scale of the gluon distribution in the proton by that in the nucleus. This initial saturation scale indeed depends on the impact parameter in the nucleus and we introduce nuclear thickness function to study the impact parameter dependence. For quarkonium production, we firstly employ the color evaporation model and use appropriate heavy quark fragmentation function for open heavy flavor meson production. We show the transverse momentum spectrum and nuclear modification factor ( $R_{pA}$ ) of the quarkonium ( $J/\psi$ ,  $\Upsilon(1S)$ ) and the heavy meson

$(D, B)$  productions at collider energy. The important result is that the our CGC calculation shows the strongly suppression of the  $R_{pA}$  at RHIC and further suppression of  $R_{pA}$  at the LHC. We next discuss the transverse momentum, rapidity, and initial saturation scale dependence of the  $R_{pA}$ , the transverse momentum broadening, and furthermore the azimuthal angle correlation of open heavy flavor meson pair. Subsequently, we discuss the impact parameter dependence of the quarkonium production. by using the Glauber model with simple thickness function. As to the  $R_{pA}$ , we actually find our computations reproduce the data for minimum bias event and central collisions event at RHIC but can not describe the peripheral data. Finally, we discuss the quarkonium production within non-relativistic QCD (NRQCD) effective field theory. Quarkonium production mechanism is not fully understood even in proton-proton collisions, then model dependence of quarkonium production is important study. In this framework, both the color singlet and octet channel productions are treated in a unified way. We notice that the color singlet production depends on the quadratic correlator in the target nucleus, and this may bring enhancement effect of the quarkonium production although the  $J/\psi$  production cross section itself in our model in this paper is smaller than inclusive  $J/\psi$  production data at RHIC. This effect brings a possibility what we should do in our future work.

# Acknowledgment

I would like to thank Prof. Hirotugu Fujii for crucial comments and careful reading of the manuscript. I also thank to him for useful discussions about heavy quark pair production from the CGC and topics related to pQCD and helping numerical computations. I thank Prof. Tetsuo Matsui for his continuous encouragements, advices, giving a better environment in laboratory and also helpful discussions about quarkonium production mechanism in pp collisions. I have constructed Bethe-Salpeter amplitude based on discussions with him and his note. I thank Profs. Kazunori Itakura, Kenji Fukushima, Sumio Wada, and Yoshio Kikukawa for their encouragement and useful comments and discussing my work. I would like to thank Dr. Larry McLerran, Dr. Robert D. Pisarski, and Dr. Raju Venugopalan for their interests, discussions about my Ph.D. project and kind advices during my stay in RIKEN BNL Research Center. As for computations of heavy meson production, I thank Dr. Marco Stratmann for useful comment on heavy quark fragmentation function. I thank all the member of Komaba nuclear theory group and also particle physics theory group. Finally, I would like to give a special thanks to my family in Fukushima and Tokyo for their support.

# Contents

<b>1</b>	<b>Introduction</b>	<b>6</b>
1.1	Quantum Chromodynamics . . . . .	6
1.2	QCD phase transition . . . . .	6
1.3	Standard picture of Heavy ion collisions . . . . .	7
1.3.1	Initial condition nuclear wave function . . . . .	8
1.3.2	Pre-equilibrium state . . . . .	8
1.3.3	QGP phase . . . . .	8
1.3.4	Hadronization and Freeze-out . . . . .	9
1.4	Observables . . . . .	9
1.4.1	Quarkonium . . . . .	9
1.4.2	Open heavy flavor meson . . . . .	11
1.5	Cold nuclear matter effect . . . . .	11
1.5.1	Absorption in target nucleus . . . . .	11
1.5.2	Nuclear parton distribution function . . . . .	11
1.5.3	Energy loss in medium . . . . .	12
1.5.4	Parton saturation . . . . .	12
1.6	Heavy quark production in pA collision . . . . .	12
1.7	Framework . . . . .	13
1.8	Purpose of this paper . . . . .	15
<b>2</b>	<b>Parton structure</b>	<b>17</b>
2.1	Deep Inelastic Scattering . . . . .	17
2.2	Parton distribution in hadron . . . . .	18
2.3	Quantum evolution . . . . .	21
2.3.1	DGLAP equation . . . . .	22
2.3.2	BFKL equation . . . . .	24

2.3.3	BK equation . . . . .	28
2.4	The Color Glass Condensate . . . . .	31
2.4.1	Classical valence quark . . . . .	31
2.4.2	JIMWLK equation . . . . .	34
<b>3</b>	<b>Heavy quark pair production from the Color Glass Condensate</b>	<b>39</b>
3.1	Background gauge field in pA collisions . . . . .	39
3.2	Quark pair production from the CGC . . . . .	45
3.2.1	Quark pair production amplitude . . . . .	45
3.2.2	Multi parton function . . . . .	50
3.3	Collinear limit on proton side: Hybrid description . . . . .	57
3.4	Quantum evolution effect . . . . .	59
<b>4</b>	<b>Quarkonium production in Color Evaporation Model</b>	<b>67</b>
4.1	Factorization assumption . . . . .	67
4.2	Expression of production cross section . . . . .	68
4.3	$x_{1,2}$ coverage . . . . .	69
4.4	Transverse momentum spectrum of $J/\psi$ . . . . .	70
4.4.1	RHIC . . . . .	72
4.4.2	LHC . . . . .	76
4.5	$\Upsilon$ production at the LHC . . . . .	80
4.6	Rapidity dependence of $R_{pA}$ of $J/\psi$ and $\Upsilon$ . . . . .	85
4.7	$P_{\perp}$ broadening . . . . .	89
4.8	Short summary . . . . .	92
<b>5</b>	<b>Heavy meson production</b>	<b>94</b>
5.1	Cross section formula of heavy meson production . . . . .	94
5.2	Kinematical coverage . . . . .	95
5.3	Transverse momentum spectrum . . . . .	97
5.3.1	pp collisions . . . . .	97
5.3.2	pA collisions . . . . .	100
5.4	Transverse momentum dependence of $R_{pA}$ . . . . .	100
5.5	Rapidity dependence of $R_{pA}$ . . . . .	104
5.6	Azimuthal angle correlation . . . . .	106
5.6.1	pp collisions . . . . .	108

5.6.2	pA collisions . . . . .	110
5.7	Short summary . . . . .	111
<b>6</b>	<b>Impact parameter dependence of <math>J/\psi</math> Nuclear modification factor</b>	<b>113</b>
6.1	$Q_{s0,A}^2$ dependence of $R_{pA}$ of $J/\psi$ . . . . .	113
6.2	Revisit the definition of $R_{pA}$ . . . . .	114
6.3	Semi-classical description of proton-nucleus collisions . . . . .	117
6.4	Numerical Results . . . . .	119
6.5	Short summary . . . . .	125
<b>7</b>	<b>Quarkonium production within the NRQCD factorization approach</b>	<b>126</b>
7.1	Quarkonium production cross section . . . . .	127
7.1.1	Quark pair in the color singlet state : $^3S_1^{(1)}$ . . . . .	130
7.1.2	Quark pair in the color octet state : $^3S_1^{(8)}$ and $^1S_0^{(8)}$ . . . . .	136
7.2	Color singlet model for quarkonium production with multi parton correlator	142
7.3	Numerical results . . . . .	147
7.3.1	Transverse momentum spectrum of direct $J/\psi$ production . . . . .	147
7.3.2	Nuclear modification factor of direct $J/\psi$ production . . . . .	150
7.3.3	$J/\psi$ production from heavy quark pair in color octet state . . . . .	152
7.4	Short summary . . . . .	154
<b>8</b>	<b>Summary</b>	<b>156</b>
<b>A</b>	<b>Notations and Identities</b>	<b>160</b>
A.1	Notation . . . . .	160
A.2	$\gamma$ -matrices . . . . .	161
A.3	SU(3) algebra . . . . .	161
A.4	Clebsh-Gordon coefficient . . . . .	163
A.5	Fierz identities . . . . .	163
A.6	Formulae . . . . .	163
<b>B</b>	<b>Hard part of the cross section</b>	<b>165</b>
<b>C</b>	<b>Quarkonium and Heavy meson</b>	<b>168</b>
C.1	Color Singlet Model . . . . .	169
C.2	Color Evaporation Model . . . . .	170

C.3	Non-Relativistic QCD approach . . . . .	172
C.3.1	Factorization . . . . .	172
C.3.2	Short distance coefficient . . . . .	174
C.4	Heavy meson fragmentation . . . . .	177
<b>D</b>	<b>Bethe-Salpeter amplitude</b>	<b>179</b>
D.1	General definition of BS equation . . . . .	179
D.2	BS amplitude in the non-relativistic limit . . . . .	180
D.3	BS amplitude in the NRQCD . . . . .	184
<b>E</b>	<b>Quadrupole amplitude in Gaussian approximation</b>	<b>186</b>
E.1	Dipole amplitude . . . . .	186
E.2	Quadrupole amplitude . . . . .	191



# Chapter 1

## Introduction

First of all, let us start by giving introduction and background of our study in the context of both high energy heavy ion collisions and small- $x$  physics.

### 1.1 Quantum Chromodynamics

The Standard Model of particle physics consists of quarks and leptons, and gauge bosons such as gluon, today [1]. The quarks have color quantum number in the 3-dimension intrinsic space and are classified in terms of SU(3) group in the fundamental representation. The gluons, which are relevant to the strong interaction, also carry the color quantum number in the SU(3) adjoint representation. Quantum Chromodynamics (QCD) is a fundamental theory to describe the dynamics of the quarks and the gluons. Baryons and mesons are bound states consisting of the quarks and gluons and referred to as hadrons because they feel the strong interaction. As the lightest meson, the pion is regarded as the Nambu-Goldstone boson of chiral symmetry breaking. Quarks and gluons themselves have never been captured alone so far due to the confinement nature of QCD.

### 1.2 QCD phase transition

In the QCD, many-body system consisting of the hadron at high temperature and density makes phase transition into a deconfined state referred to as Quark-Gluon Plasma (QGP). The existence of the QGP was predicted long time ago in the context of condition at high baryon density [5] and high temperature [6]. At finite temperature  $T \neq 0$  but zero baryon chemical potential  $\mu = 0$ , the QCD phase transition actually can be investigated by

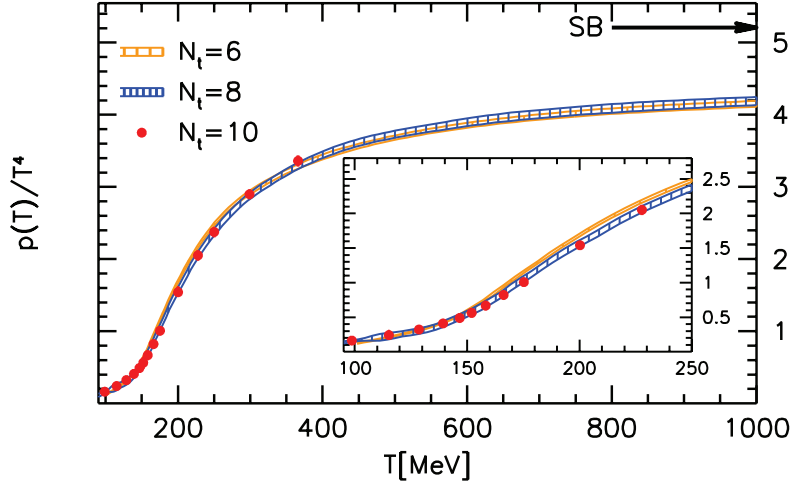


Figure 1.1: Equation of state as a function of temperature computed by Lattice QCD method. Figure is cited from Ref. [7].

Lattice QCD Monte-Carlo simulations. Fig. 1.1 displays a result of equation of state as a function of temperature  $T$  obtained by Lattice QCD computations. The result shows that the pressure of the system normalized by  $T^4$  increases rapidly around  $T \sim 200$  MeV, and gets closer to the Stefan-Boltzmann limit where the quark and gluon are in a gas state. We can interpret this rapid increase of the degrees of freedom as the phase transition from hadronic phase to QGP phase.

### 1.3 Standard picture of Heavy ion collisions

It is considered that QGP exists in early universe, inside high density neutron stars, and can be created in high energy heavy ion collisions (HICs) experiments. Relativistic Heavy Ion Collider (RHIC) at BNL and the Large Hadron Collider (LHC) at CERN are actually the unique machine to create the QGP in laboratory. By analyzing direct photons produced in HICs [12], it has been demonstrated that the initial temperature in HICs at RHIC is estimated to be higher than critical temperature  $T_c$  where the phase transition is occurred. Furthermore, creation of strong collective flows observed in the HICs is successfully analyzed with relativistic fluid dynamics. As for hard probes, quarkonium suppression and jet quenching confirms the high density medium consisting of colored partons. These measurements gradually establish the creation of QGP in HICs.

Then, next, by assuming the creation of QGP in heavy ion collision experiments, let us explain briefly a standard time evolution picture of heavy ion collisions.

### 1.3.1 Initial condition nuclear wave function

In high energy heavy ion collisions, two heavy nuclei become thin pancakes like discs due to the Lorentz contraction in the longitudinal direction<sup>1</sup>. Due to the Lorentz time dilation, quantum fluctuation emerges as parton (gluon) with small Bjorken's  $x$ , and the heavy nucleus at small- $x$  can be recognized as a novel state with large gluon occupation number referred to as Color Glass Condensate (CGC), which we will explain later. In fact, this small- $x$  gluons mainly contribute to particle productions in hadronic collisions. The CGC-inspired model [10] has been used as specific initial condition for relativistic fluid dynamic simulation to analyze bulk properties observed in the HICs.

### 1.3.2 Pre-equilibrium state

There is an open question how to form QGP from initial pre-equilibrium state. In terms of the CGC, strong coherent color field referred to as Glasma is created for an extreme short time in the HICs. Now, we introduce  $\tau_0$  as the proper time where the system achieves local equilibrium. By hydrodynamic analyzing of bulk properties in HICs, it is suggested that  $\tau_0$  is about or shorter than 1 fm/c. This is very short time scale and recently a new mechanism between the Glasma and local equilibrium state QGP has been studied actively.

### 1.3.3 QGP phase

At  $\tau > \tau_0$ , thermal QGP rapidly cools through expansion of the system. As a very amazing fact at RHIC, the space-time evolution of the system is well described by the relativistic hydro dynamics. This analysis is quite nontrivial and suggests that the produced QGP at RHIC behaves as nearly perfect fluid with small correction of transport coefficients, such as viscosity [8,9]. Transport coefficients decrease with increasing the strength of the particle interaction if the system is like gas. The smallness of the transport coefficient correction indicates that the QGP created at RHIC is just a strongly coupled plasma (sQGP).

---

<sup>1</sup>Longitudinal is parallel to a beam axis while transverse is perpendicular to it.

### 1.3.4 Hadronization and Freeze-out

As the system expands hydrodynamically, the deconfined matter begins to hadronize and quarks and gluons are re-confined in hadrons. In this stage, inelastic scatterings become less frequent and the number of each hadron species is effectively fixed around  $\tau \sim 5 - 10$  fm, which is called chemical freeze-out. Next, the system is more cooled and kinetic thermal freeze-out starts at  $\tau \sim 10 - 20$  fm/c breaking the local equilibrium in the system, which results in fixing the momentum distribution of produced particles. Finally, the produced hadrons, leptons, and photons are observed in detectors.

This is a schematic standard picture now from the first impact in a heavy ion collision to final particle observation.

## 1.4 Observables

In fact, we can not observe QGP directly due to the confinement nature of QCD. We need to confirm the creation of QGP via careful analysis of observed hadrons and leptons in the final state. For instance, creation of strong collective flows observed in HICs is successfully described with relativistic fluid dynamics simulation for QGP as stated above. As for hard probes, strong jet quenching is regarded as an evidence for the high density medium consisting of colored partons. Heavy quarks production is also an useful probe to the HIC physics and has been studied actively for a long time. In the following subsections, we introduce two important observables concerning the heavy quark pair production in the HICs.

### 1.4.1 Quarkonium

Quarkonium ( $J/\psi$ ) suppression is for a long time suggested as a clear signature of QGP creation in HICs because the hot matter screens the potential between the quark and antiquark and prevents the quark pair from binding [11]. The original reason to regard the quarkonium as an ideal probe of QGP is listed as follows: a small number of heavy quarks are produced in pair only in initial hard process, and then the bulk medium produced at later stage would destroy the pair's correlation to bound into quarkonium.

In addition, at RHIC and the LHC, a large number of  $c\bar{c}$  pairs produced in AA collisions and  $c$  and  $\bar{c}$  produced independently can be combined into a quarkonium in the hadronization [144], which may result in an enhancement of the quarkonium yield. This is

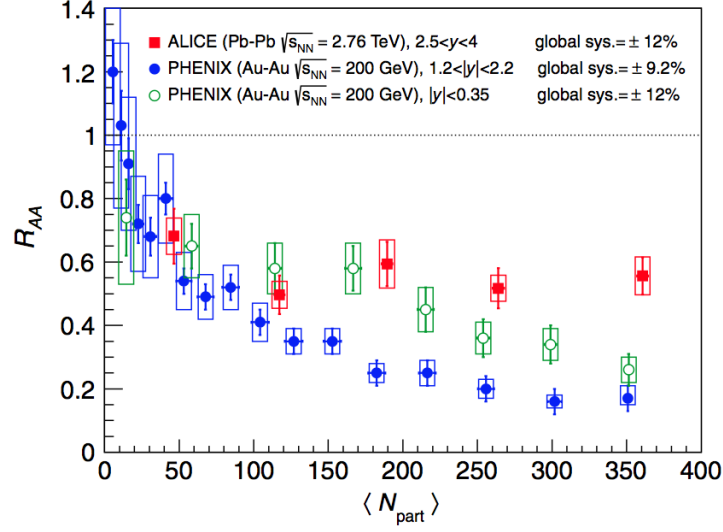


Figure 1.2: Nuclear modification factor  $R_{AA}$  of inclusive  $J/\psi$  in the forward rapidity range  $2.5 < y < 4$  as a function of the number of participating nucleons measured in Pb-Pb collisions at  $\sqrt{s} = 2.76$  TeV compared to PHENIX results in Au-Au collisions at  $\sqrt{s} = 200$  GeV at mid rapidity and forward rapidity. The number of mean participants corresponds to centrality estimated at experiments. Figure is cited from Ref. [105].

referred to as recombination scenario which has already been discussed extensively [142, 143].

The production and propagation of  $J/\psi$  in AA collisions can be quantified by the nuclear modification factor defined by

$$R_{AA} = \frac{\left. \frac{dN_{J/\psi}}{d^2P_{\perp}dy} \right|_{AA}}{N_{coll} \left. \frac{dN_{J/\psi}}{d^2P_{\perp}dy} \right|_{pp}} \quad (1.1)$$

where  $N_{coll}$  is the average number of inelastic AA collisions in a given centrality class and  $\left. \frac{dN_{J/\psi}}{d^2P_{\perp}dy} \right|_{pp (AA)}$  is the transverse momentum ( $P_{\perp}$ ) and rapidity ( $y$ ) differential multiplicity per event in pp (AA) collisions. Fig. 1.2 shows nuclear modification factor of inclusive  $J/\psi$  production as a function of the number of participating nucleons measured in Pb-Pb collisions in the forward rapidity region at the LHC, compared to PHENIX results in Au-Au collisions at  $\sqrt{s} = 200$  GeV at mid rapidity and forward rapidity. One can immediately find a strong suppression with increasing the number of participants at both RHIC and the LHC. As the primary suppression by melting in QGP can compete with the subsequent enhancement effect, a careful analysis is necessary to interpret the data.

### 1.4.2 Open heavy flavor meson

Open heavy flavor meson (Heavy meson) production itself is also very valuable probes in HIC experiments [77], in order to quantify properties of hot and dense matter or the QGP transiently created in the events. For example, energy loss in medium [136–140] and collective flow of  $D$  and  $B$  mesons [141], have been studied. The heavy meson production in AA collisions measured at RHIC [104, 106] and the LHC [114, 115] actually shows a strong suppression at large transverse momentum (compared to that in pp collisions with appropriate normalization), similar in magnitude to that of light hadrons, which is interpreted as a large energy loss of the heavy quark in the hot medium. This is a puzzling problem because energy loss via gluon radiation in the hot medium is expected to be suppressed by  $1/m$  with particle's mass  $m$ .

## 1.5 Cold nuclear matter effect

In fact, the systematic studies of quarkonium and heavy meson production in pp and pA collisions are indispensable in order to quantify the effects of QGP precisely. pp collisions provide fundamental information on the production mechanism of the quarkonia and heavy mesons. pA collisions can be regarded as a controlled baseline in the context of HIC physics and playing a crucial role to separate cold nuclear matter (CNM) effects from hot plasma effects. We briefly introduce some typical CNM effects.

CNM effects in the target nucleus include absorption of particles such as breakup of quarkonium during traversing medium, multiple scattering of partons, modification of the initial parton distribution (e.g. shadowing), and parton saturation effects.

### 1.5.1 Absorption in target nucleus

$J/\psi$  suppression in pA collisions at SPS-NA60 [103] has been analyzed by use of incoherent Glauber model:  $S_{\text{nucl}} = \exp(-\rho_{\text{nm}}\sigma_{\text{abs}}^{J/\psi}L)$  where  $\rho_{\text{nm}} = 0.16 \text{ fm}^{-3}$  is mean nuclear density,  $L$  is the effective pass length which  $J/\psi$  passes through in the target nucleus.  $\sigma_{\text{abs}}^{J/\psi}$  is an effective absorption cross section of  $J/\psi$  in the nucleus which is obtained by fitting data.

### 1.5.2 Nuclear parton distribution function

Parton distribution function (pdf) in proton  $f_i^p(x, Q^2)$  is studied in deep inelastic  $e + p$  scattering experiments.  $x$  is a momentum fraction of parton  $i$  and  $Q^2$  is a virtuality

of probe. On the other hand, the pdf in nucleus  $f_i^A(x, Q^2)$  is not fully understood and phenomenologically determined by several experiments. For example, in Ref. [134], by assuming the nuclear pdf as  $f_i^A(x, Q^2) = R_i^A(x, Q^2)f_i^p(x, Q^2)$ , the fit function  $R_i^A(x, Q^2)$  is determined by deep inelastic lepton-nucleus scattering, Drell-Yan di-lepton production in pA, and inclusive pion production in d+Au at RHIC. If no nuclear effects exist,  $R_i^A(x, Q^2) = 1$  exactly. However, the behavior of  $f_i^A(x, Q^2)$  is actually quite different from  $f_i^p(x, Q^2)$ . Particularly,  $R_i^A(x, Q^2) < 1$  can be found at  $x \leq 10^{-2}$  for large nucleus (A=Pb) and this  $R_i^A(x, Q^2) < 1$  is called nuclear shadowing where the parton apparently hides in other many partons.

### 1.5.3 Energy loss in medium

Heavy quark energy loss by medium induced gluon radiation in the nucleus is studied in Ref. [159]. The calculation is carried out in nucleus rest frame and the energy loss depends on the path length crossed in the target nucleus. We comment that quark and gluon can be rotated in their color space without their recoil when they radiate gluons. This is a feature in QCD.

### 1.5.4 Parton saturation

In high energy hadronic scattering, parton saturation scale  $Q_{sA}^2(x)$  of the gluon distribution in heavy nucleus with atomic mass number  $A$  is enhanced by the larger valence color charges seen at moderate value of  $x = x_0$ . Indeed, the empirical formula [31, 32]  $Q_{sA}^2(x) = Q_{s0}^2 A^{1/3} (x_0/x)^\lambda$  with  $Q_{s0}^2 = 0.2 \text{ GeV}^2$ ,  $x_0 = 0.01$  and  $\lambda \sim 0.3$  suggests that the saturation scale is already comparable to the charm quark mass  $m_c \sim 1.5 \text{ GeV}$  with  $A = 200$  at RHIC energy  $\sqrt{s} = 200 \text{ GeV}$ . Therefore, in the saturation point of view, quantitative analysis of particle production in pA collisions is very crucial [13]. In this paper, we mainly consider this parton saturation effect in the nucleus based on the Color Glass Condensate framework which we will show later.

## 1.6 Heavy quark production in pA collision

We focus on heavy quark pair production in this paper. The reason why we study heavy quark production is in order here. Heavy quark mass is larger than typical  $\lambda_{\text{QCD}}$  and it is clear that the heavy quark is produced only in initial hard gluon fusion and calculated

by perturbative QCD method. Then the heavy quark can be used as ideal probe to investigate the medium properties of nucleus. Heavy quark production in high energy pA collisions at RHIC and the LHC is actually very important to evaluate the CNM effects and also provides us with a unique opportunity to investigate the so-called parton saturation phenomenon [28, 29] at small Bjorken's  $x$  of gluon in the incoming nucleus. The large heavy quark mass allows perturbative calculation of the quark production from the gluons as stated above, while high center of mass collision energy  $\sqrt{s}$  makes the relevant  $x$  of the gluons still small. These low  $x$  gluons are abundantly generated from the valence partons with large  $x$  in view of the quantum evolution in  $x$ . Then the saturation momentum scale  $Q_s^2(x)$  emerges dynamically as a semi-hard scale below which virtuality  $Q^2 < Q_s^2(x)$ , coherence and nonlinearity of the  $x$  evolution become important. This dynamics of small- $x$  degrees of freedom in hadrons is systematically described with the Color Glass Condensate (CGC) effective theory [38].

## 1.7 Framework

In this paper, we study quantitatively the quarkonium ( $J/\psi$ ,  $\Upsilon(1S)$ ) and heavy meson ( $D$ ,  $B$ ) productions in pA collisions at RHIC and the LHC in order to quantify the effects of gluon saturation.

The quark-pair production cross section from the CGC in pA collisions is obtained by Blaizot, Gelis and Venugopalan [64, 65], where a pA collision is treated as a dilute-dense system and the cross section is evaluated at leading order in the strong coupling constant  $\alpha_s$  and the color charge density  $\rho_p$  in the proton, but in all orders in the color charge density  $g^2\rho_A \sim gA = O(1)$  in the nucleus.

As to hadronization of quarkonium and heavy meson productions, the heavy meson production is calculated with a heavy meson fragmentation function, while the quarkonium production is computed in the Color Evaporation model (CEM) where a hadronization dynamics is treated simply because all the quark pair form the quarkonium with a constant transition probability.

In the CGC framework, multiple scatterings and gluon merging dynamics are encoded in the unintegrated gluon distribution (uGD) function of the heavy nucleus. These effects cause relative depletion of the quark production yields and azimuthal momentum imbalance between the produced quark and antiquark. In forward particle production, the momentum fraction  $x_1$  of the gluons from the proton is not small, and the uGD of the



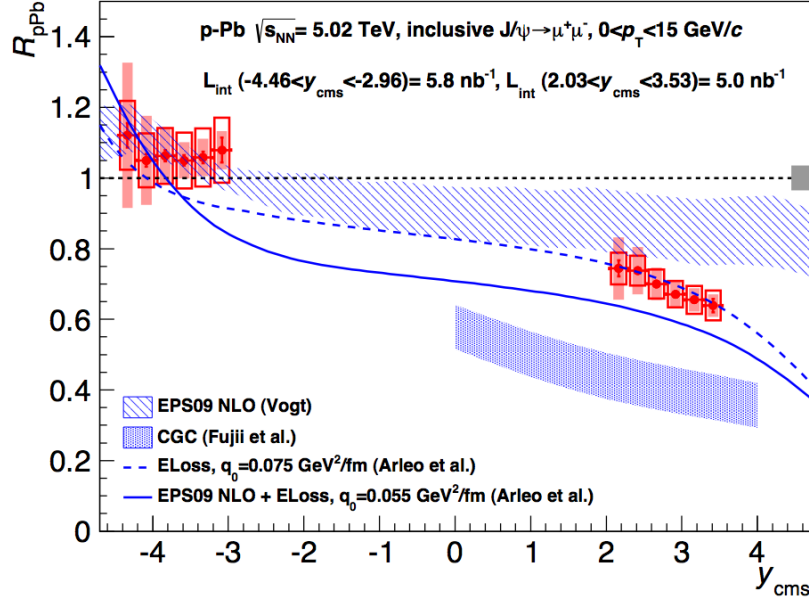


Figure 1.3: Nuclear modification factor  $R_{pA}$  of inclusive  $J/\psi$  at forward and backward rapidity as a function of rapidity in p-Pb collisions at  $\sqrt{s} = 5.02$  TeV compared to some theoretical results [13, 17] based on nuclear pdf and energy loss effects. Figure is cited from Ref. [108].

proton may be better described with the ordinary collinear gluon distribution function. This kind of asymmetric treatment is well known for the hadron production from the CGC [59], and often referred to as hybrid model.

In the nucleus side, multi-parton function such as the three point function  $\phi^{q\bar{q},g}$  appears in quark pair production and obeys JIMWLK quantum evolution equation. However, in the large- $N_c$  limit,  $\phi^{q\bar{q},g}$  can be obtained by using only the dipole amplitude. At the present day, it is standard to use nonlinear Balitsky-Kovchegov (BK) equation [47, 48] for describing the  $x$  dependence of the dipole amplitude. It is argued that the inclusion of running coupling corrections to the BK equation (now called rcBK equation) is essential to phenomenology [49–51]. Indeed, the rcBK equation with an appropriate initial condition can fit the HERA DIS data quite well [53, 54] and are successful in reproducing/predicting the data at hadron colliders quantitatively [55–58]. We use the numerical solution of the rcBK equation to describe the  $x$  dependence of the uGD in the proton, and change the initial saturation scale of the three point function  $\phi^{q\bar{q},g}$  for the heavy nucleus.

We predicted in Ref. [68] that the nuclear modification factor ( $R_{pA}$ ) of  $J/\psi$  and  $D$  meson in pA collisions at the LHC are suppressed than those at RHIC due to the nonlinear QCD evolution effect in the small- $x$  region. However, our results draw attention as a

surprise since the  $R_{pA}$  of  $J/\psi$  in p+Pb collisions at the LHC is similar to the one in d+Au collisions at RHIC in the forward rapidity region, which shown in Fig. 1.3 with some theoretical results [13,17].

## 1.8 Purpose of this paper

CGC is the effective theory in the context of perturbative QCD (pQCD). If we believe the pQCD can describes the QCD phenomena, then the CGC picture is also valid. In particular, pQCD method becomes more reliable at the LHC because of the typical characteristic energy is much larger than any other collider experiments and then the particle production should be studied from the CGC. Our purpose in this paper is to study the heavy quark production from the CGC quantitatively and investigate the parton saturation in the nucleus by using the heavy quark production. Our results for quarkonium and heavy meson production in pA collisions from the CGC bring now tense relations between theoretical and experimental study and it is required to adopt a cautious attitude to interpretation of data. In this paper, we firstly start with a review of detail our calculation of quarkonium production in the CEM for minimum bias event and also heavy meson production with an appropriate fragmentation function. Next, we consider what we can do soon and then we investigate the impact parameter dependence of quarkonium production. Furthermore we attempt to match the heavy quark pair production formula from the CGC with the NRQCD factorization approach, in order to refine the description of hadronization process of quarkonium production. In the paper, we numerically calculate only quarkonium production cross section in color singlet model which is relevant to quadrupole amplitude as a multi parton correlator in the nucleus. This multi parton correlator may bring different feature in quarkonium production in pA collisions than pp collisions. The quadrupole amplitude is also a solution of JIMWLK equation. It is known that if the distribution of color charge density inside hadron is gaussian, the quadrupole amplitude can be expressed by only use of the dipole amplitude. Then, we advance the computation of the color singlet model for quarkonium production with the quadrupole amplitude obtained by the dipole amplitude.

This paper is organized as follows. In chapter. 2, we introduce some basic topics related to our study and review the formula for heavy quark pair production in pA collisions within the CGC framework in Chap. 3, where we also present how to include the quantum evolution effect in our numerical study. Next, we show in Chap. 4–6 our numerical results

for quarkonium and heavy meson productions at RHIC and LHC energies. We also discuss quantitatively the cross section and nuclear modification factor, and also show azimuthal angle correlation between the pair of heavy mesons. In Chap. 7, we finally discuss the quarkonium production in the NRQCD factorization approach. In practice, we show the numerical results of the color singlet model for quarkonium production without quantum evolution effect. Summary and outlook are given in Chap. 8.

# Chapter 2

## Parton structure

In this chapter, we briefly present some fundamental topics related our study such as parton structure in the hadron and heavy nucleus which include the non-perturbative long distance physics. However we can know the scale dependence of those by perturbative QCD calculation. Then we also show a quantum evolution equations which control the scale dependence of the parton structure of the hadron. Detailed discussions are found such as in Ref. [2].

### 2.1 Deep Inelastic Scattering

Let us consider the deep inelastic electron-proton/nucleus scattering:  $e + p/A \rightarrow e' + X$ , which is usually called by DIS. We assign the four momenta to incident electron, target proton, and virtual photon in this process as is found in Fig. 2.1 (Left). Very useful two important Lorentz invariant variables related with collision dynamics are introduced as

$$Q^2 \equiv -q^2 \tag{2.1}$$

$$x_{Bj} \equiv \frac{Q^2}{2P \cdot q}. \tag{2.2}$$

$Q^2$  is a virtuality of the virtual photon  $\gamma^*$  which carries a momentum transfer from the incident electron to the parton in the hadron. It is usually referred to as the resolution in the transverse plane of hadron.  $x_{Bj}$  is the Bjorken's  $x$  variable Then the DIS experiment is then characterized in the  $(x_{Bj}, Q)$  space. We simply abbreviate the Bjorken's  $x$  as just  $x$  below and will restore the sub-label “ $Bj$ ” when we need to give notice.

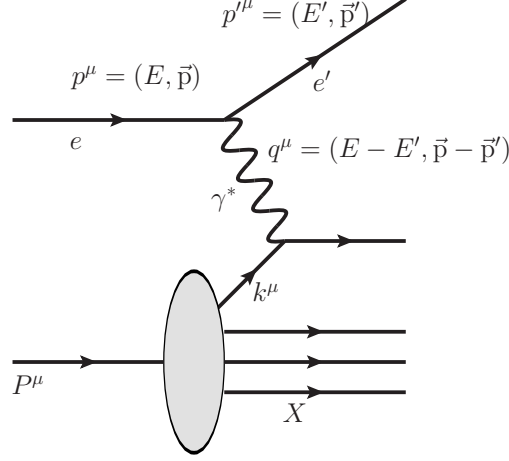


Figure 2.1: Deep inelastic electron-proton scattering. Incident electron observes the internal parton structure of the proton via virtual photon  $\gamma^*$ .

$x$  and  $Q$  can be rewritten in terms of the mandelstam variable as follows;

$$x = \frac{Q^2}{\hat{s} + Q^2 - m^2} \quad (2.3)$$

$$Q^2 = yx(s - m_p^2 - m_e^2) \sim yxs, \quad (2.4)$$

where  $m$  is a mass of the target proton.  $\hat{s} = (P + q)^2$ ,  $s = (P + p)^2$ , and  $y = \frac{E-E'}{E}$  is an energy transfer. DIS experiments are performed in the high scattering energy, then it probes the small  $x$  region inside the target.

## 2.2 Parton distribution in hadron

Next let us consider the differential cross section of the DIS process in Fig. 2.1

$$\frac{d\sigma^{ep}}{d^3p'} = \frac{\alpha_{EM}^2}{EE'Q^4} L_{\mu\nu} W^{\mu\nu} \quad (2.5)$$

where  $L_{\mu\nu}$  is a leptonic tensor which involves only the electron scattering and  $W^{\mu\nu}$  is a hadronic tensor which involves a contributions from the proton.  $\alpha_{EM}$  is the electromagnetic coupling constant. This  $L_{\mu\nu}$  actually reads

$$L_{\mu\nu} = \frac{1}{2} \sum_{s,s'} \langle p, s | j^\mu(0) | p', s' \rangle \langle p', s' | j^\nu(0) | p, s \rangle \quad (2.6)$$

where  $j^\mu(x) = \bar{u}_e(x) \gamma^\mu u_e(x)$  is the electromagnetic current of the electron with the Dirac field  $u_e$  and we have averaged the initial polarization of the electron  $s$  and summed over

the polarization in the final state  $s'$ . The expression of  $W^{\mu\nu}$  is given by

$$W^{\mu\nu} = \frac{1}{4\pi m} \frac{1}{2} \sum_{\lambda=\pm 1} \sum_X \langle P, \lambda | J^\mu(0) | X \rangle \langle X | J^\nu(0) | P, \lambda \rangle (2\pi)^4 \delta^{(4)}(P + q - P_X) \quad (2.7)$$

where we have summed over the final state  $X$  and averaged the polarization of the initial proton  $\lambda$ .  $J^\mu(x) = \sum_f Z_f \bar{u}_f(x) \gamma^\mu u_f(x)$  is the electromagnetic current of the quark and  $Z_f$  is the electric charge per unit  $e$  of the quark with flavor  $f$  and  $u_f$  is the Dirac field. By imposing the electromagnetic current conservation as  $q_\mu W^{\mu\nu} = q_\nu W^{\mu\nu} = 0$  and assuming  $W^{\mu\nu}$  is a symmetric tensor,  $W^{\mu\nu}$  is generally rewritten by

$$W^{\mu\nu} \equiv -W_1(x, Q^2) \left( g^{\mu\nu} - \frac{q^\mu q^\nu}{q^2} \right) + \frac{W_2(x, Q^2)}{m^2} \left( P^\mu - \frac{P \cdot q}{q^2} q^\mu \right) \left( P^\nu - \frac{P \cdot q}{q^2} q^\nu \right) \quad (2.8)$$

where  $W_1(x, Q^2)$  and  $W_2(x, Q^2)$  are scalar function, called structure function. These structure function can be measured experimentally and include all the non-perturbative QCD effect in the hadron.

By substituting Eqs. (2.6)(2.7) into Eq. (2.5), the differential cross section of the DIS in the laboratory frame is given by

$$\left. \frac{d\sigma^{ep}}{dE' d\Omega} \right|_{\text{Lab}} = \frac{\alpha_{EM}^2}{EE' \sin^4 \frac{\theta}{2}} \left[ W_2(x, Q^2) \cos^2 \frac{\theta}{2} + 2W_1(x, Q^2) \sin^2 \frac{\theta}{2} \right] \quad (2.9)$$

where  $\Omega$  and  $\theta$  are the solid angle and the polar angle of the scattering in the laboratory frame respectively <sup>1</sup>. Here we define the dimensionless structure functions as

$$F_1(x, Q^2) \equiv mW_1(x, Q^2), \quad (2.10)$$

$$F_2(x, Q^2) \equiv \frac{Q^2}{2mx} W_2(x, Q^2). \quad (2.11)$$

The physical meaning of  $F_1$  is the number of partons in the hadron with longitudinal momentum fraction  $x$  while the physical meaning of the  $F_2$  is that the average longitudinal momentum fraction of the partons in the hadron times the number of partons, that is,

$$F_2(x, Q^2) = \int_0^1 d\xi \sum_a C_a(x/\xi) f_a(\xi, Q^2) \quad (2.12)$$

---

<sup>1</sup>Eq. (2.9) is one of the simplest form which is found in Ref. [4].

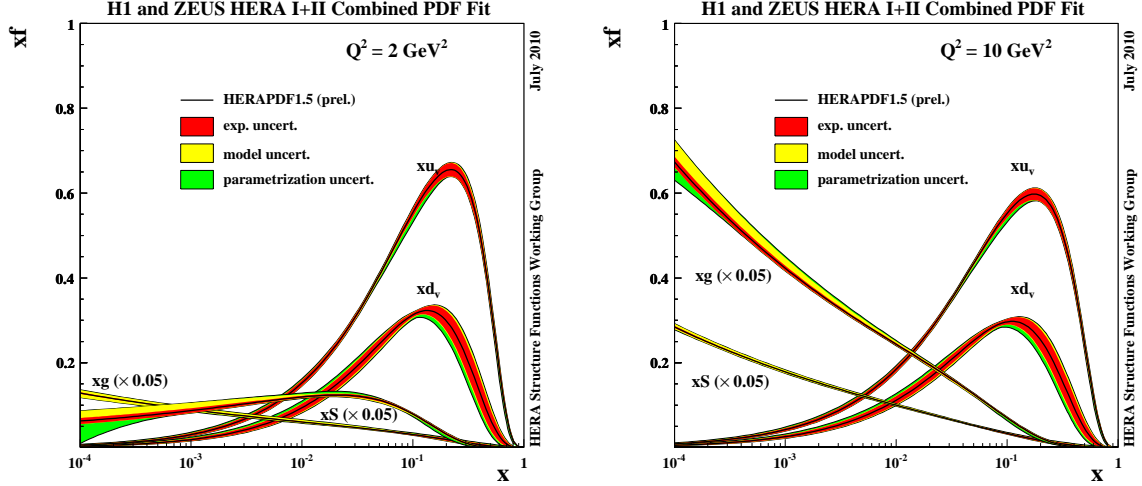


Figure 2.2: Valence and sea quark, and also gluon distributions as a function of Bjorken's  $x$  for  $Q^2 = 2$  (Left) and  $10 \text{ GeV}^2$  (Right) which are extracted by the HERA DIS data [16] Figures are cited from Ref. [15].

where  $f_a$  is the number of partons with flavor  $a$  in the proton wave function.  $C_a$  is the coefficient function which represents the information on the interaction between the parton with flavor  $a$  and the virtual photon. At the lowest order in the coupling constant, namely in the born approximation,  $C_a = e_a^2 \delta(x/\xi - 1)$  with the electromagnetic charge of the parton  $e_a$ . Then we find at the lowest order  $F_2(x, Q^2) = \sum_a x f_a(x, Q^2)$ .  $x f_a(x, Q^2)$  represents the probability to find a parton with flavor  $a$  carrying the momentum fraction between  $x$  and  $x + dx$  ( $0 \leq x \leq 1$ ) at virtuality  $Q^2$ .

As we mentioned above,  $F_2$  can be measured experimentally via Eqs. (2.9)(2.11) and Fig. 2.2 displays valence quark ( $f_v$ ) and sea quark (label " $f = S$ ") and gluon (label " $f = g$ ") distributions  $xf$  in the proton as a function of  $x$  for  $Q^2 = 2$  and  $10 \text{ GeV}^2$  which are extracted from the HERA DIS data [15]. We can notice that at larger  $x \gtrsim 0.1$  for fixed  $Q^2$  the valence quarks ( $u$  and  $d$ ) dominates in the proton while at lower  $x \ll 0.1$  the number of gluons and sea quarks increase with a decrease in  $x$ . With virtuality  $Q^2$  increases, only the gluon and sea quark distributions also increase rapidly at smaller  $x$ .

$F_1$  and  $F_2$  include all the information on the QCD dynamics in the DIS process then the non-perturbative effect is also included. However only the characteristic scale dependence of the parton distribution can be understood by the perturbative QCD calculations because the typical value of virtuality is much larger than  $\Lambda_{\text{QCD}}$  and the small- $x$  region corresponds to the high energy scattering. Of particular importance is that  $F_2$  is related

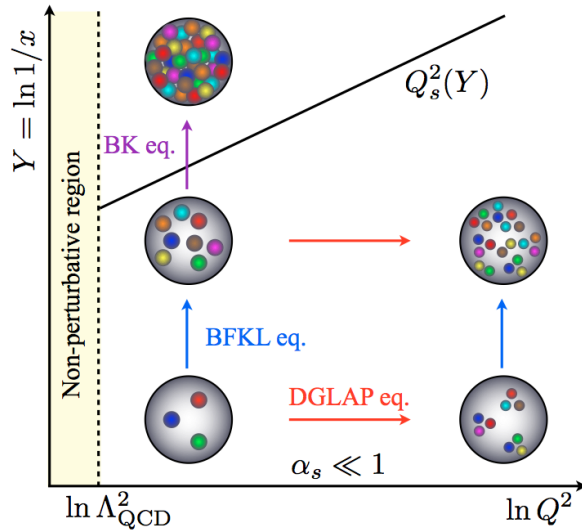


Figure 2.3: Parton structure in hadron with respect to  $Q^2$  and  $x$ .

with the gluon distribution function which is used in the particle productions in hadronic collisions. Then we will focus on how to compute the structure function  $F_2$  and understand the qualitative and also quantitative behavior of the parton distribution functions by use of the perturbative QCD method.

## 2.3 Quantum evolution

We discuss the  $Q$  and the  $x$  dependence of the parton distribution function, in particular, the gluon distribution function because we focus on the hadronic heavy quark pair production in this paper and the heavy quark itself is created by the gluon scattering. Fig. 2.3 displays the cartoon of the parton distribution in the hadron (or nucleus) as a function of  $Y = \ln(1/x)$  and  $\ln Q^2$  according to the results by using the quantum evolution equations. Here  $x$  is related with  $1/s$  (Eq. (2.3)) then  $Y$  dependence is just the energy dependence of the system. The reader notice that the entire kinematical region is divided in three part: First one is the region where the perturbative QCD method is valid and the quantum evolution equation is linear with respect to the parton distribution (DGLAP and BFKL eqs.). Second is the perturbative calculable but the system is dense where the evolution equation is non-linear with respect to the parton distribution (BK eq.). In this region, the partons in the transverse plane of hadron are localized at  $\Delta x_\perp \sim 1/Q_s$  with the new semi hard scale  $Q_s$ , usually called the saturation scale. This saturation scale roughly separates the dilute region from the dense region. Third is the non-perturbative



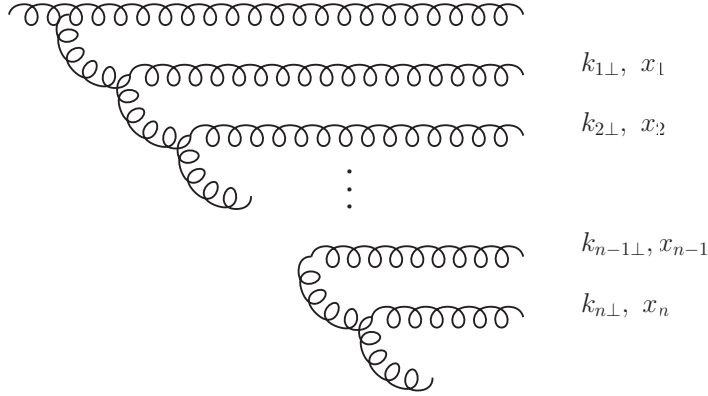


Figure 2.4: Diagrammatic representations of the gluon cascade process.

region. In this section, we consider only the perturbative region where  $\alpha_s \ll 1$ .

### 2.3.1 DGLAP equation

Firstly let us start by giving the DGLAP equation in the perturbative region  $Q^2 \gg \Lambda_{\text{QCD}}^2$  which controls the  $Q$  dependence of the parton distribution function with  $x$  fixed. Here we consider the DIS process which is shown in Fig. 2.1. Now we would focus on the integrated gluon distribution function;  $xG(x, Q^2) \equiv \int^{Q^2} d^2k_\perp \phi(x, k_\perp^2)$  then we show its evolution in  $Q$  as follows;

$$Q^2 \frac{\partial G(x, Q^2)}{\partial Q^2} = \frac{\partial G(x, Q^2)}{\partial \ln(Q^2/Q_0^2)} \approx \frac{\alpha_s(Q^2)}{2\pi} \int_x^1 \frac{dz}{z} P_{gg}(z) G(x/z, Q^2) \quad (2.13)$$

where  $Q_0^2$  is a initial virtuality scale and we have considered only the integrated gluon distribution function  $f = G$  and neglected all the quark contributions for simplicity<sup>3</sup>. If

---

<sup>2</sup>“DGLAP” stands for initial letter : Dokshitzer, Gribov, Lipatov, Altarelli, Parisi.

The QED version of this evolution equation is originally derived by Gribov and Lipatov [19]. After that, the QCD version was obtained independently by Altarelli, Parisi [20] and Dokshitzer [21].

<sup>3</sup>Strictly speaking, there is also the quark (gluon) contribution to the gluon (quark) distribution function. The exact expression of the gluon splitting function  $P_{gg}$  at leading order in the strong coupling constant is given by

$$P_{gg}(z) = 2N_c \left[ \frac{z}{(1+z)_+} + \frac{1-z}{z} + z(1-z) \right] + \frac{11N_c - 2N_f}{6} \delta(1-z), \quad (2.14)$$

with the “+” notation given by

$$\int_x^1 dz \frac{1}{(1-z)_+} f(z) = \int_x^1 dz \frac{1}{1-z} [f(z) - f(1)] + f(1) \ln(1-x) \quad (2.15)$$

for an arbitrary function  $f(z)$  defined for  $0 \leq x \leq 1$ .

$z \ll 1$ , the gluon splitting function reads

$$P_{gg}(z) \stackrel{z \ll 1}{\approx} \frac{2N_c}{z} \quad (2.16)$$

then we can simplify the DGLAP equation for the gluon distribution further as follows;

$$\begin{aligned} \frac{\partial xG(x, Q^2)}{\partial \ln(Q^2/Q_0^2)} &= \frac{\alpha_s(Q^2)N_c}{\pi} \int_x^1 \frac{dz}{z^2} xG(x/z, Q^2) \\ &= \bar{\alpha}_s(Q^2) \int_x^1 \frac{dx'}{x'} x'G(x', Q^2) \end{aligned} \quad (2.17)$$

where  $\bar{\alpha}_s \equiv \frac{\alpha_s N_c}{\pi}$  and we have redefine  $z = \frac{x}{x'}$  in the second line. This equation is linear with respect to the gluon distribution.

Here let us consider that  $Q^2 \gg Q_0^2 \sim \Lambda_{\text{QCD}}^2$  and  $x$  is small but  $\ln(Q^2/Q_0^2) \ll \ln(1/x)$  and also assume that the coupling constant is the fixed value for simplicity. In this case, even though the coupling constant is much smaller than unity, the large logarithm  $\ln(Q^2/Q_0^2)$  times the coupling constant results in  $\alpha_s \ln(Q^2/Q_0^2) \sim 1$  which should be resummed to all orders in the coupling constant. The DGLAP equation actually resums the large logarithm correction ( $\alpha_s \ln(Q^2/Q_0^2)$ ) in the  $Q$ -evolution to all orders in the coupling constant of the parton distribution function. The resummation of  $\alpha_s \ln(Q^2/Q_0^2)$  correction is referred to as the leading logarithmic approximation (LLA). On the other hand, if both  $\ln(Q^2/Q_0^2)$  and  $\ln(x_0/x)$  with a initial momentum fraction  $x_0$  are much smaller than unity but  $\alpha_s \ln(Q^2/Q_0^2) \ln(x_0/x) \sim 1$ , the resummation parameter of the DGLAP equation becomes  $\alpha_s \ln(Q^2/Q_0^2) \ln(x_0/x)$  and we can rewrite the DGLAP equation by differentiating Eq. (2.17) with respect to  $\ln(x_0/x)$  as follows;

$$\frac{\partial xG(x, Q^2)}{\partial \ln(Q^2/Q_0^2) \partial \ln(x_0/x)} = \bar{\alpha}_s(Q^2) xG(x, Q^2). \quad (2.18)$$

The resummation of  $\alpha_s \ln(Q^2/Q_0^2) \ln(x_0/x)$  correction to the parton distribution function is referred to as the double logarithmic approximation (DLA).

The physical meaning of the DGLAP equation for the gluon distribution function is given as described below. The probability for bremsstrahlung radiation of the number of

$n$  gluons from the parent parton which is shown in Fig. (2.4) is approximately given by

$$\begin{aligned}
P_{ng} &\sim \int_{Q_0^2}^{Q^2} \frac{d^2 k_{n\perp}}{k_{n\perp}^2} \alpha_s(k_{n\perp}) \int_{Q_0^2}^{k_{n\perp}^2} \frac{d^2 k_{n-1\perp}}{k_{n-1\perp}^2} \alpha_s(k_{n-1\perp}) \cdots \int_{Q_0^2}^{k_{2\perp}^2} \frac{d^2 k_{1\perp}}{k_{1\perp}^2} \alpha_s(k_{1\perp}) \\
&\sim \frac{1}{n!} \left( \alpha_s \ln \frac{Q^2}{Q_0^2} \right)^n
\end{aligned} \tag{2.19}$$

where we have assumed that the coupling constant is enough small and nearly fixed value and also that only the transverse momenta of the radiated gluons are strongly ordered as follows;

$$Q^2 \gg k_{n\perp}^2 \gg k_{n-1\perp}^2 \gg \cdots k_{1\perp}^2 \gg Q_0^2. \tag{2.20}$$

Now the probability  $P_{ng}$  is order of unity when  $Q^2 \gg Q_0^2$  then the DGLAP  $Q$ -evolution describes the multiple gluon emission in the hadron wave function <sup>4</sup> and a transverse size of the radiated gluon decreases in the  $Q$ -evolution. We can interpret the  $Q$ -dependence of the DGLAP equation from a different perspective as follows. Initially, the probe particle see the hadron structure with the coarse resolution as  $1/Q_0$ . By increasing the virtuality ( $Q > Q_0$ ), the transverse resolution of the probe becomes more finer and can see a smaller size partons. As a result, it seems that the number of partons at  $Q$  is larger than that at  $Q_0$ .

We note that the DGLAP evolution describes qualitatively the experimental data of rapid increase of the gluon distribution at small- $x$  region when the photon's virtuality increases (Fig. 2.2).

### 2.3.2 BFKL equation

Now we investigate the parton distribution in the kinematical region of  $\alpha_s \ln(x_0/x) \sim 1$  with fixed  $Q^2$ .  $x_0$  is a initial value. In such region, BFKL equation<sup>5</sup> resums the large logarithm correction ( $\alpha_s \ln(x_0/x)$ ) in the  $x$ -evolution to all orders in the coupling

---

<sup>4</sup>Even though the momentum fraction  $x$  is ordered as

$$x < x_n < x_{n-1} \cdots < x_1 < x_0 < 1, \tag{2.21}$$

the DGLAP equation also describes the multiple gluon emission but the probability for the bremsstrahlung is given by  $P_{ng} \sim \int_{Q_0^2}^{Q^2} \frac{d^2 k_{n\perp}}{k_{n\perp}^2} \int_{k_+^+}^{k_{n-1}^+} \frac{dk_n^+}{k_n^+} \alpha_s \cdots \int_{Q_0^2}^{k_{2\perp}^2} \frac{d^2 k_{1\perp}}{k_{1\perp}^2} \int_{k_+^+}^{q^+} \frac{dk_1^+}{k_1^+} \alpha_s \sim \frac{1}{n!} \left( \alpha_s \ln \frac{Q^2}{Q_0^2} \ln \frac{x_0}{x} \right)^n$ .

<sup>5</sup>"BFKL" stands for initial letter : Balitsky, Fadin, Kuraev, Lipatov.

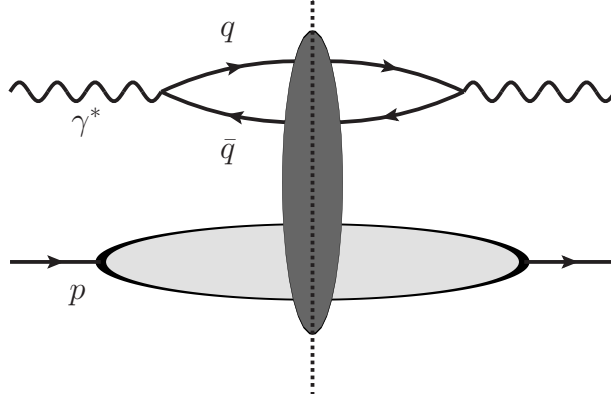


Figure 2.5: Total cross section of the  $\gamma^* p$  scattering in the dipole picture. A dotted line at the center of figure is the final state cut which means the scattering amplitude of  $\gamma^* p$  is left hand side of the dotted line and its complex conjugate is right hand side. The vertical black oval represents the interaction between the dipole and the target proton.

constant of the parton distribution function. The BFKL equation is originally derived in Refs. [22, 23], and then reconsidered in Refs. [24–26] by the use of Mueller’s dipole model. In this paper, we will review the BFKL equation from the point of view of the Mueller’s dipole model.

We first revisit the DIS process within the light cone perturbation theory [2]<sup>6</sup>. It is often convenient to consider the DIS process by use of dipole picture which is valid in high energy limit. The dipole picture which is shown in Fig. (2.5) is the same topology but different in the time ordering as shown in Fig. (2.1). Now let us consider the total  $\gamma^* p$  cross section in the dipole picture because the dimensionless structure function  $F_2$  is actually related with the total  $\gamma^* p$  cross section as follows

$$F_2(x, Q^2) = \frac{Q^2}{4\pi^2\alpha} \sigma_{tot}^{\gamma^* p}. \quad (2.22)$$

Concerning the  $F_1$ , it is found that  $2xF_1(x, Q^2) = \frac{Q^2}{4\pi^2\alpha} \sigma_T^{\gamma^* p}$ . The subindex  $T$  of the  $\sigma_T^{\gamma^* p}$  represents that the incident  $\gamma^*$  is polarized transversely<sup>7</sup>. We do not consider here the process involving the incident electron because we focus on only the parton structure in the hadron. In the dipole picture, we can factorize the DIS process as two part ; the virtual photon splits into a  $q\bar{q}$  dipole and fluctuates and subsequently the dipole interacts

<sup>6</sup>The light cone perturbation theory always imposes an ordering of the light cone time  $x^+$ .

<sup>7</sup>We immediately notice that if the longitudinal cross section  $\sigma_L^{\gamma^* A}$  remains finite, the Callan-Gross relation is broken;  $F_2 - 2xF_1 \neq 0$ .

with the target hadron. Then the  $\sigma_{tot}^{\gamma^*p}$  is given by

$$\sigma_{tot}^{\gamma^*p}(x, Q^2) = \int \frac{d^2\mathbf{r}_\perp}{4\pi} \int_0^1 \frac{dz}{z(1-z)} |\Psi^{\gamma^* \rightarrow q\bar{q}}(\mathbf{r}_\perp, z)|^2 \sigma_{tot}^{q\bar{q}p}(\mathbf{r}_\perp, Y), \quad (2.23)$$

where  $z = k^+/q^+$  and  $k^+$  is a light cone momentum of the quark and  $q^+$  is that of  $\gamma^*$ .  $\mathbf{r}_\perp$  is a transverse size between the quark and the antiquark.  $|\Psi^{\gamma^* \rightarrow q\bar{q}}(\mathbf{r}_\perp, z)|^2$  is the square of the light cone wave function for the  $\gamma^* \rightarrow q\bar{q}$  splitting process and computed by QED completely.  $Y \approx \ln(1/x)$  is the net rapidity gap between the dipole and the target proton. Furthermore, by the use of the optical theorem, the total cross section for scattering of the dipole off the target proton  $\sigma_{tot}^{q\bar{q}p}$  is given by <sup>8</sup>

$$\sigma_{tot}^{q\bar{q}p}(\mathbf{r}_\perp, Y) = 2 \int d^2\mathbf{b} N_Y(\mathbf{r}_\perp, \mathbf{b}) \quad (2.24)$$

where  $N_Y$  is imaginary part of the forward scattering amplitude of the dipole with the transverse size  $r_\perp$  at impact parameter  $\mathbf{b}$ . Then, all the information of the QCD dynamics of the parton structure in hadron is embedded in the forward scattering dipole amplitude  $N_Y$ . This  $N_Y$  itself is actually the solution of the BFKL equation.

Before the BFKL equation is shown, we note the Mueller's dipole model. In the Mueller's dipole model, the light cone wave function of the dipole changes with the scattering energy, that is, the  $x$  evolution because the the probability for bremsstrahlung of the gluon in the wave function of hadron is order of  $\alpha_s \ln(x_0/x) \sim 1$  in high energy scattering. The Mueller's dipole model assume the radiated gluon in the dipole wave function is equivalent to one  $q\bar{q}$  dipole in the large- $N_c$  limit for simplicity of the discussion. Then the (real and virtual) gluon radiation from the parent dipole is equivalent to the splitting of the parent dipole into the two daughter dipoles. Here the typical transverse size between the quark and the antiquark in the scattering process is characterized by  $\delta x_\perp \sim Lk_\perp/E$  where  $L$  is the longitudinal size of the target hadron interacting with the incident dipole and  $k_\perp$  is the transverse momentum between the quark and the antiquark and  $E$  is the energy of the dipole in laboratory frame. The coherence length of the dipole fluctuation is given by  $l_{coh} \sim 1/mx$  with the quark mass  $m$  and  $\delta x_\perp \ll l_{coh}$  at small  $x$ . Then the assumption that the transverse size of the parent dipole remains invariant in the scattering process is valid. In other words, the interaction between the partons in the hadron can

---

<sup>8</sup>The prefactor 2 in right hand side of Eq. (2.24) originates from the difference between the amplitude and its complex conjugate.

be neglected in the high energy scattering. Finally, the BFKL equation with the forward dipole amplitude is given by

$$\frac{d}{dY}N_Y(\mathbf{r}_\perp) = \int d^2\mathbf{r}_{1\perp} \mathcal{K}(\mathbf{r}_\perp, \mathbf{r}_{1\perp}) [N_Y(\mathbf{r}_{1\perp}) + N_Y(\mathbf{r}_{2\perp}) - N_Y(\mathbf{r}_\perp)], \quad (2.25)$$

with  $Y = \ln(x_0/x)$ . The interaction kernel  $\mathcal{K}$  at leading order in the coupling constant is given by

$$\mathcal{K}(\mathbf{r}_\perp, \mathbf{r}_{1\perp}) = \frac{\alpha_s N_c}{2\pi^2} \frac{r^2}{r_1^2 r_2^2} \quad (2.26)$$

where  $\mathbf{r}_\perp = \mathbf{r}_{1\perp} + \mathbf{r}_{2\perp}$  is the transverse size between the parent quark and the parent antiquark.  $r_{1\perp}$  and  $r_{2\perp}$  are the size of two daughter dipoles respectively at one step after in  $x$  evolution as is shown in Fig. 2.6. We also denote that  $r = |\mathbf{r}_\perp| = r_1 + r_2$  with  $r_1 = |\mathbf{r}_{1\perp}|$  and  $r_2 = |\mathbf{r}_{2\perp}|$ . The first two terms in Eq. (2.25) represent the real emissions of the gluon; one is coming from the quark  $N_Y(\mathbf{r}_{1\perp})$  and the other is coming from the antiquark  $N_Y(\mathbf{r}_{2\perp})$ . On the other hand, the third term corresponds to the imaginary part of the quantum correction, in other words, the virtual gluon emission. The negative sign of it is determined by the unitarity condition for the scattering amplitude. In this case, the virtual gluon emission shows no increase of the net number of radiated gluon at one step after in  $x$  evolution. The interaction kernel Eq. (2.26) is interpreted as the probability for finding the daughter dipoles in the parent dipole wave function at each step in  $x$  evolution. We note that the net quark number is conserved while the number of gluons increases in the BFKL evolution. If  $r_{2\perp} = 0$  or  $r_\perp = r_{1\perp}$ , then  $\frac{d}{dY}N_Y(\mathbf{r}_\perp) = 0$  because of  $N_Y(\mathbf{r}_{2\perp} = 0) = 0$ . This means the gluon cascade never occur in  $x$ -evolution, in other words, the colorless dipole with the transverse size  $r_\perp = 0$  never interact with the target hadron. This is called color transparency.

In contrast to the DGLAP equation, the BFKL equation imposes on the strong ordering for the momentum fraction as

$$x \ll x_n \ll x_{n-1} \cdots \ll x_1 \ll 1 \quad (2.27)$$

but no such ordering for the transverse momentum. We usually assume that all the momenta of the radiated gluons are

$$k_{n\perp}^2 \sim k_{n-1\perp}^2 \sim \cdots \sim k_{1\perp}^2 \quad (2.28)$$

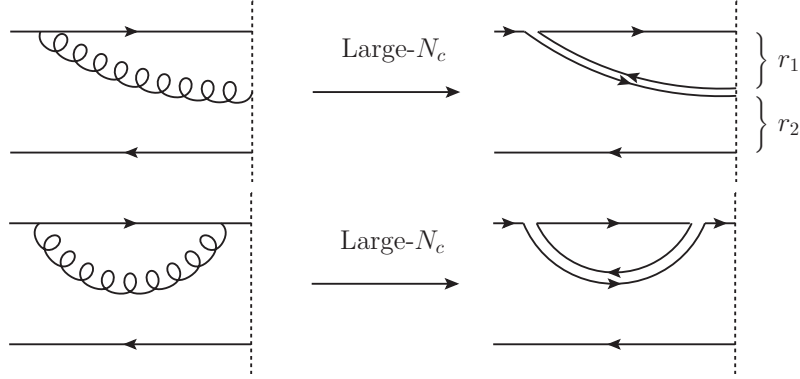


Figure 2.6: One gluon radiation from  $q\bar{q}$  dipole at one step in  $x$  evolution; (up) real emission and (down) virtual emission. The large- $N_c$  approximation allow us to substitute the  $q\bar{q}$  dipole for the gluon as shown in the right hand side. The dotted line represents the final state.

The kinematics with Eqs. (2.27)(2.28) is called the multi-Regge kinematics and we also find  $k^+ \ll k_n^+ \ll k_{n-1}^+ \cdots \ll k_1^+ \ll q^+$ .  $q^+$  is the light cone momentum of the parent parton and  $x = k^+/q^+$ . In fact, the probability for bremsstrahlung radiation of the number of  $n$  gluons from the parent parton is approximately given by

$$\begin{aligned}
 P_{ng} &\sim \int_{k^+}^{k_{n-1}^+} \frac{dk_n^+}{k_n^+} \alpha_s \int_{k^+}^{k_{n-2}^+} \frac{dk_{n-1}^+}{k_{n-1}^+} \alpha_s \cdots \int_{k^+}^{q^+} \frac{dk_1^+}{k_1^+} \alpha_s \\
 &\sim \frac{1}{n!} (\alpha_s \ln Y)^n
 \end{aligned} \tag{2.29}$$

where we have denoted  $Y = \ln(x_0/x)$  and assumed that the coupling constant is fixed value. Then the BFKL equation resums the large logarithm correction  $(\alpha_s \ln Y)$  in the  $x$ -evolution to all orders in the coupling constant of the parton distribution function via the forward scattering amplitude  $N_Y$ . The resummation of  $\alpha_s \ln(x_0/x)$  correction is also referred to as the leading logarithmic approximation (LLA).

### 2.3.3 BK equation

The BFKL evolution seemingly describes qualitatively the experimental data of rapid increase of the gluon distribution with decrease in  $x$  when the photon virtuality is fixed (Fig. 2.2). However the BFKL equation has a serious problem about unitarity. It is known that the BFKL equation violates the Froissart-Martin bound of the total cross section in

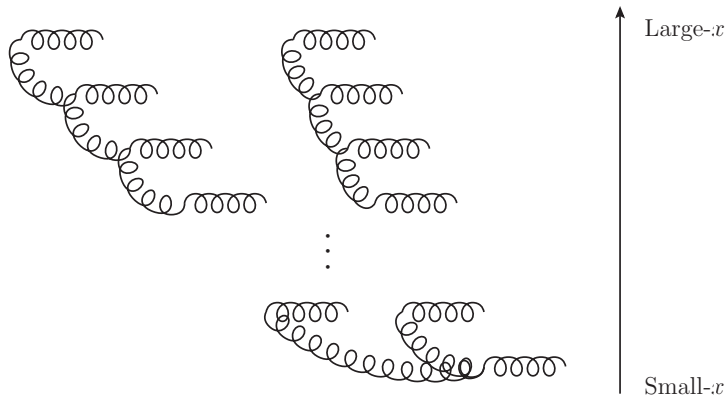


Figure 2.7: Diagrammatic representations of the gluon merging process in the BK equation.

hadron collisions;  $\sigma_{tot} \lesssim \ln^2 s$  [27]. By considering the sum from  $n = 0$  to  $n = \infty$  of Eq. (2.29), we find the total probability for bremsstrahlung of the gluons is proportional to a power of  $1/x$ ;  $\sum_n P_{ng} \sim (1/x)^\omega$  with positive number  $\omega$ . Then it can be expected that the total cross section in the hadron collisions scales as  $\sigma_{tot} \sim s^\omega$  and exceeds the Froissart-Martin bound at very large scattering energy  $s$ . We can interpret this violation as meaning that the rate of increase in the number of gluons in the BFKL evolution is too large. Then we must add new effect in the BFKL equation in order to reduce the rate of increase in the number of gluons at small  $x$ .

In fact, by introducing a nonlinear effect in the BFKL equation, the unitarity can be restored<sup>9</sup>. This is quite natural because the rapid increase in the number of gluons makes the system denser then the gluons interact with each other. In order to include the nonlinear effect, we only have to change the BFKL equation at leading order in the coupling constant as follows;

$$\frac{d}{dY} N_Y(\mathbf{r}_\perp) = \int d^2 \mathbf{r}_{1\perp} \mathcal{K}(\mathbf{r}_\perp, \mathbf{r}_{1\perp}) \left[ N_Y(\mathbf{r}_{1\perp}) + N_Y(\mathbf{r}_{2\perp}) - N_Y(\mathbf{r}_\perp) - N_Y(\mathbf{r}_{1\perp}) \mathcal{N}_Y(\mathbf{r}_{2\perp}) \right]. \quad (2.30)$$

This is called Balitsky-Kovchegov (BK) equation [47,48]. The evolution kernel  $\mathcal{K}(\mathbf{r}_\perp, \mathbf{r}_{1\perp})$  is the same as Eq. (2.26). The first three terms in the right hand side of Eq. (2.30) correspond to the BFKL equation exactly while the last nonlinear term with minus sign is the nonlinear effect and represents the gluon recombination which is shown in Fig. 2.7. As a result, this gluon recombination effect can reduce the speed of  $x$ -evolution, namely, the rapid increase of the number of gluons is suppressed. Here we note that  $\frac{d}{dY} N_Y(\mathbf{r}_\perp) = 0$

<sup>9</sup>Non linear evolution equation for the gluon distribution function was originally derived in Ref. [28] and rederived in Ref. [29].



when  $r_{2\perp} = 0$  or  $r_{\perp} = r_{1\perp}$ .

Let us consider the transverse plane of the hadron which is probed by  $\gamma^*$  in DIS process. Given the fixed virtuality  $Q$  of  $\gamma^*$ , the rapid increase of the number of gluons with decrease in  $x$  due to the BFKL evolution makes the hadron become more denser system. When the  $x$  reaches at a specific small value  $x_s$ , we can find that the valence and the radiated gluons saturate the transverse plane of the hadron completely. Here the gluon in the hadron has typically a transverse momentum  $k_{\perp} \sim Q_s$ . This  $Q_s$  is called saturation scale and corresponds to the inverse of the transverse size of the gluon approximately. Furthermore, when the  $x$  decreases to a smaller value below  $x_s$ , the wave function of the gluons begin to overlap each other and the nonlinear gluon recombination effect due to the BK evolution can no longer be neglected. If the fixed virtuality is much larger than the saturation scale;  $Q \gg Q_s$ , the transverse plane of the hadron is not dense but rather dilute. Then the  $x$ -evolution of the gluon distribution in the  $Q \gg Q_s$  region is controlled by the BFKL equation. On the other hand, for  $Q \lesssim Q_s$ , the probe particle  $\gamma^*$  can see the gluon saturation in the hadron then we should use the BK equation to describe the  $x$ -evolution of the gluon distribution.

The saturation scale  $Q_s^2$  is defined as

$$Q_s^2(x) \equiv \frac{\alpha_s N_c}{S_{\perp}} xG(x) \quad (2.31)$$

where  $\alpha_s N_c \propto (gT^a)^2$  is the color charge square of one gluon in the hadron.  $S_{\perp}$  is the transverse area in the transverse plane of the hadron. If the wavelength of the probe (e.g.  $\gamma^*$ ) is much shorter than the transverse size  $R$  of the hadron, we can well define  $S_{\perp} = \pi R^2$ . In this paper, we are just interested in the perturbative region of the probe which means that the momentum of the probe is much larger than  $\Lambda_{\text{QCD}} \sim 1/R$ , then we set  $S_{\perp} = \pi R^2$  throughout in this paper.  $xG$  is the integrated gluon distribution function and corresponds to the number of gluons per unit rapidity. When the number of gluons in hadron grows rapidly thanks to the  $x$ -evolution, the saturation scale itself becomes large. Eq. (2.31) is just as valid for the nucleus. In general, the saturation scale of the nucleus is approximately given by

$$Q_{s,A}^2(x) = \frac{\alpha_s N_c}{S_{A\perp}} xG_A(x) \propto A^{1/3} \left(\frac{1}{x}\right)^{\lambda} \quad (2.32)$$

where  $A$  is the atomic number of the nucleus and  $xG_p$  is the gluon distribution in the

proton. We have also assumed that  $R_A = A^{1/3}R_p$  with the proton radius  $R_p$  and  $xG_A = AxG_p$ . Actually, it is already known from the experimental data [158] that the gluon distribution in the proton at small  $x < 0.01$  is proportional to a power of  $1/x$  and  $\lambda \sim 0.2 - 0.3$  at  $1 < Q^2 < 10^2 \text{ GeV}^2$ . Then, the saturation scale of the nucleus is enhanced by the factor  $A^{1/3}$  and it is expected that the saturation scale in the heavy nucleus at high energy scattering can reach the hard scale which is comparable with the heavy quark mass.

## 2.4 The Color Glass Condensate

Finally, in this section, we explain the Color Glass Condensate (CGC) framework<sup>10</sup> which is used to calculate the heavy quark pair production in pA collisions in this paper. In the CGC framework, the degrees of freedom of the parton in the hadron are separated into the small  $x$  part and the large  $x$  part. The valence partons with large  $x$  are described by the classical fields which satisfy the classical Yang-Mills equation while the small  $x$  partons (mainly gluon) are emitted from a classical color sources as a result of the quantum evolution with respect to  $x$  by using the JIMWLK evolution equation<sup>11</sup> [39–46]. As we have mentioned above, the BK equation describes the energy dependence of the two point function (dipole amplitude). However, the JIMWLK equation describes the energy dependence of the multi point function in the heavy nucleus. Then the JIMWLK equation is considered to be a more general tool to include the quantum correction in the  $x$ -evolution. As a sophisticated model for an initial condition of the JIMWLK equation, it is very useful to use McLerran-Venugopalan (MV) model [33–35].

### 2.4.1 Classical valence quark

Firstly, let us consider a heavy nucleus in the nucleus rest frame. The gluon with momentum fraction  $x$  in the nucleus has a coherent length of order  $l_{coh} \sim 1/m_N x$  where  $m_N$  is a nucleon mass. If the  $x$  is much smaller than unity, the coherence length of the gluon becomes much larger than the size of the nucleus;  $l_{coh} \gg 1/\Lambda_{\text{QCD}}$ . Then, in the longitudinal direction, such small  $x$  gluon is produced coherently from the whole nucleus. On the other hand, the gluon in the transverse plane of the nucleus is localized in the area around  $x_\perp \sim 1/k_\perp$  with the transverse momentum of the gluon  $k_\perp \gg \Lambda_{\text{QCD}}$  because

<sup>10</sup>Readers are referred to Refs. [2, 36–38].

<sup>11</sup>”JIMWLK” stands for initial letter : Jalilian-Marian, Iancu, McLerran, Weigert, Leonidov, Kovner.

the gluons should be confined inside each nucleon in the transverse plane of the nucleus. Now the gluon in the nucleus with large coherence length can interact with approximately the number of  $A^{1/3}$  nucleons in the longitudinal direction at a fixed transverse position<sup>12</sup>. Then in analogy with a random walk<sup>13</sup>, the average color charge seen by the gluon is given by  $g\sqrt{A^{1/3}}$  with the QCD coupling  $g$  and atomic number  $A$ .

Next, we consider the ultrarelativistic nucleus in the infinite momentum frame where the nucleus becomes thin pancake like disc due to Lorentz contraction in the longitudinal direction. Then we only have to consider the transverse field of the gluons on the transverse plane of the nucleus. As is the case in the nucleus rest frame, we can estimate the typical average color charge fluctuations of the gluon per unit area in the transverse plane of the heavy nucleus as follows;

$$\mu_A^2 = \frac{(g\sqrt{A})^2}{S_{A\perp}} \propto \alpha_s A^{1/3} \Lambda_{\text{QCD}}^2 \quad (2.33)$$

where we have used the assumption  $S_{A\perp} = \pi(A^{1/3}R_N)^2 \sim A^{2/3}/\Lambda_{\text{QCD}}^2$ . The average color charge squared  $\mu_A^2 \gg \Lambda_{\text{QCD}}^2$  with large  $A$  seen by the gluon in the nucleus makes  $\alpha_s(\mu_A^2) \ll 1$  which allows us to calculate the gluon distribution in the nucleus by perturbative QCD method. In this case, we can assume that a quantum corrections of the valence gluon field  $A_\mu$  are neglected because the coupling constant is assumed to be enough small.

Let us define the color charge density of the valence parton with  $x$  in the transverse plane of the nucleus with the atomic mass number  $A$  which is given by

$$\rho \equiv \frac{xG_A(x, Q^2)}{S_{A\perp}} \quad (2.34)$$

which is approximately proportional to  $A^{1/3}$  by assuming  $xG_A = AxG_N$ .  $xG_N$  is the valence parton distribution in the nucleon. We note that the average color charge density  $\rho$  is static, in other words, the  $\rho$  does not depend on the light cone time  $x^+$ . The reason why the valence parton color charge is static is here in order. A wee parton with mass  $m_w$  radiated from the valence parton has a lifetime  $x_w^+$  on the light cone. This  $x_w^+$  is approximately estimated to be  $1/k_w^-$  with the light cone energy of the wee parton  $k_w^-$ . Now the on-mass shell condition is given by  $m_w^2 = 2k_w^+k_w^- - k_{w\perp}^2 = 2xP^+k_w^- - k_{w\perp}^2$  where  $x$

---

<sup>12</sup>Here we assume the Glauber model for the nucleus, namely, the nucleons inside the nucleus are independent each other.

<sup>13</sup>It is known that Brownian particle showing a random walk in medium has an average deviation  $\sigma$  from the origin in coordinate space which is proportional to  $\sqrt{t}$  at much larger time  $t$ .

is the light cone momentum fraction of the wee parton and  $P^+$  is the light cone momentum of the nucleus. Then the lifetime of the wee parton reads  $x_w^+ \sim 2xP^+/(m_w^2 + k_{w\perp}^2)$  and becomes shorter with decrease in  $x$ . In other words, by assuming the mass  $m$  is fixed, the lifetime of the valence parton is much longer than that of the wee parton and the valence parton almost freezes compared with the radiated wee parton. Thus, it is valid to assume that the valence charge does not depend on  $x^+$ .

The valence parton color charge density  $\rho$  is a random variable and distributed in the transverse plane of the nucleus according to appropriate weight function  $W_Y[\rho]$  which is normalized as unity;  $\int \mathcal{D}\rho W_Y[\rho] = 1$ .  $Y$  is a rapidity of the valence parton. In the McLerran-Venugopalan (MV) model [33–35], the weight function is assumed to be gaussian with respect to  $\rho$  as follows;

$$W_Y[\rho] = \mathcal{N} \exp \left[ - \int d^3\mathbf{x} \frac{\rho_a(x^-, \mathbf{x}_\perp) \rho_a(x^-, \mathbf{x}_\perp)}{2\mu_A^2(x^-)} \right] \quad (2.35)$$

because a lot of nucleons in the heavy nucleus support a existence of a number of valence partons ( $\sim A \times N_c$  for quark), then the central limit theorem about the number of the valence parton becomes valid. In Eq. (2.35),  $\mathcal{N}$  is normalization factor and  $\mu_A^2(x^-)$  is the average color charge squared of the valence parton per unit volume and per color with  $\mathbf{x} = (x^-, \mathbf{x}_\perp)$ . By using the gaussian weight function Eq. (2.35), the two point correlator between the different valence partons reads

$$\langle \rho_a(\mathbf{x}_\perp) \rho_{a'}^\dagger(\mathbf{y}_\perp) \rangle_Y = \delta_{aa'} \delta^{(2)}(\mathbf{x}_\perp - \mathbf{y}_\perp) \mu_A^2 \quad (2.36)$$

$$\langle \rho_a(x^-, \mathbf{x}_\perp) \rho_{a'}^\dagger(y^-, \mathbf{y}_\perp) \rangle_Y = \delta_{aa'} \delta(x^- - y^-) \delta^{(2)}(\mathbf{x}_\perp - \mathbf{y}_\perp) \mu_A^2(x^-) \quad (2.37)$$

where  $\rho(\mathbf{x}_\perp) = \int dx^- \rho(x^-, \mathbf{x}_\perp)$  and  $\mu_A^2 = \int dx^- \mu_A^2(x^-)$  has been shown in Eq. (2.33). Here a average of the operator  $\hat{\mathcal{O}}$  is defined by

$$\langle \hat{\mathcal{O}} \rangle_Y \equiv \int \mathcal{D}\rho W_Y[\rho] \hat{\mathcal{O}}. \quad (2.38)$$

The conditions Eqs. (2.37)(2.39) just satisfy the definition of “white noise”. Then, by using the Eq. (2.35) and denoting the color charge of valence parton as  $\mathcal{Q}_a = \int_{\Delta S_\perp} d^2\mathbf{x}_\perp \rho_a(\mathbf{x}_\perp)$ , the average of  $\mathcal{Q}_a$  is trivial;

$$\langle \mathcal{Q}_a \rangle_Y = 0 \quad (2.39)$$

while the average of the color charge squared is nonzero value as follows;

$$\langle \mathcal{Q}_a \mathcal{Q}_a \rangle_Y = \Delta S_\perp \frac{g^2 C_F N_c A}{\pi R_A^2} \propto \frac{A^{1/3}}{Q^2}. \quad (2.40)$$

Here  $\Delta S_\perp \sim 1/Q^2$  is a transverse area in the cylindrical tube where the valence parton is localized. We have used  $(gt^a)^2 = g^2 C_F$  by assuming the valence parton is quark. Then the commutator between the color charges of valence quarks in the large nucleus at smaller virtuality can be neglected compared with the average charge squared as follows

$$[\mathcal{Q}_a, \mathcal{Q}_b^\dagger] = if^{abc} \mathcal{Q}_c \ll \mathcal{Q}^2 \quad (2.41)$$

The commutation relation in Eq. (2.41) and the consideration as  $\alpha_s(\mu_A^2) \ll 1$  result in that the classical approximation is valid for the field of the valence quark in high energy nucleus collisions.

## 2.4.2 JIMWLK equation

The small  $x$  wave function of the ultrarelativistic nucleus is computed by using the JIMWLK equation with an appropriate initial condition such as the MV model. This wave function is referred to as the Color Glass Condensate which is usually abbreviated as CGC. The meaning of the word ‘‘Color Glass Condensate’’ is as follows. The ‘‘Color’’ refers to the gluon with colors in the nucleus and this gluon is radiated from the valence quark. The ‘‘Condensate’’ refers to the large number of the gluons emitted in high energy nucleus. We should note that the ‘‘Condensate’’ never mean the production of Bose-Einstein condensate. The bremsstrahlung of gluons with small  $x$  from the classical color sources with large  $x$  is loosely similar to spin glass in the context of the condensed matter physics. And the ultrarelativistic nucleus which is saturated by a lot of gluons seems like glass. Then these analogies result in the word ‘‘Glass’’.

Now we put an arbitrary scale  $x_0 < 1$  on the Bjorken’s  $x$  to separate between the valence quarks with larger  $x$  and the smaller  $x$  gluons. The JIMWLK equation actually describes a quantum evolution of the correlator of the number of  $n$  gauge fields and also just controls a response of the correlator when the separation scale is changed. In the CGC, the connected correlation function between the gauge fields at small  $x$  is obtained

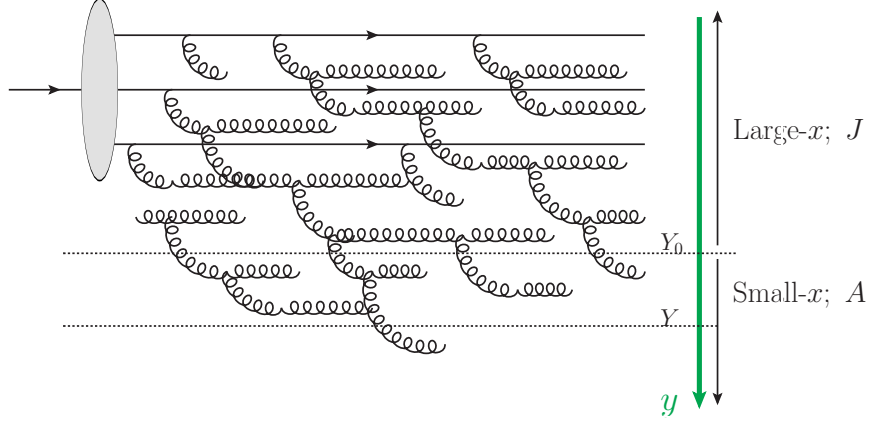


Figure 2.8: Scale separation between the large  $x$  degree of freedom corresponding to the valence parton in the hadron and the small  $x$  degree of freedom corresponding to the gluon which is emitted from the large  $x$  classical color field.  $Y = \ln 1/x$

by using the generating functional in the light cone gauge ( $A^+ = 0$ ) as follows;

$$\mathcal{Z}[j] = \int \mathcal{D}\rho \, W_Y[\rho] \ln \left( \int^Y \mathcal{D}A \delta(A^+) e^{iS[A,\rho] - i \int j \cdot A} \right) \quad (2.42)$$

where  $j$  is the external source and  $\rho$  is the valence quark color charge density in the light cone gauge. The functional integral in the bracket in Eq. (2.42) actually includes the integral with respect to the rapidity up to  $Y = \ln 1/x$  from  $Y_0 = \ln 1/x_0$  as a initial condition. This means as follows. The gauge fields at  $x \geq x_0$  firstly make the color source  $\rho_0$ . After the quantum evolution, the gauge fields between  $Y$  and  $Y_0$  are integrated out to make new color source  $\rho$  which replaces  $\rho_0$ . Here by making one step in evolution in the rapidity  $Y$  to  $Y + dY$ , the gauge fields at rapidity  $Y$  become larger  $x$  degree of freedom and behave as the classical fields making the color source current.

Let us consider a gauge invariant operator  $\mathcal{O}$  which is constructed by using the gauge fields. Most convenient gauge invariant operator is the color singlet one and actually we can construct the color singlet operator by use of the product of a Wilson line in the fundamental representation ( $\tilde{U}$ ) and its complex conjugate ( $\tilde{U}^\dagger$ ), for example,  $\text{tr}[\tilde{U}(\mathbf{x}_\perp) \tilde{U}^\dagger(\mathbf{y}_\perp)]$  and  $\text{tr}[\tilde{U}(\mathbf{x}_\perp) \tilde{U}^\dagger(\mathbf{y}_\perp) \tilde{U}(\mathbf{u}_\perp) \tilde{U}^\dagger(\mathbf{v}_\perp)]$  etc. The definition of  $\tilde{U}$  will be given later in Eq. (3.25). In high energy limit, the transverse position of a parton almost freezes during its scattering off the target hadron then the Wilson line becomes an useful degree of freedom. With increasing scattering energy, the quantum evolution of the operator  $\mathcal{O}$  reads

$$\frac{\partial \langle \hat{O} \rangle_Y}{\partial Y} = \int \mathcal{D}\rho \, W_Y[\rho] H_{\text{JIM}} \hat{O} \equiv \langle H_{\text{JIM}} \hat{O} \rangle_Y, \quad (2.43)$$

where we have used the following relation

$$\frac{\partial W_Y[\rho]}{\partial Y} = H_{\text{JIM}} W_Y[\rho] \quad (2.44)$$

because the color source  $\rho$  also varies in the quantum evolution and then we should know the alternative weight function where the quantum corrections are integrated.  $H_{\text{JIM}}$  in Eq. (2.44) stands the so-called JIMWLK Hamiltonian<sup>14</sup>.

An important remark is here. By assuming the gauge invariant operator as the dipole scattering matrix  $S_Y(\mathbf{x}_\perp - \mathbf{y}_\perp) = \frac{1}{N_c} \langle \text{tr}[\tilde{U}(\mathbf{x}_\perp) \tilde{U}^\dagger(\mathbf{y}_\perp)] \rangle_Y$ , the JIMWLK equation Eq. (2.43) reads

$$\begin{aligned} \frac{\partial}{\partial Y} \frac{1}{N_c} \langle \text{tr}[\tilde{U}(\mathbf{x}_\perp) \tilde{U}^\dagger(\mathbf{y}_\perp)] \rangle_Y &= -\frac{\alpha_s N_c}{2\pi^2} \int d^2 \mathbf{z}_\perp \frac{(\mathbf{x}_\perp - \mathbf{y}_\perp)^2}{(\mathbf{x}_\perp - \mathbf{z}_\perp)^2 (\mathbf{z}_\perp - \mathbf{y}_\perp)^2} \\ &\times \left[ \frac{1}{N_c} \langle \text{tr}[\tilde{U}(\mathbf{x}_\perp) \tilde{U}^\dagger(\mathbf{y}_\perp)] \rangle_Y - \frac{1}{N_c^2} \langle \text{tr}[\tilde{U}(\mathbf{x}_\perp) \tilde{U}^\dagger(\mathbf{z}_\perp) \text{tr}[\tilde{U}(\mathbf{z}_\perp) \tilde{U}^\dagger(\mathbf{y}_\perp)]] \rangle_Y \right]. \end{aligned} \quad (2.47)$$

We can find immediately that this equation is not closed form because the equation includes the quadrupole amplitude denoted as  $\langle \text{tr}[\tilde{U}(\mathbf{x}_\perp) \tilde{U}^\dagger(\mathbf{z}_\perp) \text{tr}[\tilde{U}(\mathbf{z}_\perp) \tilde{U}^\dagger(\mathbf{y}_\perp)]] \rangle_Y$ . Then it is difficult to find an analytical solution of the dipole amplitude after the quantum evolution. For the color singlet operator constructed by only the Wilson line, an infinite set of evolution equations are generally needed to solve the JIMWLK equation, for example, the quantum evolution of  $n$ -Wilson lines operator would be driven by an  $(n+2)$ -Wilson lines operator. This infinite system of open equations is referred to as the Balitsky's hierarchy.

However if we assume the mean field approximation in the heavy nucleus and large-

---

<sup>14</sup>In this paper, we will not use the JIMWLK hamiltonian directly but introduce the simple expression of the JIMWLK hamiltonian as follows;

$$H_{\text{JIM}} = \frac{1}{2} \int d^2 \mathbf{x}_\perp \int d^2 \mathbf{y}_\perp \frac{\delta}{\delta \alpha_Y^a(\mathbf{x}_\perp)} \eta^{ab}(\mathbf{x}_\perp, \mathbf{y}_\perp) \frac{\delta}{\delta \alpha_Y^b(\mathbf{y}_\perp)} \quad (2.45)$$

where

$$\begin{aligned} \eta^{ab}(\mathbf{x}_\perp, \mathbf{y}_\perp) &= \frac{1}{\pi} \int \frac{d^2 \mathbf{z}_\perp}{(2\pi)^2} \frac{(x_\perp^i - y_\perp^i)(x_\perp^i - y_\perp^i)}{(\mathbf{x}_\perp - \mathbf{z}_\perp)^2 (\mathbf{z}_\perp - \mathbf{y}_\perp)^2} \\ &\quad \left( 1 + \tilde{U}^\dagger(\mathbf{x}_\perp) \tilde{U}(\mathbf{y}_\perp) - \tilde{U}^\dagger(\mathbf{x}_\perp) \tilde{U}(\mathbf{z}_\perp) - \tilde{U}^\dagger(\mathbf{z}_\perp) \tilde{U}(\mathbf{y}_\perp) \right)^{ab}. \end{aligned} \quad (2.46)$$

The  $\alpha$  is defined by  $-\nabla_\perp^2 \alpha^a(\mathbf{x}_\perp) = \bar{\rho}^a(\mathbf{x}_\perp)$  where  $\bar{\rho}$  is the color charge density in the covariant gauge. We can obtain  $\bar{\rho}$  by gauge rotating of  $\rho$  with unitary operator  $S$ . For convenience, we should choose  $\alpha$  in order to satisfy  $\frac{\delta \tilde{U}(\mathbf{x}_\perp)}{\delta \alpha_Y^a(\mathbf{y}_\perp)} = ig \delta^{(2)}(\mathbf{x}_\perp - \mathbf{y}_\perp) t^a \tilde{U}(\mathbf{x}_\perp)$ .

$N_c$ , the JIMWLK equation reduces to the closed form. Here we assume in Eq. (2.47) the mean field approximation in the heavy nucleus and the large- $N_c$  limit as follows;

$$\langle \text{tr}[\tilde{U}(\mathbf{x}_\perp)\tilde{U}^\dagger(\mathbf{z}_\perp)]\text{tr}[\tilde{U}(\mathbf{z}_\perp)\tilde{U}^\dagger(\mathbf{y}_\perp)] \rangle_Y \xrightarrow{N_c \rightarrow \infty} \langle \text{tr}[\tilde{U}(\mathbf{x}_\perp)\tilde{U}^\dagger(\mathbf{z}_\perp)] \rangle_Y \langle \text{tr}[\tilde{U}(\mathbf{z}_\perp)\tilde{U}^\dagger(\mathbf{y}_\perp)] \rangle_Y. \quad (2.48)$$

In the context of the large- $N_c$  approximation, the interaction between two color singlet dipole amplitudes corresponds to a non-planar diagram which is suppressed by power of  $1/N_c^2$  and the color singlet quadrupole scattering matrix can be substituted with the product of two color singlet dipole scattering matrices. By using Eq. (2.48) and substituting the dipole forward scattering amplitude  $N_Y = 1 - S_Y$  into the Eq. (2.47), JIMWLK equation exactly reduces to BK equation shown in Eq. (2.30). Therefore, the BK equation with large- $N_c$  approximation is very convenient for numerical calculations to obtain the dipole scattering matrix for each step in quantum evolution.

Finally, let us show an appropriate initial condition of the BK equation which is obtained by assuming the MV model in the heavy nucleus. Now we denote an initial large Bjorken's  $x$  as  $x_0$  where a heavy nucleus consists of valence partons without quantum evolution. By use of the Eqs. (2.362.37), the dipole scattering matrix at  $x = x_0$  is given by [36]

$$S_{Y_0} = 1 - N_{Y_0} = \exp \left[ -\frac{r_\perp^2 Q_{s0,A}^2}{4} \ln \left( \frac{1}{r_\perp^2 \Lambda^2} \right) \right] \quad (2.49)$$

up to leading logarithmic accuracy. Here  $Y_0 = \ln 1/x_0$  and  $Q_{s0,A}^2$  is an initial saturation scale squared of the nucleus and  $\Lambda$  is a infrared cutoff and  $Q_{s0,A}^2 \equiv \alpha_s N_c \mu_A^2$ . We comment on the physical meaning of this MV model. The saturation scale in the exponent is proportional to about  $\alpha_s^2 A^{1/3}$  and then the  $\alpha_s^2 A^{1/3} = \mathcal{O}(1)$  is just resummation parameter when the atomic number is large. Roughly speaking, one  $\alpha_s$  represents a probe gluon and  $\alpha_s A^{1/3}$  represents interaction between the gluon and valence partons of  $A^{1/3}$  nucleons in the nucleus. The logarithm  $\ln(1/r_\perp^2 \Lambda^2)$  results from a quantum fluctuation of the interacting gluon and also a transverse field created by the nucleons wave function. Then the multiple scattering effect of the valence partons is included in the MV model.

We should note that all information on the nucleus is only included in the initial saturation scale in exponent of Eq. (2.49). Quantum evolution equation describes not nuclear dependence of the scattering matrix but energy dependence of that. And an impact parameter dependence is effectively included only in the initial saturation scale



$Q_{s0,A}$ . Here, if  $\mathbf{r}_\perp^2 \ll 1/Q_{s0,A}^2$ , scattering matrix  $S_{Y_0}$  is close to unity in other words  $N_{Y_0} \sim 0$  which is referred to as so-called color transparency. On the other hand, if  $\mathbf{r}_\perp^2 \gg 1/Q_{s0,A}^2$ , we find  $S_{Y_0} \sim 0$  then unitarity of the scattering amplitude is conserved.

## Chapter 3

# Heavy quark pair production from the Color Glass Condensate

In this chapter, we show the way to compute the heavy quark pair production cross section in pA collisions from the CGC in Ref. [65] by using the light cone perturbation theory [2]. In the CGC formalism, the proton-nucleus collision is described as a collision of two sets of color charge densities representing the large  $x$  degrees of freedom in the proton and the nucleus respectively. When they collide, these color densities produce a time-dependent classical color field, and this color field can in turn produce heavy quark-antiquark pairs. The CGC formalism which we use here is formulated at leading order in the color charge density of proton  $\rho_p$  while all orders in the nucleus charge density  $\rho_A^\infty$  ( $g^2\rho_A = \mathcal{O}(\infty)$ ) and includes nonlinear quantum evolution in Bjorken's  $x$  through the dipole amplitude in the numerical computations.

### 3.1 Background gauge field in pA collisions

In the CGC formula, heavy quark pair production amplitude in pA collisions is given by computing a background gauge field at large Bjorken's  $x$  in the nucleus. This background field is converted into a multi parton function in the heavy nucleus and we show it below. The multi parton function is quite different from the usual leading twist parton distribution and important for investigating the saturation effect in the nucleus.

In order to compute the background field by following Ref. [64], let us first consider

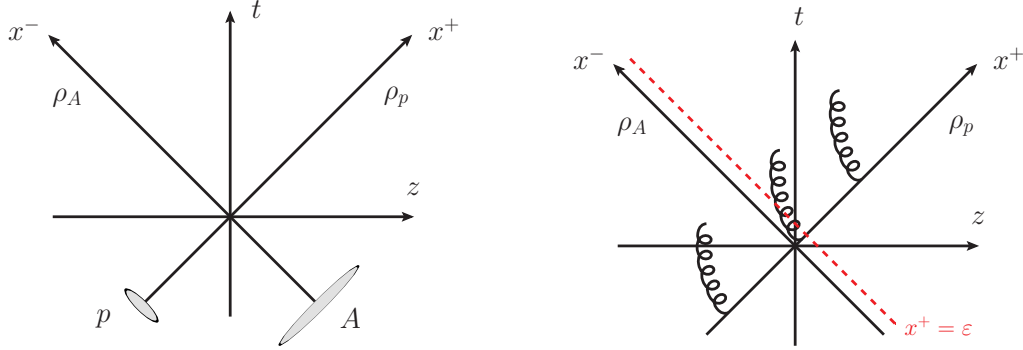


Figure 3.1: (Left) Proton-nucleus collisions in  $(x^+, x^-)$  plane. The proton (nucleus) with color charge density  $\rho_p(\rho_A)$  runs over the  $x^+(x^-)$  axis. (Right) Background field can be exactly created before the collision ( $x^+ < 0$ ), inside the nucleus ( $0 < x^+ < \epsilon$ ), and after the collision ( $\epsilon < x^+$ ).  $\epsilon$  is the thickness of the nucleus in the longitudinal direction and an infinitely small value.

the classical Yang-Mills equation in the high energy pA collisions;

$$[D_\mu, F^{\mu\nu}] = J^\nu \quad (3.1)$$

where  $J^\nu$  is a color current running over the light cone axis<sup>1</sup>. The color current on the light cone axis (Fig. 3.1) at lowest order in  $\rho_p$  and  $\rho_A$  reads

$$J_a^\nu = g\delta^{\nu+}\delta(x^-)\rho_{p,a}(\mathbf{x}_\perp) + g\delta^{\nu-}\delta(x^+)\rho_{A,a}(\mathbf{x}_\perp) \quad (3.2)$$

where  $a$  is a color and  $\rho_{p(A)}(\mathbf{x}_\perp)$  is the color charge density of proton (nucleus) localized at  $\mathbf{x}_\perp$  with large Bjorken's  $x$ . At larger  $x$ , the valence partons mainly carry the color charge. In this paper, the traveling direction of proton (nucleus) is  $x^+(x^-)$  and  $\delta^{\nu+}$  and  $\delta^{\nu-}$  mean the Lorentz contraction of the proton and the nucleus respectively in the high energy limit. The covariant color current  $J^\nu$  satisfies the current conservation condition

$$[D_\nu, J^\nu] = 0 \quad (3.3)$$

and we assume the transverse component  $J^i$  equals 0, namely the recoilless eikonal current. In addition, the gauge fixing condition is also imposed and we take the covariant gauge

---

<sup>1</sup>We have omitted a coordinate in Eq. (3.1). When we need to express the argument of the field operator, we restore the argument in the field operator below.

fixing which is given by

$$\partial^\nu A_\nu = 0. \quad (3.4)$$

Imposing the boundary condition that both gauge field and color current disappear in the remote past, then we can obtain the solution  $A_{(\rho_p^1 \rho_A^1)}^\mu$  by solving the classical Yang-Mills equation with Eq. (3.2) <sup>2</sup>. Now, we are focusing on pA collisions then we must solve the Yang-Mills equation and know the gauge field at the order in  $\rho_p^1 \rho_A^\infty$  which means the proton is being the dilute projectile while the nucleus is dense system. A way to compute the gauge field  $A_{(\rho_p \rho_A^\infty)}^\mu$  is simply shown in order below. By use of the gauge fixing condition (covariant gauge), we can rewrite the classical Yang-Mills equation and the current conservation as

$$\square A^\nu = J^\nu + ig[A_\mu, F^{\mu\nu} + \partial^\mu A^\nu], \quad (3.5)$$

$$\partial_\mu J^\mu = ig[A_\mu, J^\mu]. \quad (3.6)$$

Now we are interested in the equations at the order  $\rho_p^1$  and we must solve these equations

$$\square A_{(\rho_p^1 \rho_A^\infty)}^\nu = J_{(\rho_p^1 \rho_A^\infty)}^\nu + ig[A_{(\rho_p^1 \rho_A^\infty)_\mu}, F_{(\rho_p^0 \rho_A^\infty)}^{\mu\nu} + \partial^\mu A_{(\rho_p^0 \rho_A^\infty)}^\nu] + ig[A_{(\rho_p^0 \rho_A^\infty)_\mu}, F_{(\rho_p^1 \rho_A^\infty)}^{\mu\nu} + \partial^\mu A_{(\rho_p^1 \rho_A^\infty)}^\nu], \quad (3.7)$$

$$\partial_\mu J_{(\rho_p^1 \rho_A^\infty)}^\mu = ig[A_{(\rho_p^1 \rho_A^\infty)_\mu}, J_{(\rho_p^0 \rho_A^\infty)}^\mu] + ig[A_{(\rho_p^0 \rho_A^\infty)_\mu}, J_{(\rho_p^1 \rho_A^\infty)}^\mu]. \quad (3.8)$$

By the help of the covariant gauge fixing, the amazing relations are found as

$$A_{(\rho_p^0 \rho_A^\infty)}^\mu = A_{(\rho_p^0 \rho_A^1)}^\mu = -g\delta^{\mu-}\delta(x^+)\frac{1}{\nabla_\perp^2}\rho_A(\mathbf{x}_\perp), \quad (3.9)$$

$$J_{(\rho_p^0 \rho_A^\infty)}^\mu = J_{(\rho_p^0 \rho_A^1)}^\mu = g\delta^{\mu-}\delta(x^+)\rho_A(\mathbf{x}_\perp). \quad (3.10)$$

which are given by solving the classical Yang-Mills equation with the lowest order color current Eq. (3.2) <sup>3</sup>. Then we just have to determine the color source  $J_{(\rho_p^1 \rho_A^\infty)}^\mu$  to obtain the background field  $A_{(\rho_p^1 \rho_A^\infty)}^\mu$ .

---

<sup>2</sup>In this paper we abbreviate the gauge field at the order in  $\rho_p^n \rho_A^m$  with the positive integers  $n$  and  $m$  as  $A_{(\rho_p^n \rho_A^m)}^\mu$ . As to the color current and the field strength at the order in  $\rho_p^n \rho_A^m$ , we similarly abbreviate them as  $J_{(\rho_p^n \rho_A^m)}^\mu$  and  $F_{(\rho_p^n \rho_A^m)}^{\mu\nu}$ .

<sup>3</sup> $A_{(\rho_p^1 \rho_A^0)}^\mu$  can be obtained by exchanging  $+$   $\leftrightarrow$   $-$  and  $\rho_p \leftrightarrow \rho_A$  in  $A_{(\rho_p^0 \rho_A^1)}^\mu$ .  $J_{(\rho_p^1 \rho_A^0)}^\mu$  is the same for  $A_{(\rho_p^1 \rho_A^0)}^\mu$ .

$$U(x_\perp) = \mathcal{P} \exp \left[ ig \int dz^+ A_{(\rho_p^0 \rho_A^\infty)}^-(z^+ x_\perp) \cdot T \right]$$

Figure 3.2: Graphical representation of Wilson line in the adjoint representation. The trajectory of horizontal gluon includes the integration of a light cone time  $z^+$ . In this paper, we abbreviate the Wilson line in the adjoint representation as a horizontal gluon which is connected with a vertical gluon with a straight line shown in the right hand side of this figure. A black blob vertex represents multiple scattering of the background gauge field.

From the current conservation Eq. (3.3), we can find the solution  $J_{(\rho_p^1 \rho_A^\infty)}^+$  which is given by

$$J_{(\rho_p^1 \rho_A^\infty)}^+(x^+, x^-, \mathbf{x}_\perp) = gU(x^+, -\infty; \mathbf{x}_\perp) \delta(x^-) \rho_p(\mathbf{x}_\perp) \quad (3.11)$$

where  $U$  is the Wilson line in the adjoint representation as an eikonal phase which is given by

$$U(x_2^+, x_1^+; \mathbf{x}_\perp) \equiv \mathcal{P} \exp \left[ ig \int_{x_1^+}^{x_2^+} dz^+ A_{(\rho_p^0 \rho_A^\infty)}^-(z^+, \mathbf{x}_\perp) \cdot T \right] \quad (3.12)$$

where  $T^a$  is a generator in the adjoint representation of  $SU(N_c)$  group with the color number  $N_c$ . From Eq. (3.9), we find  $g^2 \rho_A = \mathcal{O}(1)$  (or  $gA_{(\rho_p^0 \rho_A^\infty)}^- = \mathcal{O}(1)$ ) because it is imbedded in the exponent of Eq. (3.12). Combining Eq. (3.11) with the classical Yang-Mills equation, we can find the expression for  $A_{(\rho_p^1 \rho_A^\infty)}^+$ . The solution of the classical Yang-Mills equation is given by

$$A_{(\rho_p^1 \rho_A^\infty)}^+(x) = \int dy^+ \int dy^- d\mathbf{y}_\perp G_R(x, y) J^+(y) \quad (3.13)$$

where we decompose the integral range as a three regions according to the nucleus thickness for the  $x^+$  direction which is shown in Fig. (3.1) (right). The three integral ranges and the corresponding color currents are listed below; (i)  $y^+ < 0$ ;  $J^+ = J_{(\rho_p^1 \rho_A^0)}^+$ , (ii)  $0 < y^+ < \epsilon$ ;  $J^+ = gU(y^+, 0; \mathbf{y}_\perp) \delta(y^-) \rho_p(\mathbf{y}_\perp)$ , (iii)  $\epsilon < y^+$ ;  $J^+ = gU(\epsilon, 0; \mathbf{y}_\perp) \delta(y^-) \rho_p(\mathbf{y}_\perp)$ .

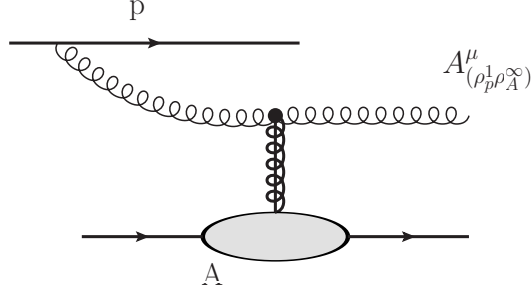


Figure 3.3: Graphical representation of the classical background gauge field  $A_{(\rho_p^1 \rho_A^\infty)}$ . The vertical gluon with solid line represents the Wilson line in the adjoint representation  $U$ . If  $U = 1$ , then  $A_{(\rho_p^1 \rho_A^\infty)} \rightarrow A_{(\rho_p^1 \rho_A^0)}$ .

We have assumed the nucleus has a infinite small thickness  $\epsilon$  for the  $x^+$  direction. Here  $G_R(x, y)$  is a retarded propagator from  $y^\mu$  to  $x^\mu$ . When the end points  $x^+$  and  $y^+$  are outside the nucleus, namely  $-\infty < x^+, y^+ < 0$  or  $\epsilon < x^+, y^+ < \infty$ , the  $G_R(x, y)$  becomes a free retarded propagator  $G_R^0(x, y)$ . On the other hand, more importantly the  $G_R(x, y)$  inside the nucleus  $[0 < y^+ < x^+ < \epsilon]$  is given by

$$G_R(x, y) = \frac{1}{2} \theta(x^- - y^-) \theta(x^+ - y^+) \delta(\mathbf{x}_\perp - \mathbf{y}_\perp) V(x^+, y^+; \mathbf{y}_\perp) \quad (3.14)$$

where  $V(x_2^+, x_1^+; \mathbf{x}_\perp) \equiv \mathcal{P} \exp \left[ \frac{ig}{2} \int_{x_1^+}^{x_2^+} dz^+ A_{(\rho_p^0 \rho_A^\infty)}^-(z^+, \mathbf{x}_\perp) \cdot T \right]$  is also the eikonal phase representing the multiple scattering effect of the background gauge field in the nucleus and differs from the  $U$  by the factor  $\frac{1}{2}$  in the exponent. From the retarded Green function, the gluon never travel toward the past (e.g. from  $y^+ > 0$  to  $x^+ < 0$ ). All the propagators in the direction of  $x^+$  and  $x^-$  can be constructed of the  $G_R^0(x, y)$  and Eq. 3.14.

Concerning the transverse component  $A_{(\rho_p^1 \rho_A^\infty)}^i$ , we can find the expression in similar way to obtain the  $A_{(\rho_p^1 \rho_A^\infty)}^+$ , by solving the Eq. (3.7) and noticing that a retarded Green function inside the nucleus involves the eikonal phase  $V$  because of the multiple scattering of the background gauge field. As to the  $A_{(\rho_p^1 \rho_A^\infty)}^-$ , a reasonable derivation of it is given in Ref. [64]. Now the covariant gauge fixing condition Eq. (3.4) is used and we can understand it as  $\partial^- A_{(\rho_p^1 \rho_A^\infty)}^+ + \partial^+ A_{(\rho_p^1 \rho_A^\infty)}^- - \partial_\perp \cdot \mathbf{A}_{(\rho_p^1 \rho_A^\infty)\perp} = 0$ . Then we obtain the expression of  $A_{(\rho_p^1 \rho_A^\infty)}^-$  by substituting  $A_{(\rho_p^1 \rho_A^\infty)}^+$  and  $A_{(\rho_p^1 \rho_A^\infty)}^-$  into Eq. (3.4). Finally, we find the background field

at the order in  $\rho_p^1 \rho_A^\infty$  in the momentum representation as

$$A_{(\rho_p^1 \rho_A^\infty)}^\mu(q) = A_{(\rho_p^1 \rho_A^0)}^\mu(q) + \frac{ig}{q^2 + iq^+ \epsilon} \int \frac{d^2 \mathbf{k}_{1\perp}}{(2\pi)^2} \left\{ C_U^\nu(q, \mathbf{k}_{1\perp}) [U(\mathbf{k}_{2\perp}) - (2\pi)^2 \delta^{(2)}(\mathbf{k}_{2\perp})] \right. \\ \left. + C_V^\nu(q) [V(\mathbf{k}_{2\perp}) - (2\pi)^2 \delta^{(2)}(\mathbf{k}_{2\perp})] \right\} \frac{\rho_p(\mathbf{k}_{1\perp})}{k_{1\perp}^2} \quad (3.15)$$

where we have used compact notations as follows;

$$\begin{aligned} \mathbf{k}_{2\perp} &\equiv \mathbf{q}_\perp + \mathbf{k}_{1\perp}, \\ U(\mathbf{k}_\perp) &\equiv \int d^2 \mathbf{x}_\perp e^{-i\mathbf{k}_\perp \cdot \mathbf{x}_\perp} U(\mathbf{x}_\perp), \\ V(\mathbf{k}_\perp) &\equiv \int d^2 \mathbf{x}_\perp e^{-i\mathbf{k}_\perp \cdot \mathbf{x}_\perp} V(\mathbf{x}_\perp), \\ \rho_p(\mathbf{k}_\perp) &\equiv \int d^2 \mathbf{x}_\perp e^{-i\mathbf{k}_\perp \cdot \mathbf{x}_\perp} \rho_p(\mathbf{x}_\perp). \end{aligned} \quad (3.16)$$

and 4-vectors  $C_U^\mu$  and  $C_V^\mu$  are given by respectively<sup>4</sup>

$$C_U^+(q, \mathbf{k}_{1\perp}) \equiv -\frac{k_{1\perp}^2}{q^-} ; C_U^-(q, \mathbf{k}_{1\perp}) \equiv \frac{k_{2\perp}^2 - q_1^2}{q^+} ; C_U^i(q, \mathbf{k}_{1\perp}) \equiv -2k_1^i \quad (3.17)$$

and

$$C_V^+(q) \equiv 2q^+ ; C_V^-(q) \equiv \frac{2q_1^2}{q^+} - 2q^- ; C_V^i(q) \equiv 2q^i . \quad (3.18)$$

$U(\mathbf{x}_\perp) \equiv U(+\infty, -\infty; \mathbf{x}_\perp)$  is the Wilson line in the adjoint representation at transverse position  $\mathbf{x}_\perp$  and  $V(\mathbf{x}_\perp) \equiv V(+\infty, -\infty; \mathbf{x}_\perp)$  is the same as  $U(\mathbf{x}_\perp)$  but with different exponent. The first term  $A_{(\rho_p^1 \rho_A^0)}^\mu(q)$  in Eq. (3.15) represents the gauge field produced from the proton color source  $\rho_p$  before the pA collisions. Thus we obtain the expression of the  $A_{(\rho_p^1 \rho_A^\infty)}^\mu(q)$  at the order in  $\rho_p^1 \rho_A^\infty$ . We note that the eikonal phase  $V$  can be dropped at last when we consider a heavy quark pair production in the background gauge field [65]. In next section, we show the heavy quark production amplitude in the classical background gauge field in pA collisions.

---

<sup>4</sup>Here  $C_L^\mu = C_U^\mu + \frac{1}{2} C_V^\mu$  corresponds to the Lipatov vertex.

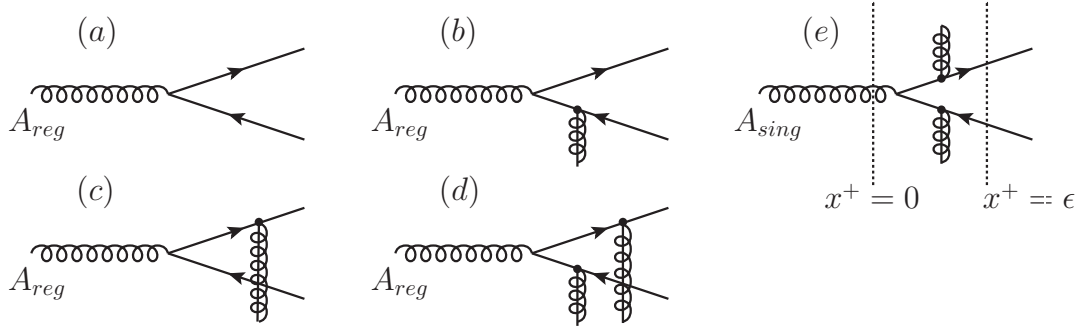


Figure 3.4: Graphical representation of a heavy quark pair production in the background gauge field. It is assumed that the nucleus has a finite small size  $\epsilon$  in the  $x^+$  direction. (a)–(d) : the heavy quark pair production from the *regular* gauge field  $A_{reg}$ , (e) : the heavy quark pair production from the *singular* field  $A_{sing}$ . The vertical gluon with straight line connected with the black blob means the eikonal phase which represents multiple scattering in the nucleus.

## 3.2 Quark pair production from the CGC

### 3.2.1 Quark pair production amplitude

Let us turn to the expression of the heavy quark pair ( $q\bar{q}$ ) production amplitude in the background gauge field in Eq. (3.15). In pA collisions, by assuming the nucleus has the finite small thickness  $\epsilon$ , the heavy quark pair can be created outside and also inside the nucleus. Here we refer the heavy quark pair production outside the nucleus as *regular* production and inside the nucleus as *singular* production. We show the graphical representation of the regular production in Fig. 3.4 (a)–(d) while the singular production in Fig. 3.4 (e). Since the  $A_{(\rho_p^1 \rho_A^\infty)}^-$  can be existed on the  $x^-$  axis, then we can decompose  $A_{(\rho_p^1 \rho_A^\infty)}^\mu$  as

$$A_{(\rho_p^1 \rho_A^\infty)}^\mu(q) \equiv A_{reg}^\mu(q) + \delta^{\mu-} A_{sing}^-(q). \quad (3.19)$$

From Eq. (3.15), the expression of the singular field is given by

$$A_{sing}^-(q) \equiv -\frac{ig}{q^+} \int \frac{d^2 \mathbf{k}_{1\perp}}{(2\pi)^2} [V(\mathbf{k}_{2\perp}) - (2\pi)^2 \delta^{(2)}(\mathbf{k}_{2\perp})] \frac{\rho_p(\mathbf{k}_{1\perp})}{k_{1\perp}^2}. \quad (3.20)$$



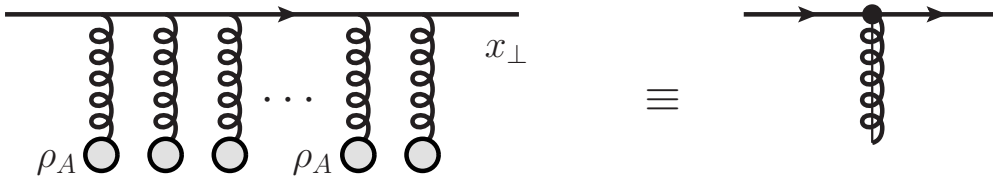
$$\tilde{U}(x_\perp) = \mathcal{P} \exp \left[ ig \int dz^+ A_{(\rho_p^0 \rho_A^\infty)}^-(x_\perp) \cdot t \right]$$


Figure 3.5: Graphical representation of Wilson line in the fundamental representation. The trajectory of horizontal quark includes the integration of a light cone time  $z^+$ . In this paper, we abbreviate the Wilson line in the fundamental representation as a horizontal quark which is connected with a vertical gluon with a straight line shown in the right hand side of this figure. A black blob vertex represents multiple scattering of the background gauge field.

Now we define a time ordered heavy quark pair production amplitude which is given by

$$\mathcal{M}_F(q(\mathbf{q})\bar{q}(\mathbf{p})) \equiv \bar{u}(\mathbf{q})\mathcal{T}_F(\mathbf{q},\mathbf{p})v(\mathbf{p}). \quad (3.21)$$

$\mathcal{T}_F(\mathbf{q},\mathbf{p})$  represents the Feynman quark propagator in the classical background field while an external lines are amputated.  $\mathbf{q}$  ( $\mathbf{p}$ ) is the momentum of the quark (antiquark). By computing all the amplitudes shown in Fig. 3.4,  $\mathcal{M}_F$  is finally given by [65]

$$\begin{aligned} \mathcal{M}_F(q(\mathbf{q})\bar{q}(\mathbf{p})) &= g^2 \int \frac{d^2\mathbf{k}_{1\perp}}{(2\pi)^2} \frac{d^2\mathbf{k}_\perp}{(2\pi)^2} \frac{\rho_{p,a}(\mathbf{k}_{1\perp})}{k_{1\perp}^2} \int d^2\mathbf{x}_\perp d^2\mathbf{y}_\perp e^{i\mathbf{k}_\perp \cdot \mathbf{x}_\perp} e^{i(\mathbf{q}_\perp + \mathbf{p}_\perp - \mathbf{k}_\perp - \mathbf{k}_{1\perp}) \cdot \mathbf{y}_\perp} \\ &\times \bar{u}(\mathbf{q}) \left\{ T_{q\bar{q}}(\mathbf{k}_{1\perp}, \mathbf{k}_\perp) [\tilde{U}(\mathbf{x}_\perp) t^a \tilde{U}^\dagger(\mathbf{y}_\perp)] + T_g(\mathbf{k}_{1\perp}) [t^b U^{ba}(\mathbf{x}_\perp)] \right\} v(\mathbf{p}), \end{aligned} \quad (3.22)$$

where

$$T_{q\bar{q}}(\mathbf{k}_{1\perp}, \mathbf{k}_\perp) \equiv \frac{\gamma^+(\not{q} - \not{k} + m)\gamma^-(\not{q} - \not{k} - \not{k}_1 + m)\gamma^+}{2p^+[(\mathbf{q}_\perp - \mathbf{k}_\perp)^2 + m^2] + 2q^+[(\mathbf{q}_\perp - \mathbf{k}_\perp - \mathbf{k}_{1\perp})^2 + m^2]}, \quad (3.23)$$

$$T_g(\mathbf{k}_{1\perp}) \equiv \frac{\not{C}_L(p + q, \mathbf{k}_{1\perp})}{(p + q)^2}, \quad (3.24)$$

with a momentum conservation  $\mathbf{k}_{2\perp} \equiv \mathbf{q}_\perp + \mathbf{p}_\perp - \mathbf{k}_{1\perp}$ . Physically,  $\mathbf{k}_{1\perp}$  ( $\mathbf{k}_{2\perp}$ ) is the momentum flow coming from the proton (nucleus), and we define  $\mathbf{k}_\perp$  as the momentum exchanged between the quark line and the nucleus while  $\mathbf{k}_{2\perp} - \mathbf{k}_\perp$  as the momentum exchanged between the antiquark line and the nucleus (Fig. 3.6).  $\tilde{U}$  is the Wilson line in

the fundamental representation which is shown in Fig. 3.5 and defined by

$$\tilde{U}(\mathbf{x}_\perp) \equiv \mathcal{P} \exp \left[ ig \int_{-\infty}^{+\infty} dz^+ A_A^-(z^+, \mathbf{x}_\perp) \cdot t \right] \quad (3.25)$$

where  $t^a$  is a generator in the fundamental representation of  $SU(N_c)$  group with the color number  $N_c$ . Here we find  $g^2 \rho_A = \mathcal{O}(1)$  in the exponent.  $\tilde{U}$  ( $\tilde{U}^\dagger$ ) appears when the quark (antiquark) is multiply scattered by the classical background field (see Fig. 3.4).  $C_L^\mu$  is the well-known gauge invariant Lipatov effective vertex whose components are

$$C_L^+(q, \mathbf{k}_{1\perp}) \equiv \frac{-k_{1\perp}^2}{q^-} + q^+ ; C_L^-(q, \mathbf{k}_{1\perp}) \equiv \frac{k_{2\perp}^2}{q^+} - q^- ; C_L^i(q, \mathbf{k}_{1\perp}) \equiv -2k_1^i + q^i \quad (3.26)$$

and satisfies the gauge invariance condition  $q \cdot C_L = 0$ . The Lipatov vertex appears in the gluon production in pA collisions [64]. Physically, the first term in the curly bracket in Eq. (3.22)  $T_{q\bar{q}}(\mathbf{k}_{1\perp}, \mathbf{k}_\perp)[\tilde{U}(\mathbf{x}_\perp)t^a\tilde{U}^\dagger(\mathbf{y}_\perp)]$  represents that the quark and the antiquark production from splitting of a gluon which is coming from the proton and subsequently the quark at  $\mathbf{x}_\perp$  and the antiquark at  $\mathbf{y}_\perp$  interact with the classical background field in the nucleus. On the other hand, the second term  $T_g(\mathbf{k}_{1\perp})[t^b U^{ba}(\mathbf{x}_\perp)]$  represents that a gluon coming from the proton interacts with the background field in the nucleus at  $\mathbf{x}_\perp$  and subsequently splits into the quark and the antiquark. The quark and the antiquark produced inside the nucleus are very close to each other until the heavy quark pair passes through the nucleus in high energy limit ( $\epsilon \rightarrow 0$ ), then we can assume that the transverse positions of the heavy quark pair almost freeze during the scattering of the quark pair off the nucleus. In this case, by use of the identity

$$\tilde{U}(\mathbf{x}_\perp)t^a\tilde{U}^\dagger(\mathbf{x}_\perp) = t^b U^{ba}(\mathbf{x}_\perp), \quad (3.27)$$

the propagator of the quark and the antiquark pair in the color octet state inside the nucleus at the same transverse position can be effectively converted into that of the gluon. This process is then included in the  $T_g(\mathbf{k}_{1\perp})[t^b U^{ba}(\mathbf{x}_\perp)]$ . Therefore, we only have to consider the quark pair production from the gluon splitting before or after the gluon scatters off the nucleus. In other words, the multiple scattering effect of the background occurs only before or after the heavy quark pair is produced and no process that the multiple scattering is involved both before and after the heavy quark pair production occur. We possibly understand that the Eq. (3.22) the gluon emission from the quark

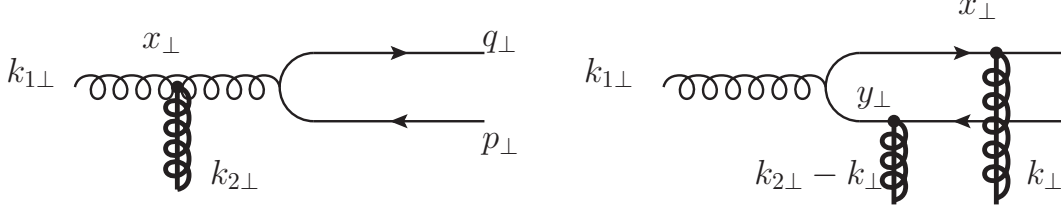


Figure 3.6: Multiple scattering effect of back ground gauge field on heavy quark pair production before the quark pair creation (Left) and after (Right).

inside the nucleus should be suppressed by inverse of a scattering energy  $1/s$  in high energy limit. At the end, we note that the eikonal phase  $V$  never appear in the final result Eq. (3.22) because it is cancelled out by summing all the amplitudes (a)–(e) in Fig. 3.4.

The total cross section of exactly one heavy quark pair ( $q\bar{q}$ ) production in the minimum bias event is computed by averaging the configurations of the classical color charge densities  $\rho_p$  and  $\rho_A$  with the distribution functions  $W_{Y_p}[\rho_p]$  and  $W_{Y_A}[\rho_A]$  [65];

$$\sigma_{q\bar{q}} = \int d^2\mathbf{b} \int \mathcal{D}\rho_p \mathcal{D}\rho_A W_{Y_p}[\rho_p] W_{Y_A}[\rho_A] P_{q\bar{q}}[\rho_p, \rho_A; \mathbf{b}]. \quad (3.28)$$

Here  $Y_{p(A)}$  is the rapidity of the gluon in the proton (nucleus). As discussed in Ref. [62], we should interpret  $P_{q\bar{q}}$  as a probability to find exactly one heavy quark pair production in the given particular configurations of  $\rho_p$  and  $\rho_A$  at the impact parameter  $\mathbf{b}$  in pA collisions. We can compute the  $P_{q\bar{q}}$  by using the heavy quark pair production amplitude Eq. (3.22) and it is given by

$$P_{q\bar{q}}[\rho_p, \rho_A; \mathbf{b}] = \int \frac{d^3\mathbf{q}}{(2\pi)^3 2E_q} \int \frac{d^3\mathbf{p}}{(2\pi)^3 2E_p} \sum |\mathcal{M}_F(q(\mathbf{q})\bar{q}(\mathbf{p}))|^2 \quad (3.29)$$

where  $E_q$  and  $E_p$  are the energy of the quark and the antiquark respectively. The saturation scale, which characterizes the behavior of the gluon coming from the nucleus, depends on the nuclear thickness function then the impact parameter dependence is encoded through the saturation scale in the square amplitude, as we show below.

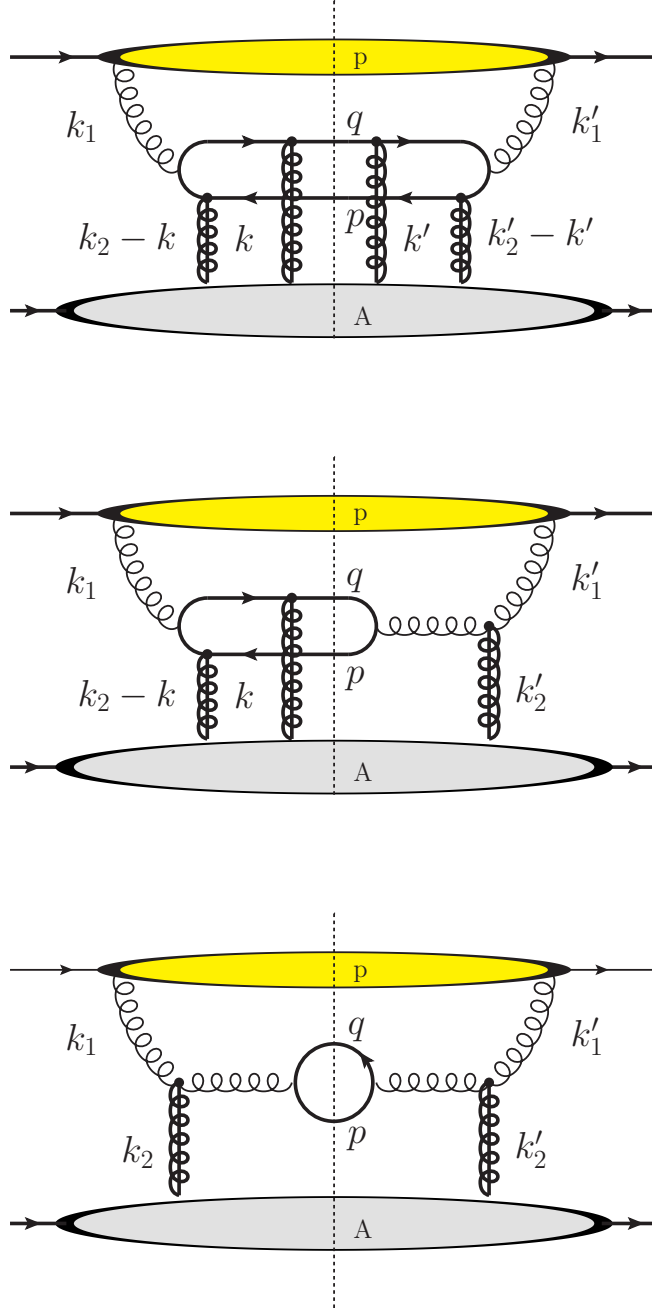


Figure 3.7: Specific diagrams of the production of the heavy quark pair. Upper figure is related to the four point function, Middle is related to the three point function, and Lower is related to the two point function. Dash line at each diagram corresponds to final state cut where the heavy quark pair is produced in the color singlet and octet state because we sum the square amplitude over all the final state. The gluons coming from the nucleus provide eikonal phases to the quark propagators which are shown in Eq. (3.22).

### 3.2.2 Multi parton function

Now we turn to the square amplitude  $\sum |\mathcal{M}_F(q(\mathbf{q})\bar{q}(\mathbf{p}))|^2$  summing over the final state of the heavy quark pair which is shown in Fig. (3.7). As we have shown in Eq. (3.28), we need to average the square amplitude over the configurations of the classical color sources  $\rho_p$  and  $\rho_A$ , then a two point correlation between the two different color charge densities which corresponds to the leading twist parton distribution function or a multi point correlation involving the four different Wilson lines because of the multiple scattering effect of the background field on the quark and the antiquark are incorporated into the cross section of the heavy quark pair production. Then, before the expression of the heavy quark production cross section, we would introduce more compact notations as to such the two point function and the multi point function.

Firstly, let us see the two point function between the different classical color sources is related with the unintegrated gluon distribution function. The detailed discussion is also found in Refs. [36, 37]. Now we consider the free transverse polarized field  $A^i$  in the light cone gauge which can be expressed by use of the creation and the annihilation operators;

$$A^i(x^+, \mathbf{x}) = \int_{k^+ > 0} \frac{d^3 k}{(2\pi)^3 2k^+} (a_c^i(x^+, \mathbf{k}) e^{i\mathbf{k} \cdot \mathbf{x}} + a_c^{i\dagger}(x^+, \mathbf{k}) e^{-i\mathbf{k} \cdot \mathbf{x}}) \quad (3.30)$$

with  $\mathbf{x} = (x^-, \mathbf{x}_\perp)$  and  $\mathbf{k} = (k^+, \mathbf{k}_\perp)$ .  $i$  is a component of the polarized vector and  $c$  is a color of the gluon. The creation and the annihilation operator should satisfy the equal time commutation relation which is given by

$$[a_c^i(x^+, \mathbf{k}), a_{c'}^{i'\dagger}(x^+, \mathbf{k}')] = \delta^{ii'} \delta_{cc'} 2k^+ (2\pi)^3 \delta^{(3)}(\mathbf{k} - \mathbf{k}') \quad (3.31)$$

at light cone time  $x^+$ . Using the production and the annihilation operators defined in the Fock space, we can compute the gluon density per unit volume in the phase space as

$$\frac{dN}{d^3 k} = \langle a_c^{i\dagger}(x^+, \mathbf{k}) a_c^i(x^+, \mathbf{k}) \rangle = \frac{2k^+}{(2\pi)^3} \langle A_c^i(x^+, \mathbf{k}) A_c^i(x^+, -\mathbf{k}) \rangle \quad (3.32)$$

where the expectation value  $\langle |\cdots| \rangle$  is given by performing the average over the hadron state  $h$ . The gauge field in the momentum space is here defined by

$$A_c^i(x^+, \mathbf{k}) \equiv \int d^3 x e^{i\mathbf{k} \cdot \mathbf{x}} A_c^i(x^+, \mathbf{x}). \quad (3.33)$$

This gluon density is usually computed in the light cone gauge. On the other hand, the collinear gluon distribution function is defined by

$$xG(x, Q^2) \equiv \int^{Q^2} d^3k \theta(Q^2 - k_\perp^2) x \delta\left(x - \frac{k^+}{P^+}\right) \frac{dN}{d^3k} \quad (3.34)$$

where  $Q^2$  is a momentum transfer between the gluon and the probe and the  $P^+$  is a longitudinal momentum of the parent hadron. Then the unintegrated gluon distribution (uGD)  $\phi$  is obtained by use of Eqs. (3.34)(3.32);

$$\begin{aligned} \phi(x, k_\perp^2) &= \left. \frac{\partial xG(x, Q^2)}{\partial Q^2} \right|_{Q^2=k_\perp^2} = k^+ \langle a_c^{i\dagger}(x^+, \mathbf{k}) a_c^i(x^+, \mathbf{k}) \rangle \\ &= \frac{1}{4\pi^3} \langle F_{LCc}^{i+}(x^+, \mathbf{k}) F_{LCc}^{i+}(x^+, \mathbf{k}) \rangle \end{aligned} \quad (3.35)$$

where we have used the fact that  $F_{LC}^{i+}(x^+, \mathbf{x}) = -\partial^+ A^i$  in the light cone gauge and the notation

$$F_c^{i+}(x^+, \mathbf{k}) \equiv \int d^3x e^{i\mathbf{k}\cdot\mathbf{x}} F_c^{i+}(x^+, \mathbf{x}). \quad (3.36)$$

When we choose the gauge field in the covariant gauge, the unintegrated gluon distribution function can be computed by performing the unitary transformation as

$$F_{LC}^{i+}(x^+, \mathbf{x}) = U(x^+, -\infty; \mathbf{x}) F_{COV}^{i+}(x^+, \mathbf{x}) U^\dagger(x^+, -\infty; \mathbf{x}) \quad (3.37)$$

where  $F_{COV}$  is the field strength in the covariant gauge and  $U$  is the Wilson line in the adjoint representation which is given in Eq. (3.12). When we consider the gluon distribution of the dilute projectile (or target) such as proton, the field strength should be given at the lowest order in the classical color source  $\rho$  and then the replacement  $U \rightarrow 1$  in Eq. (3.37) becomes valid approximately.

Here, by taking the above discussion into account, we convert the two point function  $\langle \rho_{p,a}(\mathbf{k}_{1\perp}) \rho_{p,a'}^\dagger(\mathbf{k}'_{1\perp}) \rangle_Y$ , which is averaged over the configurations of the color charge density  $\rho_p$  with the weight function  $W_Y[\rho_p]$ , into the unintegrated gluon distribution function of

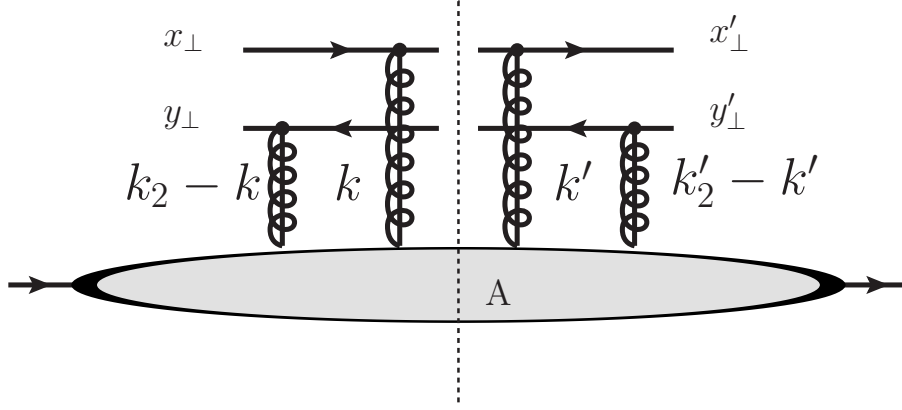


Figure 3.8: The transverse coordinates of the quark and the antiquark in the amplitude (left hand side from the dotted line) and in the complex conjugate amplitude (right hand side from the dotted line). Dotted line represents a final state cut.

the proton  $\varphi_p = 4\pi^3\phi$  as follows [64];

$$\begin{aligned}
 g^2 \langle \rho_{p,a}(\mathbf{k}_{1\perp}) \rho_{p,a'}^\dagger(\mathbf{k}'_{1\perp}) \rangle_Y &= \frac{\delta^{aa'}}{\pi d_A} \left[ \frac{\mathbf{k}_{1\perp} + \mathbf{k}'_{1\perp}}{2} \right]^2 \int_{\mathbf{X}_\perp} e^{i(\mathbf{k}_{1\perp} - \mathbf{k}'_{1\perp}) \cdot \mathbf{X}_\perp} \frac{d\varphi_{p,Y} \left( \frac{\mathbf{k}_{1\perp} + \mathbf{k}'_{1\perp}}{2} | \mathbf{X}_\perp \right)}{d^2 \mathbf{X}_\perp} \\
 &\approx \frac{\delta^{aa'}}{\pi d_A} k_{1\perp}^2 \int_{\mathbf{X}_\perp} e^{i(\mathbf{k}_{1\perp} - \mathbf{k}'_{1\perp}) \cdot \mathbf{X}_\perp} \frac{d\varphi_{p,Y}(\mathbf{k}_{1\perp} | \mathbf{X}_\perp)}{d^2 \mathbf{X}_\perp}, \quad (3.38)
 \end{aligned}$$

where we have assumed  $g^2$  is fixed value and  $d_A = N^2 - 1$ . We denote  $\int_{\mathbf{x}_\perp} = \int d^2 \mathbf{x}_\perp$ .  $\mathbf{X}_\perp$  is a coordinate running over the transverse profile of the proton and characterized by  $1/\Lambda_{\text{QCD}}$ . Then  $\mathbf{k}_{1\perp} - \mathbf{k}'_{1\perp}$  as the conjugate momentum of  $\mathbf{X}_\perp$  is the order of  $\mathcal{O}(\Lambda_{\text{QCD}})$  at most. Therefore we can validly neglected  $\mathbf{k}_{1\perp} - \mathbf{k}'_{1\perp}$  in the second line of Eq. (3.38). We are mainly interested in the perturbative region  $(\mathbf{k}_{1\perp} + \mathbf{k}'_{1\perp})/2 \gg \Lambda_{\text{QCD}}$ , then we assume  $\mathbf{k}_{1\perp} = \mathbf{k}'_{1\perp}$  below. Here by performing the integration  $\frac{d\varphi_p(\mathbf{k}_{1\perp} | \mathbf{X}_\perp)}{d^2 \mathbf{X}_\perp}$  over  $\mathbf{X}_\perp$  in Eq. (3.38), we can obtain

$$\varphi_p(\mathbf{k}_{1\perp}) = \frac{\pi^2 R_p^2 g^2}{k_{1\perp}^2} \int_{\mathbf{x}_\perp} e^{i\mathbf{k}_{1\perp} \cdot \mathbf{x}_\perp} \langle \rho_{p,a}(\mathbf{x}_\perp) \rho_{p,a}^\dagger(0) \rangle \quad (3.39)$$

where we have converted the classical source  $\rho$  into the one in the configuration space. Furthermore we have assumed the translational invariance in the transverse plane of the proton then the proton size  $\pi R_p^2$  emerges in Eq. (3.39).

On the other hand, we can not define the gluon distribution function for the nu-

cleus because the gauge field in the nucleus is given in all orders in the color charge density, in other words, many partons are relevant to the distribution function. Then we must define a multi parton correlation function. Here let us consider the correlation function between the four different Wilson lines in the fundamental representation  $\langle \text{tr}[\tilde{U}(\mathbf{x}_\perp) t^a \tilde{U}^\dagger(\mathbf{y}_\perp) \tilde{U}(\mathbf{y}'_\perp) t^a \tilde{U}^\dagger(\mathbf{x}'_\perp)] \rangle_Y$ , where  $\langle \cdots \rangle_Y$  represents the average over the configurations of the color charge density  $\rho_A$  with the weight function  $W_Y[\rho_A]$ .

By referring to the definition of the two point function in the proton, we define the four point parton function which is shown in Fig. (3.8) by analogy with Eq. (3.38) as follows;

$$\begin{aligned} & \delta^{aa'} \int_{\mathbf{x}_\perp, \mathbf{x}'_\perp, \mathbf{y}_\perp, \mathbf{y}'_\perp} e^{i(\mathbf{k}_\perp \cdot \mathbf{x}_\perp - \mathbf{k}'_\perp \cdot \mathbf{x}'_\perp)} e^{i(\mathbf{k}_{2\perp} - \mathbf{k}_\perp) \cdot \mathbf{y}_\perp} e^{-i(\mathbf{k}'_{2\perp} - \mathbf{k}'_\perp) \cdot \mathbf{y}'_\perp} \\ & \quad \times \langle \text{tr}[\tilde{U}(\mathbf{x}_\perp) t^a \tilde{U}^\dagger(\mathbf{y}_\perp)] \text{tr}[\tilde{U}(\mathbf{y}'_\perp) t^{a'} \tilde{U}^\dagger(\mathbf{x}'_\perp)] \rangle_Y \\ & = \frac{g^2 N_c}{2\pi k_{2\perp}^2} \int_{\mathbf{Y}_\perp} e^{i(\mathbf{k}_{2\perp} - \mathbf{k}'_{2\perp}) \cdot \mathbf{Y}_\perp} \frac{d\phi_{A,Y}^{q\bar{q},q\bar{q}}(\mathbf{k}_\perp, \mathbf{k}_{2\perp} - \mathbf{k}_\perp; \mathbf{k}'_\perp, \mathbf{k}'_{2\perp} - \mathbf{k}'_\perp | \mathbf{Y}_\perp)}{d^2 \mathbf{Y}_\perp}, \end{aligned} \quad (3.40)$$

where we have assumed  $g^2$  is fixed value.  $\mathbf{x}_\perp$  and  $\mathbf{y}_\perp$  are a transverse coordinates of the quark and the antiquark respectively in the production amplitude and  $\mathbf{x}'_\perp$  and  $\mathbf{y}'_\perp$  are the same but in the complex conjugate.  $\mathbf{Y}_\perp$  is a transverse position on the nucleus and its conjugate variable is  $\mathbf{k}_{2\perp} - \mathbf{k}'_{2\perp}$ . We have also assumed that the difference  $\mathbf{k}_{2\perp} - \mathbf{k}'_{2\perp}$  is small ( $\mathcal{O}(\Lambda_{\text{QCD}})$ ) and then we take  $\mathbf{k}_{2\perp} = \mathbf{k}'_{2\perp}$  because we focus on the perturbative region.

Here by use of the Fierz identity;  $(t^a)_{ij}(t^a)_{kl} = \frac{1}{2} \left( \delta_{il}\delta_{jk} - \frac{1}{N_c} \delta_{ij}\delta_{kl} \right)$ , we can rewrite the four point correlator in Eq. (3.40) as

$$\begin{aligned} & \langle \text{tr}[\tilde{U}(\mathbf{x}_\perp) t^a \tilde{U}^\dagger(\mathbf{y}_\perp) \tilde{U}(\mathbf{y}'_\perp) t^a \tilde{U}^\dagger(\mathbf{x}'_\perp)] \rangle_Y \\ & = \frac{1}{2} \langle \text{tr}[\tilde{U}(\mathbf{x}_\perp) \tilde{U}^\dagger(\mathbf{x}'_\perp)] \text{tr}[\tilde{U}(\mathbf{y}_\perp) \tilde{U}^\dagger(\mathbf{y}'_\perp)] \rangle_Y - \frac{1}{2N_c} \langle \text{tr}[\tilde{U}(\mathbf{x}_\perp) \tilde{U}^\dagger(\mathbf{y}_\perp) \tilde{U}(\mathbf{y}'_\perp) \tilde{U}^\dagger(\mathbf{x}'_\perp)] \rangle_Y \\ & \stackrel{LN_c}{=} \frac{N_c^2}{2} S_Y(\mathbf{x}_\perp, \mathbf{x}'_\perp) S_Y(\mathbf{y}_\perp, \mathbf{y}'_\perp) \end{aligned} \quad (3.41)$$

where we have used the large- $N_c$  approximation in the second line and the dipole amplitude is given by  $S_Y(\mathbf{x}_\perp, \mathbf{y}_\perp) \equiv \frac{1}{N_c} \langle \text{tr}[\tilde{U}(\mathbf{x}_\perp) \tilde{U}^\dagger(\mathbf{y}_\perp)] \rangle_Y$ . We have abbreviated the large- $N_c$  limit as “ $LN_c$ ”<sup>5</sup>. In the large- $N_c$  limit, we have also assumed the mean field approxima-

---

<sup>5</sup>Unless we give notice to the reader, we use the same abbreviation for the large- $N_c$  limit.



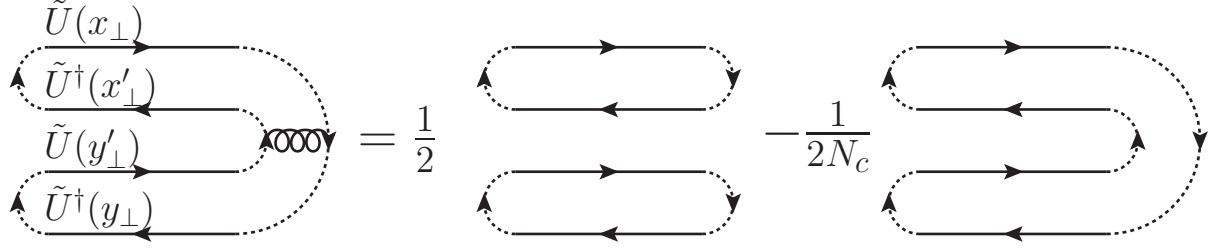


Figure 3.9: Graphical representation of the four point correlator between the different four Wilson line in the fundamental representation. The horizontal solid line represents the fundamental Wilson line.

tion in the heavy nucleus Eq. (2.48). The third line in Eq. (3.41) is very important result in this paper because the quantum evolution effect can be included through the dipole amplitude  $S_Y$  not the quadruple amplitude which is related to the four point correlator. It is known that the quantum evolution of the dipole amplitude is controlled by the BK equation. In this paper, we compute the cross section of the heavy quark pair production in the large- $N_c$  limit and use Eq. (3.41).

In addition to the four point function  $\phi_{A,Y}^{q\bar{q},q\bar{q}}$ , we need to define a three point function  $\phi_{A,Y}^{q\bar{q},g}$  and a two point function  $\phi_{A,Y}^{g,g}$  which are related with  $\langle \text{tr}[\tilde{U}(\mathbf{x}_\perp)t^a\tilde{U}^\dagger(\mathbf{y}_\perp)t^b U^{\dagger ab}(\mathbf{x}'_\perp)] \rangle_Y$  (Fig. (3.7) (mid)) and  $\langle \text{tr}[t^b U^{ba}(\mathbf{x}_\perp)t^{b'} U^{\dagger ab'}(\mathbf{x}'_\perp)] \rangle_Y$  (Fig. (3.7) (lower)) respectively in order to compute the heavy quark pair production cross section. However they can be obtained as a special limits of the four point function thanks to the identity  $\tilde{U}(\mathbf{x}_\perp)t^a\tilde{U}^\dagger(\mathbf{x}_\perp) = t^b U^{ba}(\mathbf{x}_\perp)$ . Without lacking generality, we can find the following sum rule [65, 67],

$$\begin{aligned}
& \int_{\mathbf{k}_\perp, \mathbf{k}'_\perp} \frac{d\phi_{A,Y}^{q\bar{q},q\bar{q}}(\mathbf{k}_\perp, \mathbf{k}_{2\perp} - \mathbf{k}_\perp; \mathbf{k}'_\perp, \mathbf{k}_{2\perp} - \mathbf{k}'_\perp | \mathbf{Y}_\perp)}{d^2 \mathbf{Y}_\perp} \\
&= \int_{\mathbf{k}_\perp} \frac{d\phi_{A,Y}^{q\bar{q},g}(\mathbf{k}_\perp, \mathbf{k}_{2\perp} - \mathbf{k}_\perp; \mathbf{k}_{2\perp} | \mathbf{Y}_\perp)}{d^2 \mathbf{Y}_\perp} \\
&= \frac{d\phi_{A,Y}^{g,g}(\mathbf{k}_{2\perp}; \mathbf{k}_{2\perp} | \mathbf{Y}_\perp)}{d^2 \mathbf{Y}_\perp}.
\end{aligned} \tag{3.42}$$

Here we denote  $\int_{\mathbf{k}_\perp} = \int d^2 \mathbf{k}_\perp / (2\pi)^2$ . Then we use this relation in computing the heavy quark pair production cross section below.

Finally, let us consider the heavy quark pair production cross section by squaring the amplitude and summing the square amplitude over the final state and averaging the configurations of the classical color charge density with the weight function in the proton

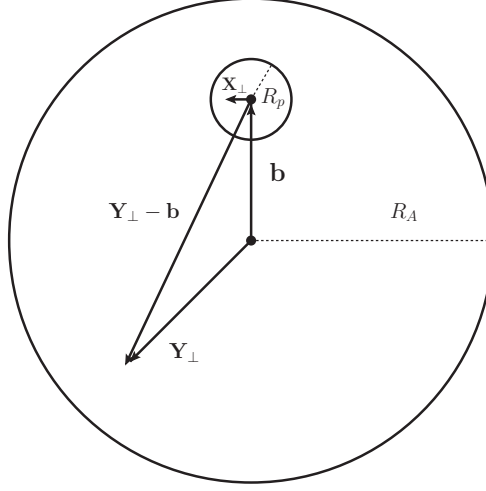


Figure 3.10: Transverse plane of the nucleus in pA collisions.  $\mathbf{X}_\perp(\mathbf{Y}_\perp)$  runs over the transverse plane of the proton (nucleus) having a radius  $R_p(R_A)$ .  $\mathbf{b}$  is the impact parameter characterized the distance from the center of nucleus to the center of proton.

and the nucleus. Here we indicate the impact parameter dependence of the heavy quark pair production cross section. The saturation scale  $Q_{s,A}^2$ , which depends on the impact parameter, is embedded in the dipole amplitude in the large- $N_c$  limit however when we treat the nucleus as cylindrical one and assume the translational invariance in the nucleus, we can effectively convert the impact parameter dependence into the initial saturation scale at larger Bjorken's  $x$ . Therefore If once we fix the initial saturation scale, the  $\phi_{A,Y}$  itself does not depend on the impact parameter and the impact parameter dependence should be encoded in the exponential phase in Eq. (3.40) as  $(\mathbf{k}_{1\perp} - \mathbf{k}'_{1\perp}) \cdot (\mathbf{X}_\perp - \mathbf{Y} + \mathbf{b})$ . By the shift  $\mathbf{Y}_\perp \rightarrow \mathbf{Y}_\perp - \mathbf{b}$ ,  $\mathbf{Y}_\perp$  becomes a relative transverse coordinate from the center of proton as is shown in Fig. (3.10). When we focus on the production cross section in the minimum bias event, we integrate out the impact parameter by use of

$$\int_b e^{i(\mathbf{k}_{1\perp} - \mathbf{k}'_{1\perp}) \cdot \mathbf{b}} = (2\pi)^2 \delta^{(2)}(\mathbf{k}_{1\perp} - \mathbf{k}'_{1\perp}). \quad (3.43)$$

After the performing of the integral over the impact parameter, we can treat the  $\mathbf{X}_\perp$  and the  $\mathbf{Y}_\perp$  independently in  $\varphi_p$  and  $\phi_A$  and we can also perform the integral over the  $\mathbf{X}_\perp$  and the  $\mathbf{Y}_\perp$ . Then the heavy quark pair production cross section in minimum bias event

is given by

$$\frac{d\sigma_{q\bar{q}}}{d^2\mathbf{p}_\perp d^2\mathbf{q}_\perp dy_p dy_q} = \frac{\alpha_s^2 N_c}{8\pi^4 d_A} \frac{1}{(2\pi)^2} \int_{\mathbf{k}_{2\perp}, \mathbf{k}_\perp} \frac{\Xi(\mathbf{k}_{1\perp}, \mathbf{k}_{2\perp}, \mathbf{k}_\perp)}{\mathbf{k}_{1\perp}^2 \mathbf{k}_{2\perp}^2} \phi_{A,y_2}^{q\bar{q},g}(\mathbf{k}_{2\perp}, \mathbf{k}_\perp) \varphi_{p,y_1}(\mathbf{k}_{1\perp}), \quad (3.44)$$

where  $y_1$  and  $y_2$  are rapidities of the gluon coming from the proton and the nucleus respectively. We have used the relations in Eq. (3.42) then only the three point function emerges. The hard matrix element  $\Xi$  is given by

$$\begin{aligned} \Xi(\mathbf{k}_{1\perp}, \mathbf{k}_{2\perp}, \mathbf{k}_\perp) &= \text{tr}_d \left[ (\not{q} + m) T_{q\bar{q}} (\not{p} - m) \gamma^0 T_{q\bar{q}}^\dagger \gamma^0 \right] \\ &\quad + \text{tr}_d \left[ (\not{q} + m) T_{q\bar{q}} (\not{p} - m) \gamma^0 T_g^\dagger \gamma^0 + \text{h.c.} \right] \\ &\quad + \text{tr}_d \left[ (\not{q} + m) T_g (\not{p} - m) \gamma^0 T_g^\dagger \gamma^0 \right]. \end{aligned} \quad (3.45)$$

This production formula corresponds to the unpolarized cross section of the heavy quark pair production<sup>6</sup>. The three point function is given by

$$\phi_{A,Y}^{q\bar{q},g}(\mathbf{k}_{2\perp}, \mathbf{k}_\perp) = \frac{\pi R_A^2 N_c \mathbf{k}_{2\perp}^2}{4\alpha_s} \tilde{S}_Y(\mathbf{k}_\perp) \tilde{S}_Y(\mathbf{k}_{2\perp} - \mathbf{k}_\perp) \quad (3.46)$$

where we have assumed the translational invariance in the nucleus and introduced the dipole scattering matrix  $\tilde{S}_Y$  in the momentum representation as follows;

$$\tilde{S}_Y(\mathbf{k}_\perp) \equiv \int_{\mathbf{x}_\perp} e^{-i\mathbf{k}_\perp \cdot \mathbf{x}_\perp} S_Y(\mathbf{x}_\perp). \quad (3.47)$$

Single heavy quark production cross section is obtained by integrating the pair production cross-section (3.44) over the anti-quark phase space:

$$\frac{d\sigma_q}{d^2\mathbf{q}_\perp dy_q} = \int \frac{dp^+}{p^+} d^2\mathbf{p}_\perp \frac{d\sigma_{q\bar{q}}}{d^2\mathbf{p}_\perp d^2\mathbf{q}_\perp dy_p dy_q}. \quad (3.48)$$

By dividing the production cross section Eq. (3.44) or (3.48) with the total inelastic cross section  $\sigma_{inel}^{pA}$ , which we estimate as  $\sigma_{inel}^{pA} = \pi(R_A + R_p)^2 \approx \pi R_A^2$ , we can obtain the average

---

<sup>6</sup>We note that the production formula here strictly breaks  $k_\perp$ -factorization due to the multi parton correlator [66,67]. We mean that the single momentum  $\mathbf{k}_{2\perp}$  only characterizes the gluon exchange between the quark or the antiquark and the gluon coming from the nucleus in  $k_\perp$ -factorization.

multiplicity per event<sup>7</sup>. If we compute the multiplicity per event, the total inelastic cross section is effectively canceled out with the transverse size of nucleus  $\pi R_A^2$  in  $\phi_{A,y_2}^{q\bar{q},g}(\mathbf{k}_{2\perp}, \mathbf{k}_\perp)$  and therefore the proton size only remains explicitly in the expression of multiplicity. We show the multiplicity of the quark pair production as follows;

$$\frac{dN_{q\bar{q}}}{d^2\mathbf{p}_\perp d^2\mathbf{q}_\perp dy_p dy_q} = \frac{1}{\pi R_A^2} \frac{\alpha_s^2 N_c}{8\pi^4 d_A} \frac{1}{(2\pi)^2} \int_{\mathbf{k}_{2\perp}, \mathbf{k}_\perp} \frac{\Xi(\mathbf{k}_{1\perp}, \mathbf{k}_{2\perp}, \mathbf{k}_\perp)}{\mathbf{k}_{1\perp}^2 \mathbf{k}_{2\perp}^2} \phi_{A,y_2}^{q\bar{q},g}(\mathbf{k}_{2\perp}, \mathbf{k}_\perp) \varphi_{p,y_1}(\mathbf{k}_{1\perp}) . \quad (3.49)$$

### 3.3 Collinear limit on proton side: Hybrid description

When the momentum fraction  $x_1$  probed in the proton is not small or even more at forward rapidity where  $x_1 = \mathcal{O}(1)$ , the gluons in the proton have the typical transverse momentum of the order of  $\mathcal{O}(\Lambda_{\text{QCD}})$  or larger. In this case, we can neglect  $\mathbf{k}_{1\perp}$  in the matrix element  $\Xi$  in Eq. (3.45) compared to other hard scale such as heavy quark mass and the larger transverse momentum of the heavy quark, and then the taking of the collinear approximation on the proton side becomes valid. This limit is well defined thanks to the fact that the expression on the second line in the amplitude in Eq. (3.22) goes to zero as  $\mathbf{k}_{1\perp} \rightarrow 0$  [65] :

$$\mathcal{M}_F(\mathbf{q}, \mathbf{p})_{\mathbf{k}_{1\perp} \rightarrow 0} = \mathbf{A} \cdot \mathbf{k}_{1\perp} + \mathcal{O}(\mathbf{k}_{1\perp}^2) . \quad (3.50)$$

In fact, in the  $\mathbf{k}_{1\perp}$  limit, the two terms in the curly bracket of Eq. (3.22) become

$$\begin{aligned} T_{q\bar{q}}(\mathbf{k}_{1\perp}, \mathbf{k}_\perp) [\tilde{U}(\mathbf{x}_\perp) t^a \tilde{U}^\dagger(\mathbf{y}_\perp)] &\rightarrow \frac{\gamma^+}{p^+ + q^+} [\tilde{U}(\mathbf{x}_\perp) t^a \tilde{U}^\dagger(\mathbf{y}_\perp)] \\ T_g(\mathbf{k}_{1\perp}) [t^b U^{ba}(\mathbf{x}_\perp)] &\rightarrow -\frac{\gamma^+}{p^+ + q^+} [t^b U^{ba}(\mathbf{x}_\perp)] + \left[ -\frac{\gamma^- k_{1\perp}^2}{(p+q)^2 (p^- + q^-)} \right. \\ &\quad \left. + \frac{\gamma^+}{(p+q)^2 (p^+ + q^+)} [k_{1\perp}^2 - 2(\mathbf{p}_\perp + \mathbf{q}_\perp) \cdot \mathbf{k}_{1\perp}] + \frac{2\gamma_\perp \cdot \mathbf{k}_{1\perp}}{(p+q)^2} \right] [t^b U^{ba}(\mathbf{x}_\perp)] \end{aligned} \quad (3.51)$$

---

<sup>7</sup>The expression Eq. (3.44) is for *single* quark pair production. Ref. [119] reports that double charm production amounts to 10 % of single charm production in forward rapidity region in pp collisions at  $\sqrt{s} = 7$  TeV.

where we have used the identity  $\gamma^+ \gamma^- \gamma^+ = 2\gamma^+$  and  $\bar{u}(\mathbf{q})(\not{q} - m) = 0$  and  $(\not{p} + m)v(\mathbf{p}) = 0$ . And in Eq. (3.52), we have left the  $\mathbf{k}_{1\perp}$  dependent terms explicitly. By combining Eq. (3.51) with Eq. (3.52) except for the  $\mathbf{k}_{1\perp}$  dependent terms and performing the integral over the  $\mathbf{k}_{\perp}$ , we can find

$$\int_{\mathbf{k}_{\perp}} e^{i\mathbf{k}_{\perp} \cdot (\mathbf{x}_{\perp} - \mathbf{y}_{\perp})} \left\{ \frac{\gamma^+}{p^+ + q^+} [\tilde{U}(\mathbf{x}_{\perp}) t^a \tilde{U}^\dagger(\mathbf{y}_{\perp})] - \frac{\gamma^+}{p^+ + q^+} [t^b U^{ba}(\mathbf{x}_{\perp})] \right\} = 0 \quad (3.53)$$

where we have used the identity Eq. (3.27) because the inside in the curly bracket does not depend on  $\mathbf{k}_{\perp}$  then the delta function  $\delta^{(2)}(\mathbf{x}_{\perp} - \mathbf{y}_{\perp})$  emerges after the integration.

Therefore, the squared amplitude  $\Xi$  is quadratic in  $\mathbf{k}_{1\perp}$  when  $\mathbf{k}_{1\perp} \rightarrow 0$ , which cancels the factor  $k_{1\perp}^2$  in the denominator of Eq. (3.44). Note that the three vector  $\mathbf{A}$  in this formula contains spinors and Dirac matrices. In this approximation, we can write the integral in Eq. (3.44) as

$$\int_{\mathbf{k}_{1\perp}, \mathbf{k}_{\perp}} \frac{\text{tr}_d(\mathbf{A}^i \mathbf{A}^j) \mathbf{k}_{1\perp}^i \mathbf{k}_{1\perp}^j}{\mathbf{k}_{1\perp}^2 \mathbf{k}_{2\perp}^2} \phi_{A, y_2}^{q\bar{q}, g}(\mathbf{k}_{2\perp}, \mathbf{k}_{\perp}) \varphi_{p, y_1}(\mathbf{k}_{1\perp}), \quad (3.54)$$

where it is now implicit that  $k_{1\perp}$  should not exceed the typical transverse momentum scale set by the produced final state. Using  $d^2\mathbf{k}_{1\perp} = \frac{1}{2}d\theta_1 d(k_{1\perp}^2)$  and defining the collinear gluon distribution from Eq. (3.34) as <sup>8</sup>

$$\frac{1}{4\pi^3} \int_0^{Q^2} d(k_{\perp}^2) \varphi_{p, y}(\mathbf{k}_{\perp}) \equiv x G_p(x = e^{-y}, Q^2), \quad (3.55)$$

and then we obtain

$$\frac{d\sigma_{q\bar{q}}}{d^2\mathbf{p}_{\perp} d^2\mathbf{q}_{\perp} dy_p dy_q} = \frac{\alpha_s^2 N_c}{8\pi^2 d_A} \frac{1}{(2\pi)^2} \int_{\mathbf{k}_{\perp}} \frac{\Xi_{\text{coll}}(\mathbf{k}_{2\perp}, \mathbf{k}_{\perp})}{\mathbf{k}_{2\perp}^2} \phi_{A, y_2}^{q\bar{q}, g}(\mathbf{k}_{2\perp}, \mathbf{k}_{\perp}) x_1 G_p(x_1, Q^2), \quad (3.56)$$

where we have now  $\mathbf{k}_{2\perp} = \mathbf{p}_{\perp} + \mathbf{q}_{\perp}$  and we denote  $\Xi_{\text{coll}}(\mathbf{k}_{2\perp}, \mathbf{k}_{\perp}) \equiv \frac{1}{2}\text{tr}_d(\mathbf{A}^2)$ . The squared matrix element  $\Xi_{\text{coll}}$  in the collinear approximation can be obtained by expanding the

---

<sup>8</sup> $Q^2$  is a renormalization scale limited by the transverse resolution determined by an external probe such as virtual photon. Large  $\alpha_s \ln Q^2$  correction is controlled by DGLAP equation.

amplitude in Eq. (3.22) to linear order in the transverse momentum  $\mathbf{k}_{1\perp}$ :

$$\Xi_{\text{coll}} = \Xi_{\text{coll}}^{q\bar{q},q\bar{q}} + \Xi_{\text{coll}}^{q\bar{q},g} + \Xi_{\text{coll}}^{g,g} , \quad (3.57)$$

with

$$\begin{aligned} \Xi_{\text{coll}}^{q\bar{q},q\bar{q}} &= \frac{8p^+q^+}{(p^+ + q^+)^2(\mathbf{a}_\perp^2 + m^2)^2} \left[ m^2 + \frac{(p^+)^2 + (q^+)^2}{(p^+ + q^+)^2} \mathbf{a}_\perp^2 \right] , \\ \Xi_{\text{coll}}^{q\bar{q},g} &= -\frac{16}{(p+q)^2(\mathbf{a}_\perp^2 + m^2)} \left[ m^2 + \frac{(p^+)^2 + (q^+)^2}{(p^+ + q^+)^3} \mathbf{a}_\perp \cdot (p^+ \mathbf{q}_\perp - q^+ \mathbf{p}_\perp) \right] , \\ \Xi_{\text{coll}}^{g,g} &= \frac{8}{(p+q)^4} \left[ (p+q)^2 - \frac{2}{(p^+ + q^+)^2} (p^+ \mathbf{q}_\perp - q^+ \mathbf{p}_\perp)^2 \right] . \end{aligned} \quad (3.58)$$

In these formulas, we denote  $\mathbf{a}_\perp \equiv \mathbf{q}_\perp - \mathbf{k}_\perp$  and the squared invariant mass of the pair  $(p+q)^2$  is given by

$$(p+q)^2 = (p^+ + q^+) \left[ \frac{\mathbf{p}_\perp^2 + m^2}{p^+} + \frac{\mathbf{q}_\perp^2 + m^2}{q^+} \right] - (\mathbf{p}_\perp + \mathbf{q}_\perp)^2 . \quad (3.59)$$

We will evaluate how the collinear description works in the quarkonium production below.

### 3.4 Quantum evolution effect

So far we have shown the two point gluon distribution and the multi parton function but these functions describe the behavior of only the valence parton in the proton and the nucleus. In fact, the creation of the smaller- $x$  parton results from the quantum evolution of the gluon distribution and multi parton function. Energy dependence of the heavy quark production cross section is implicit in the multi parton function  $\phi_{A,Y}^{q\bar{q},g}(\mathbf{k}_{2\perp}, \mathbf{k}_\perp)$  shown in Eq. (3.46) through the rapidity  $Y = \ln(1/x)$  evolution of the dipole amplitude.

We have already shown that the BK equation controls the energy dependence of the dipole amplitude. As a recent theoretical development, it has been demonstrated [50, 51] that the BK equation with the running coupling corrections includes the important part of the NLO corrections<sup>9</sup>. That means the quark loops run over the gluon line which is emitted from the parent dipole through the one step rapidity evolution (Fig. 3.11). In Balitsky's prescription [49] but without the subtraction term in the evolution kernel, we refer BK equation with running coupling kernel as rcBK equation and the running

---

<sup>9</sup>The full NLO corrections of the BK equation at leading order has been computed in Ref. [52].

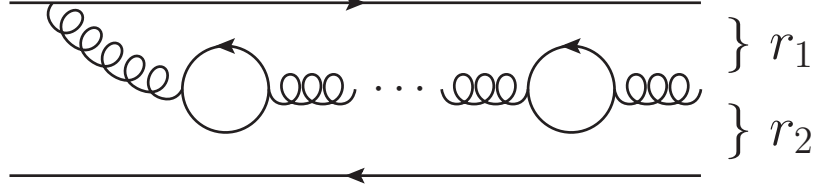


Figure 3.11: One of the running coupling corrections of the BK equation.

coupling kernel is given by

$$\mathcal{K}_{\text{Bal}}(\mathbf{r}_\perp, \mathbf{r}_{1\perp}) = \frac{\alpha_s(r^2) N_c}{2\pi^2} \left[ \frac{1}{r_1^2} \left( \frac{\alpha_s(r_1^2)}{\alpha_s(r_2^2)} - 1 \right) + \frac{r^2}{r_1^2 r_2^2} + \frac{1}{r_2^2} \left( \frac{\alpha_s(r_2^2)}{\alpha_s(r_1^2)} - 1 \right) \right] \quad (3.60)$$

where both  $r_1$  ( $r_2$ ) is the transverse size between the emitted gluon and the parent quark (antiquark). In this paper, we use the rcBK equation to include the quantum evolution effect into the dipole amplitude because it is manageable for numerical calculations.

In order to use the rcBK equation, we need to determine the initial condition of the dipole amplitude at  $x = x_0$ . Global fit analysis of the compiled HERA e+p data at  $x < x_0 = 0.01$  was performed in [53, 54] using the rcBK equation with the initial condition of the dipole amplitude in the proton side at  $x = x_0$

$$S_{Y=0}(\mathbf{r}_\perp) = \exp \left[ -\frac{(r^2 Q_{s0,p}^2)^\gamma}{4} \ln \left( \frac{1}{\Lambda r} + e_c \cdot e \right) \right]. \quad (3.61)$$

where  $e_c \cdot e$  is a infrared regulator. Here, in the quantum evolution, we modify the infrared regularization of the running coupling in the coordinate space to the smooth one [57]:

$$\alpha_s(r^2) = \left[ b_0 \ln \left( \frac{4C^2}{r^2 \Lambda^2} + a \right) \right]^{-1} \quad (3.62)$$

with  $b_0 = 9/(4\pi)$ . The constant  $a$  is introduced so as to freeze the coupling constant smoothly at  $\alpha_s(r \rightarrow \infty) = \alpha_{fr}$  and  $\Lambda$  is a width and we fix  $\Lambda = 0.241$  GeV in this paper. The global fitted parameter values  $Q_{s0,p}^2$ ,  $\gamma$ ,  $\alpha_{fr}$ , and  $C$  are listed in Table 3.1. We also list a parameter set with the McLerran-Venugopalan (MV) model initial condition  $\gamma = 1$  which is also used in our numerical computations, for comparison. We also refer the constrained initial condition by fitting data as MV $^\gamma$  model below <sup>10</sup>.

<sup>10</sup>The origin of  $\gamma \neq 1$  in the initial condition for the proton is not fully understood yet. In the case of MV model with  $\gamma = 1$  which is valid for the very large nucleus, the classical color source density  $\rho$  is distributed as gaussian in the transverse plane of the nucleus due to the central limit theorem. On the

set	$Q_{s0,p}^2/\text{GeV}^2$	$\gamma$	$\alpha_{fr}$	$C$
g1118	0.1597	1.118	1.0	2.47
MV	0.2	1	0.5	1

Table 3.1: Parameter values of the initial dipole amplitude with  $e_c = 1$  at  $x_0 = 0.01$ .  $\Lambda = 0.241$  GeV is fixed. The data fit with  $MV^\gamma$  initial condition yields a best fit  $\chi^2/d.o.f. \approx 1.1$ .

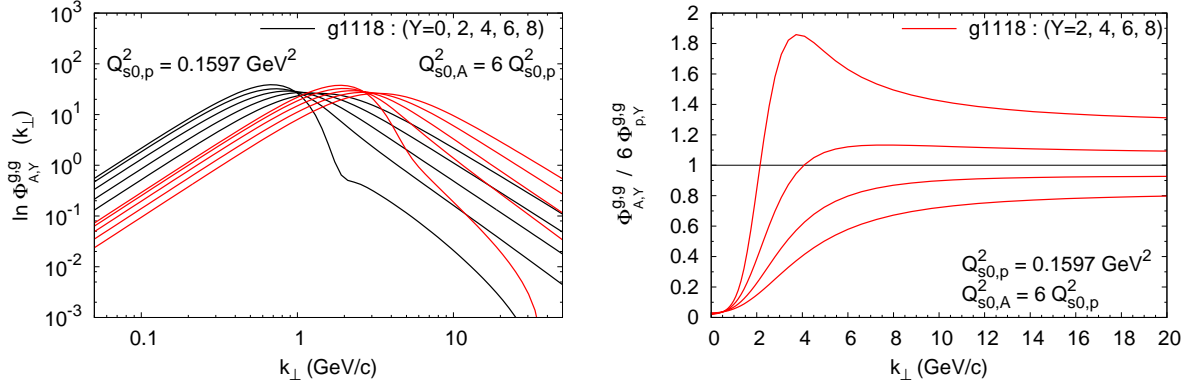


Figure 3.12: (Left) Two point function  $\phi_{A,Y}^{g,g}$  with respect to each initial saturation scale  $Q_{s0}^2$  and its evolution in rapidity  $Y = \ln(x_0/x)$  with  $x_0 = 0.01$ . Black solid lines correspond to the uGD in the proton with  $Q_{s0,p}^2 = 0.1597$  GeV<sup>2</sup> at  $Y = 0, 2, 4, 6, 8$ . The uGD in the nucleus is shown as red solid line with  $Q_{s0,A}^2 = 6 Q_{s0,p}^2$ . (Right) The ratio of uGD in the proton to the one in nucleus, which is defined by  $\phi_{pA}/(6\phi_{pp})$  at  $Y = 2, 4, 6, 8$ .

For a heavy nucleus  $A$ , the saturation scale at moderate values of  $x$  will be enhanced by a factor of the nuclear thickness  $T_A(\mathbf{b})$  at the impact parameter  $\mathbf{b}$ . However, as we limit our analysis to the minimum bias events, we assume a simpler relation

$$Q_{s,A}^2(x_0) = A^{1/3} Q_{s,p}^2(x_0) \quad (3.63)$$

which is the only information about the nucleus and embedded in the initial condition Eq. (3.61). We shall allow the saturation scale of the nucleus with  $A = 200$  in the range  $Q_{s,A}^2 = (4 - 6) \times Q_{s,p}^2$  at initial point  $x_0 = 0.01$ .

other hand, the distribution of the  $\rho$  for the proton is not necessarily gaussian. Then we could interpret  $\gamma \neq 1$  as meaning that it possibly results from higher order corrections of the gaussian distribution of the  $\rho$  [156]. We also comment that the infrared cutoff  $e_c$  dependence on the global data fitting is studied in Ref. [157]. When  $e_c$  becomes an additional fitting parameter, it is possible to find another best fit parameters set ( $\chi^2/d.o.f. \approx 1.1$ ) even though  $\gamma = 1$ . In any case, we should now understand that  $\gamma$  is just the parameter of the initial condition.



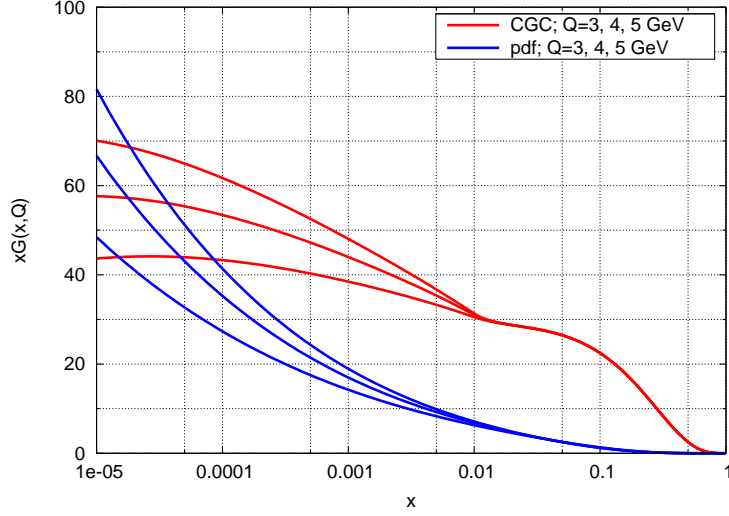


Figure 3.13: Collinear gluon distribution function as a function of  $x$  at each  $Q$ . (Blue line) CTEQ6LO parametrization [61], (Red line) The gluon distribution function in the CGC formula which is obtained by integrating Eq. (3.39) over the transverse momentum.

We show in Fig. 3.12 (Left) two point function  $\phi^{g,g} = \int_{\mathbf{k}_\perp} \phi^{q\bar{q},g}$ <sup>11</sup> with respect to each saturation scale for proton ( $Q_{s0,p}^2$ ) and nucleus ( $Q_{s0,A}^2$ ) and its evolution in rapidity  $Y = \ln(x_0/x)$ . Black solid lines correspond to the  $\phi^{g,g}$  with  $Q_{s0,p}^2 = 0.1597 \text{ GeV}^2$  at  $Y = 0, 2, 4, 6, 8$ . The  $\phi^{g,g}$  in the nucleus is shown as red solid line with  $Q_{s0,A}^2 = 6Q_{s0,p}^2$ . The peak value of the  $\phi^{g,g}$  determines the typical momentum scale  $Q_s$  of the gluon inside the hadron. One can immediately note that the quantum evolution modifies the gluon distribution and the peak of the  $\phi^{g,g}$  moves. For both the proton and the nucleus, the number of gluon at lower  $k_\perp$  is strongly suppressed due to the gluon merging, while more gluons are emitted at higher  $k_\perp$  by the BFKL cascade in  $x$  evolution. Taking a ratio of the  $\phi_{A,Y}^{g,g}$  in the nucleus to the  $\phi_{p,Y}^{g,g}$  in the proton times the effective thickness  $A^{1/3}$  (Fig. 3.12 (Right)), we can find the large suppression of the ratio at low  $k_\perp$  which means that the gluon density in the nucleus becomes totally harder compared with the one in the proton while the net number of gluon in the nucleus is much larger than that in the proton.

We note how to compute the multi point function at larger  $x > x_0$  in this paper. For  $x_0 \leq x \leq 1$ , we apply the following phenomenological Ansatz [67]:

$$\phi_{A,Y}^{q\bar{q},g}(\mathbf{l}_\perp, \mathbf{k}_\perp) = \phi_{A,Y_0}^{q\bar{q},g}(\mathbf{l}_\perp, \mathbf{k}_\perp) \left( \frac{1-x}{1-x_0} \right)^4 \left( \frac{x_0}{x} \right)^{0.15}, \quad (3.64)$$

<sup>11</sup>In fact, the dipole amplitude with parameter set g1118 has a negative value at high  $k_\perp$  region due to the non-gaussian initial condition.

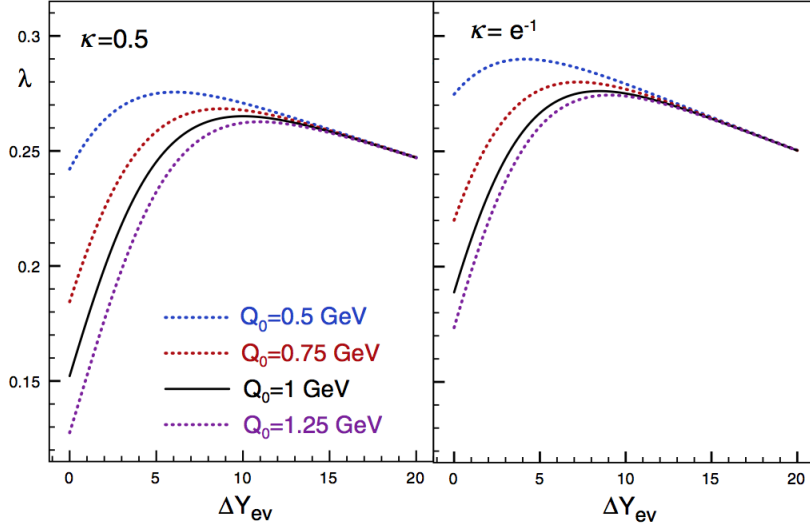


Figure 3.14: Evolution speed  $\lambda = d \ln Q_s^2(Y)/dY$  for each initial saturation scale  $Q_0 = 0.5, 0.75, 1.0$ , and  $1.25$  GeV. Left (Right) figure corresponds to the different matching condition to determine the saturation scale;  $\mathcal{N}_Y(r = 1/Q_s(Y)) = 0.5$  ( $e^{-1}$ ). Figure cited from Ref. [51].

where  $Y_0 \equiv \ln(1/x_0)$ . In this formula, the power 4 for the factor  $1 - x$  comes from the behavior at large  $x$  of the gluon distributions, as inferred from sum rules. Note that this extrapolation implies that the saturation scale is frozen at large  $x$ , which may lead to a harder  $k_\perp$ -spectrum for  $x > x_0$  than expected, possibly overestimating the Cronin peak. Here we note the difference between the collinear gluon distribution function obtained from Eq. (3.39) by performing the integral over the transverse momentum  $k_\perp$  and the CTEQ6LO parametrization [61] which is used in our numerical computations. The extrapolated gluon distribution with the Ansatz Eq. (3.64) is actually larger than the CTEQ6LO parametrized gluon distribution at  $x_0 \leq x \leq 1$ . This fact can provide the difference of the magnitude of the heavy quark pair production cross section between the CGC formula and the hybrid formula at forward rapidity.

Here we show the behavior of the saturation scale which is extracted from the rcBK equation, as is studied in Ref. [51]. Fig. 3.14 displays the speed of evolution  $\lambda \equiv d \ln Q_s^2(Y)/dY$  which is extracted from numerical solution of Eq. (2.30) with the evolution kernel Eq. (3.60). The initial forward scattering amplitude is given by  $\mathcal{N}_{Y=0}(r) = 1 - S_{Y=0}(r)$  where  $S_{Y=0}(r)$  is Eq. (3.61) and  $\gamma = 1$  and  $\Lambda = 0.2$  GeV. The saturation scale is determined by the condition  $\mathcal{N}_Y(r = 1/Q_s(Y)) = \kappa$  with  $\kappa = 0.5$  (Fig. 3.14 (left)) or  $e^{-1}$  (Fig. 3.14 (right)) for each different initial condition  $Q_{s0} = 0.5, 0.75, 1.0$ , and  $1.25$

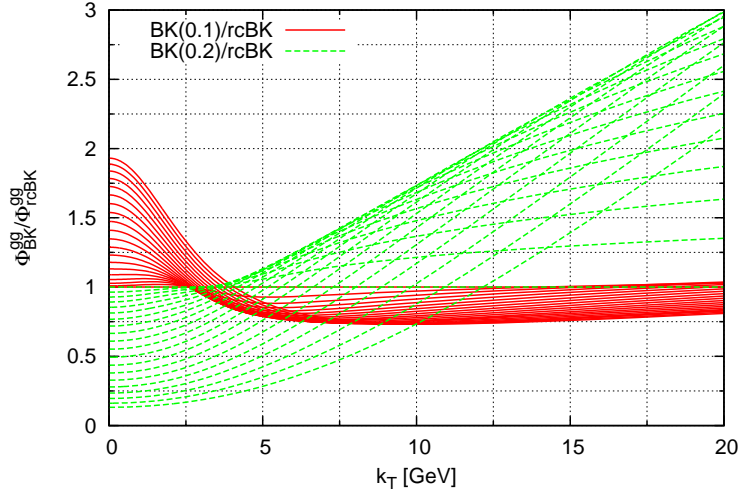


Figure 3.15: The ratio of  $\phi^{g,g}$  which is obtained by using fixed coupling BK equation to the one which is obtained by using rcBK equation as a function of  $k_{\perp}$  at each rapidity  $Y = \ln(x_0/x)$ . The ratio is unity at the start point of the  $x$ -evolution  $Y = 0$ . The red solid (dashed green) lines are the ratio by using fixed BK equation with  $\alpha_s = 0.1$  (0.2). The initial condition for both the fixed coupling BK equation and the rcBK equation is set MV model.

GeV. At  $\Delta Y \sim 0$ , the  $\lambda$  strongly depends on the initial condition while at larger  $\Delta Y$  the  $\lambda$  for different initial condition gets close to the same value and the initial condition dependence of the  $\lambda$  disappears. We can find that the  $\lambda$  at larger  $Y$ , which is determined by the rcBK equation whether the matching condition is  $\kappa = 0.5$  or  $e^{-1}$ , is compatible with approximately  $\lambda = 0.288$  which is constrained by global fitting of HERA data [30].

In this paper, we adopt the rcBK equation to include the quantum evolution effect in the heavy quark pair production cross section and we remark here about a difference between the  $\phi^{g,g}$  with the rcBK equation and the one which is obtained by use of the leading order BK equation with fixed coupling kernel. Fig. 3.15 displays that a ratio of the  $\phi^{g,g}$  which is computed with the rcBK equation to the one which is computed with the leading order BK equation as a function of  $k_{\perp}$  at each rapidity  $Y = \ln(x_0/x)$ . The solid red (dashed green) lines correspond to the results which is obtained by using  $\alpha_s = 0.1$  (0.2) in the leading order BK equation. As the rapidity increases, the ratio with the leading order BK equation with  $\alpha_s = 0.2$  deviates from unity both at lower and higher  $k_{\perp}$  while the one with  $\alpha_s = 0.1$  deviates from unity only at lower  $k_{\perp}$ . This fact indicates that the  $x$ -evolution of the  $\phi^{g,g}$  with the leading order BK equation with  $\alpha_s = 0.2$  is too fast at larger  $k_{\perp}$  and we need to fix  $\alpha_s = 0.1$  in the leading order BK equation to reproduce

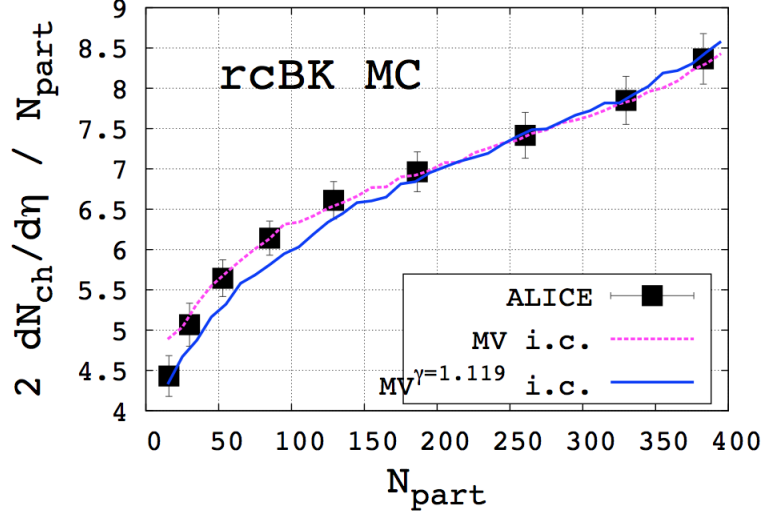


Figure 3.16: Centrality dependence of charged particles multiplicity at mid rapidity in Pb+Pb collisions at  $\sqrt{s} = 2.76$  TeV which is computed by using the rcBK equation in Ref. [56].  $\eta$  is a pseudo rapidity and  $N_{\text{part}}$  is a number of Dotted (Solid) line is the result with MV (MV $^{\gamma}$ ) model as the initial condition in the rcBK equation Figure cited from Ref. [56].

reasonably the evolution speed which is obtained by the rcBK equation at larger  $k_{\perp}$ . As long as we use the rcBK equation with the suitable running coupling constant, we can reproduce automatically the  $x$ -evolution speed extracted from the data fitting.

As is mentioned above, the saturation scale characterizes not only light hadron production and also the heavy quark production, particularly in high energy collisions at forward rapidity. Concerning the light hadron production, there is already the previous work to compute charged particles multiplicity by using the rcBK equation ([56]). Then although we will show a results of the heavy quark pair production in this paper, we finally present the result of the multiplicity of charged particle which is computed by use of the rcBK equation in Ref. ([56])<sup>12</sup>. In Fig. 3.16, we show the charged particle multiplicity at mid rapidity for Pb+Pb collisions at the LHC  $\sqrt{s} = 2.76$  TeV by use of the unintegrated

<sup>12</sup>In Ref. [56], the number of gluons produced at a transverse position  $\mathbf{R}$  in the Pb-Pb collisions is computed in  $k_{\perp}$ -factorization formula;

$$\frac{dN_g}{dy d^2 p_{\perp} d^2 R} \propto \frac{1}{\sigma} \frac{\alpha_s(Q)}{p_{\perp}^2} \varphi\left(\frac{|p_{\perp} + k_{\perp}|}{2}, x_1; b\right) \otimes \varphi\left(\frac{|p_{\perp} - k_{\perp}|}{2}, x_2; R - b\right) \quad (3.65)$$

where  $\sigma$  is the effective inelastic interaction area in Pb-Pb collisions and  $p_{\perp}$  is the transverse momentum of the produced gluon with the rapidity  $y$  and  $\frac{|p_{\perp} + k_{\perp}|}{2}$  ( $\frac{|p_{\perp} - k_{\perp}|}{2}$ ) is the transverse momentum of the gluon with  $x_{1,2} = p_{\perp}/\sqrt{s}e^{\pm y}$  coming from the projectile (target) nucleus.  $Q$  is a scale of the running

gluon distribution with the rcBK equation and by assuming that the produced gluon is the dominant source of the charged particle. As to the initial condition for the rcBK equation, both MV model and  $MV^\gamma$  model with  $\gamma = 1.119$  are used in the computations of charged particles multiplicity for comparison. We should note that no hot matter effect is considered. Nevertheless, it seems that the theoretical results has been successful in describing the data at ALICE whether the initial condition of the rcBK equation is MV model or  $MV^\gamma$  model. Then, we expect the use of the rcBK equation might also provide a good possibility to describe the heavy quark pair production.

---

coupling and the unintegrated gluon distribution  $\varphi$  is given by

$$\varphi(k, x; b) \propto \int d^2\mathbf{r} e^{-i\mathbf{k}\cdot\mathbf{r}} \nabla_{\mathbf{r}}^2 N_Y(r, b). \quad (3.66)$$

where  $N_Y(r, b)$  is the dipole amplitude and depends on the transverse coordinate  $b$  through the saturation scale  $Q_{s0,A}^2(b) = N(\mathbf{b})Q_{s0,p}^2$  in the initial condition of the dipole amplitude.  $N(\mathbf{b})$  is the number of nucleons overlap at  $\mathbf{b}$  from the two nucleus.

# Chapter 4

## Quarkonium production in Color Evaporation Model

In this chapter, we show the numerical results of quarkonium production from the CGC in the Color Evaporation Model. In particular, transverse momentum spectrum and nuclear modification factor are presented. For the gluons in the proton, we examine two possible descriptions, unintegrated gluon distribution and ordinary collinear gluon distribution.

### 4.1 Factorization assumption

In the high energy collisions at RHIC and the LHC, a production time of the heavy quark pair in the lab frame  $t_p$  is determined by the mass  $m$ , the transverse momentum  $P_\perp$  and the rapidity  $y$ . For example,  $t_p$  of the charm quark pair is given by about  $1/m_c \sim 0.1$  fm and the charmonium formation time  $t_f$  is given by about  $1/m_c v^2 \sim 0.5$  fm in the charm pair rest frame. Here we have assumed that the binding energy of the charmonium  $E_B \sim m_c v^2$  is about 0.5 GeV. These times are strongly retarded by the Lorentz boost in the forward rapidity region as follows

$$t_p \sim \frac{1}{m_c} \xrightarrow{\text{Boost}} \frac{1}{m_c} \frac{M_\perp}{M} \cosh y, \quad (4.1)$$

$$t_f \sim \frac{1}{m_c v^2} \xrightarrow{\text{Boost}} \frac{1}{m_c v^2} \frac{M_\perp}{M} \cosh y. \quad (4.2)$$

Here the  $M \sim 2m_c$  is an invariant mass of the pair with small relative momentum between the quark and the antiquark in the rest frame and  $M_\perp = \sqrt{M^2 + P_\perp^2}$ . The passing time of the heavy quark pair through the Lorentz contracted nucleus  $t_0$  is estimated as

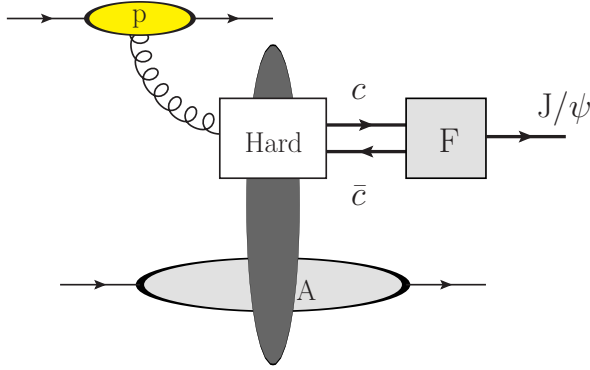


Figure 4.1:  $J/\psi$  production process in pA collisions. The charm quark pair is created in the hard process (white box) and interacts with the nucleus (dark grey oval). At very forward rapidity, the  $J/\psi$  is produced far away from the nucleus (the symbol F inside grey box).

$2R_A/\gamma \sim 0.1 - 0.01$  fm at RHIC and the LHC respectively. Then if the retarded quark pair creation time is large than  $t_0$ , the heavy quark pair creation is affected by the nucleus coherently. Furthermore if  $t_f \gg t_p$ , we can regard the hadronization of the heavy quark pair is almost frozen when the quark pair passes through the nucleus. In that case, the quarkonium is produced far away from the nucleus and a dynamics of the quarkonium production is not related to the nuclear effect.

In our model at leading order in coupling constant, the quarkonium is produced in the collisions of two gluons which are coming from proton and nucleus. Then the quarkonium transverse momentum is almost determined by the saturation scale of the gluon in the nucleus which becomes larger at forward rapidity. Namely, from Eqs. (4.1)(4.2), the order  $t_f \gg t_p \gg t_0$  can be valid at very forward rapidity in the lab frame and the factorization between the heavy quark pair production and the quarkonium formation becomes a feasible assumption (Fig. 4.1).

## 4.2 Expression of production cross section

Quarkonium production in the CEM is straightforward. For instance,  $J/\psi$  production cross section reads

$$\frac{d\sigma_{J/\psi}}{d^2\mathbf{P}_\perp dy} = F_{J/\psi} \int_{4m_c^2}^{4M_D^2} dM^2 \frac{d\sigma_{c\bar{c}}}{d^2\mathbf{P}_\perp dM^2 dy}, \quad (4.3)$$

where  $m_c$  ( $M_D$ ) is the charm quark ( $D$  meson) mass. This expression is obtained by using Eq. (3.44) with change of variables. A phenomenological constant  $F_{J/\psi}$  represents the non-perturbative transition rate for the charm pairs, produced in the invariant mass range  $M \in [2m_c, 2M_D]$ , to be bound into a quarkonium. In this model, we do not include a bottom quark decay contribution to the  $J/\psi$  and also a higher state feed down contribution. We should understand Eq. (4.3) as the inclusive production. For  $\Upsilon(1S)$  production, the expression of production cross section is the same as  $J/\psi$  except that we should use the different non-perturbative probability  $F_\Upsilon(1S)$ .

A remark is here in order. In the multiplicity of the quark pair production (3.49), the inelastic cross section which estimated as  $\pi R_A^2$  in the denominator in Eq. 3.49 effectively cancels out with the same factor in  $\phi_{A,y}^{q\bar{q},g}$ , and the cross section is proportional to the effective transverse area  $\pi R_p^2$  of the proton appearing in  $\varphi_{p,y}$ . In the following calculations, we choose the proton size  $R_p = 0.9$  fm for heavy meson and quarkonium production. We also cancel  $\alpha_s^2$  in front of the cross section by  $\alpha_s$  appearing in the denominator in  $\phi_{A,y}$  and in  $\varphi_{p,y}$ . In the case of collinear approximation on the proton side, we set  $\alpha_s = 0.2$  in this paper. The proton uGD  $\varphi_{p,y}$  may be estimated by replacing the transverse area  $R_A^2$  and the amplitude  $S_Y$  with those for the proton in the two point function  $\phi_{A,Y}^{g,g} = \int_{\mathbf{k}_\perp} \phi_{A,Y}^{q\bar{q},g}$

<sup>1</sup>.

### 4.3 $x_{1,2}$ coverage

In Fig. 4.2, we show the  $x_{1,2}$  coverage of the charm pair production in the plane of the rapidity  $y$  and the transverse momentum  $P_\perp$  of the pair at RHIC and LHC energies;  $\sqrt{s}=200$  GeV and 5.02 TeV. Here we fix the charm pair's invariant mass  $M = 3.1$  GeV, and draw the curves determined by  $x_{1,2} = e^{\pm y}(\sqrt{P_\perp^2 + M^2}/\sqrt{s})$ , on which either  $x_1$  or  $x_2$  is constant. The kinematically disallowed region where  $x_{1,2} > 1$  is indicated by the shaded grey area. We see that, at the RHIC energy,  $J/\psi$  is produced from the gluons of moderate  $x_{1,2} \sim 0.01 - 0.05$  at mid-rapidities, while at forward rapidities  $y \sim 2$  the process gets sensitivity to the gluons at small  $x_2 < 0.01$ . On the other hand, at the LHC energy,  $J/\psi$  production is already sensitive to the small  $x_2$  gluon even at mid-rapidity, and at forward rapidity it probes  $x_2$  as low as  $\sim 10^{-4}$  to  $10^{-5}$ .

However, one must take account that in the small  $x_2$  region but  $J/\psi$  has large  $P_\perp$ ,

---

<sup>1</sup>In this paper, we always compute the heavy quark pair production cross section by using  $\phi_{p,Y}^{g,g}$  in the proton side.



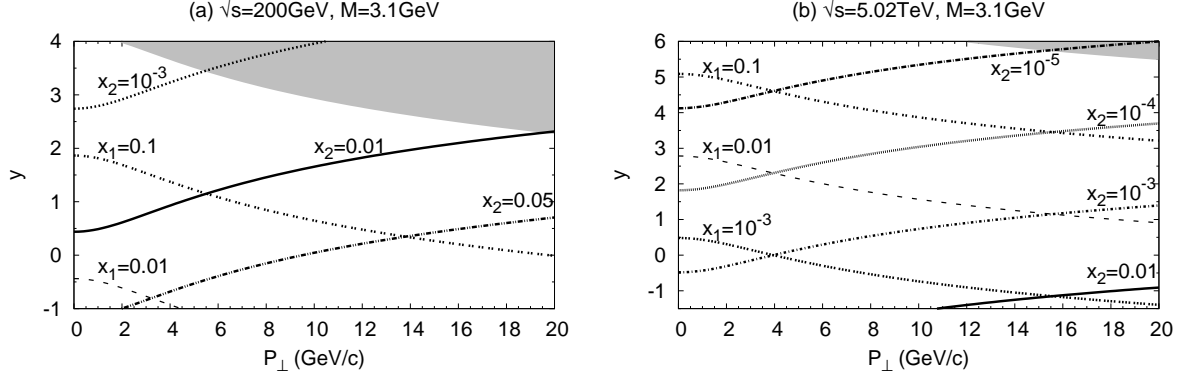


Figure 4.2: Kinematical coverage of the pair production in the plane of rapidity  $y$  and transverse momentum  $P_{\perp}$  for invariant mass  $M = 3.1$  GeV at (a)  $\sqrt{s} = 200$  GeV and (b)  $\sqrt{s} = 5.02$  TeV. Shown are the curves of constant  $x_{1,2} = (\sqrt{P_{\perp}^2 + M^2}/\sqrt{s})e^{\pm y}$ . The shade region is kinematically forbidden.

the gluon with large  $k_{1\perp}$  in the proton can participate in the production of  $J/\psi$ , which reduces the saturation effect.

Thus one can find that the heavy quark production, which may be evaluated with perturbation method, can be used to probe the small- $x$  dynamics by studying the open heavy flavor production and also the quarkonium production at lower transverse momentum in the forward rapidity region at the LHC.

## 4.4 Transverse momentum spectrum of $J/\psi$

In this section, we estimate the quarkonium production from the quark-pair production cross section in the CEM (Eq. 4.3). We choose the  $J/\psi$  formation fraction  $F_{J/\psi} = 0.02$  as representative values. One should keep in mind that the absolute normalization of the cross section depends on these parameters. In addition, the framework in our calculations is valid in the small- $x$  region and the transverse momentum  $P_{\perp}$  corresponds to about the saturation scale of the gluon coming from the nucleus. Then the reader should focus on the spectrum of  $J/\psi$  productions at lower  $P_{\perp}$  up to about the saturation scale in the nucleus which is here approximately estimated as  $Q_{sA}^2(x) \sim 0.2 A^{1/3} \left(\frac{0.01}{x}\right)^{0.3} \text{ GeV}^2$  or a few times higher than it.

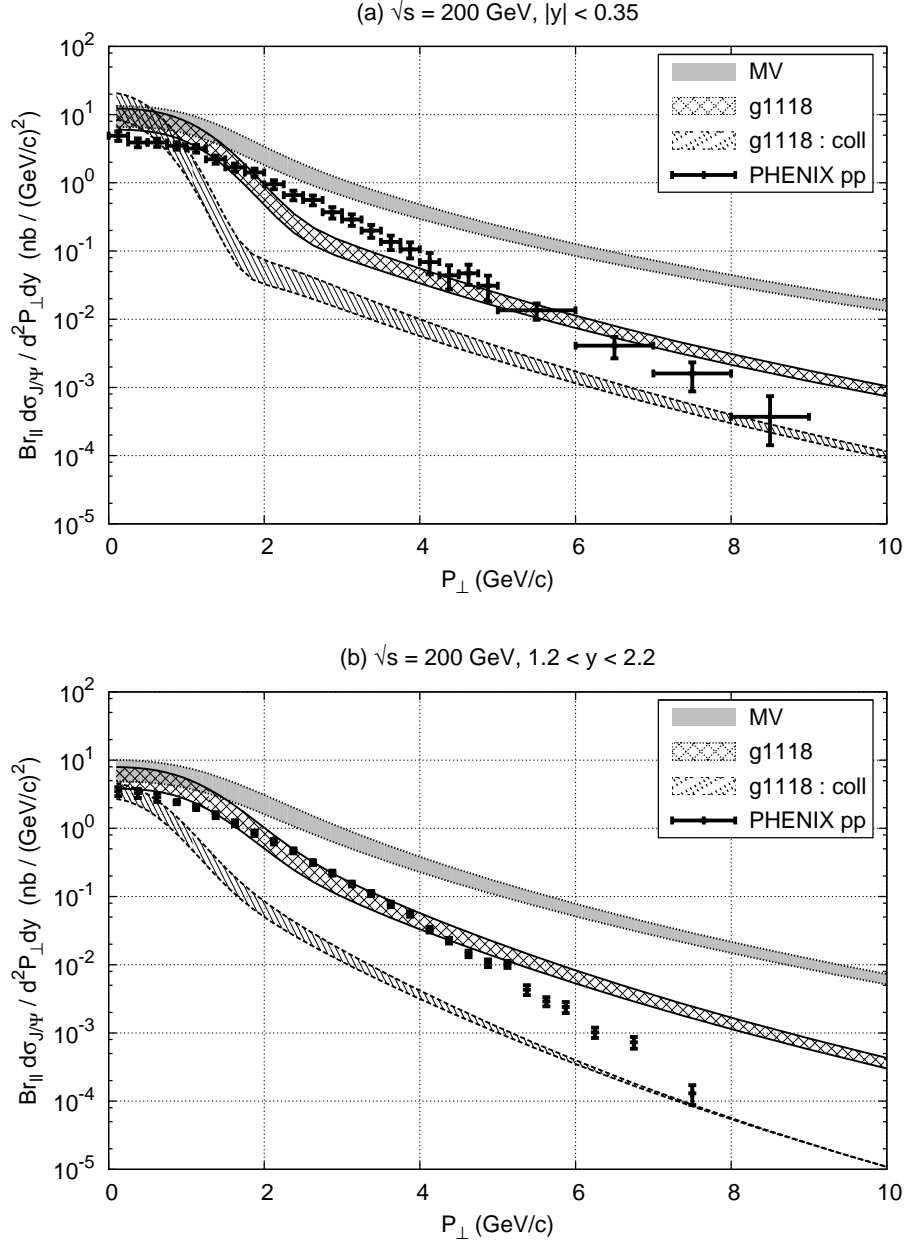


Figure 4.3: Transverse momentum spectrum of  $J/\psi$  in di-lepton channel in pp collisions at  $\sqrt{s} = 200$  GeV for rapidity ranges (a)  $|y| < 0.35$  and (b)  $1.2 < y < 2.2$ .  $Br_{ll}$  is a branching ratio of the  $J/\psi$  decay into di-lepton channel;  $Br_{ll} = 0.0594$  for  $e^+e^-$  at mid rapidity and  $Br_{ll} = 0.0593$  for  $\mu^+\mu^-$  at forward rapidity. CEM model results using the pair production (3.44) with sets MV and g1118 are shown in gray and doubly-hatched bands, respectively, and the result using collinear approximation (3.56) with set g1118 is in hatched band. The upper (lower) curve of the band corresponds to the result with  $m_c = 1.2$  (1.5) GeV, and the scale of pdf is chosen at  $2M_\perp$  ( $M_\perp/2$ ) in the collinear approximation. Data from [110].

#### 4.4.1 RHIC

We first show in Fig. 4.3 the transverse momentum spectrum of the produced  $J/\psi$  in pp collisions at  $\sqrt{s} = 200$  GeV, using the uGD set g1118 given in Table 3.1. The upper (lower) curve of each band indicates the result with charm quark mass  $m_c = 1.2$  (1.5) GeV. In the collinear approximation on the larger- $x_1$  side, we adopt CTEQ6LO parametrization [61], and the band in Fig. 4.3 includes the change of the factorization scale from  $2M_\perp$  to  $M_\perp/2$  with  $M_\perp = \sqrt{M^2 + P_\perp^2}$ , where  $M$  is the pair's invariant mass. Here we note that no  $K$ -factor have been included in our computations which means we set  $K = 1$ . We just compare the results in  $k_\perp$ -factorization like formalism to that in the hybrid formalism in this paper. This fact is the same for the results in pA collisions.

As mentioned above, the quarkonium production at mid-rapidity  $|y| < 0.35$  is largely determined by the gluon distributions at moderate  $x_{1,2} \gtrsim 0.01$ . Then, we notice a difficulty with set g1118: the peculiar dip structure of g1118 seen in Fig. 3.12 remains in the  $J/\psi$  spectrum as a similar dip around  $P_\perp \sim 2$  GeV, which must be an artifact of this initial condition. In contrast, we don't see such a structure with the MV initial condition. At forward-rapidity  $1.2 < y < 2.2$ , the dip is smeared to be less noticeable by the imbalance between  $x_1$  and  $x_2$  and by the  $x_2$  evolution of the uGD. As a whole, the  $P_\perp$  spectrum obtained with set g1118 is closer to the observed data [110] than with set MV. In this pp case, the collinear approximation on the large- $x_1$  side does not improve the description of the data. The  $k_\perp$  kick from only the one of the protons cannot give enough  $P_\perp$  for the pair.

In Fig. 4.4 shown is the transverse momentum spectrum of the  $J/\psi$  in pA collisions in our model. We set the initial saturation scale of the uGD for the heavy nucleus as  $Q_{s0,A}^2(x = x_0) = 6Q_{s0,p}^2$ . The upper (lower) curve of the bands indicate the result with  $m_c = 1.2$  (1.5) GeV. We overlay d-Au data observed by PHENIX at  $\sqrt{s} = 200$  GeV [107], presuming here that the difference between pA and dA results only in normalization difference of order  $O(1)$ <sup>2</sup>. We find that  $P_\perp$ -dependence of  $J/\psi$  production is better described with set g1118<sup>3</sup> than that with set MV. Indeed, here the collinear approximation on the proton side gives a better description of the data both at mid- and forward-rapidity regions. At forward rapidities, where we are approaching the small- $x_2$  region and the kinematical boundary for  $x_1$  at the same time (see Fig. 5.1), we expect a nontrivial

<sup>2</sup>Recall that our model already has an uncertainty of  $O(1)$  in the normalization of the uGD.

<sup>3</sup>Possible dip structure from the proton uGD is smeared out here in Fig. 4.4 by the multiple scattering effects in the nuclear uGD.

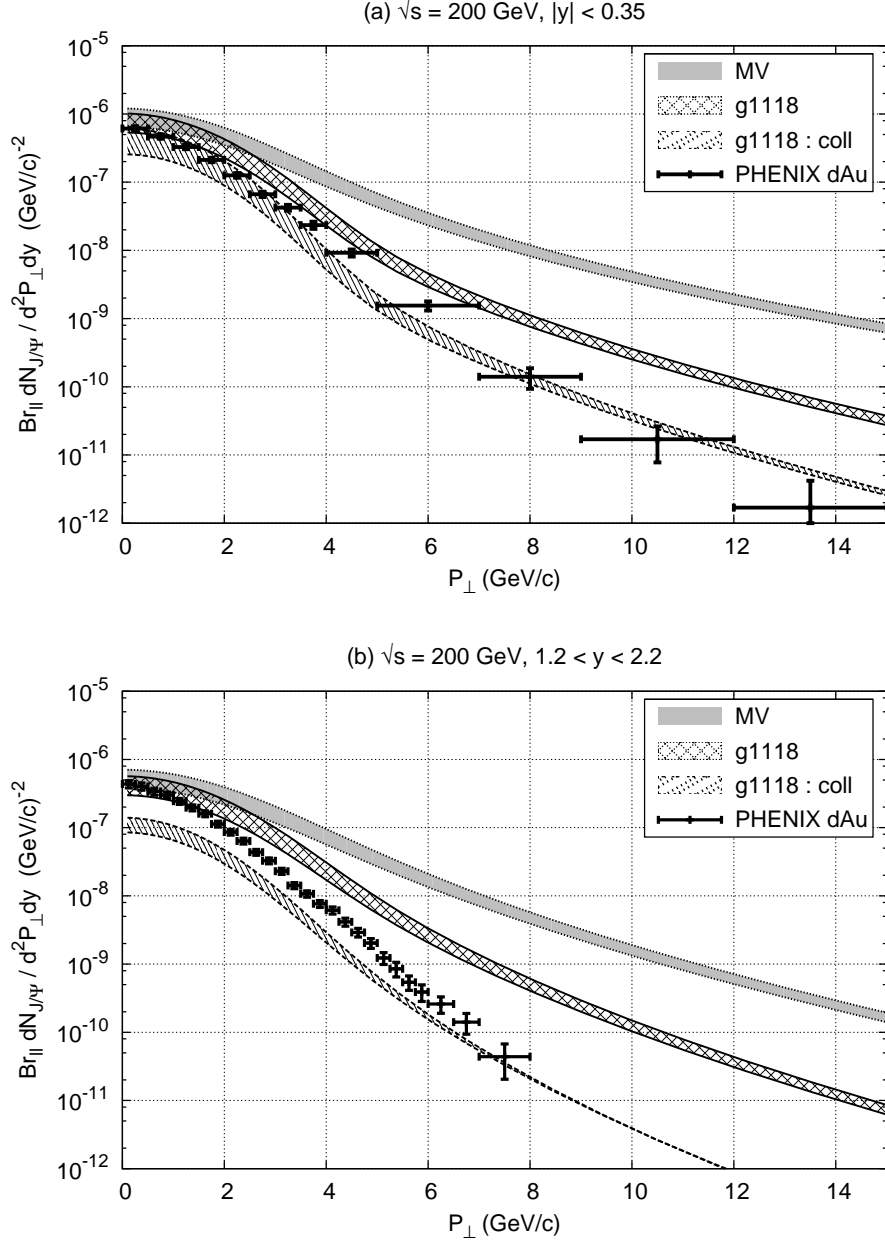


Figure 4.4: Transverse momentum spectrum of  $J/\psi$  in di-lepton channel in pA collisions at  $\sqrt{s} = 200$  GeV for rapidity ranges (a)  $|y| < 0.35$  and (b)  $1.2 < y < 2.2$ . Notations are the same as in Fig. 4.3. Data in d+Au collisions [107] are overlaid for comparison.

interplay between large  $x_1$  and small  $x_2$ . Besides the saturation dynamics of  $x_2$  gluons, one may need to consider energy loss of large- $x_1$  gluons in the heavy target [17] in order to understand the  $P_\perp$  spectrum of  $J/\psi$  in the very forward region. These effects are not included in our present treatment.

We notice in Fig. 4.4 (b) that the  $J/\psi$  production is more suppressed nearly by one order of magnitude in the collinear approximation than those in the full calculation. This is caused by a difference in the large  $x_1$  behavior of gluon distributions on the proton side. As  $x \rightarrow 1$ , the CTEQ gluon distribution decreases much more rapidly than our model uGD  $\varphi_{p,y}$ , which is assumed to behave as  $\propto (1-x)^4$ . Furthermore, in the collinear approximation, the pair's  $P_\perp$  is solely provided from the nucleus side,  $P_\perp = k_2$ , and uGD  $\phi_{A,y}$  for the heavy target is more suppressed at low  $k_2$  by multiple scatterings.

Now let us take a ratio of the cross section of  $J/\psi$  in pA collisions to that in pp collisions, which is called nuclear modification factor  $R_{pA}$ . We expect that model uncertainties cancel out to some extent in the ratio. We define  $R_{pA}$  for  $J/\psi$  in our model as

$$R_{pA} = \frac{dN_{J/\psi}/d^2P_\perp dy|_{pA}}{N_{\text{coll}} dN_{J/\psi}/d^2P_\perp dy|_{pp}}, \quad (4.4)$$

where  $dN_{J/\psi}/d^2P_\perp dy$  is the average multiplicity of  $J/\psi$  per event. Here we set the number of nucleon-nucleon collisions in pA to  $N_{\text{coll}} = A^{\gamma/3}$  as stated in the heavy meson case.

In Fig. 4.5 we compare the model results for  $R_{pA}$  at  $\sqrt{s} = 200$  GeV with the data of  $R_{dAu}$ . Note that the projectile is different between the model calculation and the data. The notations are the same as in Fig. 4.3. We stress here that  $R_{pA}$  is indeed little dependent on the choice of the quark mass and factorization scale. Unfortunately, however, one immediately recognizes an unphysically strong Cronin peak in the model calculations with set g1118 both at mid- and forward rapidities, which is obviously caused by the dip seen in the pp collisions (Fig. 4.3). In contrast, the  $R_{pA}$  result with set MV looks more reasonable; we see a moderate Cronin peak at mid-rapidity due to the multiple scatterings, while it almost disappears at forward rapidity  $y \sim 2$  by the  $x_2$  evolution. In low- $P_\perp$  region, we also notice a stronger suppression than the experimental data. This would imply the importance of the fragmentation process in the formation of  $J/\psi$ , which is missing in the simple CEM treatment.

To summarize the results at RHIC energy, the  $J/\psi$  production spectrum is sensitive to the moderate value of  $x_{1,2}$ , where the initial condition for the  $x$ -evolution is set. We have a difficulty to describe the pp data and therefore the ratio  $R_{pA}$  with the constrained uGD

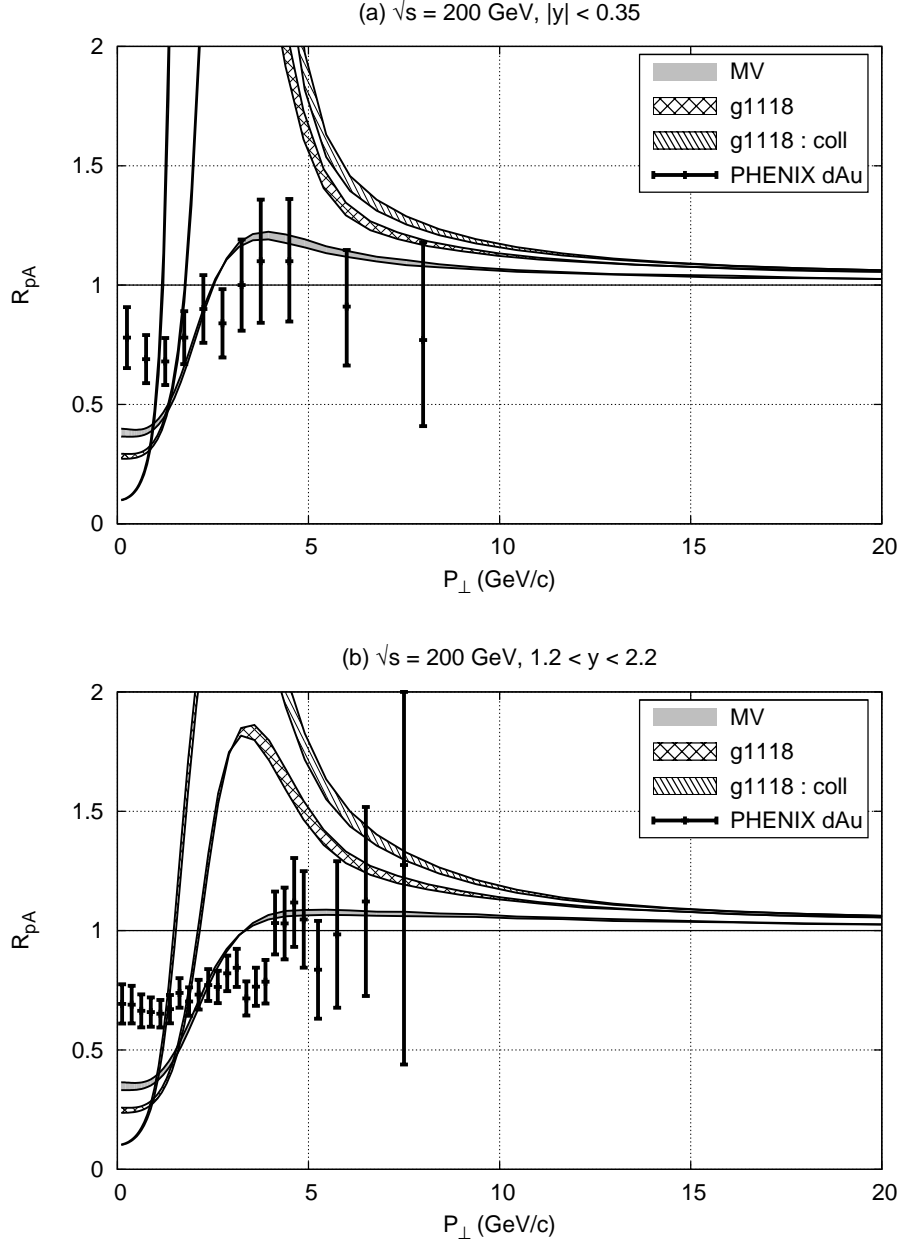


Figure 4.5: The ratio of  $J/\psi$  productions in pA and pp collisions  $R_{pA}(P_{\perp})$  at  $\sqrt{s} = 200$  GeV for (a)  $|y| < 0.35$  and (b)  $1.2 < y < 2.2$ . The results with uGD sets MV and g1118 are shown in gray and doubly-hatched bands, respectively, and the result in collinear approximation with set g1118 is shown in a hatched band. Notations are the same as in Fig. 4.3. Data of  $R_{dAu}$  taken from [107].

g1118. In contrast the set MV gives more reasonable behavior for  $R_{pA}$ . The  $P_\perp$  spectrum in pA collisions is better described with set g1118 at mid- and forward-rapidities. In forward rapidity,  $P_\perp$  slope is still steeper in the data than in the model, hinting a possible energy loss of the large- $x_1$  gluon from the proton. Actually  $R_{dA}$  of  $J/\psi$  at RHIC energy has been studied in several approaches (e.g.) with introducing nuclear parton distribution and nuclear absorption effects to a  $J/\psi$  production model for pp [147,148], or with taking account of the multiple scatterings and energy loss of the projectile gluons [17,18].

#### 4.4.2 LHC

Now we compute the  $J/\psi$  production at the LHC energy, where we expect that the wider  $x_2$ -evolution of uGD on the nucleus side will manifest in the production spectrum. In fact, both  $x_{1,2}$  are small ( $\sim 10^{-3} < x_0$ ) already in mid-rapidity production of the charm pair as seen in Fig. 5.1, and as moving to larger rapidities we can probe smaller values of  $x_2$  on the nucleus side down to  $x_2 \sim 10^{-5}$ .

We show in Fig. 4.6 the  $J/\psi$  cross section in pp collision at  $\sqrt{s} = 7$  TeV, obtained in CEM from charm quark spectrum (3.44). Notations are same as in the case of the RHIC energy. In order to assess the uncertainty, we again vary the charm quark mass from  $m_c = 1.2$  to 1.5 GeV, and change in the collinear approximation the factorization scale from  $2M_\perp$  to  $M_\perp/2$ . The observed data [113] is fairly well reproduced with set g1118 in this  $P_\perp$  region both at  $|y| < 0.9$  and  $2.5 < y < 4$ , indicating that  $y$ -dependence is appropriately captured by  $x$  evolution of uGD. The  $P_\perp$  slope in the collinear approximation (3.56) with set g1118 seems to be slightly off the data, while the full result with set MV gives harder  $P_\perp$  spectrum. The situation is expected to be similar in pp collisions at  $\sqrt{s} = 5.02$  TeV.

Results in pA collisions at  $\sqrt{s} = 5.02$  TeV are plotted at mid- and forward-rapidities in Fig. 4.7. The MV initial condition gives a harder spectrum of  $J/\psi$  than g1118. But the  $P_\perp$  slope is almost the same at  $P_\perp \gtrsim 10$  GeV, hinting the BFKL tail of uGD generated during the evolution. Compared to the case at  $\sqrt{s} = 200$  GeV, the collinear approximation (with set g1118) results in the spectral shape rather similar to the full result at this energy  $\sqrt{s} = 5.02$  TeV, where the collinear approximation on the proton side would be more appropriate since the saturation scale of the nucleus is much larger than that of the proton:  $Q_{s,A}^2(x_2) \gg Q_{s,p}^2(x_1)$ , especially in the forward region.

In Fig. 4.8, we show the results of  $J/\psi$  cross section in pA collisions with set g1118 in the forward rapidity region ( $1.5 < y < 4$ ) at the LHC, and put recent data [109] on our results. The upper (lower) curve of the band is corresponds to the result with

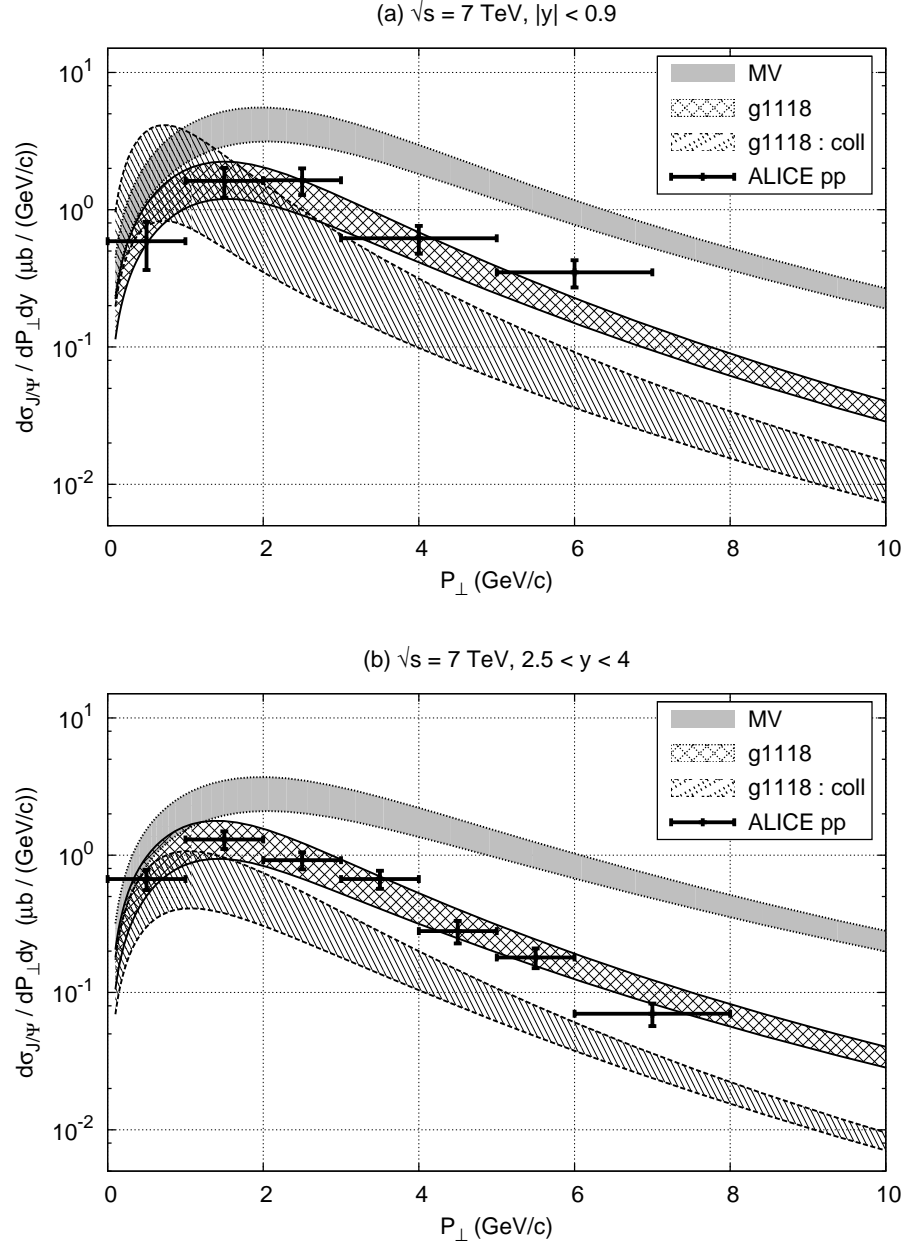


Figure 4.6: Differential  $J/\psi$  yield in pp collisions at  $\sqrt{s} = 7 \text{ TeV}$  for (a)  $|y| < 0.9$  and (b)  $2.5 < y < 4$ . Notations are the same as in Fig. 4.3. Data from [113].



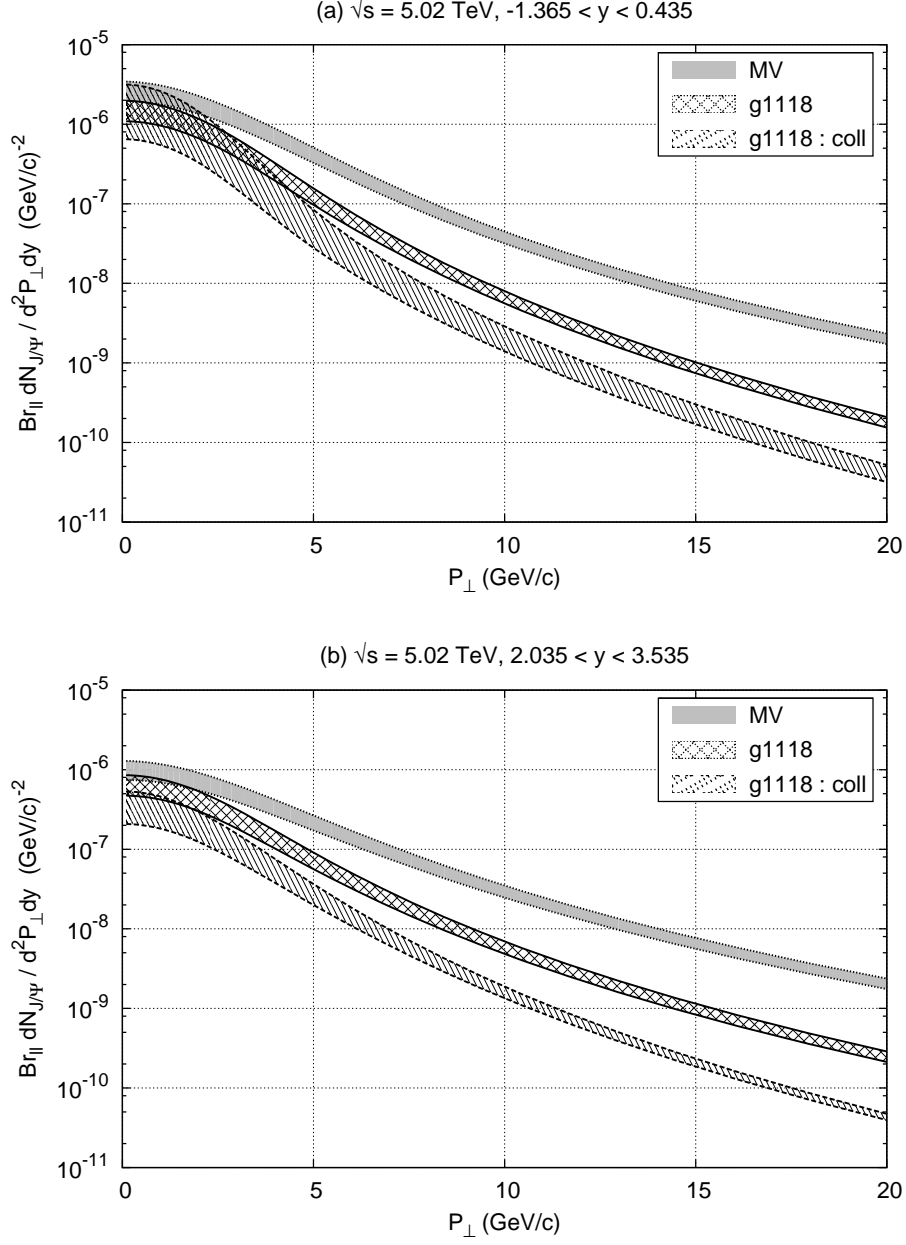


Figure 4.7: Transverse momentum spectrum of  $J/\psi$  in di-lepton channel in pA collisions at  $\sqrt{s} = 5.02 \text{ TeV}$  for (a)  $-1.4 < |y| < 0.4$  and (b)  $2 < y < 3.5$ . Notations are the same as in Fig. 4.3.

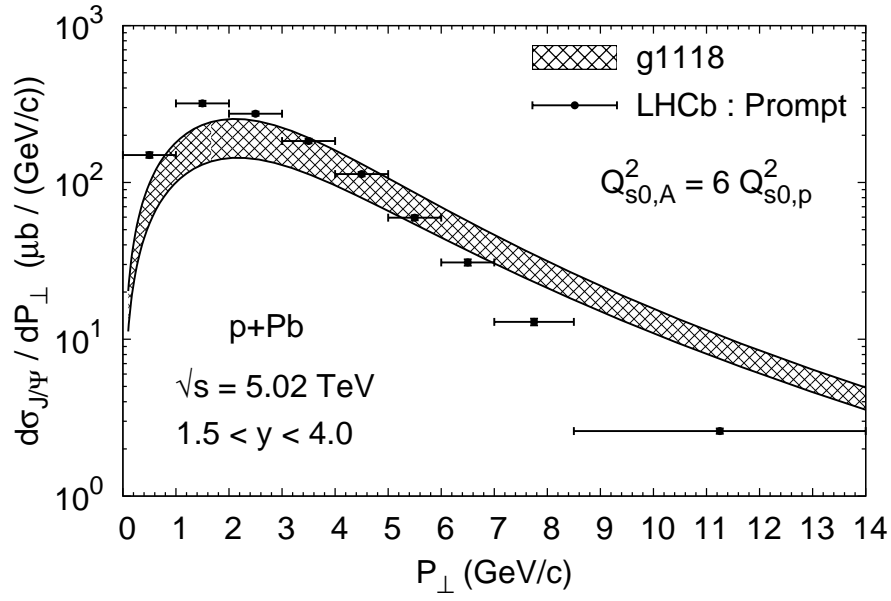


Figure 4.8: Transverse momentum spectrum of  $J/\psi$  production cross section in pA collisions at  $\sqrt{s} = 5.02$  TeV for  $1.5 < y < 4.0$  with set g1118 which shown in doubly-hatched band. The upper (lower) curve of the band is corresponds to the result with  $m_c = 1.2(1.5)$  GeV and  $Q_{sA}^2 = 6Q_{sp}^2$ . We choose the nuclear radius as  $R_A = 6R_p$ . Data from [109].

$m_c = 1.2(1.5)$  GeV and  $Q_{sA}^2 = 6Q_{sp}^2$ . We choose the nuclear radius as  $R_A = 6R_p$ . Our result seems to be reasonable at low- $P_\perp$  while harder than data in the high- $P_\perp$  region. We can expect the collinear approximation on the proton side provides more reasonable  $P_\perp$  slope at forward rapidity. As stated above, one should keep in mind that the absolute normalization of the cross section depends on  $R_A$ ,  $Q_s^2$ , and  $m_c$  and so on.

We show in Fig. 4.9 the ratio  $R_{pA}$  of  $J/\psi$  as a function of  $P_\perp$  at  $\sqrt{s} = 5.02$  TeV. We have assumed  $N_{\text{coll}} = A^{\gamma/3}$  as mentioned before. We find that each band almost collapses into a single line, which means that the ratio  $R_{pA}$  is insensitive to the variation of the charm quark mass (and the factorization scale in the collinear approximation) within the range considered here.

At mid-rapidities (Fig. 4.9 (a)), we see that the ratio  $R_{pA}$  of  $J/\psi$  production is suppressed at low  $P_\perp$ , while it approaches unity at higher  $P_\perp$  for both sets of g1118 and MV. In the collinear approximation on the proton side,  $R_{pA}$  shows a Cronin-like peak around  $P_\perp \sim 4$  GeV and remains larger than unity at larger  $P_\perp$ , which largely reflects  $R_{pA}$  of  $\phi_{A,y}$  at the gluon level. At forward rapidities (Fig. 4.9 (b)), however, this difference due to different uGD sets and approximations becomes much weaker to yield a systematic suppression for all three cases <sup>4</sup>.

We examine the initial-scale ( $Q_{s0,A}^2$ ) dependence of the ratio  $R_{pA}$  in Fig. 4.10, by plotting the results with the saturation scale  $Q_{s0,A}^2 = 4Q_{s0,p}^2$  (upper) and  $6Q_{s0,p}^2$  (lower) in Eq. (3.61) at  $x = x_0$ . It is found that the  $Q_{s0,A}^2$  dependence of  $R_{pA}$  is relatively weak within the range. At low  $P_\perp$  we have strong suppression, but one should keep in mind that this suppression may be filled to some extent by the nonperturbative fragmentation of  $J/\psi$ , as is seen in the RHIC case in Fig. 4.5.

To summarize the result at LHC energy, We can probe a wide  $x_2$ -evolution of the uGD  $\phi_{A,y_2}(\mathbf{k}_2)$  through the  $J/\psi$  production, and the ratio  $R_{pA}$  will be a good indicator for it.

## 4.5 $\Upsilon$ production at the LHC

Here we consider  $\Upsilon(1S)$  production. Non-linear effects are generally suppressed by the inverse power of the heavy quark mass. However, since the bottom quark mass  $m_b$  is just three times as heavy as the charm quark mass  $m_c$ , the relevant value of  $x$  for the  $\Upsilon(1S)$  production becomes larger by the same factor at low  $P_\perp$ , as compared to the  $J/\psi$ . At the

---

<sup>4</sup> We note a preliminary data in p-Pb collisions at the LHC shows that our results with set g1118 overestimate a suppression of the  $R_{pA}$  at lower  $P_\perp$  [154].

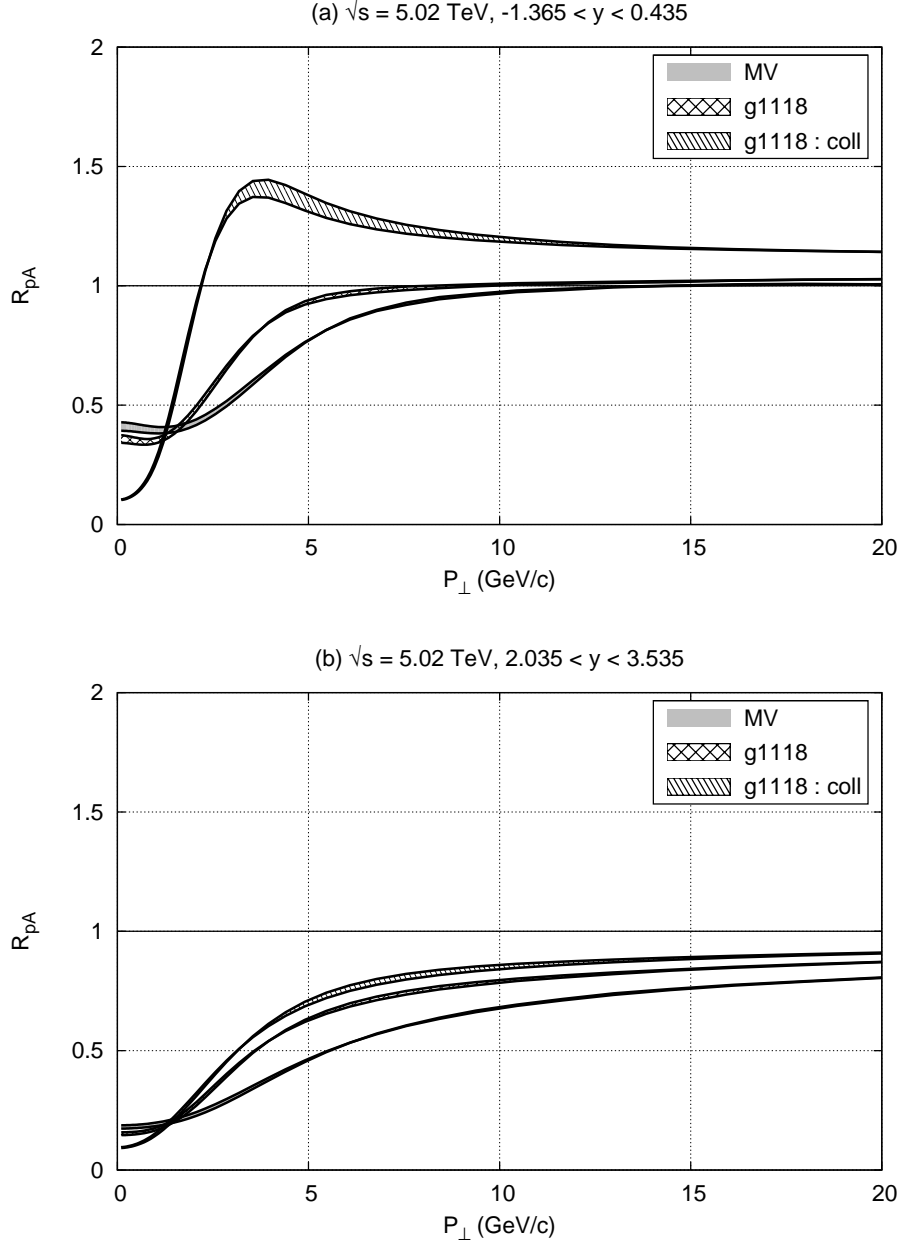


Figure 4.9: The ratio  $R_{pA}(P_{\perp})$  for  $J/\psi$  at  $\sqrt{s} = 5.02$  TeV for (a)  $-1.4 < y < 0.4$  and (b)  $2 < y < 3.5$ . Notations are the same as in Fig. 4.3.

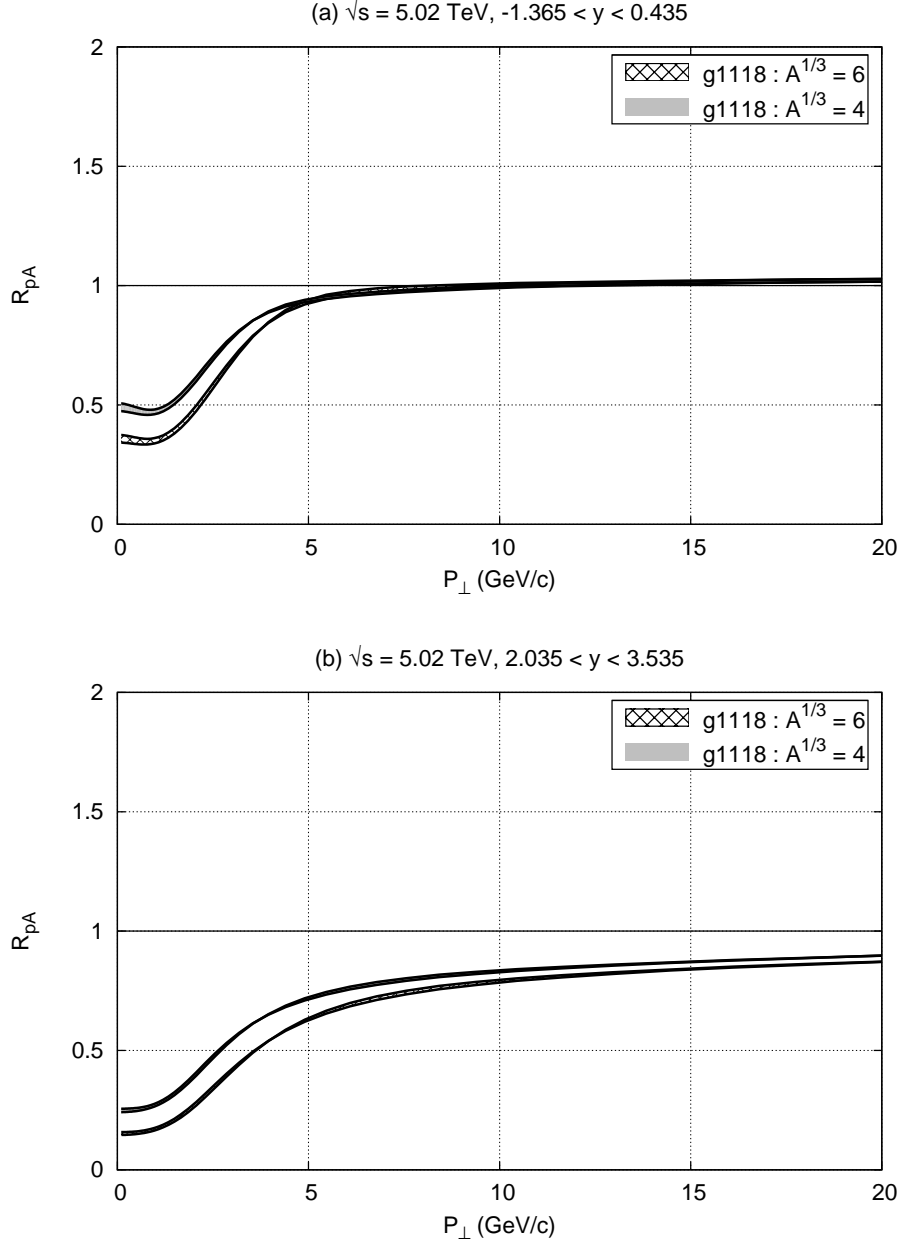


Figure 4.10: Initial-scale dependence of the ratio  $R_{pA}(P_{\perp})$  for  $J/\psi$  at (a) mid- and (b) forward-rapidity at  $\sqrt{s} = 5.02$  TeV.  $Q_{s0,A}^2$  is set to  $4Q_{s0,p}^2$  (upper) and  $6Q_{s0,p}^2$  (lower).

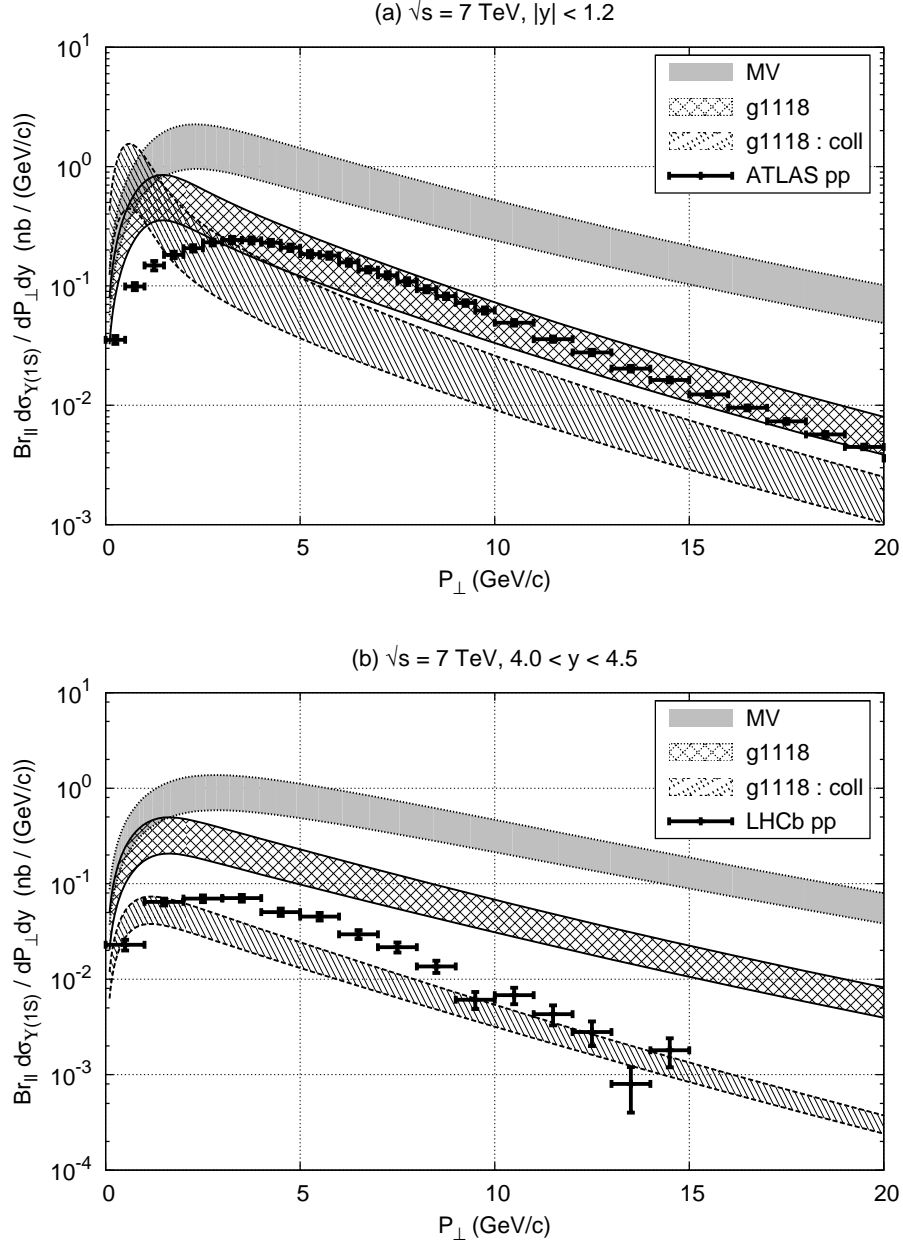


Figure 4.11: Transverse momentum spectrum of  $\Upsilon(1S)$  in di-lepton channel in pp collisions at  $\sqrt{s} = 7 \text{ TeV}$  for (a)  $|y| < 1.2$  and (b)  $4 < y < 4.5$ . Notations are the same as in Fig. 4.3 except for a branching ratio of the  $\Upsilon(1S)$  decay into di-lepton channel.  $Br_u = 0.0238$  for  $e^+e^-$  at mid rapidity and  $Br_u = 0.0248$  for  $\mu^+\mu^-$  at forward rapidity. Data from [111, 112].

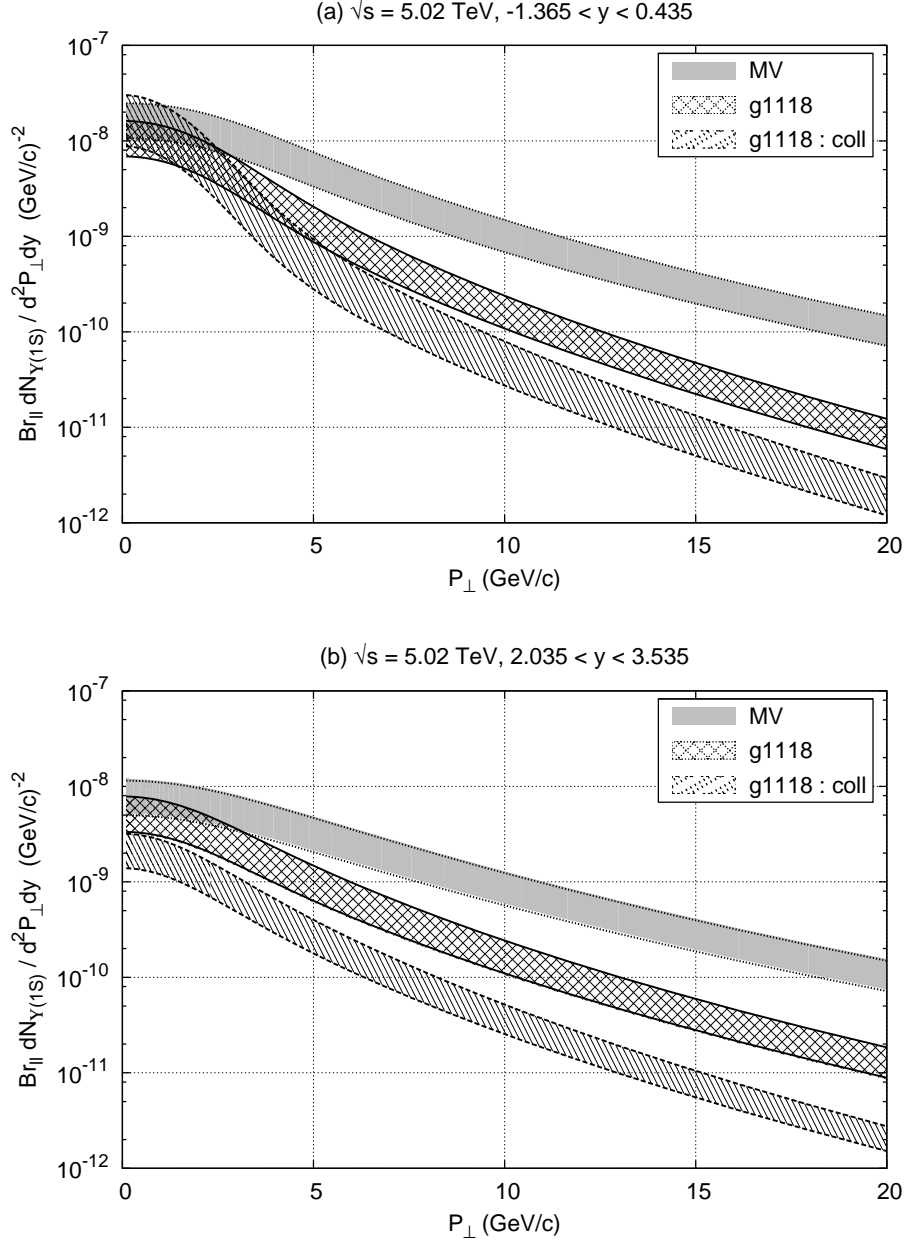


Figure 4.12: Transverse momentum spectrum of  $\Upsilon(1S)$  in di-lepton channel in pA collisions at  $\sqrt{s} = 5.02$  TeV for (a)  $-1.4 < y < 0.4$  and (b)  $2 < y < 3.5$ . Notations are the same as in Fig. 4.3 except for a branching ratio of the  $\Upsilon(1S)$  decay into di-lepton channel.  $Br_u = 0.0238$  for  $e^+e^-$  at mid rapidity and  $Br_u = 0.0248$  for  $\mu^+\mu^-$  at forward rapidity.

LHC energy, this  $x$  value may be still small enough for multiple scatterings and saturation to be important in the  $\Upsilon$  production.

We plot the  $P_\perp$  spectrum of  $\Upsilon(1S)$  in pp and pA collisions at  $\sqrt{s} = 7$  and 5.02 TeV in Figs. 4.11 and 4.12, respectively, together with the data measured by ATLAS and LHCb [111,112] for the pp case. Here we have chosen the CEM parameter as  $F_{\Upsilon(1S)} = 0.01$ , and varied  $m_b$  from 4.5 to 4.8 GeV. Other notations are the same as in the  $J/\psi$  case. In pp collisions, the coincidence between the model and the data for  $\Upsilon(1S)$  state is not as good as that for  $J/\psi$  at low  $P_\perp$  and at forward rapidity.

The model uncertainty from the quark mass value and the factorization scale would cancel out by taking the ratio of the cross-sections in the pp and pA collisions. We present in Fig. 4.13 the nuclear modification factor  $R_{pA}$  for  $\Upsilon(1S)$  as a function of  $P_\perp$ . Indeed, each band collapses into a thin line whose width is almost unnoticeable.

The result for  $\Upsilon(1S)$  is qualitatively very similar to that for  $J/\psi$ . At mid-rapidity, we see a suppression  $R_{pA}$  in low  $P_\perp$  region below 5 GeV, while it turns to be unity at larger  $P_\perp$ . Only in the collinear approximation, we see the Cronin-like enhancement, which is largely caused by the dip structure in the proton uGD at moderate  $x_1$ . At forward rapidities  $2 < y < 3.5$ , the  $\Upsilon$  production is suppressed in a wide  $P_\perp$  region from 0 to 20 GeV, irrespective of the model uGD's, g1118 or MV, or of the use of collinear approximation. In the forward region,  $\Upsilon(1S)$  production has the sensitivity to the small- $x$  evolution of uGD in the nucleus.

We have also checked the initial-scale ( $Q_{s0,A}^2$ ) dependence by comparing the result with  $Q_{s0,A}^2 = 4Q_{s0,p}^2$  and  $6Q_{s0,p}^2$  to find that the change is very similar to the case with  $J/\psi$  (Fig. 4.10).

## 4.6 Rapidity dependence of $R_{pA}$ of $J/\psi$ and $\Upsilon$

We study the rapidity dependence of the  $R_{pA}$  integrated over  $P_\perp$ . The computation is performed with set g1118. In Fig. 4.14 shown is  $R_{pA}(y)$  of  $J/\psi$  at  $\sqrt{s} = 0.2$  and 5.02 TeV with experimental data at RHIC [106] and the LHC [108,109]. Note that our assumption of dilute-dense colliding system applies only in the positive rapidity region, especially for pp, which appears in the denominator of  $R_{pA}$ . We see systematically a stronger suppression of  $R_{pA}$  as the rapidity increases both at RHIC and LHC energies. This is in accord with  $x$ -evolution of uGD in the heavy target.  $R_{pA}(y)$  of  $J/\psi$  flattens out at  $y \lesssim 1$  at RHIC energy because the  $J/\psi$  is produced there by the gluons with  $x_2 > x_0 = 0.01$  and



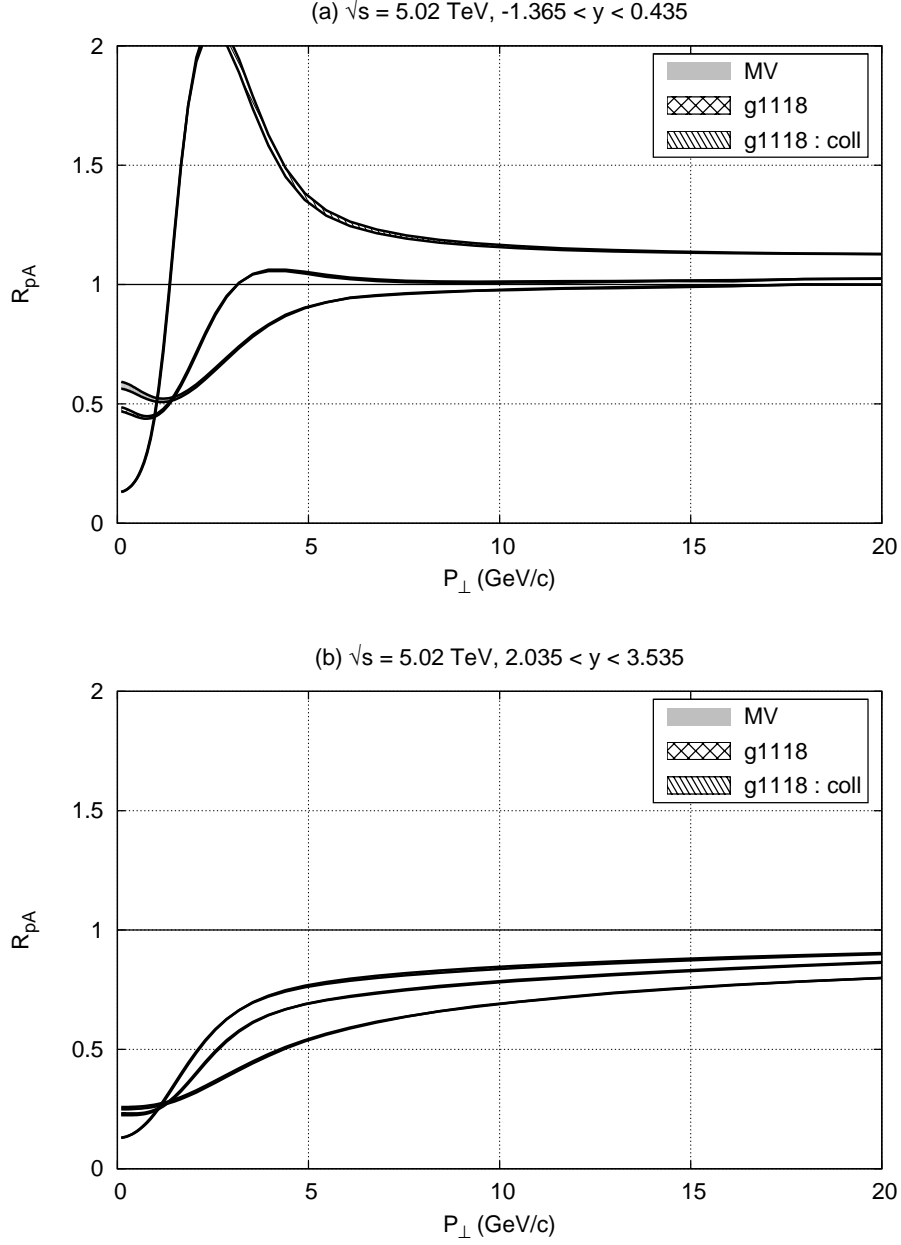


Figure 4.13: The ratio  $R_{pA}$  for  $\Upsilon(1S)$  at  $\sqrt{s} = 5.02$  TeV as a function of the transverse momentum. (a)  $-1.4 < y < 0.4$  and (b)  $2 < y < 3.5$ . Notations are the same as in Fig. 4.11.

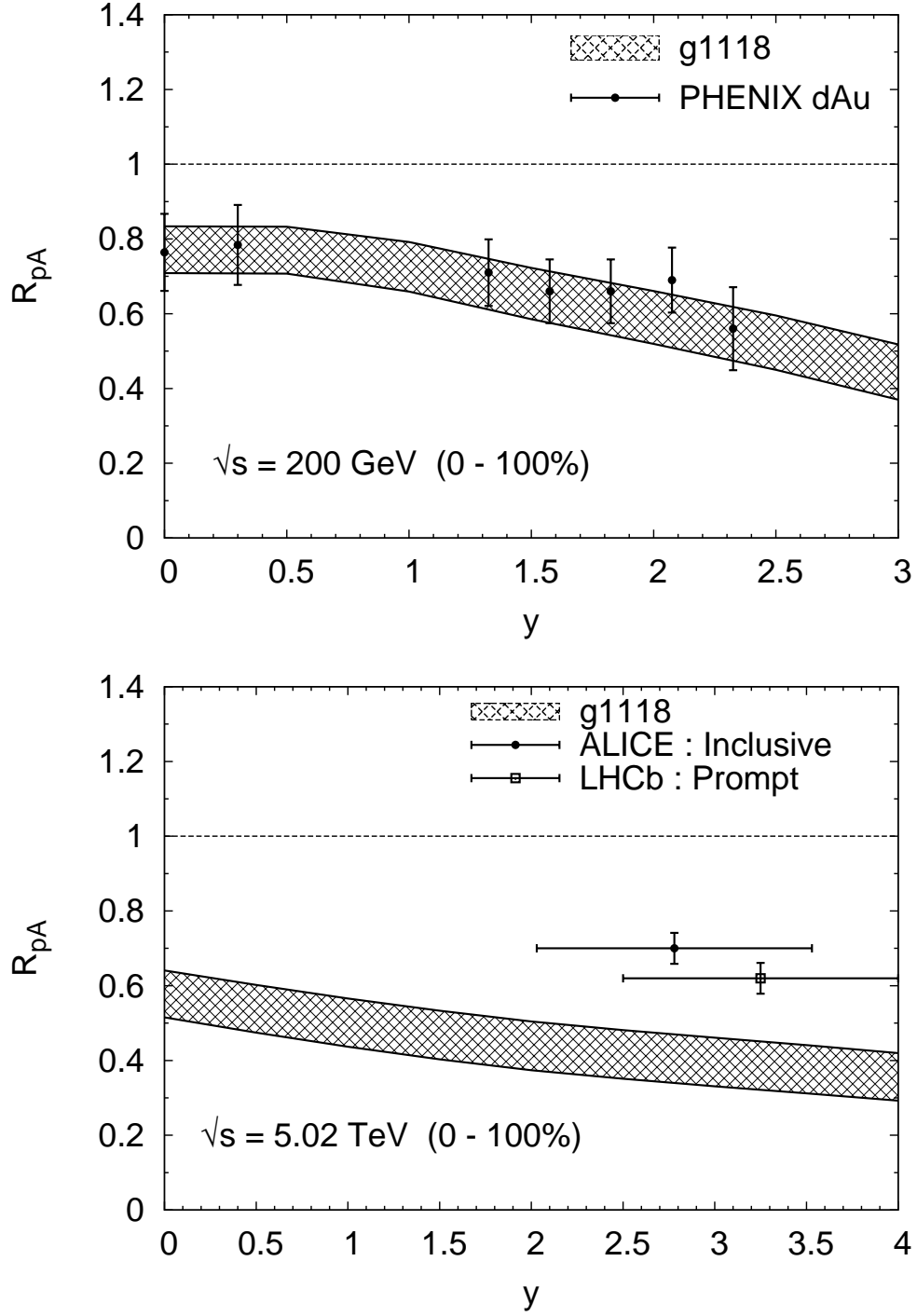


Figure 4.14: Nuclear modification factor  $R_{pA}$  for  $J/\psi$  integrated over  $P_{\perp}$  as a function of rapidity, in pA collisions at  $\sqrt{s} = 200 \text{ GeV}$  (top) and  $\sqrt{s} = 5.02 \text{ TeV}$  (down). The band includes uncertainty for  $m_c = 1.2 \text{ GeV}$  to  $1.5 \text{ GeV}$  and  $Q_{s0,A}^2 = (4 - 6)Q_{s0,p}^2$ . RHIC data from [106] and LHC data from [108, 109]

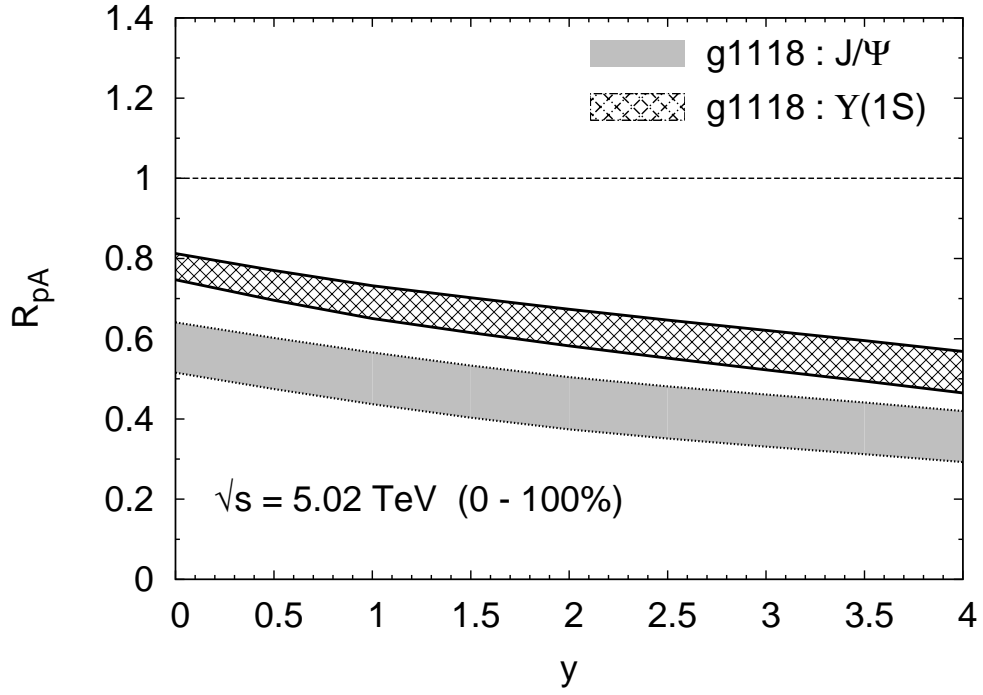


Figure 4.15: Nuclear modification factor  $R_{pA}$  for  $J/\psi$  integrated over  $P_\perp$  as a function of rapidity, in pA collisions at  $\sqrt{s} = 5.02$  TeV. The band includes uncertainty for  $m_c = 1.2$  GeV to 1.5 GeV and  $Q_{s0,A}^2 = (4 - 6)Q_{s0,p}^2$ .  $R_{pA}$  of  $\Upsilon(1S)$  is also shown where we vary  $m_b = 4.5$  to 4.8 GeV.

we freeze the saturation scale to its initial value at  $x = x_0$ . Although our computation shows the strong suppression of  $R_{pA}$  at the LHC, but the data represent that the  $R_{pA}$  at the LHC in the forward rapidity is similar to the one at RHIC forward rapidity. We will leave the investigation of the cause of this similarity in the future work.

Comparing the results of  $J/\psi$  and  $\Upsilon(1S)$  at LHC, we note that the suppression of  $\Upsilon(1S)$  is less than that of  $J/\psi$ , but is still significant to be observed. It would be quite important to study these systematics in experimental data in order to quantify the saturation effects in the heavy nuclear target.

## 4.7 $P_\perp$ broadening

Finally, we study the mean transverse momentum of quarkonium in pA collisions. The momentum broadening in the nuclear target has been discussed in the literature [76–79]. In our framework, the multiple scatterings of the incident gluon and the produced quark pair in the nuclear target, encoded in  $U$  and  $\tilde{U}$  terms in Eq. (3.45) respectively, cause the momentum broadening of the pair. Typical momentum transfer of the multiple scatterings in the nucleus should be characterized by the saturation scale  $Q_{s,A}(x_2)$ . We define here the broadening of  $P_\perp$  as the deviation of the mean transverse momentum  $\langle P_\perp^2 \rangle$  of  $J/\psi$  in pA collisions from that in pp collisions:

$$\Delta\langle P_\perp^2 \rangle_{pA} \equiv \langle P_\perp^2 \rangle_{pA} - \langle P_\perp^2 \rangle_{pp} = \frac{\int d\sigma_{pA} P_\perp^2}{\int d\sigma_{pA}} - \frac{\int d\sigma_{pp} P_\perp^2}{\int d\sigma_{pp}}. \quad (4.5)$$

In Fig. 4.16 we plot  $\Delta\langle P_\perp^2 \rangle_{pA}$  as a function of  $Q_{s0,A}^2$ . We use uGD set g1118 with the quark masses  $m_c = 1.5$  GeV and  $m_b = 4.8$  GeV. We have found that for each rapidity the  $Q_{s0,A}^2$  dependence of the broadening can be fitted in a simple form:

$$\Delta\langle P_\perp^2 \rangle_{pA} = a[(Q_{s0,A}^2/Q_{s0,p}^2)^\alpha - 1] \quad (4.6)$$

with  $a$  and  $\alpha$  being fitting parameters.

At  $\sqrt{s} = 200$  GeV, the broadening at mid-rapidity is obviously linear in  $Q_{s0,A}^2$ , which indicates the random walk nature of the multiple scatterings in the momentum space. In the forward rapidity region, we expected an increase of the mean momentum by the stronger multiple scatterings, but actually found the opposite, i.e., a decrease from the mid-rapidity value. This is because of the kinematical boundary of  $x_1$  in the forward region (see Fig. 5.1).

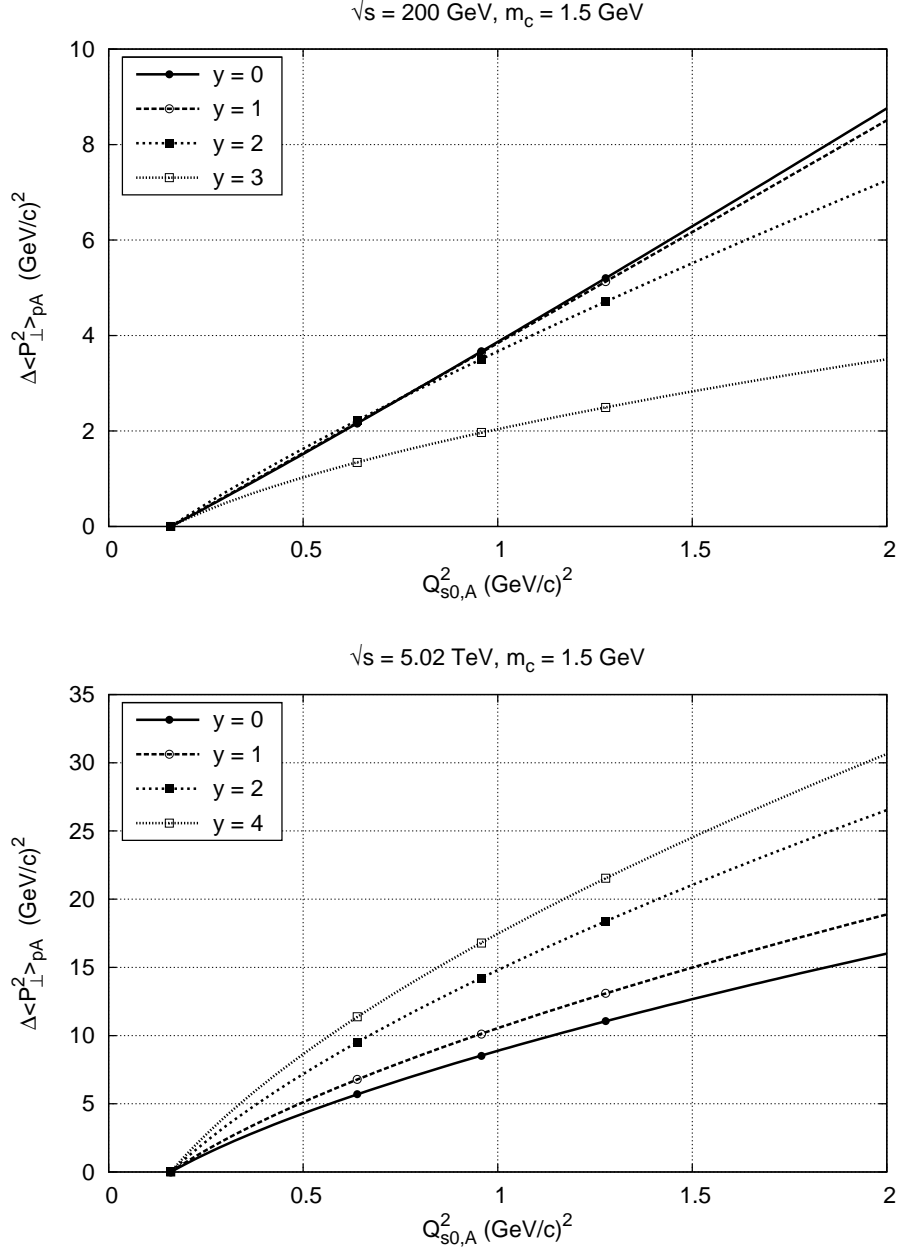


Figure 4.16: Mean transverse momentum square  $\Delta\langle P_{\perp}^2 \rangle_{pA}$  for  $J/\psi$  as a function of  $Q_{s0,A}^2$  at  $\sqrt{s} = 200 \text{ GeV}$  (top) and  $\sqrt{s} = 5.02 \text{ TeV}$  (down). Fit with a form  $a[(Q_{s0,A}^2/Q_{s0,p}^2)^\alpha - 1]$  is also shown.

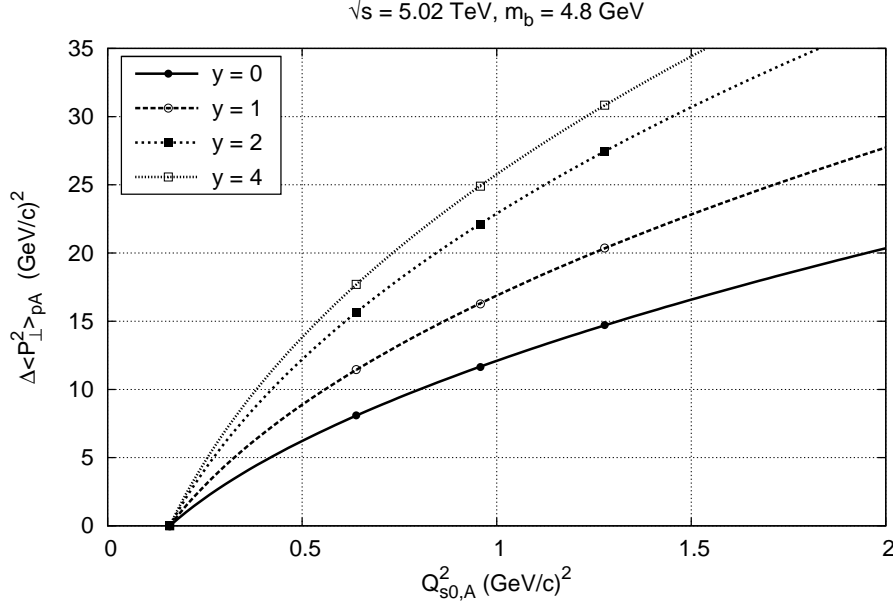


Figure 4.17: Mean transverse momentum square  $\Delta\langle P_{\perp}^2 \rangle_{pA}$  for  $\Upsilon(1S)$  as a function of  $Q_s^2$  at  $\sqrt{s} = 5.02\text{TeV}$ . Fit with a form  $a[(Q_{s0,A}^2/Q_{s0,p}^2)^\alpha - 1]$  is also shown.

The measured value of  $\Delta\langle P_{\perp}^2 \rangle_{dAu}$  at RHIC [107] seems to be smaller by a factor of 5 than that in Fig. 4.16, if we naively translate  $Q_{s0,A}^2$  to the centrality parameter  $N_{\text{coll}}$  evaluated for dAu collisions. This strong broadening originates probably from the fact that our model has too hard  $P_{\perp}$  spectrum at RHIC energy. But it is at least consistent with data that  $P_{\perp}$  broadening at forward rapidities  $\sim 2$  is weaker than that at mid-rapidity  $y \sim 0$ . At  $\sqrt{s} = 5.02\text{ TeV}$ , a wider phase space opens up and we instead see an increase of the mean momentum of  $J/\psi$  as moving to the forward-rapidity region. We have checked that  $\Delta\langle P_{\perp}^2 \rangle_{pA}$  gets back to be smaller at  $y = 6$  than that of mid-rapidity, just as seen in the case of  $\sqrt{s} = 200\text{ GeV}$ . Non-linear dependence on  $Q_{s0,A}^2$  may imply the different evolution speed of multiple scattering strength for different initial values  $Q_{s0,A}^2$ . The result for  $\Upsilon(1S)$  in Fig. 4.17 is similar to the  $J/\psi$  case, but interestingly the broadening becomes more remarkable; The heavier bottom quark pair can acquire the larger transverse momentum  $P_{\perp}$  in multiple scatterings before going beyond the threshold set on the pair's invariant mass  $M^2 < 4M_B^2$ .

## 4.8 Short summary

We have computed the  $J/\psi$  and  $\Upsilon(1S)$  production in pA collision at collider energies within the CEM based on the CGC quark pair production, and have discussed sensitivity of the quarkonium observables to the parton saturation in the target nucleus. We have presented the two types of calculation: one is using the uGD set g1118 which is constrained with DIS data at  $x < x_0 = 0.01$ , and the other is to use uGD set MV for comparison.

At the RHIC energy  $\sqrt{s} = 200$  GeV, the  $J/\psi$  at mid-rapidity is produced not from small- $x_2$  gluons, but rather from moderate- $x_2$  gluons, and the  $P_\perp$  spectrum in pp collisions is unfortunately sensitive to an unphysical dip structure of the uGD set g1118, which was constrained only for  $x < x_0$ . We need better extrapolation of our framework to  $x \geq x_0$ . In pA collisions, multiple scatterings smear out the dip of the uGD and the  $P_\perp$  spectrum of  $J/\psi$  becomes closer to the observed one in dAu collisions.

At the LHC energy  $\sqrt{s} = 5.02$  TeV, the small- $x$  gluons dominate the charm production, and we have found that our model with the uGD set g1118 works for  $J/\psi$  production in pp collisions both at mid- and forward-rapidities. Then we have shown our model prediction on  $J/\psi$  production in pA collisions. The ratio  $R_{pA}(P_\perp)$  for  $J/\psi$  shows a suppression for  $P_\perp < 5$  GeV at mid-rapidity due to saturation effects, and it is further suppressed in wider range of  $P_\perp$  as moving to forward rapidities.

When integrated over  $P_\perp$ ,  $R_{pA}(y)$  of  $J/\psi$  is more suppressed with increasing rapidity, which is consistent with RHIC data. At the LHC energy  $R_{pA}(y)$  is further suppressed, which reflects through CEM the stronger effects of multiple scatterings and gluon saturation in the quark-pair production process. However, the recent data at the LHC p-Pb collisions indicates that the suppression of  $R_{pA}(y)$  of  $J/\psi$  at the LHC is comparable to the one at RHIC in the forward rapidity region. We have also shown that the  $\Upsilon(1S)$  production in pA collisions at the LHC has a good sensitivity to the gluon saturation of the nucleus, provided that the effect is smaller than that in the  $J/\psi$  case. In our model, when integrated over  $P_\perp$ , the ratio  $R_{pA}(y)$  for  $\Upsilon(1S)$  at the LHC shows a suppression similar to that of  $J/\psi$  at RHIC energy.

The collinear approximation on the proton side unsatisfactorily describe the data. It seems that some  $k_\perp$  smearing is necessary in view of our numerical results. The proton collinear approximation in the CGC framework is also studied in Ref. [145].

Transverse momentum broadening of the quarkonium shows an increasing behavior as a function of  $Q_{s0,A}^2$ . Because our model gives harder  $P_\perp$  spectrum than the data, the broadening is likely to be overestimated at RHIC energy in our calculation. Transverse

momentum broadening is also investigated recently by taking account of the multiple scatterings in the target in [146].



# Chapter 5

## Heavy meson production

In this chapter, we firstly show the numerical results of open heavy flavor meson productions such as  $D$ -meson and  $B$ -meson in pA collisions. In addition to the transverse momentum and nuclear modification factor which are discussed in the quarkonium case, we present azimuthal angle correlation between the heavy meson pair. We expect this particle correlation can bring some information about the saturation effect in the nucleus. In the following calculations, we choose the proton size  $R_p = 0.9$  fm.

### 5.1 Cross section formula of heavy meson production

Heavy meson pair production cross-section can be written as

$$\frac{d\sigma_{h\bar{h}}}{d^2\mathbf{p}_{h\perp}d^2\mathbf{p}_{\bar{h}\perp}dy_qdy_p} = f_{q\rightarrow h}f_{\bar{q}\rightarrow\bar{h}} \int_{z_{1\min}, z_{2\min}}^1 dz_1 dz_2 \frac{D_q^h(z_1)}{z_1^2} \frac{D_{\bar{q}}^{\bar{h}}(z_2)}{z_2^2} \frac{d\sigma_{q\bar{q}}}{d^2\mathbf{q}_{\perp}d^2\mathbf{p}_{\perp}dy_qdy_p} \quad (5.1)$$

Here  $\mathbf{p}_{h\perp}$  ( $\mathbf{p}_{\bar{h}\perp}$ ) and  $y_q$  ( $y_{\bar{q}}$ ) are respectively transverse momentum and rapidity of the produced meson  $h$  ( $\bar{h}$ ). The longitudinal momentum fraction  $z_1$  ( $z_2$ ) of the heavy meson fragmented from the heavy quark (anti-quark) is defined as  $p_{h\perp} = z_1 q_{\perp}$  ( $p_{\bar{h}\perp} = z_2 p_{\perp}$ ). The lower limit  $z_{\min}$  is set by the momentum fraction of the meson fragmented from the heavy quark with the maximum  $q_{\perp}$  allowed kinematically. Here we assume that the meson and the quark have the same rapidity,  $y_q = y_h$  ( $y_p = y_{\bar{h}}$ ).

For the heavy meson fragmentation function  $D(z)$ <sup>1</sup>, we use the Kartvelishvili frag-

---

<sup>1</sup>For recent study of the fragmentation functions for charm and bottom quarks, including the factorization scale dependence, we refer to Refs. [127, 128].

mentation function [126],

$$D_q^h(z) = (\alpha + 1)(\alpha + 2)z^\alpha(1 - z) . \quad (5.2)$$

This is originally not a Lorentz invariant quantity but useful to evaluate the cross section of the heavy meson production. Here we assume that the non-perturbative parameter  $\alpha$  in Eq. (5.2) is the same both in  $D$  ( $B$ ) production and  $D^*$  ( $B^*$ ) production. The value of  $\alpha$  is set to 3.5 (13.5) for  $D$  ( $B$ ) which is determined by fitting the data [129, 130]. The factor  $f_{q \rightarrow h}$  represents the transition probability of the heavy quark  $q$  to evolve the heavy meson  $h$ .  $f_{q \rightarrow h}$  should satisfy the condition as  $\sum_h f_{q \rightarrow h} = 1$  for all the heavy meson  $h$  from  $q$ . Empirical values,  $f_{c \rightarrow D^0} = 0.565$ ,  $f_{c \rightarrow D^{*+}} = 0.224$ , and  $f_{b \rightarrow \bar{B}^0} = 0.401$  are taken from [131, 132, 152]. For the charge conjugate states, we assume  $D_q^h(z) = D_{\bar{q}}^{\bar{h}}(z)$  and  $f_{\bar{q} \rightarrow \bar{h}} = f_{q \rightarrow h}$ .

Similarly single heavy meson production cross-section is expressed in convolution form of quark production cross-section <sup>2</sup> (3.48) and the fragmentation function  $D_q^h(z)$ ,

$$\frac{d\sigma_h}{d^2\mathbf{p}_{h\perp} dy} = f_{q \rightarrow h} \int_{z_{\min}}^1 dz \frac{D_q^h(z)}{z^2} \frac{d\sigma_q}{d^2\mathbf{q}_{\perp} dy} . \quad (5.5)$$

Again we set  $p_{h\perp} = zq_{\perp}$  and  $y_q = y_h = y$ .

## 5.2 Kinematical coverage

It would be instructive to show the relevant kinematical coverage of  $x$  variable in the open heavy flavor production at RHIC and LHC energies.

We assign the momentum fraction  $x_1(x_2)$  to the gluon from proton (nucleus), and it

---

<sup>2</sup>The lower limit of the  $z$  integration in Eq. (5.5) is given explicitly as

$$z_{\min} = \frac{q_{h\perp} \cosh y}{\sqrt{\frac{s}{4} - m^2 \cosh^2 y}} . \quad (5.3)$$

This can be readily derived by noting that the maximum energy of the produced quark and anti-quark in the center-of-mass frame is  $E_q^{\max} = E_{\bar{q}}^{\max} = \frac{\sqrt{s}}{2}$ . For the on-mass-shell quark, we have

$$E_q^{\max} = \sqrt{m^2 + (q_{\perp}^{\max})^2} \cosh y , \quad (5.4)$$

where  $y$  is the quark rapidity, which we set the same as the rapidity of the produced meson  $h$ . Then  $z_{\min} \equiv q_{h\perp}/q_{\perp}^{\max}$  gives the desired expression.

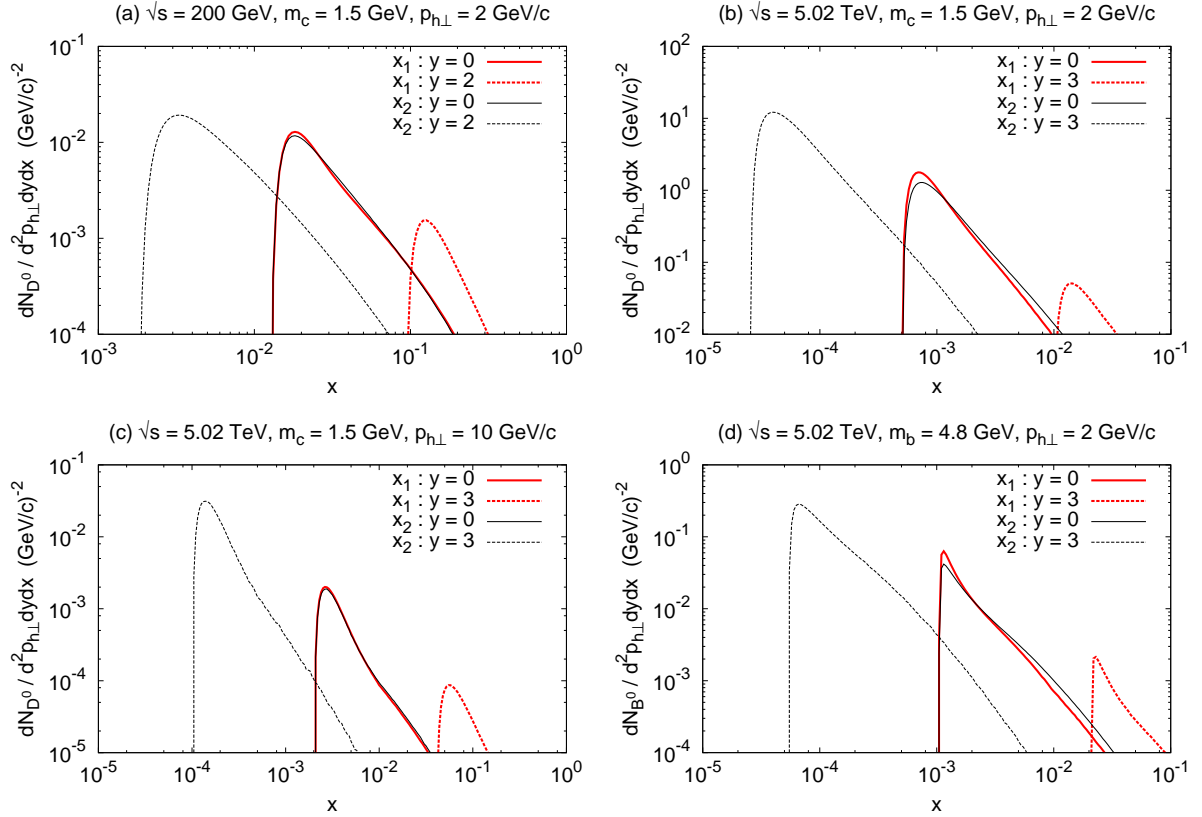


Figure 5.1:  $x_1$  (black) and  $x_2$  (red) coverages of  $D^0$  production at mid and forward rapidities, for fixed  $p_{h\perp} = 2$  GeV at  $\sqrt{s} = 200$  GeV (a), and for fixed  $p_{h\perp} = 2$  GeV (b) and 10 GeV (c) at  $\sqrt{s} = 5.02$  TeV.  $x_{1,2}$  coverages of  $B^0$  production are shown in (d) for fixed  $p_{h\perp} = 2$  GeV at  $\sqrt{s} = 5.02$  TeV.

is expressed in terms of the produced quark momenta as

$$x_{1,2} = \frac{1}{\sqrt{s}} \left( \sqrt{m^2 + q_{\perp}^2} e^{\pm y_q} + \sqrt{m^2 + p_{\perp}^2} e^{\pm y_p} \right). \quad (5.6)$$

We plot in Fig. 5.1 the  $x_{1,2}$  distribution of single heavy meson production at a particular transverse momentum and rapidity. We find in Fig. 5.1 (a) that both  $x_1$  and  $x_2$  contributing to single charmed meson production at  $p_{h\perp} = 2$  GeV and  $y = 0$  at  $\sqrt{s} = 200$  GeV are larger than  $x_0 = 0.01$ , while at forward rapidity  $y = 2$  the production gets sensitivity to small  $x_2 < x_0$ . In other words, the mid-rapidity production of single heavy mesons is sensitive to the initial  $\phi_{A,Y}^{\bar{q}q,g}$  and  $x$ -evolution effect shows up only at forward meson production at RHIC energy. However, it is seen in Fig. 5.1 (b) and (c) that at  $\sqrt{s} = 5.02$  TeV small  $x$  gluons around  $10^{-3}$  dominate the production even at mid rapidity. In the

forward-rapidity production, the  $x_2$  value of the gluons from the nucleus can become lower than  $10^{-4}$ , where one would expect good sensitivity of heavy meson production to  $x$ -evolution and parton saturation. Even for bottomed meson production the situation is similar, as seen in Fig. 5.1 (d). Thus heavy quark productions, which may be evaluated with perturbation method, can be used to probe the small- $x$  dynamics by studying the heavy meson production at lower  $p_{h\perp}$  and forward rapidity at the LHC.

## 5.3 Transverse momentum spectrum

### 5.3.1 pp collisions

We calculate  $D$  meson production cross-section at mid rapidity in pp collisions at  $\sqrt{s} = 200$  GeV and 5.02 TeV. Although the expression (5.5) is derived for a dilute-dense system such as pA, we apply it here by substituting the numerical solution for the proton into  $\phi_{A,Y}^{q\bar{q},g}(\mathbf{l}_\perp, \mathbf{k}_\perp)$ . By comparing the result with available data, we can examine the applicability of our formula. Furthermore we actually need the cross-sections in pp collisions as the normalization when we study the nuclear modification of the cross-sections in pA collisions.

We compute transverse momentum ( $p_\perp$ ) spectrum of  $D$  meson production cross-section with uGD sets g1118 and MV in Table 3.1, and show the results in Fig. 5.2 together with the available data at  $|y| < 1$  and at  $\sqrt{s} = 200$  GeV [120] and at  $|y| < 0.5$  and at  $\sqrt{s} = 5.02$  TeV [116]. The upper (lower) curve of each band indicates the result with charm quark mass  $m_c = 1.2$  (1.5) GeV. We find that  $p_\perp$  dependence of  $D$  production is better described with uGD set g1118, although it gives still harder spectrum at high  $p_\perp$ .

Next we show forward  $B^0$  production cross-section in  $2 < y < 4.5$  in pp collisions at  $\sqrt{s} = 5.02$  TeV as a function of  $p_\perp$  in Fig. 5.3 (a) and the  $p_\perp$ -integrated cross-section as a function of  $y$  in Fig. 5.3 (b). The upper (lower) curve of each band indicates the result with the bottom quark mass  $m_b = 4.5$  (4.8) GeV. The result with uGD set g1118 describes  $p_\perp$  and  $y$  dependence of the data [121] better than that with set MV. But the magnitude of cross-section is larger than the data by about a factor of 2 – 3. We comment here that large- $x_1$  gluons in the proton become relevant in  $B^0$  production at forward rapidity and/or at high  $p_\perp$ . Therefore the numerical result is sensitive to the extrapolation Ansatz Eq. (3.64) of the uGD for large  $x$ .

The framework in our calculations is valid in the small- $x$  region then the reader should focus on the spectrum of  $D$  meson and also  $B$  meson productions at low  $p_\perp$  up to about

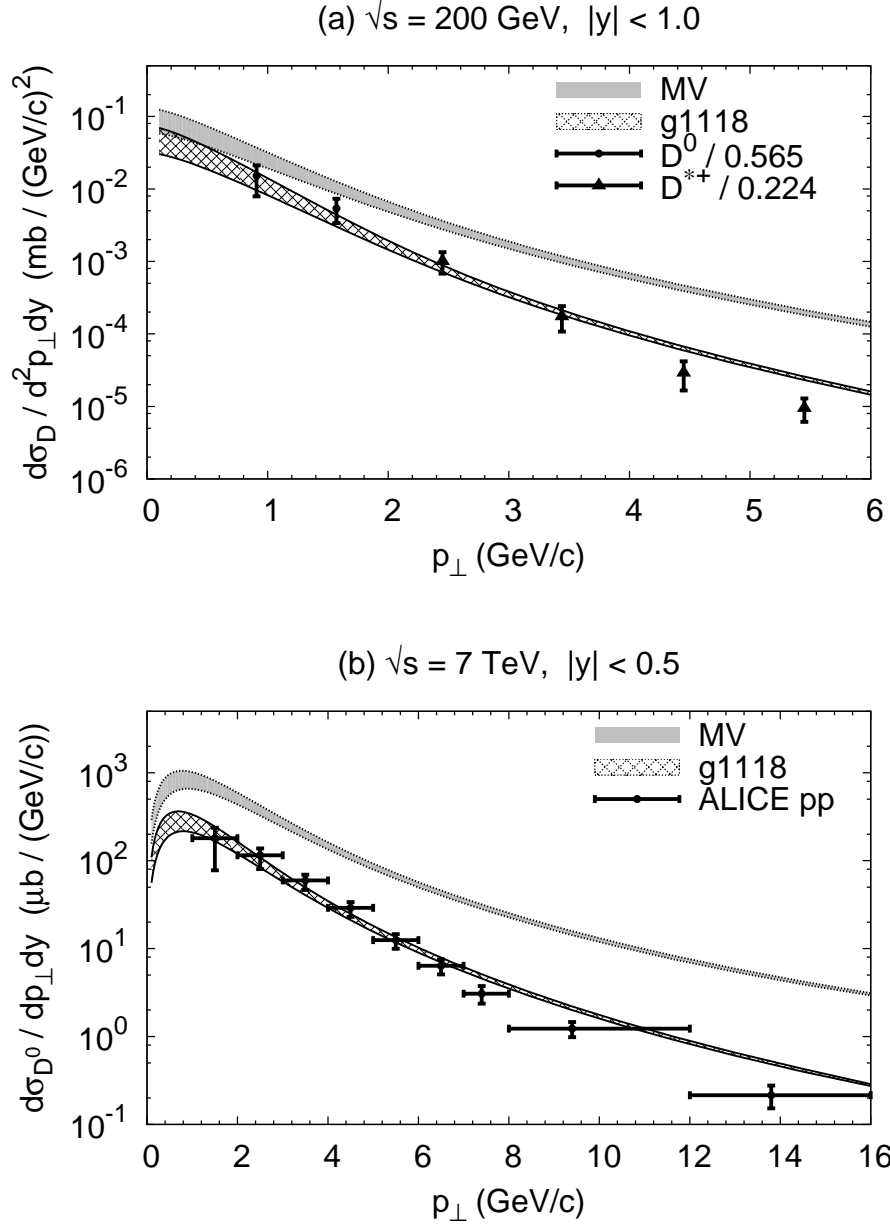


Figure 5.2: (a) Differential cross-section of  $D$  (rescaled as  $D^0/f_{c \rightarrow D^0}$  and  $D^{*+}/f_{c \rightarrow D^{*+}}$ ) vs transverse momentum  $p_\perp$  for rapidity range  $|y| < 1.0$  in pp collisions at  $\sqrt{s} = 200$  GeV, computed with Eq. (5.5) with uGD sets MV (gray band) and g1118 (double-hatched). The upper (lower) curve of the band corresponds to the result with  $m_c = 1.2$  (1.5) GeV. The data is taken from Ref. [120]. (b) Differential cross-section of  $D^0$  vs transverse momentum  $p_\perp$  at  $|y| < 0.5$  in pp collisions at  $\sqrt{s} = 5.02$  TeV. The ALICE data is taken from Ref. [116].

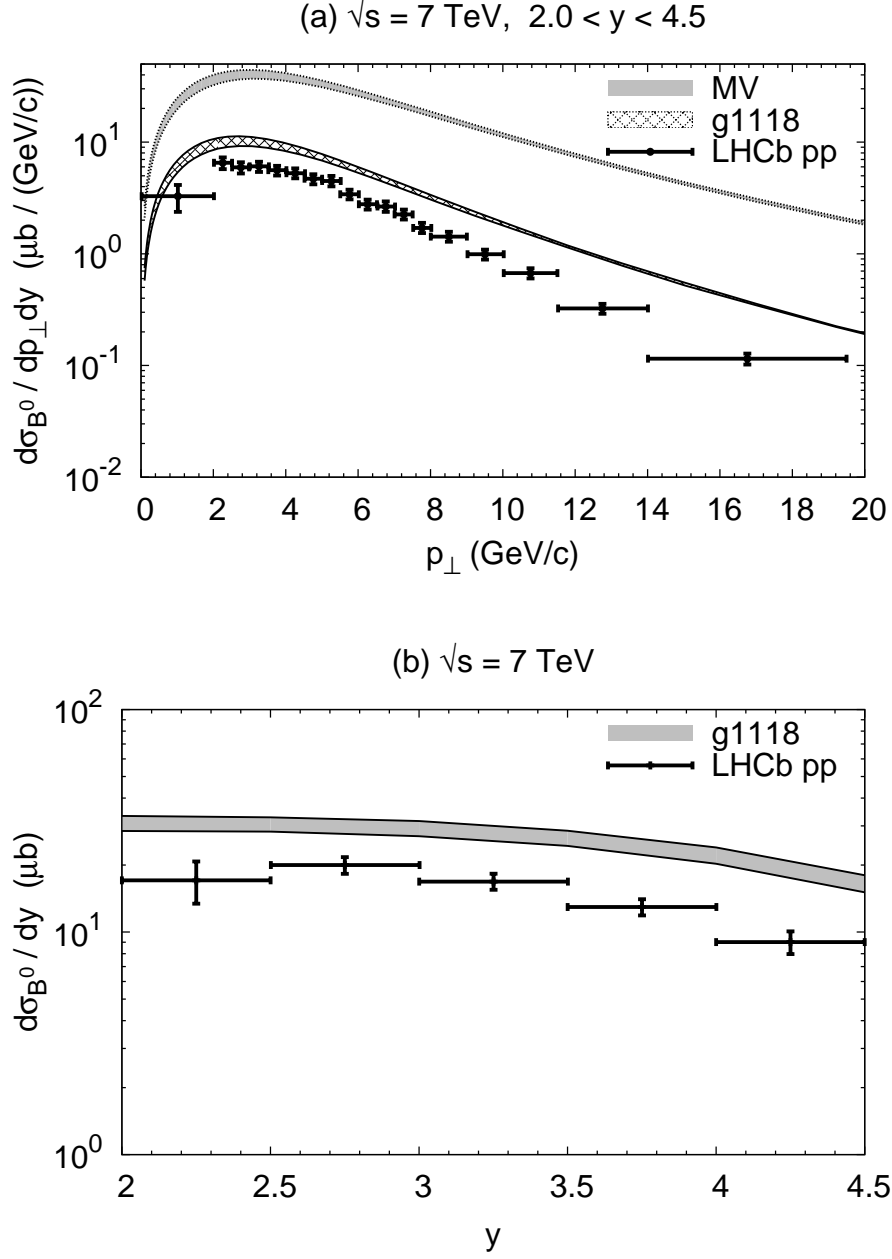


Figure 5.3: (a) Differential cross-section of  $B^0$  vs transverse momentum  $p_{\perp}$  for rapidity range  $2 < y < 4.5$  in pp collisions at  $\sqrt{s} = 5.02 \text{ TeV}$ , computed with Eq. (5.5) with uGD sets MV (gray band) and g1118 (double-hatched). The upper (lower) curve of the band corresponds to the result with  $m_b = 4.5$  (4.8) GeV. (b) Differential cross-section of  $B^0$  vs  $y$  in the range  $0 < p_{\perp} < 40 \text{ GeV}$  in pp collisions at  $\sqrt{s} = 5.02 \text{ TeV}$ . The notation of the curve is the same as in (a). The LHCb data is taken from Ref. [121].

2 GeV or a few times higher than it.

### 5.3.2 pA collisions

We plot in Fig. 5.4 (a) the transverse momentum spectrum of  $D^0$  multiplicity in the rapidity range  $|y| < 1.0$  in pA collisions at  $\sqrt{s} = 200$  GeV. We choose the initial saturation scale of the uGD in the heavy nucleus as  $Q_{s0,A}^2(x = x_0) = 6Q_{s0,p}^2$ . The upper (lower) curve of the bands indicate the result with  $m_c = 1.2$  (1.5) GeV. We find that the results obtained with sets g1118 and MV fairly describe the available data at low  $p_\perp \lesssim 2$  GeV [117] although high- $p_\perp$  behaviors are different. We show in Fig. 5.4 (b)  $D^0$  production spectrum in  $-1 < y < 0$  at  $\sqrt{s} = 5.02$  TeV <sup>3</sup>. The uGD sets MV and g1118 give different  $p_\perp$  dependence of the  $D$  meson spectrum: Set MV yields harder  $p_\perp$  spectrum.

## 5.4 Transverse momentum dependence of $R_{pA}$

Now let us discuss the nuclear modification factor for pA collisions defined as

$$R_{pA} = \frac{dN_h/d^2p_\perp dy|_{pA}}{N_{\text{coll}} dN_h/d^2p_\perp dy|_{pp}}. \quad (5.7)$$

where  $dN_h/d^2p_\perp dy$  is the average multiplicity of hadron per event. Here we set the number of binary nucleon-nucleon collisions <sup>4</sup> to  $N_{\text{coll}} = A^{\gamma/3}$  because the uGD  $\phi_{A,y_0}(\mathbf{k}_\perp)$  scales as  $(Q_{s0}^2)^\gamma \propto A^{\gamma/3}$  at large  $k_\perp$  [58]. Model uncertainties in our calculation will largely cancel out in the ratio of multiplicity per event in pA collisions to that in pp collisions.

In Fig. 5.5 we plot  $R_{pA}$  of (a)  $D$  and (b)  $B$  productions as a function of  $p_\perp$  at mid rapidity ( $|y| < 1.0$ ) at  $\sqrt{s} = 200$  GeV. We use the uGD set g1118 in this subsection. We have checked that  $R_{pA}$  is insensitive to the variation of the heavy quark mass within the range considered here, and we show the results with  $m_c = 1.5$  GeV for  $D$  production and  $m_b = 4.8$  GeV for  $B$  production.

The nuclear modification factor  $R_{pA}$  of  $D$  production is suppressed at lower  $p_\perp \lesssim 2$  GeV while enhanced at higher  $p_\perp$  larger than 2 GeV. As seen in Fig. 5.1 (a), heavy mesons are produced from the gluons with moderate values of  $x$ , whose distribution is fixed by

---

<sup>3</sup>Rapidity in the center-of-mass frame in pA collisions at  $\sqrt{s} = 5.02$  TeV is shifted by  $\Delta y = 0.465$  from that in the laboratory frame.

<sup>4</sup>Of course, we have an ambiguity of definition of  $N_{\text{coll}}$ . We discuss in the Appendix chapter a quantitative difference between  $R_{pA}$  of the  $J/\psi$  with  $N_{\text{coll}} = A^{\gamma/3}$  and that with  $N_{\text{coll}} = A^{1/3}$ .

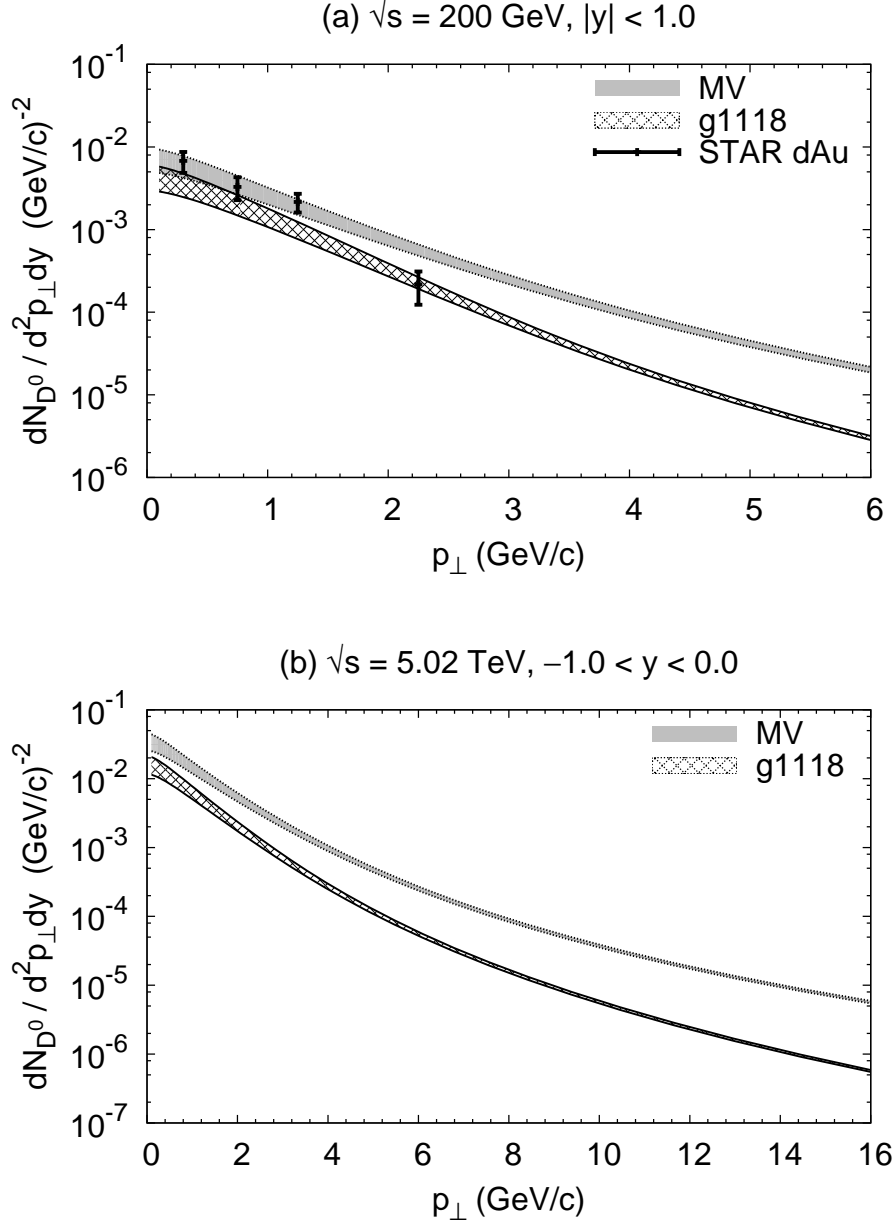


Figure 5.4: Transverse momentum spectrum of  $D^0$  multiplicity per event in pA collisions, computed with Eq. (5.5) with uGD sets MV (gray) and g1118 (double-hatch), in rapidity range  $|y| < 1.0$  at  $\sqrt{s} = 200 \text{ GeV}$  (a) and in  $-1.0 < y < 0.0$  at  $\sqrt{s} = 5.02 \text{ GeV}$  (b). The upper (lower) curve of the band corresponds to the result with  $m_c = 1.2$  (1.5) GeV. dAu data is taken from [117].



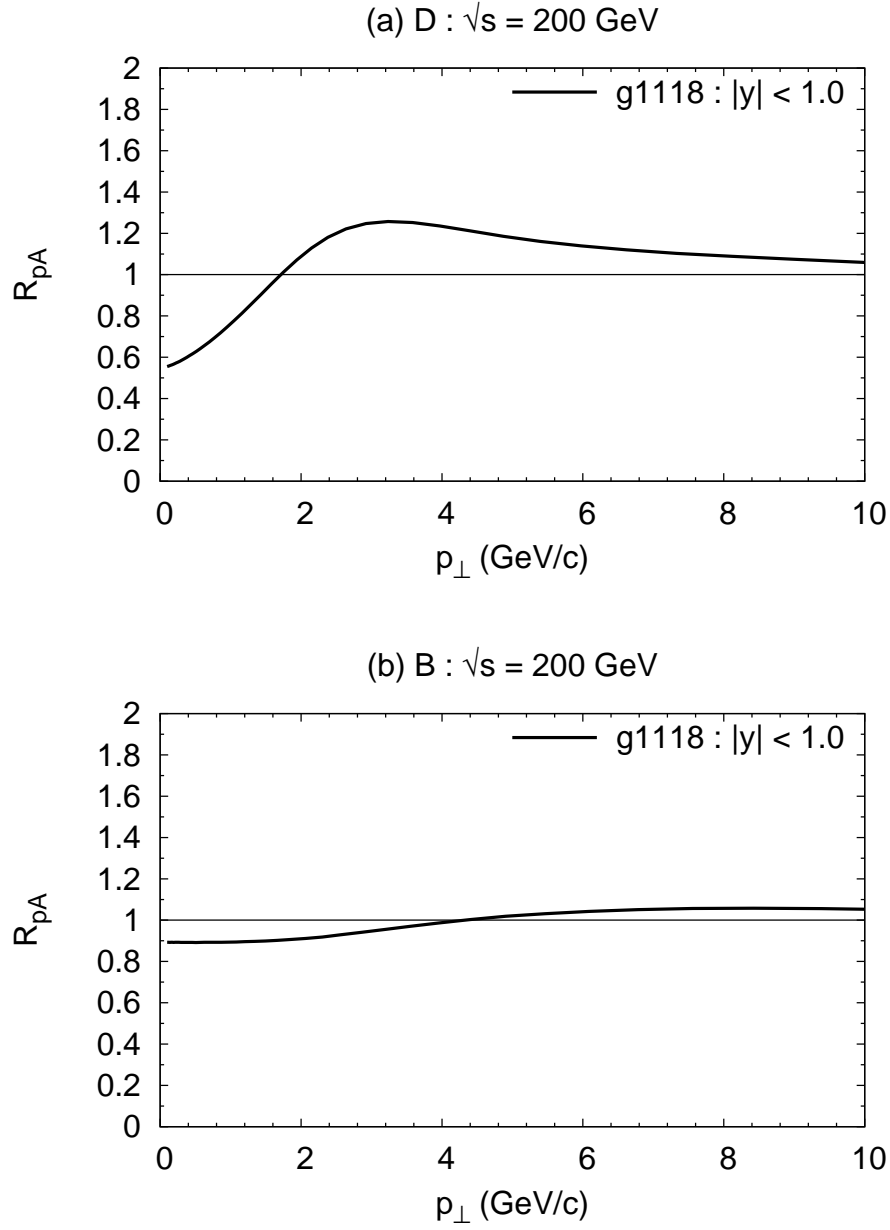


Figure 5.5: (a) Nuclear modification factor  $R_{pA}$  of  $D$  production vs  $p_{\perp}$  computed with Eq. (5.7) with uGD set g1118 with  $m_c = 1.5$  GeV in the rapidity range  $|y| < 1.0$  at  $\sqrt{s} = 200$  GeV. (b)  $R_{pA}(p_{\perp})$  of  $B$  production with  $m_b = 4.8$  GeV.

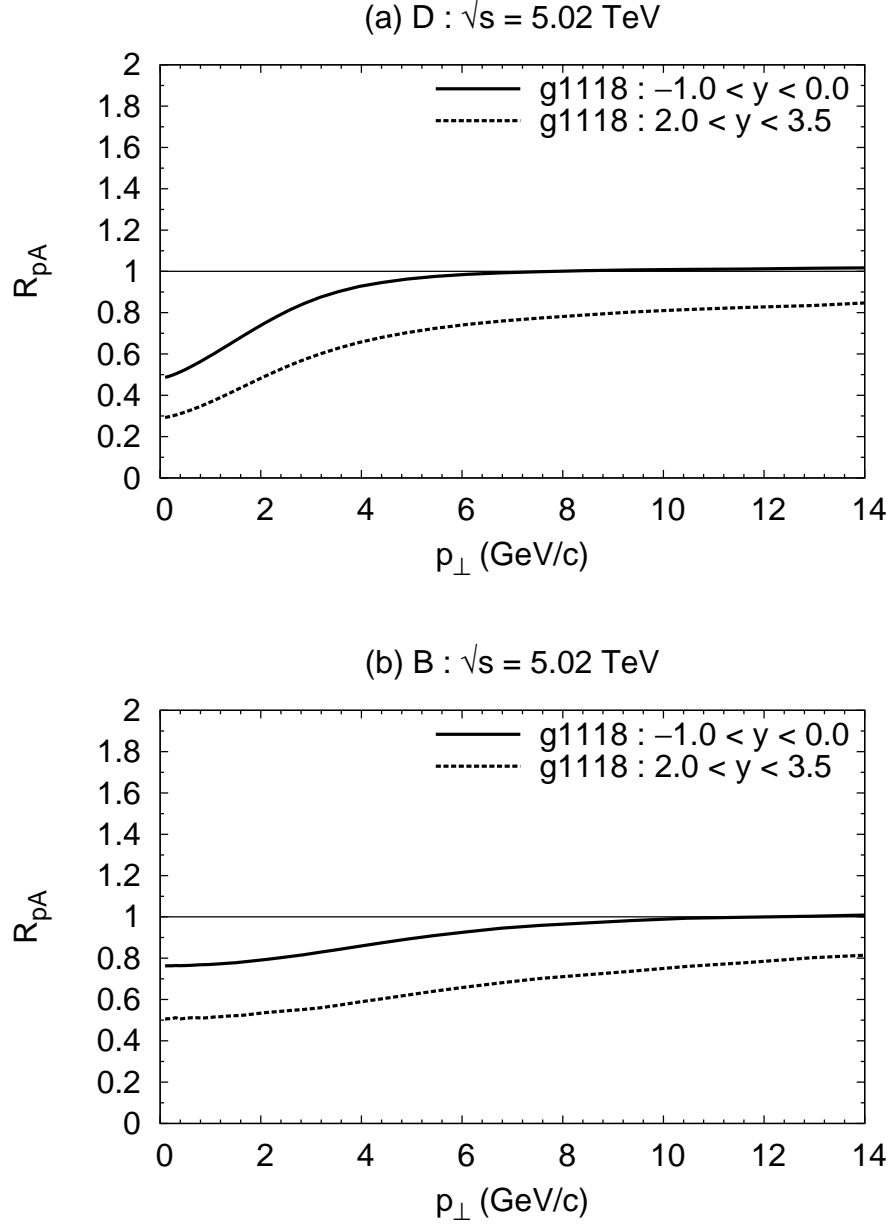


Figure 5.6: Nuclear modification factor  $R_{pA}(p_{\perp})$  of (a)  $D$  and (b)  $B$  productions for  $-1 < y < 0$  (solid line) and  $2 < y < 3.5$  (dotted line) at  $\sqrt{s} = 5.02 \text{ TeV}$ .

the extrapolation Ansatz (3.64) from  $x = x_0$  to larger  $x > x_0$ . Thus the suppression and enhancement of  $R_{pA}$  should be interpreted as the effects of the multiple scatterings in the nucleus encoded in  $\phi_{A,Y_0}$ . On the other hand,  $R_{pA}$  of  $B$  production in Fig. 5.5 (b) shows little structure as a function of  $p_\perp$ , even though it is dominated by the larger- $x$  gluons. This is because the larger bottom mass suppresses the effects of multiple scatterings, i.e.,  $Q_{A,y_0}^2/m_b^2 \ll 1$ . That is,  $B$  production scales with  $N_{\text{coll}}$  at RHIC energy.

Next, we study the nuclear modification  $R_{pA}$  of  $D$  and  $B$  productions at  $\sqrt{s} = 5.02$  TeV.  $R_{pA}$  of  $D$  production shown in Fig. 5.6 (a) indicates that there is a strong suppression at lower  $p_\perp$  and that no Cronin-like peak structure is seen at mid rapidity ( $-1 < y < 0$ ) by the quantum  $x$ -evolution effects on the small  $x_2$  gluons<sup>5</sup>. We see the stronger suppression of  $R_{pA}$  in the wider range of  $p_\perp$  at forward rapidity ( $2 < y < 3.5$ ), compared to that at mid rapidity. At  $\sqrt{s} = 5.02$  TeV,  $B$  production at low  $p_\perp$  shows a suppression similar to but weaker than the  $D$  production as shown in Fig. 5.6 (b).

## 5.5 Rapidity dependence of $R_{pA}$

The nuclear modification factor ( $R_{pA}(y)$ ) of the heavy meson multiplicities  $dN/dy$  in pA collisions as a function of  $y$  provides important information about how the saturation effect evolves as moving to forward rapidity region. In Fig. 5.7 shown are the  $R_{pA}$  of  $D$  (gray band) and  $B$  (double hatched band) mesons as a function of rapidity at  $\sqrt{s} = 200$  GeV (a) and 5.02 TeV (b).

We have allowed the variation of the initial saturation scale at  $x = x_0$  in the heavy nucleus as  $Q_{s0,A}^2(x = x_0) = (4 - 6)Q_{s0,p}^2$  with  $A^{1/3} = 4 - 6$  here. The upper (lower) curve of the band of  $D$  production in Fig. 5.7 now corresponds to the result with  $m_c = 1.5$  (1.2) GeV and  $A^{1/3} = 4$  (6). For  $B$  production, the upper (lower) curve corresponds to the result obtained with  $m_b = 4.8$ (4.5) GeV and  $A^{1/3} = 4$ (6). The width of the band here comes mainly from the change of  $A^{1/3} = 4 - 6$ .

We find in Fig. 5.7 (a) that  $R_{pA}$  of the  $D$  production at mid rapidity at  $\sqrt{s} = 200$  GeV is suppressed, which reflects the multiple scattering effect as we have discussed in Fig. 5.5. Stronger suppression of  $D$  production is seen with increasing the rapidity, in accord with the quantum evolution of the gluon distribution  $\phi_A$ . On the other hand, for  $B$  production,  $R_{pA}$  shows no appreciable change with the increasing rapidity at RHIC

---

<sup>5</sup>A preliminary data of  $R_{pA}$  as a function of  $p_\perp$  of  $D$  meson production in the mid rapidity region at the LHC seems to be consistent with our result within a certain error [118, 155].

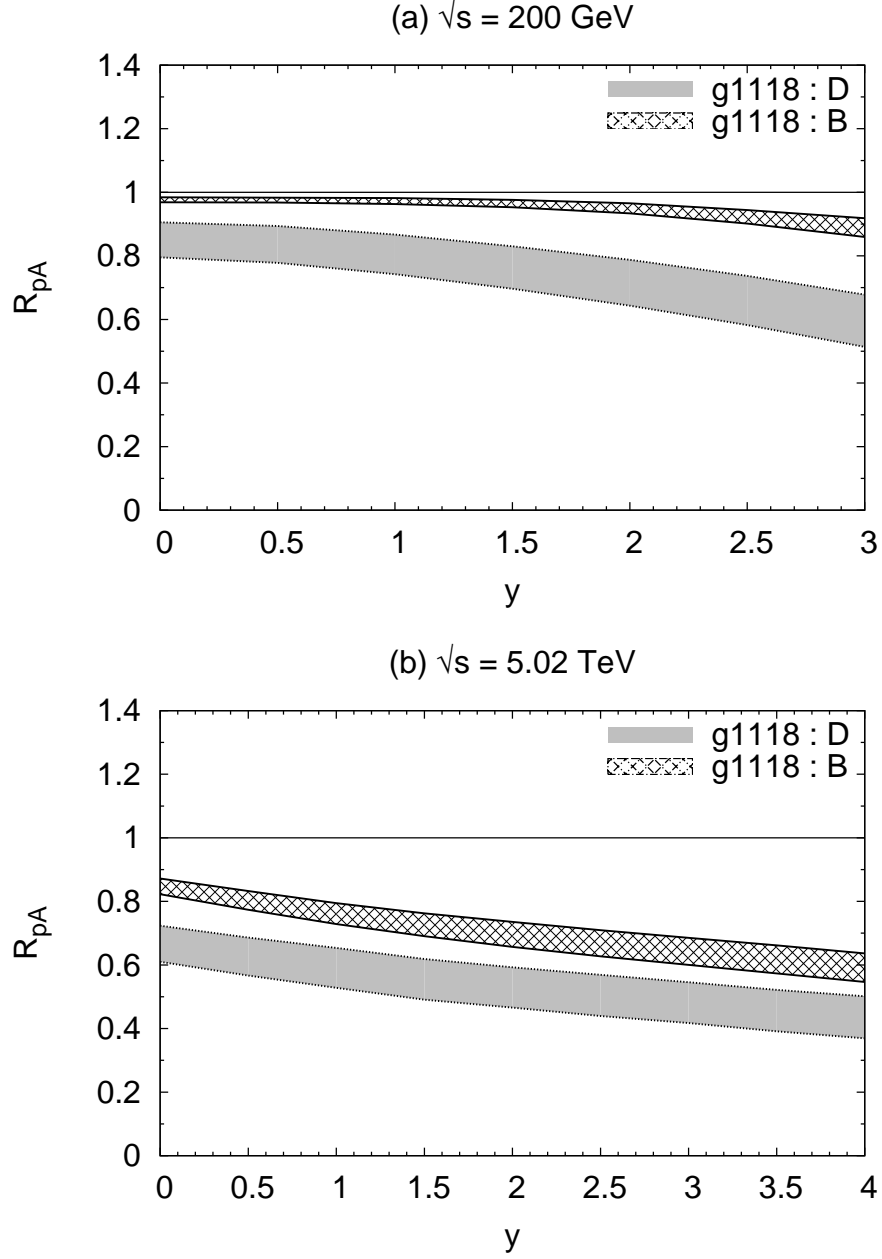


Figure 5.7: Nuclear modification factor  $R_{pA}$  for  $D$  (gray) and  $B$  (double-hatched) vs rapidity  $y$  in pA collisions at (a)  $\sqrt{s} = 200$  GeV and (b)  $\sqrt{s} = 5.02$  TeV. The uGD set g1118 is used. The bands indicate uncertainties from the variations  $m_c = 1.2 - 1.5$  GeV for  $D$ , and  $m_b = 4.5 - 4.8$  GeV for  $B$  and also  $Q_{s0,A}^2 = (4 - 6)Q_{s0,p}^2$ .

energy, besides a subtle suppression at very forward rapidities.

At  $\sqrt{s} = 5.02$  TeV,  $R_{pA}$  of both  $D$  and  $B$  productions show large depletion even at mid rapidity as seen in Fig. 5.7 (b). Since the large colliding energy of the LHC gives rise to much smaller  $x_2 < x_0$  of participating gluons (Fig. 5.1 (b)–(d)), small- $x$  effects have already become relevant at mid rapidity, and even  $B$  production shows a suppression with increasing rapidity.

Here, we compare  $R_{pA}$  for  $D$  and  $J/\psi$  productions as a function of rapidity at (a)  $\sqrt{s} = 200$  GeV and (b)  $\sqrt{s} = 5.02$  TeV in Fig. 5.7. We notice that  $J/\psi$  production is more suppressed than  $D$  meson. This is because, in addition to the saturation effects of the initial gluons, the produced quark pair experiences the multiple scatterings with the gluons in the target. This effect increases the invariant mass of the pair on average. In the CEM, if the quark pair is kicked beyond the invariant mass threshold, the quark pair cannot bound into the quarkonium, which results in a stronger suppression of the quarkonium than the  $D$  meson production. We have also found that  $\Upsilon(1S)$  is more suppressed than  $B$  in our calculation, although it is not shown here.

## 5.6 Azimuthal angle correlation

Pair production of open heavy flavor covers wider kinematic region of the participating partons than quarkonium production. In this subsection we examine nuclear modification of the azimuthal angle correlation of the heavy meson pair  $h\bar{h}$  in pA collisions [55, 122].

Although azimuthal angle correlation measurement for charmed meson pair is inaccessible at RHIC so far due to limited statistics, LHCb collaboration recently measured the angle correlation at forward rapidity in pp collisions [119, 123]. We expect that it will become also available in AA collisions at the LHC. In AA collisions, the interactions of the heavy quarks with the hot medium will distort the angle correlation of the pair and may generate a new correlation by collective flow [124]. For a precise evaluation, again, we need to take account of the initial state effects.

We define the azimuthal angle correlation between  $h$  and  $\bar{h}$  as the pair-production multiplicity per event integrated over certain momentum and rapidity ranges with fixed angle  $\Delta\Phi$  between the pair:

$$CP[\Delta\Phi] = \frac{2\pi}{N_{\text{tot}}} \int p_{h\perp} dp_{h\perp} p_{\bar{h}\perp} dp_{\bar{h}\perp} dy_h dy_{\bar{h}} \frac{dN_{h\bar{h}}}{d^2\mathbf{p}_{h\perp} d^2\mathbf{p}_{\bar{h}\perp} dy_h dy_{\bar{h}}}, \quad (5.8)$$

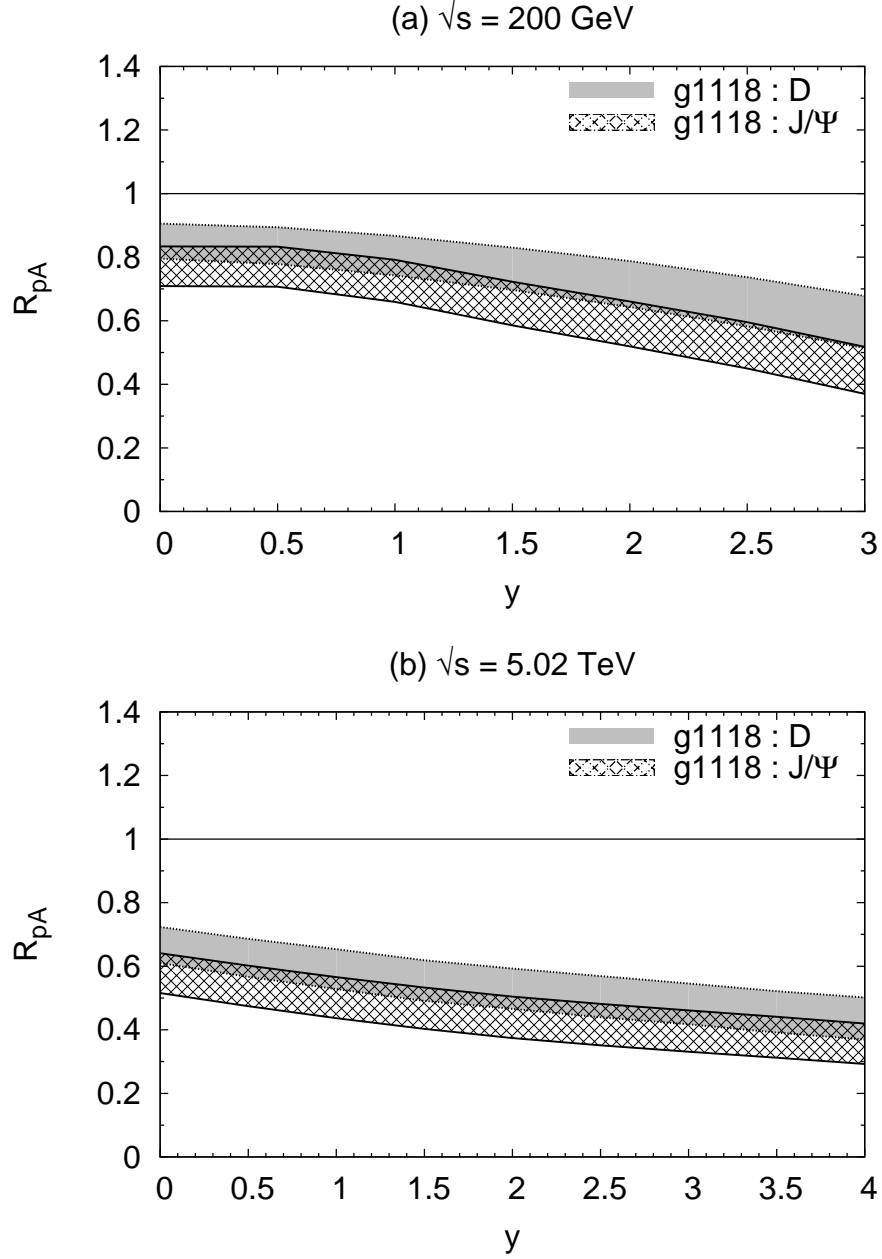


Figure 5.8: Nuclear modification factor  $R_{pA}$  for  $D$  and  $J/\psi$  vs  $y$  in pA collisions at (a)  $\sqrt{s} = 200$  GeV and (b)  $\sqrt{s} = 5.02$  TeV. The bands indicate the uncertainties from the variations  $m_c = 1.2 - 1.5$  GeV and  $Q_{s0,A}^2 = (4 - 6)Q_{s0,p}^2$ .

where  $N_{\text{tot}}$  is the pair multiplicity per event integrated over the same kinematic region and further integrated over the angle between the pair. The pair production cross-section of the heavy mesons is given in Eq. (5.1).

### 5.6.1 pp collisions

We compute the azimuthal angle correlation in  $D^0\bar{D}^0$  pair production at the forward rapidity in pp collisions at  $\sqrt{s} = 7$  TeV, using the uGD sets g1118 and MV for studying the sensitivity to the initial condition. We use  $m_c = 1.5$  GeV. In order to compare the result with LHCb data [119], we set the kinematical range as  $2 < y_D, y_{\bar{D}} < 4$  and  $3 < p_{D\perp}, p_{\bar{D}\perp} < 12$  GeV, as plotted in Fig. 5.9 (a). In [119] the bin size of the azimuthal angle is chosen as  $\Delta\Phi/\pi = 0.05$ .

We immediately notice the near-side ( $|\Delta\Phi| \sim 0$ ) and away-side ( $|\Delta\Phi| \sim \pi$ ) enhancements in the numerical result. The away-side peak is naturally expected from the back-to-back kinematics of the LO quark-pair production from two gluons in the collinear factorization framework, but no near-side peak can be explained unless the higher-order processes are considered. In the CGC framework, on the other hand, gluon bremsstrahlung and multiple scatterings, which are encoded in  $\phi_p^{q\bar{q},g}$ , provide *intrinsic transverse momentum*  $k_\perp \sim Q_s$  of incident gluons. This  $k_\perp$  smears the away-side peak and generates the near-side peak in the angle correlation. In the LHCb data, indeed, we see the near-side peak but an only subtle away-side enhancement. The numerical result with set MV fairly reproduces this LHCb angle correlation, whereas in the result with set g1118 the away-side peak still remains. This is presumably reflecting the fact that the uGD set MV has harder  $k_\perp$  spectrum than set g1118. But one should recall that the uGD set MV is already disfavored in the global fit [53, 54] and in hadron production analysis at collider energies [56, 58].

The invariant mass spectrum of  $D^0\bar{D}^0$  pair production in pp collisions at  $\sqrt{s} = 7$  TeV is also measured in [119]. We compare in Fig. 5.9 (b) our numerical results with the data. The bin size for  $M$  is 0.5 GeV. The dip structure seen at low  $M$  is understood as the effect of the lower momentum cut at 3 GeV. Apparently the numerical result yields much harder invariant mass spectrum than the observed data.

Several remarks are here in order: First, large  $M$  pair production probes the gluons at large  $x_1$ , where as explained in Sec. 2 we extrapolate the uGD with a simple Ansatz (3.64), which is likely to overestimate the uGD in large  $x$  region and needs more refinement. Furthermore the back-to-back kinematics corresponds to the pair with the large  $M$  and

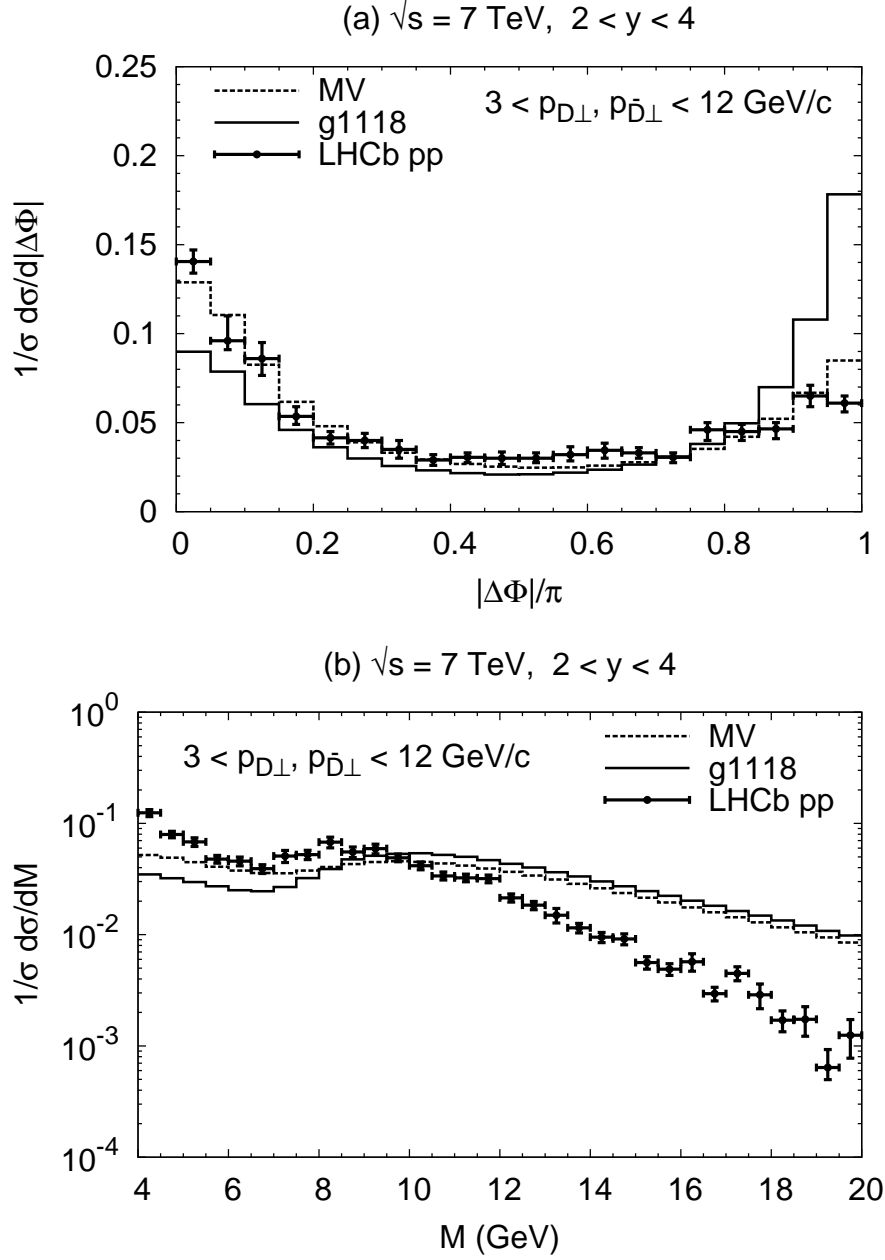


Figure 5.9: Azimuthal angle correlation (a) and invariant mass  $M_{D\bar{D}}$  spectrum of  $D^0\bar{D}^0$  pair production (b) in the rapidity and transverse momentum coverages,  $2 < y_D, y_{\bar{D}} < 4$  and  $3 < p_{D\perp}, p_{\bar{D}\perp} < 12 \text{ GeV}$  in pp collisions at  $\sqrt{s} = 7 \text{ TeV}$ , normalized by the total cross-section in the same fiducial region. For binning,  $\Delta\Phi/\pi = 0.05$  in (a) and  $\Delta M = 0.5 \text{ GeV}/c^2$  in (b). Solid line denotes numerical result of Eq. (5.1) with uGD set g1118, the data points with error bars are taken from [119].



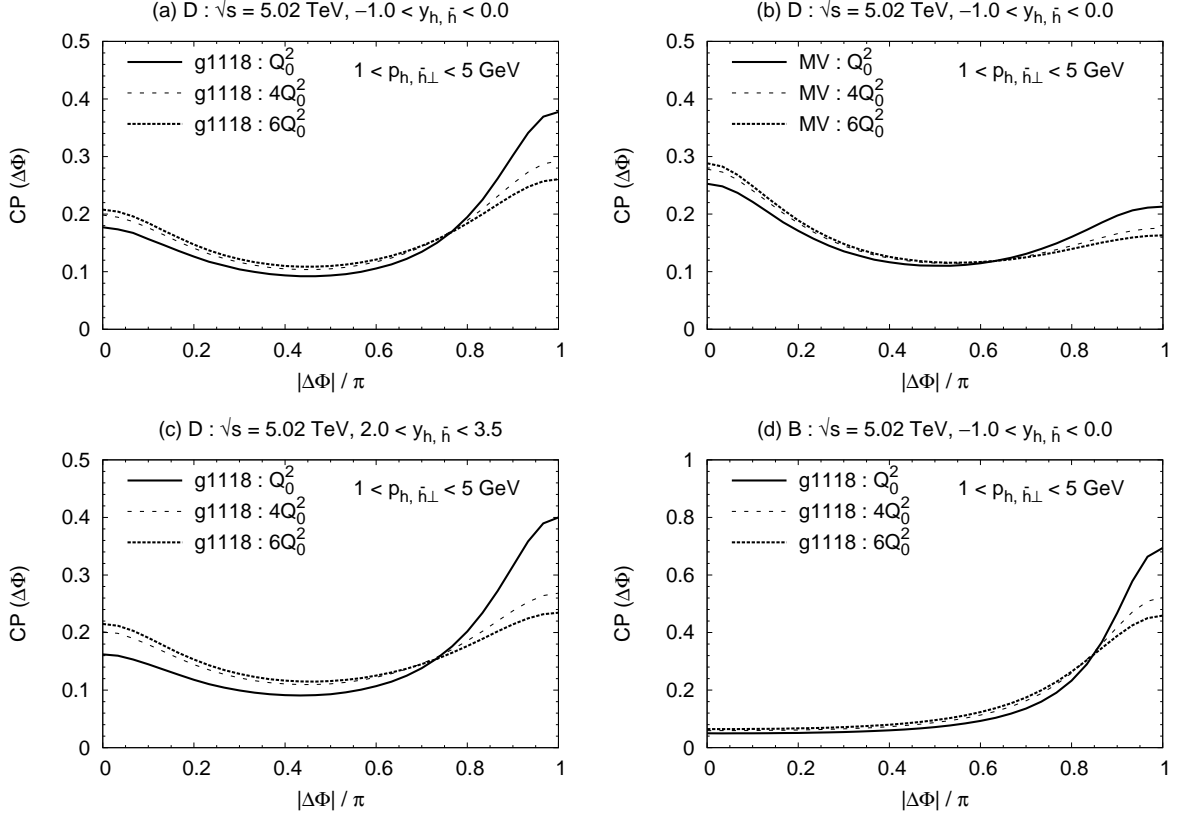


Figure 5.10: Nuclear modification of azimuthal angle correlation of heavy meson pair production in pA collision at  $\sqrt{s} = 5.02$  TeV. Results with the initial saturation scale  $Q_0^2$ ,  $4Q_0^2$  and  $6Q_0^2$  are plotted in solid, dashed and dotted lines, respectively. (a)  $D\bar{D}$  correlation with set g1118 for  $-1 < y_{h,\bar{h}} < 0$ , (b) the same as (a) but with set MV, (c) the same as (b) but for  $2 < y_{h,\bar{h}} < 3.5$ , and (d)  $B\bar{B}$  correlation with set g1118 for  $-1 < y_{h,\bar{h}} < 0$ . The momentum coverage is  $1 < p_{h,\bar{h}\perp} < 5$  GeV, and  $m_c = 1.5$  GeV for  $D\bar{D}$  and  $m_b = 4.8$  GeV for  $B\bar{B}$ .

small transverse momentum, where soft gluon emissions will be important and should be resummed [150]. Regarding small  $M$  pair on the near-side, full NLO extension of the pair production formula may be important although gluon splitting processes are partially included in the LO CGC formula (3.44).

## 5.6.2 pA collisions

Here we discuss modification of the azimuthal angle correlation between open heavy flavor meson ( $h$ ) and open anti-flavor meson ( $\bar{h}$ ) in pA collisions at  $\sqrt{s} = 5.02$  TeV. We set the momentum coverage to  $1 < p_{h\perp}, p_{\bar{h}\perp} < 5$  GeV.

In Fig. 5.10 (a) we plot the numerical result obtained with uGD set g1118 for the  $D\bar{D}$  production at mid rapidity ( $-1 < y < 0$ ). The away-side peak seen at  $|\Delta\Phi| \sim \pi$  in pp collisions (initial scale  $Q_0^2$ ) is gradually suppressed in pA collisions with increasing the (initial) saturation scale in the nucleus as  $(4 - 6)Q_0^2$ , while the near-side peak is slightly enhanced. This is due to the stronger multiple scatterings and saturation effects in the heavy nucleus. Then nuclear effects make  $D\bar{D}$  correlation at low momentum closer to isotropic distribution. For comparison, we show the same plot but with the uGD set MV in Fig. 5.10 (b). Stronger enhancement of the correlation on the near side than on the away side is seen with increasing the saturation scale of the uGD in the nucleus. Different uGD sets result in quantitatively different correlation, but the qualitative features remain the same.

The nuclear modification of the angle correlation becomes more prominent in the forward rapidity region as seen in Fig. 5.10 (c). We have also computed the angle correlation in higher momentum region,  $5 < p_{h,\bar{h}\perp} < 10$  GeV. We saw a strong away-side peak suppressed in pA collisions than in pp, while the near-side structure is unaffected. Note that the transverse momentum on the near side is provided solely by the intrinsic  $k_\perp$  of the gluons in (5.5). The gluon saturation at  $k_\perp \lesssim Q_s$  does not affect the particle production in such a high momentum region.

Finally, let us study  $B\bar{B}$  correlations in the same kinematic region as  $D\bar{D}$ , to see the quark mass dependence of the correlation. As seen in Fig. 5.10 (d), despite that the momentum region is as low as in Fig. 5.10 (a), we do not confirm any correlation on the near side since intrinsic momentum of gluon is still insufficient to produce the pair there. The away-side peak exists and is suppressed with increasing  $Q_{A,0}^2(x_0)$ .

## 5.7 Short summary

In this chapter, we have shown the numerical results of  $D$  and  $B$  meson productions in pA collisions at the collider energy.

At RHIC energy, numerical result with the constrained gluon distribution g1118 fairly reproduces single  $D$  meson spectrum data at mid-rapidity in pp and pA collisions, whereas the result with set MV is too hard. The nuclear modification factor  $R_{\text{pA}}$  of  $D$  shows a suppression at low  $p_\perp$  and a Cronin-like enhancement at larger  $p_\perp$  reflecting the multiple scattering effects implemented in the initial gluon distribution at  $x = x_0$ . In contrast,  $R_{\text{pA}}(p_\perp)$  of  $B$  is almost flat in  $p_\perp$ .

At LHC energy,  $D^0$  production with constrained gluon distribution g1118 reasonably reproduces the  $p_\perp$ -dependence of the mid-rapidity data in pp collisions. The  $R_{pA}$  of  $D$  shows stronger suppression at low  $p_\perp$  and no enhancement in the computed  $p_\perp$  region. The  $R_{pA}(y)$  for  $p_\perp$ -integrated multiplicity shows a systematic suppression from mid rapidity to forward rapidity, which is due to the quantum  $x$ -evolution effect of the gluons in the heavy nucleus. We have also found that the  $R_{pA}(y)$  of  $J/\psi$  production is more suppressed than that of  $D$  production.

The azimuthal angle correlation for  $D\bar{D}$  and  $B\bar{B}$  pair in pp and pA collisions at LHC energy shows that the near-side peak emerges in  $D\bar{D}$  correlation in addition to the smeared away-side peak. The near-side peak is also seen in LHCb pp data [119]. We have a difficulty to reproduce quantitatively the angle correlation and the invariant mass spectrum of the pp data at the same time. Nevertheless, we have calculated the  $D\bar{D}$  correlation in pA collisions, in order to estimate qualitatively the nuclear dependence of the saturation effect. We have found that the away-side peak is more smeared and the near-side peak is slightly enhanced for the larger saturation scale, i.e., with the heavier nucleus and/or at more forward rapidity. For  $B\bar{B}$  correlation, we do not see the near-side peak. This is probably because the saturation scale is not large enough to produce the  $B\bar{B}$  in the same azimuthal direction.

# Chapter 6

## Impact parameter dependence of $J/\psi$ Nuclear modification factor

We investigate the dependence of  $R_{pA}$  on the saturation scale parameter  $Q_{s0,A}^2$ , which may be translated to the effective thickness of the target. We can effectively translate the initial saturation scale dependence of  $R_{pA}$  shown in previous section into the effective impact parameter dependence in the heavy nucleus.

### 6.1 $Q_{s0,A}^2$ dependence of $R_{pA}$ of $J/\psi$

In this section, we compute  $R_{pA}$  of  $J/\psi$  integrated over  $P_\perp$  as a function of  $Q_{s0,A}^2$  at several values of  $y$ . We fix here the uGD set g1118 and the quark masses as  $m_c = 1.5$  GeV. In Fig. 6.1 we plot  $R_{pA}$  of  $J/\psi$  at  $\sqrt{s} = 200$  GeV and  $\sqrt{s} = 5.02$  TeV. We found that for each rapidity  $Q_{s0,A}^2$ -dependence of  $R_{pA}$  can be fitted nicely by a model function:

$$R_{pA} = \frac{a}{(b + Q_{s0,A}^2)^\alpha} \quad (6.1)$$

with  $a$ ,  $b$  and  $\alpha$  being fitting parameters<sup>1</sup>. This functional form is motivated by QCD analog of superpenetration of a electron-positron pair through a medium [67, 101]. The stronger suppression at the larger value of  $Q_{s0,A}^2$  is naturally understood as a result of stronger multiple scatterings and saturation effects in the heavier target

---

<sup>1</sup>We can fit the  $R_{pA}$  of  $\Upsilon(1S)$  production at  $\sqrt{s} = 5.02$  TeV by the same function, which is not shown here. Energy and rapidity dependences may be qualitatively inferred from the increase of  $Q_{s,A}^2(y)$  as increasing  $y$ . Thus we tried to fit the rapidity dependence of  $R_{pA}$  by replacing in Eq. (6.1)  $Q_{s0,A}^2 \rightarrow Q_{s0,A}^2 e^{\lambda y}$  with a free parameter  $\lambda$ , but it was unsuccessful.

Energy and rapidity dependences may be qualitatively inferred through the increase of  $Q_{s,A}^2(y)$  with increasing  $y$ . We remark here that quarkonium suppression due to parton saturation in our treatment is twofold: a relative depletion of the gluon source and multiple scatterings of the quark pair in the target. The latter disturbs the bound state formation, by increasing the pair's invariant mass on average in CEM [102]. It appears hard to describe energy and rapidity dependence of the suppression at the same time through a single function  $Q_{s,A}^2(x)$ .

In Table 6.1, we list the specific numerical values of the least chi-square fitting of  $R_{pA}$  of  $J/\psi$  integrated over  $P_\perp$  as a function of  $Q_{s0,A}^2$  by simple parametrized function at each rapidity.

## 6.2 Revisit the definition of $R_{pA}$

We define  $R_{pA}$  of the  $J/\psi$  production in our model as

$$R_{pA}(\mathbf{b}, y) = \frac{\frac{1}{\sigma_{inel}^{pA}} \frac{d\sigma_{J/\psi}^{pA}(\mathbf{b})}{dy}}{N_{coll}(\mathbf{b}) \cdot \frac{1}{\sigma_{inel}^{pp}} \frac{d\sigma_{J/\psi}^{pp}}{dy}}, \quad (6.2)$$

where the cross sections are integrated over  $P_\perp$ . in this paper, we replace  $\sigma_{inel}^{pp}$  with  $\sigma_{inel}^{NN}$  for nucleon-nucleon collisions.

We shift the saturation scale for heavy nucleus as

$$Q_{s0,A}(\mathbf{b}) = N_{coll}^{1/\gamma}(\mathbf{b}) Q_{s0,p} \quad (6.3)$$

since the uGD  $\phi_{A,y_0}(\mathbf{k}_\perp)$  in (3.44) scales as  $(Q_{s0,A}^2)^\gamma$  at large  $k_\perp$ . We also consider another simple expression given by

$$Q_{s0,A}(\mathbf{b}) = N_{coll}(\mathbf{b}) Q_{s0,p}. \quad (6.4)$$

Through this chapter, we call Eq. (6.4) natural definition and Eq. (6.3) effective definition [14]. Within these definitions, the uncertainties of  $R_{pA}$  exist.

In the rest of this chapter, we will show the model in our calculations describing  $\sigma_{inel}^{pA}$  and  $N_{coll}(\mathbf{b})$ . Of particular importance of this calculations is that we include the impact parameter dependence in the saturation scale explicitly. Our aim in this chapter is to clarify whether we should explicitly include the impact parameter dependence in the

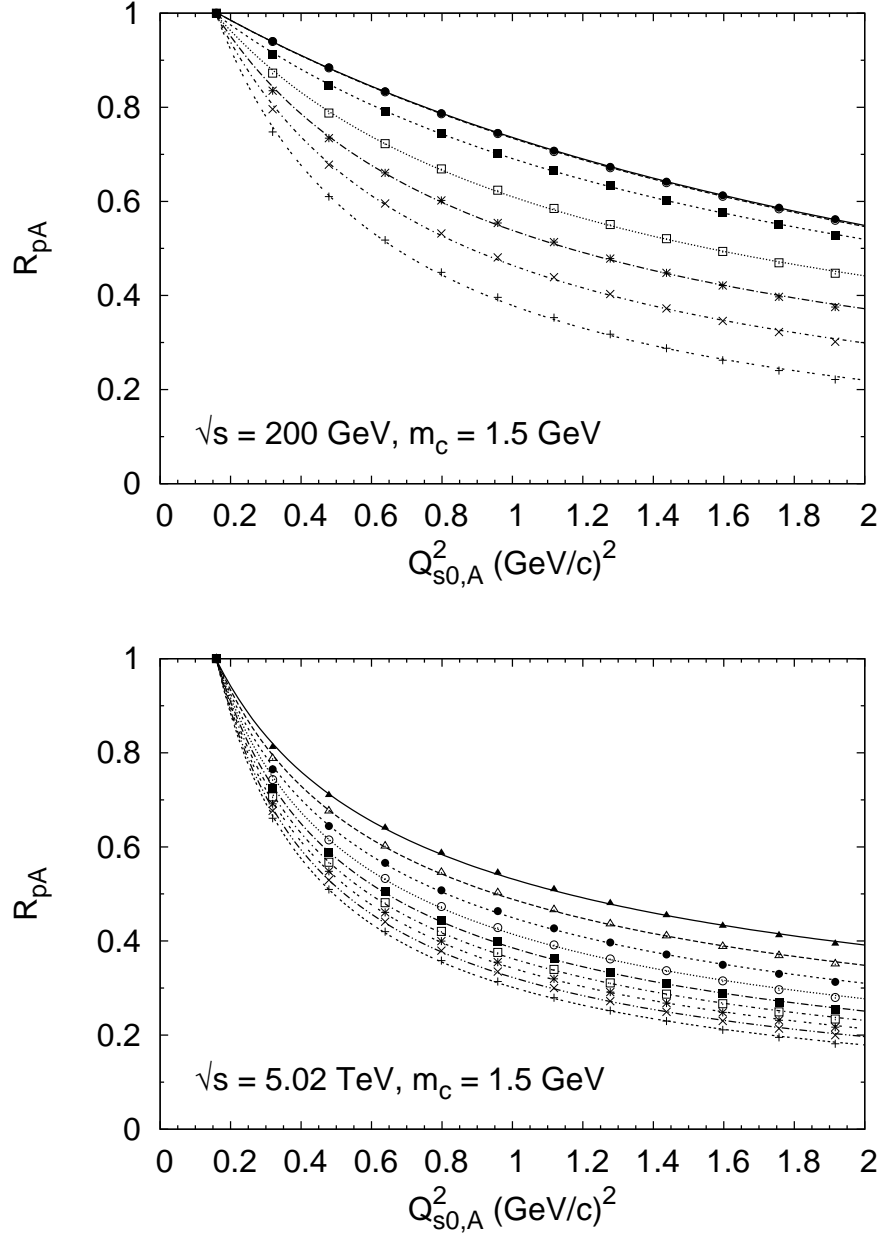


Figure 6.1: Nuclear modification factor  $R_{pA}$  for  $J/\psi$  as a function of  $Q_{s0,A}^2$  at  $y = 0 - 3$  with respect to each 0.5 rapidity interval at  $\sqrt{s} = 200 \text{ GeV}$  and at  $y = 0 - 4$  with respect to each 0.5 rapidity interval at  $\sqrt{s} = 5.02 \text{ TeV}$ . We choose charm quark mass as  $m_c = 1.5 \text{ GeV}$ . Fitted curves are also shown.

$\sqrt{s} = 200 \text{ GeV}$						
$m_c = 1.5 \text{ GeV}$				$m_c = 1.2 \text{ GeV}$		
y	$A_y$	$B_y$	$C_y$	$A_y$	$B_y$	$C_y$
0.0	4.93	3.11	1.35	8.89	3.42	1.71
0.5	5.08	3.13	1.36	8.53	3.36	1.70
1.0	1.26	1.20	0.762	1.31	1.20	0.901
1.5	0.844	0.622	0.671	0.846	0.653	0.785
2.0	0.697	0.442	0.703	0.681	0.463	0.800
2.5	0.596	0.366	0.799	0.574	0.378	0.886
3.0	0.499	0.330	0.967	0.475	0.332	1.042

$\sqrt{s} = 5.02 \text{ TeV}$						
$m_c = 1.5 \text{ GeV}$				$m_c = 1.2 \text{ GeV}$		
y	$A_y$	$B_y$	$C_y$	$A_y$	$B_y$	$C_y$
0.0	0.575	0.169	0.496	0.550	0.181	0.554
0.5	0.526	0.146	0.540	0.502	0.156	0.596
1.0	0.483	0.130	0.585	0.459	0.138	0.641
1.5	0.445	0.117	0.630	0.422	0.125	0.686
2.0	0.412	0.105	0.665	0.389	0.112	0.723
2.5	0.386	0.094	0.693	0.363	0.101	0.752
3.0	0.364	0.087	0.722	0.341	0.092	0.779
3.5	0.343	0.083	0.755	0.321	0.087	0.811
4.0	0.321	0.080	0.796	0.300	0.084	0.851

Table 6.1: The parameter sets of least squared fitting  $R_{\text{pA}}$  of the  $J/\psi$  with parametrized function Eq. (6.11) at  $\sqrt{s} = 200 \text{ GeV}$  and  $5.02 \text{ TeV}$  :  $R_{\text{pA}} = A_y/(B_y + Q_{s,A0}^2)^{C_y}$  with  $m_c = 1.5$  and  $1.2 \text{ GeV}$ .

heavy nucleus or we can exchange  $N_{coll}(\mathbf{b})$  with effective value in the minimum bias event.

### 6.3 Semi-classical description of proton-nucleus collisions

Here, we approximate a density of atomic mass number as

$$\rho_A = \frac{A}{\frac{4}{3}\pi R_A^3} \sim 1.17\text{fm}^{-3} . \quad (6.5)$$

In general,  $\rho_A$  might depend on a configuration of nucleon within the nucleus which is characterized with impact parameter:  $\mathbf{b}$  in the transverse plane and longitudinal position:  $z$  [58].

Then, we can define a nuclear thickness function given by

$$T_A(\mathbf{b}) = \int dz \rho_A = \frac{3A}{2\pi R_A^3} \sqrt{R_A^2 - b^2} \theta(R_A - b) , \quad (6.6)$$

with the density of the nuclear mass number (6.5). This function is of course normalized as  $\int d^2\mathbf{b} T_A(\mathbf{b}) = A$ . Thickness function takes a crucial role for the calculation of impact parameter dependence of  $R_{pA}$  for the  $J/\psi$  production.

Using the semi-classical Glauber theory, the number of overlapping nucleons at the impact parameter  $\mathbf{b}$  in proton-nucleus collisions is given by

$$N_{coll}(\mathbf{b}) = \int d^2\mathbf{s} \sigma_{inel}^{NN} T_A(\mathbf{s}) T_p(\mathbf{s} - \mathbf{b}) = \sigma_{inel}^{NN} T_A(\mathbf{b}) , \quad (6.7)$$

where the thickness function of the proton has been assumed to be  $T_p(\mathbf{s} - \mathbf{b}) = \delta(\mathbf{s} - \mathbf{b})$ . (See Fig. 6.2.) Here  $\sigma_{inel}^{NN}$  is an input parameter to estimate  $N_{coll}$  at  $x = x_0$  encoded into the saturation scale. Initial saturation scale is proper to the heavy nucleus, therefore we should take  $\sigma_{inel}^{NN}$  as energy independent one. Here  $\sigma_{inel}^{NN} = 42$  mb is used for the calculation of both RHIC and LHC energy.

Next, we present briefly how to obtain the total inelastic cross section in pA collisions. We take  $n$  as the number of nucleon-nucleon collision in pA collisions and  $(A - n)$  as the number of binary nucleon's pair passing through each other. Following the Glauber



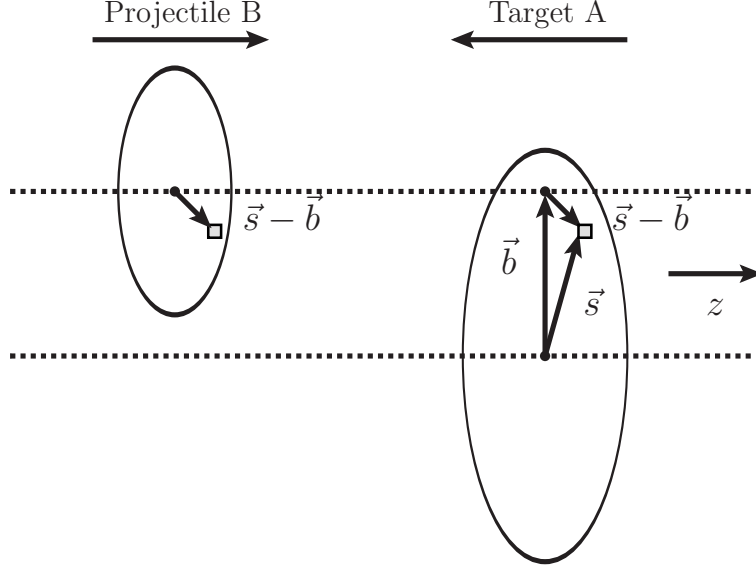


Figure 6.2: Schematic representation of the Glauber Model geometry, with transverse views.

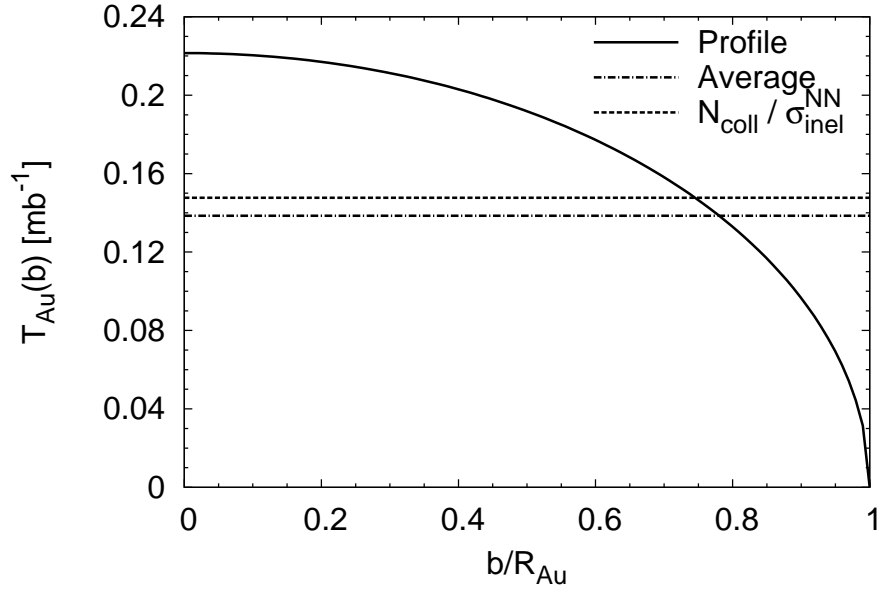


Figure 6.3: Thickness function  $T(b)$  plotted by using Eq. (6.6) which is compared with averaged thickness labeled *Average*. We also plot the value  $N_{coll}/\sigma_{inel}^{NN}$  for MB event.

theory,

$$\frac{d^2\sigma_{inel}^{pA}}{db^2} = \left\{ \sum_{n=1}^A \binom{A}{n} \left[ \hat{T}_A(b) \sigma_{inel}^{NN} \right]^n \left[ 1 - \hat{T}_A(b) \sigma_{inel}^{NN} \right]^{A-n} \right\}, \quad (6.8)$$

where  $\hat{T}_A(b) = T_A(b)/A$ . Therefore, total inelastic cross section in pA collisions is given by

$$\sigma_{inel}^{pA} = \int d^2b \left\{ 1 - \left[ 1 - \hat{T}_A(b) \sigma_{inel}^{NN} \right]^A \right\}. \quad (6.9)$$

Now we have replaced  $T_A(\mathbf{b}) = T_A(b)$  since  $T_A(\mathbf{b})$  is the scalar function given in Eq. (6.5).

Finally, we remark a centrality which is measured in the experiences. Centrality corresponds to the ratio of produced J/ $\psi$  cross section in the certain range of impact parameter to its total cross section. The cross section at  $\mathbf{b} \sim \mathbf{0}$  is larger than any other point in the impact parameter space in our model, then the centrality is measured from the center of target nucleus in the transverse plane. For instance,  $X\%$ -centrality for each rapidity means

$$\frac{\int_0^{b_X} 2\pi b db \frac{dN_{J/\psi}^{pA}(b)}{dy}}{\int_0^{R_A} 2\pi b db \frac{dN_{J/\psi}^{pA}(b)}{dy}} = \frac{X}{100}, \quad (6.10)$$

and we note the heavy nucleus has a sharp edge:  $\theta(R_A - b)$ .

## 6.4 Numerical Results

As stated above, we have found that for each rapidity  $Q_{s0,A}^2$ -dependence of  $R_{pA}$  can be fitted nicely by a following parametrized function:

$$R_{pA}(b, y) = \frac{\frac{1}{\sigma_{inel}^{pA}} \frac{d\sigma_{J/\psi}^{pA}(\mathbf{b})}{dy}}{N_{coll}(\mathbf{b}) \cdot \frac{1}{\sigma_{inel}^{pp}} \frac{d\sigma_{J/\psi}^{pp}}{dy}} \simeq \frac{\frac{1}{\pi R_A^2} \frac{d\sigma_{J/\psi}^{pA}(\mathbf{b})}{dy}}{N_{coll}(\mathbf{b}) \cdot \frac{1}{\pi R_p^2} \frac{d\sigma_{J/\psi}^{pp}}{dy}} = \frac{A_y}{(B_y + Q_{s0,A}^2(b))^{C_y}} \quad (6.11)$$

with  $Q_{s0,A}(\mathbf{b}) = N_{coll}^{1/\gamma}(\mathbf{b}) Q_{s0,p}$ .  $A_y$ ,  $B_y$  and  $C_y$  are fitting parameters at each rapidity, and specific values of these parameters are listed in Table. 6.1. This data analysis procedure can be also found in Ref. [67] but for different parameter set. Above suppression pattern

might be caused by the scattering of produced quark pair off the heavy nucleus coherently known as a QCD analog of superpenetration. in this paper, using the above expression of Eq. (6.11), we redefine  $R_{pA}$  as follows

$$R_{pA}^{\text{eff}}(b, y; Q_{s0,A}(\mathbf{b}) = N_{coll}^{1/\gamma}(\mathbf{b})Q_{s0,p}) = \frac{\frac{1}{\sigma_{inel}^{pA}} \frac{d\sigma_{J/\psi}^{pA}(\mathbf{b})}{dy}}{N_{coll}(\mathbf{b}) \cdot \frac{1}{\sigma_{inel}^{NN}} \frac{d\sigma_{J/\psi}^{pp}}{dy}} = \frac{A_y}{(B_y + Q_{s0,A}^2(b))^{C_y}} \cdot \frac{A^{2/3} \sigma_{inel}^{NN}}{\sigma_{inel}^{pA}} \quad (6.12)$$

for effective definition and

$$R_{pA}^{\text{nat}}(b, y; Q_{s0,A}(\mathbf{b}) = N_{coll}(\mathbf{b})Q_{s0,p}) = \frac{R_{pA}^{\text{eff}}(b, y; Q_{s0,A}(\mathbf{b}) = N_{coll}(\mathbf{b})Q_{s0,p}) \cdot N_{coll}^{\gamma}(\mathbf{b})}{N_{coll}(\mathbf{b})} \quad (6.13)$$

for natural definition.

In the minimum bias event,

$$\langle R_{pA}(y) \rangle_{\text{MB}} = \frac{\frac{1}{\pi R_A^2} \int d^2b \frac{dN_{J/\psi}^{pA}(b)}{dy}}{\frac{1}{\pi R_A^2} \int d^2b N_{coll}(b) \cdot \frac{dN_{J/\psi}^{pp}}{dy}} = \frac{\int d^2b R_{pA}(b, y) N_{coll}(b)}{\int d^2b N_{coll}(b)} \quad (6.14)$$

and for the centrality  $(X_1 - X_2)\%$ , we integrate the impact parameter over  $b \in [b_1, b_2]$ . We take  $R_A = A^{1/3} R_p$  with  $R_p = 1.12\text{fm}$  and  $A = {}^{197}\text{Au}$  at RHIC and  $A = {}^{208}\text{Pb}$  at LHC as default parameters in our calculations.

We show in Fig. 6.4 and Fig. 6.5 the  $R_{pA}$  of  $J/\psi$  production at  $\sqrt{s} = 200\text{ GeV}$  as a function of rapidity for each centrality, computed with Eq. (6.12) and (6.13). We found the results in the central collisions (0 – 20%) and the minimum bias event (0 – 100%), which is shown in Fig. 6.6, can reproduce the data at RHIC. On the other hand, for peripheral collisions (60 – 88%) it seems the discrepancies between our results and the data at forward rapidity.

Fig. 6.7 shows the  $R_{pA}$  in the minimum bias event at  $\sqrt{s} = 5.02\text{ TeV}$ . Contrast to the results at RHIC, the results indicate a stronger suppression of  $R_{pA}$  at forward rapidity, however, the data of the LHC provide the similar suppression of that of RHIC.

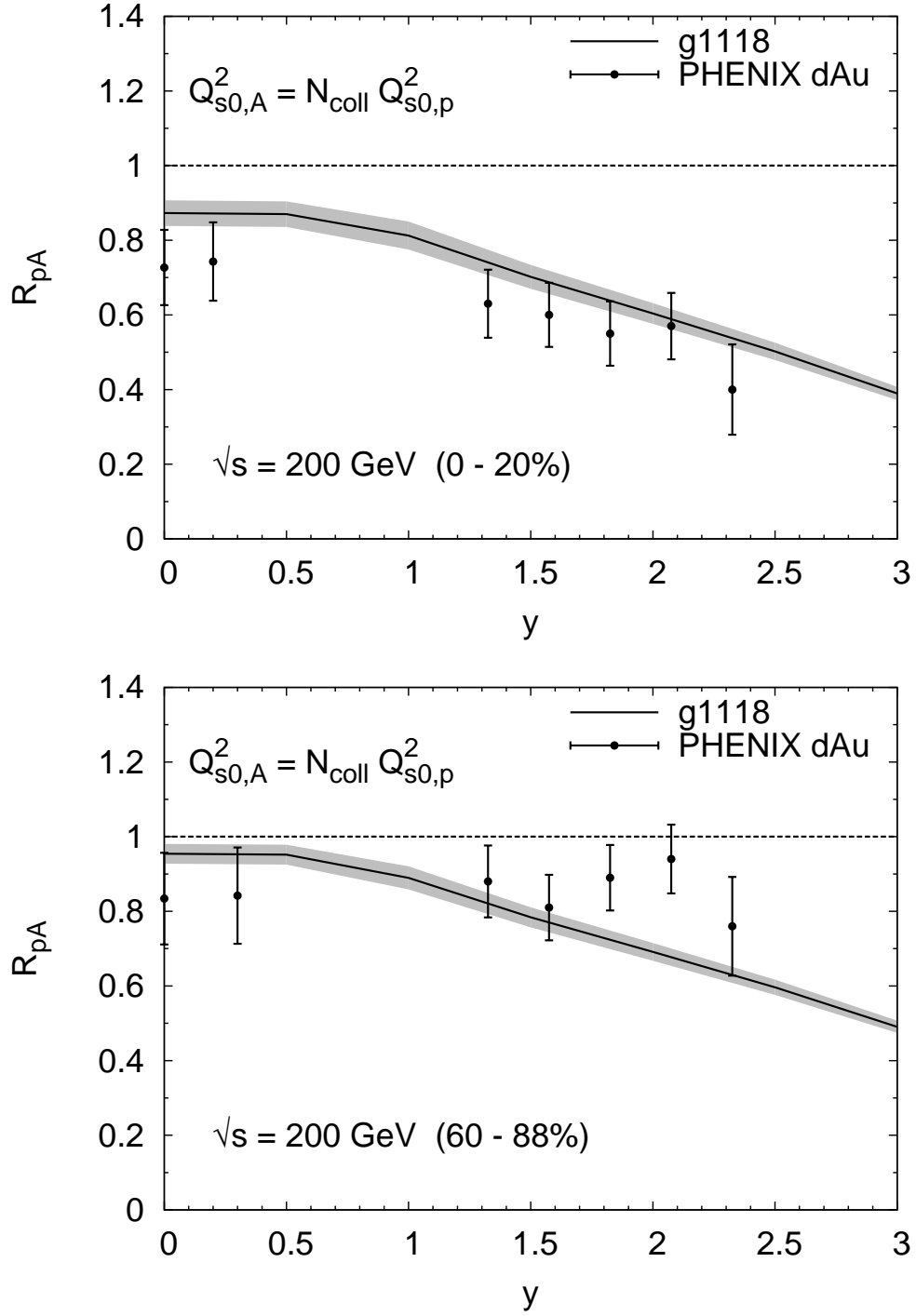


Figure 6.4: Nuclear modification factor as a function of rapidity at  $\sqrt{s} = 200$  GeV, for each centrality. Grey band includes uncertainty for changing the charm mass  $m_c = 1.2$  GeV to 1.5 GeV. Data at RHIC are taken from Ref. [106].

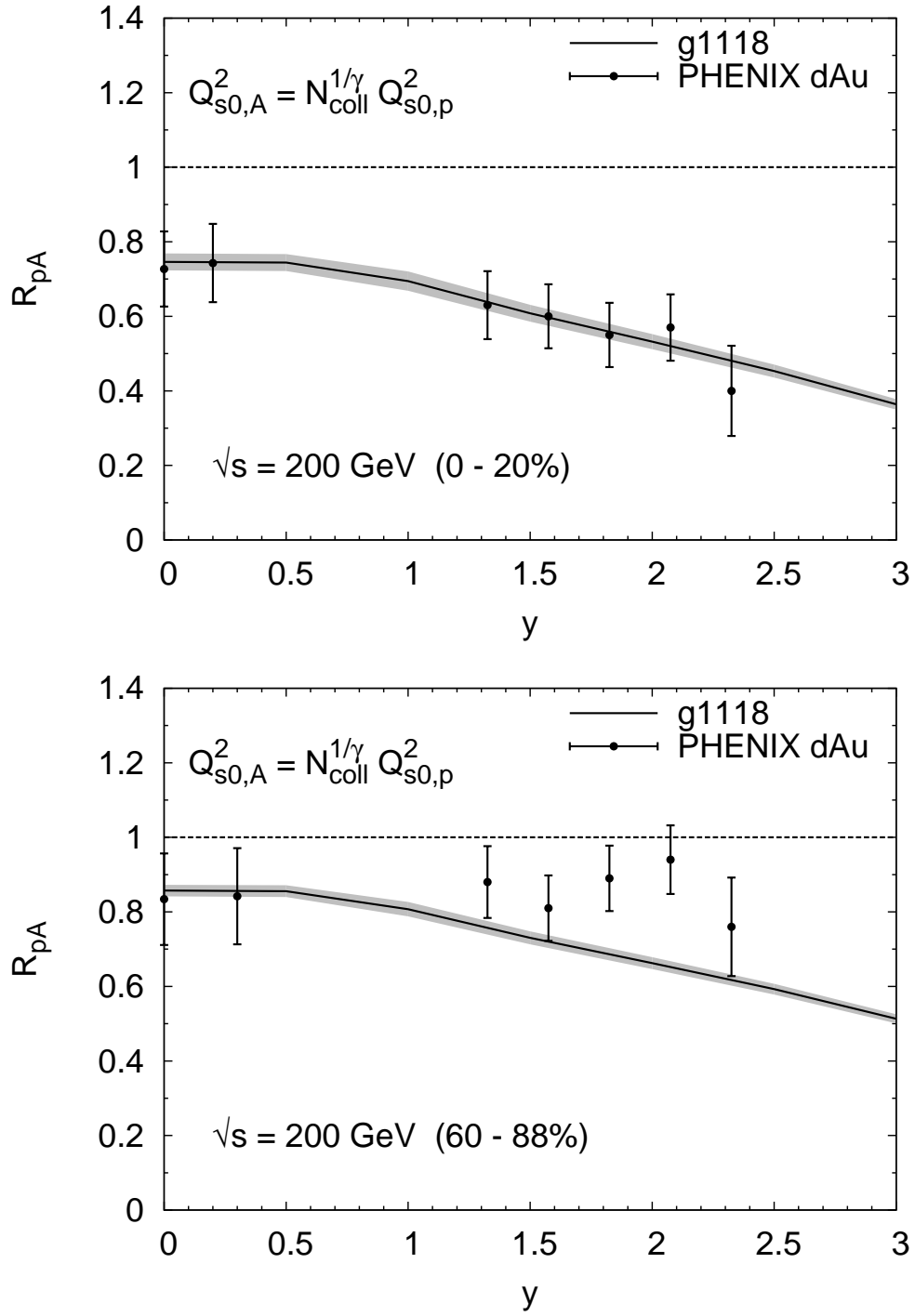


Figure 6.5: Nuclear modification factor as a function of rapidity at  $\sqrt{s} = 200$  GeV, for each centrality. Notations are the same as Fig. 6.4. Data at RHIC are taken from Ref. [106].

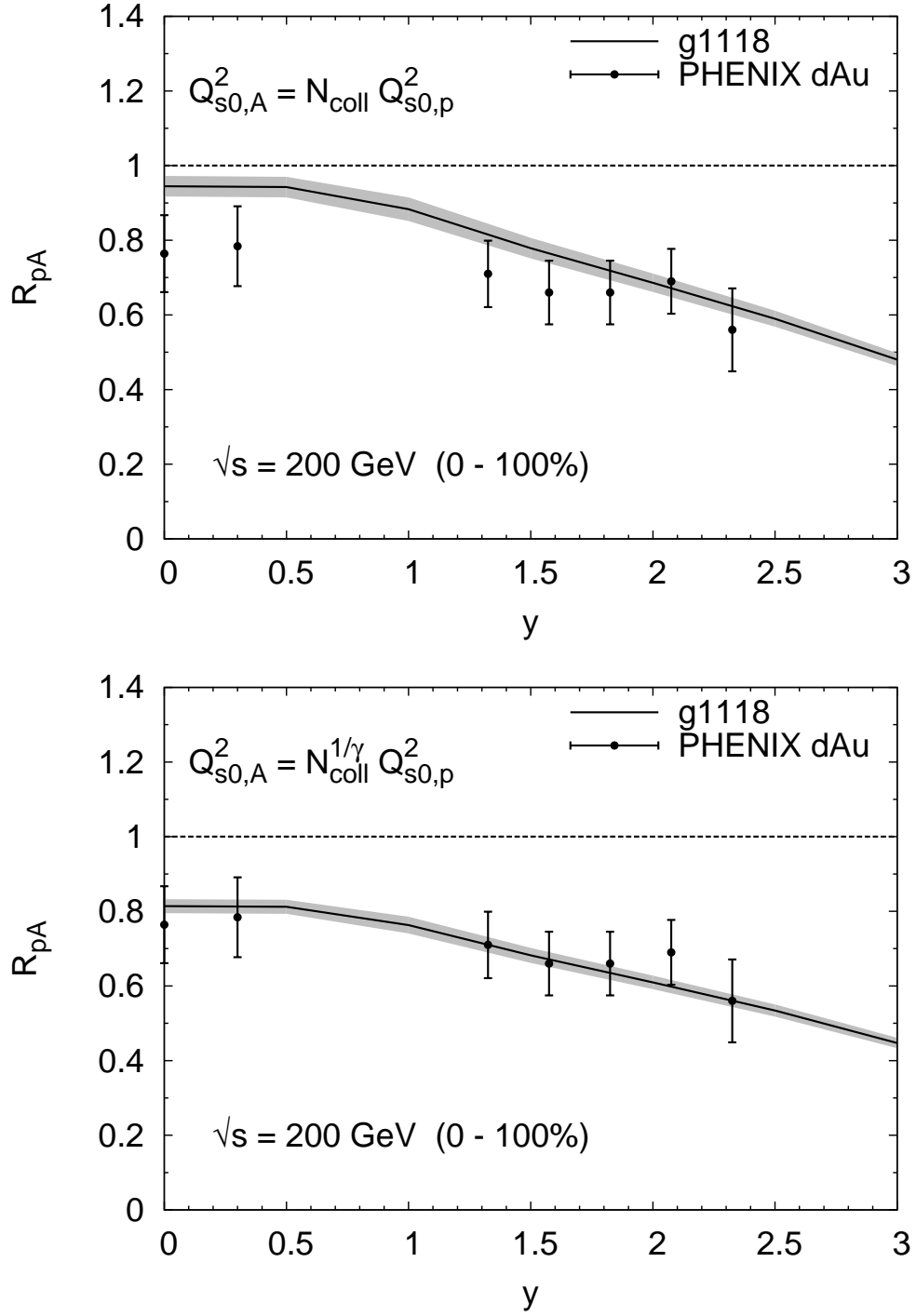


Figure 6.6: Nuclear modification factor as a function of rapidity at  $\sqrt{s} = 200$  GeV in the minimum bias event. Notations are the same as Fig. 6.4. Data at RHIC are taken from Ref. [106].

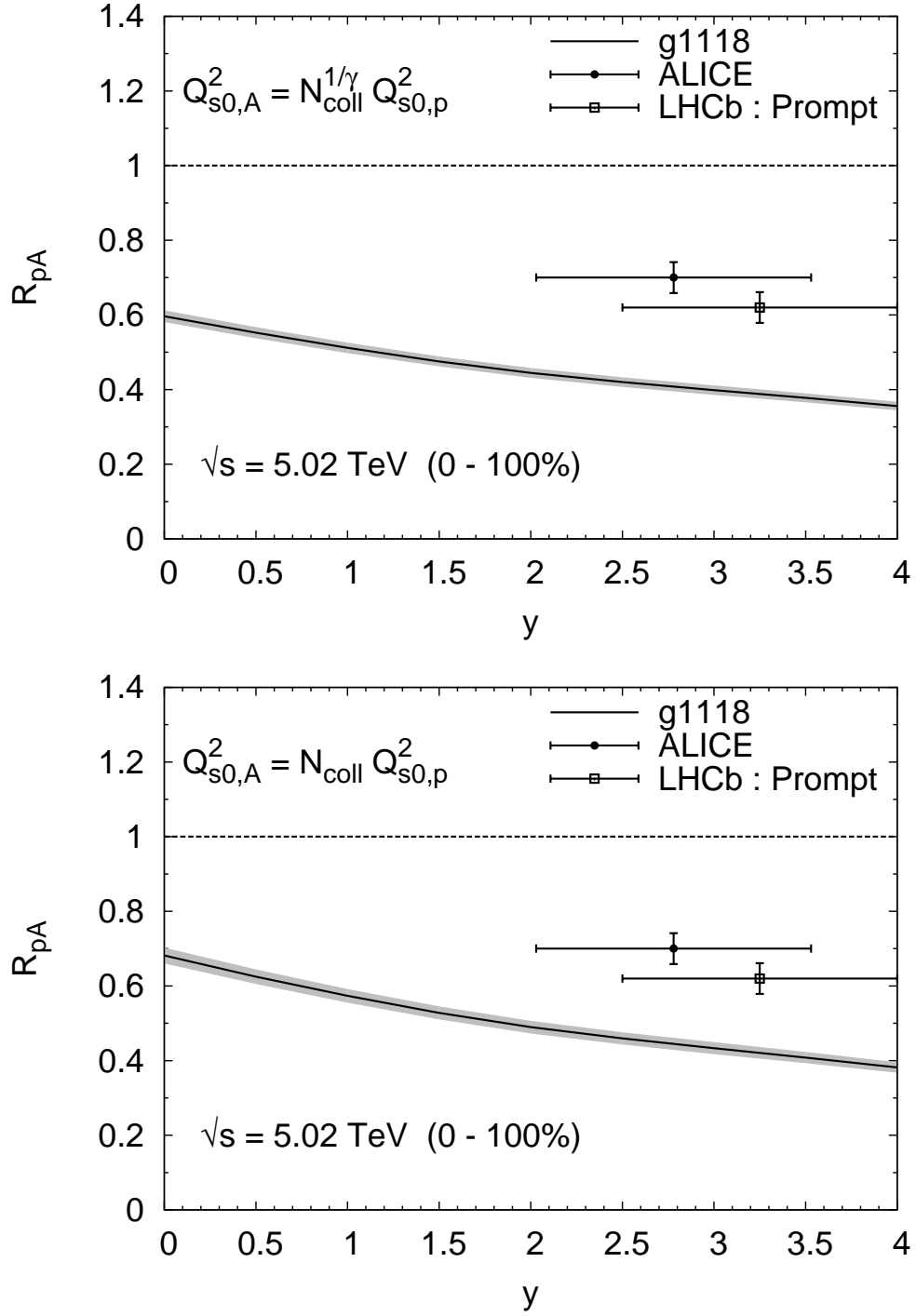


Figure 6.7: Nuclear modification factor as a function of rapidity at  $\sqrt{s} = 5.02$  TeV in the minimum bias event. Notations are the same as Fig. 6.4. Data at the LHC are taken from Ref. [108, 109].

## 6.5 Short summary

We have found the  $R_{pA}$  of quarkonium production as a function of initial saturation scale in the 3-point  $\phi^{q\bar{q},g}$  can be fitted nicely by simple model function. We have computed the effective centrality dependence of the nuclear modification factor of the quarkonium production, but we have found taking into account the nuclear profile does not modify the results in our model drastically. Namely, as to the minimum bias event, the results of the  $J/\psi$  production which are computed with the nucleus regarded as cylindrical is possibly reasonable in our computations. As to central collisions, we found our computations reproduce the data of the  $R_{pA}$  of the  $J/\psi$  production at RHIC qualitatively, on the other hand, it might be difficult to reproduce the data in peripheral collisions by use of the CGC model only. We can rather conclude that the peripheral are of the nucleus behaves like as a group of free nucleons then we should discuss the peripheral collisions carefully. In this paper, we have used the simple thickness function Eq. (6.6) with the constant nuclear density however, for example, the woods-saxon distribution, which is differ from Eq. (6.6) in a tail of the thickness function at edge of the nucleus, can change the results in the peripheral collisions. We leave a study of the thickness function dependence of the  $J/\psi$   $R_{pA}$  in the peripheral collisions in future work.

So far we have investigated only the initial interaction of the gluon coming from the nucleus to the heavy quark pair production. As to the quarkonium production, the fundamental quarkonium production mechanism is not fully understood even in elementary pp collisions. Then, a dynamics of bound state formation, which is the lack in our calculations, might modify the  $R_{pA}$  of the  $J/\psi$  quantitatively. In next chapter, we will consider the dynamics of quarkonium production in pA collisions by using a little sophisticated model in order to study whether the  $R_{pA}$  of the  $J/\psi$  is affected or not by the dynamics of the bound state.



## Chapter 7

# Quarkonium production within the NRQCD factorization approach

In the view of quantitative study, when we compare our results with data, we should include the other effects such as energy loss of the heavy quark in cold nuclear matter and a higher order corrections of the amplitude in terms of the coupling constant. Focusing on the saturation effect and the multiple scattering effect of the heavy quark pair production, our computation of the CGC shows in Chapter 4 that the stronger suppression of the  $R_{pA}$  of the  $J/\psi$  at low  $p_\perp$  and forward rapidity at the LHC as compared to the one at RHIC. However, the quarkonium production mechanism is not fully understood in elementary pp collisions yet, so that a dynamics of the bound state formation might modify the  $R_{pA}$  of the  $J/\psi$  quantitatively. In this chapter, we attempt to evaluate the direct quarkonium production from the heavy quark pair in the color singlet state in terms of the NRQCD factorization within the CGC framework<sup>1</sup>. Particularly, we focus on a direct quarkonium production taking a static limit as  $v \rightarrow 0$  with the relative velocity  $v$  between the quark and the antiquark in the quarkonium rest frame. In this case, the quarkonium production amplitude reduces to the same as the amplitude in the color singlet model exactly. Then, in other words, we investigate whether the color singlet model can contribute to the total quarkonium production cross section. If the quarkonium production cross section from the heavy quark pair in the color singlet state is remained a comparable order by comparing it with the total cross section of the quarkonium production, we can expect that the  $R_{pA}$  of the  $J/\psi$  at RHIC and also the LHC one become larger than our results in the color evaporation model which are shown in Fig. 4.14. This is because the background color

---

<sup>1</sup>Our model of the computation is similar to that found in Ref. [70].

field created in pA collisions does not affect the heavy quark pair in the color singlet state, whereas in the color evaporation model the heavy quark pair in the color octet state which is created in the initial collisions dominantly contributes to the quarkonium production later.

## 7.1 Quarkonium production cross section

Let us start by giving a general way to compute the quarkonium cross section in the CGC. We follow the discussion about one quark pair production as a reference, so then the cross section to produce exactly one quarkonium ( $\psi$ ) in pA collisions is defined by

$$\sigma_{\psi_Q} = \int d^2\mathbf{b} \int \mathcal{D}\rho_p \mathcal{D}\rho_A W_{Y_p}[\rho_p] W_{Y_A}[\rho_A] P_{\psi_Q}[\rho_p, \rho_A; \mathbf{b}] \quad (7.1)$$

with

$$P_{\psi_Q}[\rho_p, \rho_A; \mathbf{b}] = \int \frac{d^3\mathbf{P}}{(2\pi)^3 2E_P} \sum |\mathcal{M}_{\psi_Q}(P)|^2. \quad (7.2)$$

$P_{\psi_Q}[\rho_p, \rho_A; \mathbf{b}]$  is the probability to find a quarkonium with the given  $\rho_p$  and  $\rho_A$  at the impact parameter  $\mathbf{b}$ .  $\mathcal{M}_{\psi_Q}$  is a time-ordered amplitude to produce the quarkonium with spacial momentum  $\mathbf{P}$  and energy  $E_P$  at  $\mathbf{b}$ . Here, we consider only the minimum bias event then the impact parameter  $\mathbf{b}$  should be integrated out in Eq. (7.1). And we have also averaged the probability  $P_{\psi_Q}[\rho_p, \rho_A; \mathbf{b}]$  over  $\rho_p$  and  $\rho_A$  with the appropriate weight functions  $W_{Y_p}$  and  $W_{Y_A}$ . Then what we must do is to compute the quarkonium production amplitude  $\mathcal{M}_{\psi_Q}$ .

In order to compute it, we first consider the production amplitude of the heavy quark pair in the  $^{2S+1}L_J^{(1,8c)}$  state by inserting the projection operators in the final state [96] with use of Eq. (3.22);

$$\begin{aligned} & \mathcal{M}_{q\bar{q}} \left( q\bar{q} [^{2S+1}L_J^{(1,8c)}](P) \right) \\ &= \sum_{L_z, S_z} \sum_{s_1, s_2} \sum_{i, j} \int \frac{d^3l}{(2\pi)^3 2l^0} \delta \left( l^0 - \frac{l^2}{M} \right) Y_{LLz}(\hat{l}) \langle \tfrac{1}{2}, s_1; \tfrac{1}{2}, s_2 | S, S_z \rangle \langle L, L_z; S, S_z | J, J_z \rangle \\ & \quad \times \langle 3i; \bar{3}j | 1, 8c \rangle \mathcal{M}_F \left( q^i \left( \frac{P}{2} + l; s_1 \right) \bar{q}^j \left( \frac{P}{2} - l; s_2 \right) \right), \end{aligned} \quad (7.3)$$

where  $S$ ,  $L$ ,  $J$  are spin, angular momentum, and total spin of the heavy quark pair re-

spectively with  $S_z$ ,  $L_z$ ,  $J_z$  which are a component of  $S$ ,  $L$ ,  $J$  respectively. And  $Y_{LL_z}$  is spherical harmonics and  $M = 2m$ . The index 1 and 8c in the left hand side of Eq. (7.3) represent color singlet and octet state respectively. Before inserting the projection operators, the heavy quark (antiquark) has a spin component  $s_1$  ( $s_2$ ) and color  $i$  ( $j$ ) with the relative momentum  $l$  between the quark and the antiquark and the total momentum  $P$ .  $\delta$ -function for the relative energy in the right hand side of Eq. (7.3) restricts relative momentum to  $|\mathbf{l}| = \sqrt{Ml^0}$ . In the quarkonium rest frame, the kinetic energy of the system is estimated  $\sim Mv^2$  then the relative energy between the quark and the antiquark is assumed to  $l^0 \simeq Mv^2 \ll M = 2m$  if the relative velocity of the quark is enough small compared with the speed of light. Color projection operators in the  $SU(N_c)$  algebra are given by

$$\begin{aligned}\langle 3i; \bar{3}j | 1 \rangle &= \frac{\delta^{ji}}{\sqrt{N_c}} \\ \langle 3i; \bar{3}j | 8c \rangle &= \sqrt{2}(t^c)_{ji}\end{aligned}\tag{7.4}$$

for the color singlet and the octet state respectively. The relation between the differential cross section of the heavy quark pair production and the amplitude Eq. (7.3) is given by

$$\frac{d\sigma_{q\bar{q}}}{d\mathbf{P}_\perp^2 dy} = \int d^2\mathbf{b} \int \mathcal{D}\rho_p \mathcal{D}\rho_A W_{Y_p}[\rho_p] W_{Y_A}[\rho_A] \frac{1}{(2\pi)^3 2} \sum |\mathcal{M}_{q\bar{q}}(P)|^2.\tag{7.5}$$

where  $\mathbf{P}_\perp$  is the transverse momentum and  $y$  is the rapidity of the quark pair. We notice immediately Eq. (7.3) breaks the Lorentz invariance due to the  $\delta$ -function which depends on the frame dependent relative energy. However such Lorentz non-invariant terms should be compensated with other terms in the long distance matrix element of the heavy quark pair production. This is proper since the total cross section should be defined as the Lorentz invariant quantity.

To confirm this fact, let us consider the NRQCD factorization assumption;

$$d\sigma(q\bar{q}[^{2S+1}L_J^{(1,8c)}]) = C(q\bar{q}[^{2S+1}L_J^{(1,8c)}])_{\text{short}} \langle 0 | \mathcal{O}_{1,8c}^{q\bar{q}}(^{2S+1}L_J) | 0 \rangle.\tag{7.6}$$

This is the rewrite of Eq. (C.9) and the short distance coefficient  $C_{\text{short}}$  involving the heavy quark pair production is essential for computing the quarkonium cross section. As we discuss in Appendix C, once  $C_{\text{short}}$  is determined from Eq. (7.6) then we can compute the quarkonium production cross section with use of the same  $C_{\text{short}}$ . The amplitude

$\langle 0 | \mathcal{O}_{1,8c}^{q\bar{q}}(^{2S+1}L_J) | 0 \rangle$  is given in the NRQCD explicitly. Then, by combining Eq. (7.6) with Eq. (7.5), what we must do to obtain the differential cross section of the quarkonium production in the minimum bias event is computing the short distance coefficient as follows;

$$C(q\bar{q}[^{2S+1}L_J^{(1,8c)}])_{\text{short}} = \frac{1}{\langle 0 | \mathcal{O}_{1,8c}^{q\bar{q}}(^{2S+1}L_J) | 0 \rangle} \int d^2\mathbf{b} \int \mathcal{D}\rho_p \mathcal{D}\rho_A W_{Y_p}[\rho_p] W_{Y_A}[\rho_A] \frac{1}{(2\pi)^{32}} \sum |\mathcal{M}_{q\bar{q}}(P)|^2. \quad (7.7)$$

In Appendix C, we actually show the long distance matrix element  $\langle 0 | \mathcal{O}_{1,8c}^{q\bar{q}}(^{2S+1}L_J) | 0 \rangle$  also includes the Lorentz non-invariant  $\delta$ -function which is canceled out by the same  $\delta$ -function in the  $\mathcal{M}_{q\bar{q}}$ . Then, we find finally the Lorentz invariant quarkonium cross section with use of this short distance coefficient which is given by

$$\frac{d\sigma_{\psi_Q}}{d\mathbf{P}_\perp^2 dy} = C(q\bar{q}[^{2S+1}L_J^{(1,8c)}])_{\text{short}} \frac{1}{m} \langle 0 | \mathcal{O}_{1,8c}^{\psi_Q}(^{2S+1}L_J) | 0 \rangle \quad (7.8)$$

where  $\langle 0 | \mathcal{O}_{1,8c}^{\psi_Q}(^{2S+1}L_J) | 0 \rangle$  is the non-perturbative long distance matrix element which describes the hadronization from the heavy quark pair in the  $^{2S+1}L_J^{(1,8c)}$  state to the quarkonium in the  $^{2S+1}L_J$  state. And this is fitted or determined by experiments and lattice calculation. Here we assume that the quantum numbers of the heavy quark are preserved through its hadronization. The factor  $1/m$  is required to compensate for the dimension of the cross section. As we already stated, in this paper we focus on the quarkonium production in terms of the color singlet model. Especially, we are interested in the direct  $J/\psi$  (and also  $\Upsilon(1S)$ ) production and then we compute the short distance coefficient of the S-wave heavy quark pair production in color singlet state and octet state in the following sections.

### 7.1.1 Quark pair in the color singlet state : ${}^3S_1^{(1)}$

Firstly, we consider the amplitude of the quark pair production in the color singlet and spin triplet state;  ${}^3S_1^{(1)}$  which is given by

$$\begin{aligned} \mathcal{M}_{q\bar{q}}\left({}^3S_1^{(1)}(S_z); P\right) &= \int_0^\pi \sin\theta d\theta \int_0^{2\pi} d\phi \frac{M}{4(2\pi)^3} \sqrt{\frac{M}{l^0}} \sqrt{\frac{1}{4\pi}} \frac{1}{\sqrt{N_c}} \\ &\times g^2 \int \frac{d^2\mathbf{k}_{1\perp}}{(2\pi)^2} \frac{d^2\mathbf{k}_\perp}{(2\pi)^2} \frac{\rho_{p,a}(\mathbf{k}_{1\perp})}{k_{1\perp}^2} \int d^2\mathbf{x}_\perp d^2\mathbf{y}_\perp e^{i\mathbf{k}_\perp \cdot \mathbf{x}_\perp} e^{i(\mathbf{P}_\perp - \mathbf{k}_\perp - \mathbf{k}_{1\perp}) \cdot \mathbf{y}_\perp} \\ &\times \text{tr}_d [\mathcal{P}_{1S_z}(P; l) T_{q\bar{q}}(\mathbf{k}_{1\perp}, \mathbf{k}_\perp)]_{|l|=\sqrt{l^0 M}} \text{tr}[\tilde{U}(\mathbf{x}_\perp) t^a \tilde{U}^\dagger(\mathbf{y}_\perp)] \end{aligned} \quad (7.9)$$

where we assume the quark pair in the final state has a spin component  $S_z$ . The covariant spin projection operator is given by <sup>2</sup> [74, 75]

$$\mathcal{P}_{SS_z}(P; l) = \sum_{s_1, s_2} v\left(\frac{P}{2} - l; s_2\right) \bar{u}\left(\frac{P}{2} + l; s_1\right) \langle \tfrac{1}{2}, s_1; \tfrac{1}{2}, s_2 | S, S_z \rangle. \quad (7.12)$$

Here we have neglected the term involving  $T_g$  because no transition process from color octet state to color singlet state exists and vice versa. The color singlet quark pair does not interact with background fields and no gluon absorption occurs. Then this is one of the phenomena of color transparency in the medium.

Furthermore, by averaging the configurations of the color charge densities  $\rho_p$  and  $\rho_A$  with the weight functions  $W_{Y_p}[\rho_p]$  and  $W_{Y_A}[\rho_A]$ , and summing over the spin states of

---

<sup>2</sup>The expressions for the spin singlet and triplet state read

$$\mathcal{P}_{00}(P; l) = \frac{-1}{2\sqrt{2}m} \left(\frac{P}{2} - l - m\right) \gamma^5 \left(\frac{P}{2} + l + m\right) \quad (7.10)$$

$$\mathcal{P}_{1S_z}(P; l) = \frac{-1}{2\sqrt{2}m} \left(\frac{P}{2} - l - m\right) \not{\epsilon}^*(P; S_z) \left(\frac{P}{2} + l + m\right) \quad (7.11)$$

respectively. Here  $\epsilon$  is a three components polarization vector of the produced quarkonium according to the spin direction  $S_z = 0, \pm 1$ .

produced quarkonium and the configurations of  $\rho_p$  and  $\rho_A$ , we obtain a square amplitude

$$\begin{aligned}
& \overline{\sum} \left| \mathcal{M}_{q\bar{q}} \left( {}^3S_1^{(1)}(S_z); P \right) \right|^2 = \int \mathcal{D}\rho_p \mathcal{D}\rho_A W_{Y_p}[\rho_p] W_{Y_p}[\rho_A] \sum_{S_z} \left| \mathcal{M}_{q\bar{q}} \left( {}^3S_1^{(1)}(S_z); P \right) \right|^2 \\
& \simeq \sum_{S_z} (4\pi)^2 \frac{M^3}{16(2\pi)^6 l^0} \frac{1}{4\pi} \frac{1}{N_c} g^4 \int \frac{\langle \rho_{p,a}(\mathbf{k}_{1\perp}) \rho_{p,a'}^\dagger(\mathbf{k}'_{1\perp}) \rangle_{Y_p}}{k_{1\perp}^2 k'_{1\perp}{}^2} \\
& \times \int_{\mathbf{x}_\perp, \mathbf{x}'_\perp, \mathbf{y}_\perp, \mathbf{y}'_\perp} e^{i(\mathbf{k}_\perp \cdot \mathbf{x}_\perp - \mathbf{k}'_\perp \cdot \mathbf{x}'_\perp)} e^{i(\mathbf{P}_\perp - \mathbf{k}_\perp - \mathbf{k}_{1\perp}) \cdot \mathbf{y}_\perp} e^{-i(\mathbf{P}_\perp - \mathbf{k}'_\perp - \mathbf{k}'_{1\perp}) \cdot \mathbf{y}'_\perp} \\
& \times \text{tr}_d[\mathcal{P}_{1S_z}(P; l) T_{q\bar{q}}(\mathbf{k}_{1\perp}, \mathbf{k}_\perp)] \text{tr}_d[T_{q\bar{q}}^\dagger(\mathbf{k}'_{1\perp}, \mathbf{k}'_\perp) \mathcal{P}_{1S_z}^\dagger(P; l')] \\
& \times \langle \text{tr}[\tilde{U}(\mathbf{x}_\perp) t^a \tilde{U}^\dagger(\mathbf{y}_\perp)] \text{tr}[\tilde{U}(\mathbf{y}'_\perp) t^{a'} \tilde{U}^\dagger(\mathbf{x}'_\perp)] \rangle_{Y_A}, \tag{7.13}
\end{aligned}$$

where we can neglect the relative momenta  $l^\mu$  and  $l'^\mu$  in the hard matrix elements since we suppose that  $l^0 \simeq l'^0 \simeq Mv^2 \ll M$  and  $|\mathbf{l}| \sim |\mathbf{l}'| = \sqrt{l^0 M} \simeq Mv \ll M$  with quark velocity  $v \ll c = 1$ . We denote  $\int_{\mathbf{k}_\perp} = \int d^2\mathbf{k}_\perp / (2\pi)^2$  and  $\int_{\mathbf{x}_\perp} = \int d^2\mathbf{x}_\perp$  in the above expression.  $\mathbf{x}_\perp$  and  $\mathbf{y}_\perp$  are a transverse coordinates of the quark and the antiquark respectively in the production amplitude and  $\mathbf{x}'_\perp$  and  $\mathbf{y}'_\perp$  are the same but in the complex conjugate (see Fig. 3.8).

Here as we have defined  $\phi_A$  in Chapter 3, we define the non-perturbative 4-point correlator  $\phi_{A,Y}^{\text{CS}}$  relevant to the color singlet quark pair production which is given as follows;

$$\begin{aligned}
& \delta^{aa'} \int_{\mathbf{x}_\perp, \mathbf{x}'_\perp, \mathbf{y}_\perp, \mathbf{y}'_\perp} e^{i(\mathbf{k}_\perp \cdot \mathbf{x}_\perp - \mathbf{k}'_\perp \cdot \mathbf{x}'_\perp)} e^{i(\mathbf{P}_\perp - \mathbf{k}_\perp - \mathbf{k}_{1\perp}) \cdot \mathbf{y}_\perp} e^{-i(\mathbf{P}_\perp - \mathbf{k}'_\perp - \mathbf{k}'_{1\perp}) \cdot \mathbf{y}'_\perp} \\
& \times \langle \text{tr}[\tilde{U}(\mathbf{x}_\perp) t^a \tilde{U}^\dagger(\mathbf{y}_\perp)] \text{tr}[\tilde{U}(\mathbf{y}'_\perp) t^{a'} \tilde{U}^\dagger(\mathbf{x}'_\perp)] \rangle_Y \\
& = \int_{\mathbf{k}_{2\perp}} (2\pi)^2 \delta^{(2)}(\mathbf{P}_\perp - \mathbf{k}_{1\perp} - \mathbf{k}_{2\perp}) \frac{g^2 N_c}{2\pi k_{2\perp}^2} \\
& \times \int_{\mathbf{Y}_\perp} e^{i(\mathbf{k}_{2\perp} - \mathbf{k}'_{2\perp}) \cdot \mathbf{Y}_\perp} \frac{d\phi_{A,Y}^{\text{CS}}(\mathbf{k}_\perp, \mathbf{k}_{2\perp} - \mathbf{k}_\perp; \mathbf{k}'_\perp, \mathbf{k}_{2\perp} - \mathbf{k}'_\perp | \mathbf{Y}_\perp)}{d^2\mathbf{Y}_\perp}, \tag{7.14}
\end{aligned}$$

where we have assumed  $g^2$  is fixed value.  $Y$  is the rapidity and  $\mathbf{P}_\perp = \mathbf{k}_{1\perp} + (\mathbf{k}_{2\perp} - \mathbf{k}_\perp) + \mathbf{k}_\perp$  is the transverse momentum conservation condition.  $\mathbf{Y}_\perp$  is the transverse position running over the transfers plane of the nucleus and conjugate variable to  $\mathbf{k}_{2\perp} - \mathbf{k}'_{2\perp}$ . We have also assumed that the differences  $\mathbf{k}_{1\perp} - \mathbf{k}'_{1\perp}$  and  $\mathbf{k}_{2\perp} - \mathbf{k}'_{2\perp}$  are small ( $\mathcal{O}(\Lambda_{\text{QCD}})$ ) and we assume  $\mathbf{k}_{2\perp} \approx \mathbf{k}'_{2\perp}$  and  $\mathbf{k}_{1\perp} \approx \mathbf{k}'_{1\perp}$  because we focus on the perturbative region. This function is

a quite different from the four point function introduced in the quark pair production because this new 4-point correlator is not related to the multi-parton function  $\phi_A$ . The only allowed configuration of the color singlet quark pair production is shown in Fig. 7.2 where the gluons coming from the nucleus present the multiple scattering effects. Then the square amplitude with use of the multi parton function  $\phi_{A,Y}^{\text{CS}}$  is rewritten as

$$\begin{aligned}
& \sum \left| \mathcal{M}_{q\bar{q}} \left( {}^3S_1^{(1)}(S_z); P \right) \right|^2 \\
&= \frac{M^3}{4(2\pi)^5 l^0} \frac{g^4}{d_A} \int_{\mathbf{k}_{1\perp}, \mathbf{k}'_{1\perp}, \mathbf{k}_{\perp}, \mathbf{k}'_{\perp}, \mathbf{k}_{2\perp}} \frac{\delta^{(2)}(\mathbf{P}_{\perp} - \mathbf{k}_{1\perp} - \mathbf{k}_{2\perp})}{k_{1\perp}^2 k_{2\perp}^2} \Xi^{3S_1^{(1)}}(\mathbf{k}_{1\perp}, \mathbf{k}_{2\perp}, \mathbf{k}_{\perp}, \mathbf{k}'_{\perp}) \\
&\quad \times \int_{\mathbf{X}_{\perp}} e^{i(\mathbf{k}_{1\perp} - \mathbf{k}'_{1\perp}) \cdot (\mathbf{X}_{\perp} + \mathbf{b})} \frac{d\varphi_{p,Y_1}(\mathbf{k}_{1\perp} | \mathbf{X}_{\perp})}{d^2 \mathbf{X}_{\perp}} \\
&\quad \times \int_{\mathbf{Y}_{\perp}} e^{i(\mathbf{k}_{2\perp} - \mathbf{k}'_{2\perp}) \cdot \mathbf{Y}_{\perp}} \frac{d\phi_{A,Y_2}^{\text{CS}}(\mathbf{k}_{\perp}, \mathbf{k}_{2\perp} - \mathbf{k}_{\perp}; \mathbf{k}'_{\perp}, \mathbf{k}'_{2\perp} - \mathbf{k}'_{\perp} | \mathbf{Y}_{\perp})}{d^2 \mathbf{Y}_{\perp}} \tag{7.15}
\end{aligned}$$

where we have abbreviated the hard matrix part as  $\Xi^{3S_1^{(1)}}$  which is explicitly given in the Appendix B.  $Y_1$  ( $Y_2$ ) is a rapidity of the gluon coming from proton (nucleus). In the amplitude, we have replaced the correlation between the color charge densities of the proton with the gluon distribution  $\varphi$  defined in Eq. (3.38).  $\mathbf{X}_{\perp}$  is a transverse coordinate in the proton. Then we find the probability of production of one heavy quark pair,

$$\begin{aligned}
& \frac{dP_{q\bar{q}}^{3S_1^{(1)}}[\mathbf{b}]}{d^2 \mathbf{P}_{\perp} dy} = \frac{1}{2(2\pi)^3} \sum \left| \mathcal{M}_{q\bar{q}} \left( {}^3S_1^{(1)}(S_z); P \right) \right|^2 \\
&= \frac{1}{2(2\pi)^3} \frac{M^3}{4(2\pi)^5 l^0} \frac{g^4}{d_A} \int_{\mathbf{k}_{1\perp}, \mathbf{k}'_{1\perp}, \mathbf{k}_{\perp}, \mathbf{k}'_{\perp}, \mathbf{k}_{2\perp}} \frac{\delta^{(2)}(\mathbf{P}_{\perp} - \mathbf{k}_{1\perp} - \mathbf{k}_{2\perp})}{k_{1\perp}^2 k_{2\perp}^2} \Xi^{3S_1^{(1)}}(\mathbf{k}_{1\perp}, \mathbf{k}_{2\perp}, \mathbf{k}_{\perp}, \mathbf{k}'_{\perp}) \\
&\quad \times \int_{\mathbf{X}_{\perp}, \mathbf{Y}_{\perp}} e^{i(\mathbf{k}_{1\perp} - \mathbf{k}'_{1\perp}) \cdot (\mathbf{X}_{\perp} - \mathbf{Y}_{\perp} + \mathbf{b})} \frac{d\varphi_{p,Y_1}(\mathbf{k}_{1\perp} | \mathbf{X}_{\perp})}{d^2 \mathbf{X}_{\perp}} \frac{d\phi_{A,Y_2}^{\text{CS}}(\mathbf{k}_{\perp}, \mathbf{k}_{2\perp} - \mathbf{k}_{\perp}; \mathbf{k}'_{\perp}, \mathbf{k}'_{2\perp} - \mathbf{k}'_{\perp} | \mathbf{Y}_{\perp})}{d^2 \mathbf{Y}_{\perp}}. \tag{7.16}
\end{aligned}$$

The impact parameter dependence should be encoded in the exponential phase and we have shifted the exponent as  $(\mathbf{k}_{1\perp} - \mathbf{k}'_{1\perp}) \cdot (\mathbf{X}_{\perp} - \mathbf{Y}_{\perp} + \mathbf{b})$ . By the shift  $\mathbf{Y}_{\perp} \rightarrow \mathbf{Y}_{\perp} - \mathbf{b}$ ,  $\mathbf{Y}_{\perp}$  becomes a relative transverse coordinate from the center of proton as is shown in Fig. (3.10). Here, we have assumed that the saturation scale is not sensitive to the transverse profile of the nucleus. Now we focus on the production cross section in the

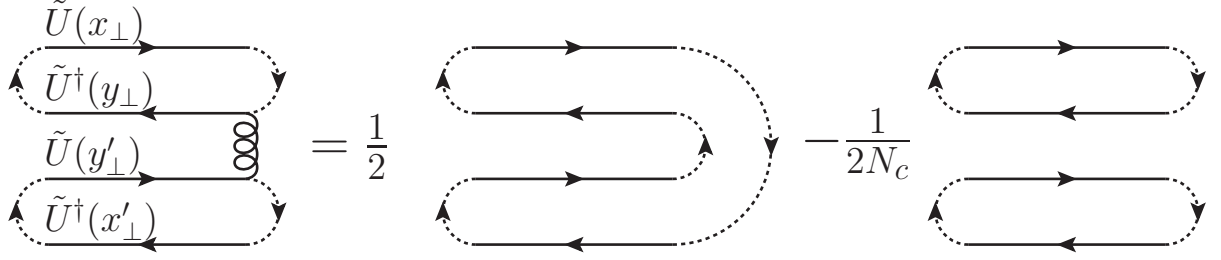


Figure 7.1: Graphical representation of the four point correlator between the different four Wilson line in the fundamental representation. The horizontal solid line represents the fundamental Wilson line.

minimum bias event, therefore we integrate out the impact parameter by use of

$$\int_{\mathbf{b}} e^{i(\mathbf{k}_{1\perp} - \mathbf{k}'_{1\perp}) \cdot \mathbf{b}} = (2\pi)^2 \delta^{(2)}(\mathbf{k}_{1\perp} - \mathbf{k}'_{1\perp}). \quad (7.17)$$

Finally, we obtain the formula of the cross section of the color singlet quark pair production in the minimum bias event as follows;

$$\begin{aligned} \frac{d\sigma_{q\bar{q}}^{3S_1^{(1)}}}{d^2\mathbf{P}_\perp dy} &= \int_{\mathbf{b}} \frac{dP_{q\bar{q}}^{3S_1^{(1)}}[\mathbf{b}]}{d^2\mathbf{P}_\perp dy} \\ &= \frac{1}{2(2\pi)^3} \frac{M^3}{4(2\pi)^7 l^0} \frac{g^4}{d_A} \int_{\mathbf{k}_\perp, \mathbf{k}'_\perp, \mathbf{k}_{2\perp}} \frac{\Xi^{3S_1^{(1)}}(\mathbf{k}_{2\perp}; \mathbf{k}_\perp, \mathbf{k}'_\perp)}{k_{1\perp}^2 k_{2\perp}^2} \varphi_{p, Y_1}(\mathbf{k}_{1\perp}) \phi_{A, Y_2}^{\text{CS}}(\mathbf{k}_{2\perp}; \mathbf{k}_\perp, \mathbf{k}'_\perp) \end{aligned} \quad (7.18)$$

where the multi parton function in the minimum bias event is defined as

$$\begin{aligned} \phi_{A, Y_2}^{\text{CS}}(\mathbf{k}_{2\perp}; \mathbf{k}_\perp, \mathbf{k}'_\perp) &\equiv \int_{\mathbf{Y}_\perp} \frac{d\phi_{A, Y_2}^{\text{CS}}(\mathbf{k}_\perp, \mathbf{k}_{2\perp} - \mathbf{k}_\perp; \mathbf{k}'_\perp, \mathbf{k}_{2\perp} - \mathbf{k}'_\perp | \mathbf{Y}_\perp)}{d^2\mathbf{Y}_\perp} \\ &= \frac{2\pi k_{2\perp}^2}{g^2 N_c} \int_{\mathbf{x}_\perp, \mathbf{x}'_\perp, \mathbf{y}_\perp, \mathbf{y}'_\perp} e^{i(\mathbf{k}_\perp \cdot \mathbf{x}_\perp - \mathbf{k}'_\perp \cdot \mathbf{x}'_\perp)} e^{i(\mathbf{k}_{2\perp} - \mathbf{k}_\perp) \cdot \mathbf{y}_\perp} e^{-i(\mathbf{k}_{2\perp} - \mathbf{k}'_\perp) \cdot \mathbf{y}'_\perp} \\ &\quad \times \langle \text{tr}[\tilde{U}(\mathbf{x}_\perp) t^a \tilde{U}^\dagger(\mathbf{y}_\perp)] \text{tr}[\tilde{U}(\mathbf{y}'_\perp) t^{a'} \tilde{U}^\dagger(\mathbf{x}'_\perp)] \rangle. \end{aligned} \quad (7.19)$$

To simplify this function further, by the systematic use of the Fierz identities;  $(t^a)_{ij}(t^a)_{kl} = \frac{1}{2} \left( \delta_{il} \delta_{jk} - \frac{1}{N_c} \delta_{ij} \delta_{kl} \right)$ , the four point function is arranged as follows



$$\begin{aligned}
& \frac{1}{N_c} \langle \text{tr}[\tilde{U}(\mathbf{x}_\perp) t^a \tilde{U}^\dagger(\mathbf{y}_\perp)] \text{tr}[\tilde{U}(\mathbf{y}'_\perp) t^a \tilde{U}^\dagger(\mathbf{x}'_\perp)] \rangle_Y \\
&= \frac{1}{2N_c} \langle \text{tr}[\tilde{U}^\dagger(\mathbf{y}_\perp) \tilde{U}(\mathbf{x}_\perp) \tilde{U}^\dagger(\mathbf{x}'_\perp) \tilde{U}(\mathbf{y}'_\perp)] \rangle_Y - \frac{1}{2N_c^2} \langle \text{tr}[\tilde{U}^\dagger(\mathbf{y}_\perp) \tilde{U}(\mathbf{x}_\perp)] \text{tr}[\tilde{U}^\dagger(\mathbf{x}'_\perp) \tilde{U}(\mathbf{y}'_\perp)] \rangle_Y
\end{aligned} \tag{7.20}$$

which is shown in Fig. 7.1. Here we have defined a quadrupole scattering matrix as

$$Q_Y(\mathbf{x}_\perp, \mathbf{y}_\perp; \mathbf{y}'_\perp, \mathbf{x}'_\perp) \equiv \frac{1}{N_c} \text{tr} \langle \tilde{U}(\mathbf{x}_\perp) \tilde{U}^\dagger(\mathbf{x}'_\perp) \tilde{U}(\mathbf{y}'_\perp) \tilde{U}^\dagger(\mathbf{y}_\perp) \rangle_Y, \tag{7.21}$$

and then we can rewrite the 4 point function as

$$\begin{aligned}
& \frac{1}{N_c} \langle \text{tr}[\tilde{U}(\mathbf{x}_\perp) t^a \tilde{U}^\dagger(\mathbf{y}_\perp)] \text{tr}[\tilde{U}(\mathbf{y}'_\perp) t^a \tilde{U}^\dagger(\mathbf{x}'_\perp)] \rangle_Y \\
& \stackrel{LN_c}{=} \frac{1}{2} [Q_Y(\mathbf{x}_\perp, \mathbf{y}_\perp; \mathbf{y}'_\perp, \mathbf{x}'_\perp) - S_Y(\mathbf{x}_\perp, \mathbf{y}_\perp) S_Y(\mathbf{y}'_\perp, \mathbf{x}'_\perp)],
\end{aligned} \tag{7.22}$$

where we have abbreviated the large- $N_c$  limit as “ $LN_c$ ”. Finally Eq. (7.19) in the large- $N_c$  limit becomes

$$\begin{aligned}
\phi_{A,Y}^{\text{CS}}(\mathbf{k}_{2\perp}; \mathbf{k}_\perp, \mathbf{k}'_\perp) & \stackrel{LN_c}{=} \frac{\pi^2 R_A^2 k_{2\perp}^2}{g^2} \int_{\mathbf{r}, \mathbf{r}', \mathbf{\Delta}} e^{i(\mathbf{k}_\perp \cdot \mathbf{x}_\perp - \mathbf{k}'_\perp \cdot \mathbf{x}'_\perp)} e^{i(\mathbf{k}_{2\perp} - \mathbf{k}_\perp) \cdot \mathbf{y}_\perp} e^{-i(\mathbf{k}_{2\perp} - \mathbf{k}'_\perp) \cdot \mathbf{y}'_\perp} \\
& \times [Q_Y(\mathbf{x}_\perp, \mathbf{y}_\perp; \mathbf{y}'_\perp, \mathbf{x}'_\perp) - S_Y(\mathbf{x}_\perp, \mathbf{y}_\perp) S_Y(\mathbf{y}'_\perp, \mathbf{x}'_\perp)]
\end{aligned} \tag{7.23}$$

where  $\mathbf{r} = \mathbf{x}_\perp - \mathbf{x}'_\perp$ ,  $\mathbf{r}' = \mathbf{y}_\perp - \mathbf{y}'_\perp$ , and  $\mathbf{\Delta} = \mathbf{x}'_\perp - \mathbf{y}'_\perp$ . We have assumed the translational invariance in the nucleus then the area of the nucleus  $\pi R_A^2$  emerges.

Combining Eq. (7.18) with Eq. (C.19) in Appendix C, the short distance coefficient for the heavy quark pair production in the color singlet  $^3S_1$  state is determined as

$$C(q\bar{q}[^3S_1^{(1)}])_{\text{short}} = \frac{\alpha_s^2}{3(2\pi)^3 N_c^2 C_F} \int_{\mathbf{k}_\perp, \mathbf{k}'_\perp, \mathbf{k}_{2\perp}} \frac{\Xi^{^3S_1^{(1)}}(\mathbf{k}_{2\perp}; \mathbf{k}_\perp, \mathbf{k}'_\perp)}{k_{1\perp}^2 k_{2\perp}^2} \varphi_{p,Y_1}(\mathbf{k}_{1\perp}) \phi_{A,Y_2}^{\text{CS}}(\mathbf{k}_{2\perp}; \mathbf{k}_\perp, \mathbf{k}'_\perp) \tag{7.24}$$

where  $C_F = t^a t^a = (N_c^2 - 1)/2N_c$ . As a results, by the shift of mass dimension, the

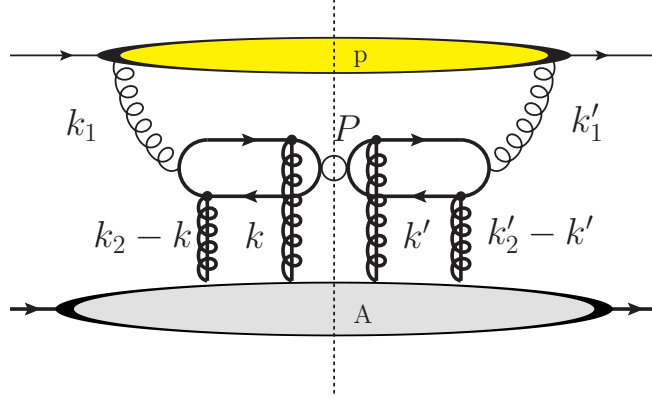


Figure 7.2: Graphical diagram of the production of the quark pair in  $^3S_1^{(1)}$  state. Dash line at each diagram corresponds to final state cut. White blob represents color singlet state. The gluons from the nucleus provide eikonal phases to the quark propagators.

production cross section of the quarkonium in the  $^3S_1$  state is given by

$$\begin{aligned} \frac{d\sigma_{\psi_Q}^{^3S_1^{(1)}}}{d^2\mathbf{P}_\perp dy} &= C(q\bar{q}[^3S_1^{(1)}])_{\text{short}} \frac{1}{m} \langle 0 | \mathcal{O}_1^{\psi_Q}(^3S_1) | 0 \rangle \\ &= \frac{2\alpha_s^2 \langle 0 | \mathcal{O}_1^{\psi_Q}(^3S_1) | 0 \rangle}{3(2\pi)^3 N_c^2 C_F M} \int_{\mathbf{k}_\perp, \mathbf{k}'_\perp, \mathbf{k}_{2\perp}} \frac{\Xi^{^3S_1^{(1)}}(\mathbf{k}_{2\perp}; \mathbf{k}_\perp, \mathbf{k}'_\perp)}{k_{1\perp}^2 k_{2\perp}^2} \varphi_{p,Y_1}(\mathbf{k}_{1\perp}) \phi_{A,Y_2}^{\text{CS}}(\mathbf{k}_{2\perp}; \mathbf{k}_\perp, \mathbf{k}'_\perp), \end{aligned} \quad (7.25)$$

where non-perturbative transition rate  $\langle 0 | \mathcal{O}_1^{\psi_Q}(^3S_1) | 0 \rangle$  corresponds to the non-relativistic BS amplitude exactly which reads

$$\langle 0 | \mathcal{O}_1^{\psi_Q}(^3S_1) | 0 \rangle = \frac{3N_c}{2\pi} |R(0)|^2 [1 + \mathcal{O}(v^4)]. \quad (7.26)$$

$R(0)$  is a radial wave function at origin and it has been computed in the QCD motivated potential model <sup>3</sup> and we find  $|R(0)|^2 = 0.81 \text{GeV}^3$  in Ref. [99, 100]. We use this value in

---

<sup>3</sup>For another phenomenological estimation, we can use a correspondence of decay width to the wave function at origin as follows,

$$\Gamma(J/\psi \rightarrow e^+ e^-) = \frac{4\alpha_{EM}^2 e_Q^2 |R(0)|^2}{M^2} \left[ 1 - \frac{16}{3\pi} \alpha_s \right], \quad (7.27)$$

where the input parameters  $\Gamma_{e^+e^-} = 5.55 \text{keV}$ ,  $\alpha_{EM} = 1/137$ , and  $M = 3.1 \text{GeV}$ . This expression includes the radiative correction [99].

numerical computations.

### 7.1.2 Quark pair in the color octet state : ${}^3S_1^{(8)}$ and ${}^1S_0^{(8)}$

In the similar way for the color singlet heavy quark pair production, the production amplitude of the quark pair in the color octet and  ${}^3S_1$  state is given by

$$\begin{aligned}
\mathcal{M}_{q\bar{q}}\left({}^3S_1^{(8)}(S_z); P\right) = & \sqrt{2} \int \frac{d^3l}{(2\pi)^3 2l^0} \delta\left(l^0 - \frac{l^2}{M}\right) \sqrt{\frac{1}{4\pi}} \\
& \times g^2 \int \frac{d^2\mathbf{k}_{1\perp}}{(2\pi)^2} \frac{d^2\mathbf{k}_{\perp}}{(2\pi)^2} \frac{\rho_{p,a}(\mathbf{k}_{1\perp})}{k_{1\perp}^2} \int d^2\mathbf{x}_{\perp} d^2\mathbf{y}_{\perp} e^{i\mathbf{k}_{\perp} \cdot \mathbf{x}_{\perp}} e^{i(\mathbf{P}_{\perp} - \mathbf{k}_{\perp} - \mathbf{k}_{1\perp}) \cdot \mathbf{y}_{\perp}} \\
& \times \left\{ \text{tr}_d [\mathcal{P}_{1S_z}(P; l) T_{q\bar{q}}(\mathbf{k}_{1\perp}, \mathbf{k}_{\perp})] \text{tr} \left[ t^c \tilde{U}(\mathbf{x}_{\perp}) t^a \tilde{U}^{\dagger}(\mathbf{y}_{\perp}) \right] \right. \\
& \left. + \text{tr}_d [\mathcal{P}_{1S_z}(P; l) T_g(\mathbf{k}_{1\perp})] \text{tr} \left[ t^c t^b U^{ba}(\mathbf{x}_{\perp}) \right] \right\}. \tag{7.28}
\end{aligned}$$

In this case, the color matrix in the fundamental representation  $t^c$  for the color octet heavy quark pair production enters into the color trace of the amplitude. By averaging the configurations of the color charge densities  $\rho_p$  and  $\rho_A$ , and summing over the spin states of produced quarkonium and the configurations of  $\rho_p$  and  $\rho_A$ , a square amplitude is given as follows;

$$\begin{aligned}
\overline{\sum} \left| \mathcal{M}_{q\bar{q}}\left({}^3S_1^{(8)}(S_z); P\right) \right|^2 = & \frac{M^3 g^2}{4(2\pi)^5 l^0 \pi d_A} \int_{\mathbf{k}_{1\perp}, \mathbf{k}_{\perp}, \mathbf{k}'_{1\perp}, \mathbf{k}'_{\perp}} \frac{1}{k_{1\perp}^{\prime 2}} \int_{\mathbf{X}_{\perp}} e^{i(\mathbf{k}_{1\perp} - \mathbf{k}'_{1\perp}) \cdot \mathbf{X}_{\perp}} \frac{d\varphi_{p,Y_1}(\mathbf{k}_{1\perp} | \mathbf{X}_{\perp})}{d^2\mathbf{X}_{\perp}} \\
& \times \int_{\mathbf{x}_{\perp}, \mathbf{y}_{\perp}, \mathbf{x}'_{\perp}, \mathbf{y}'_{\perp}} e^{i\mathbf{k}_{\perp} \cdot \mathbf{x}_{\perp} - i\mathbf{k}'_{\perp} \cdot \mathbf{x}'_{\perp}} e^{i(\mathbf{P}_{\perp} - \mathbf{k}_{\perp} - \mathbf{k}_{1\perp}) \cdot \mathbf{y}_{\perp}} e^{-i(\mathbf{P}_{\perp} - \mathbf{k}'_{\perp} - \mathbf{k}'_{1\perp}) \cdot \mathbf{y}'_{\perp}} \\
& \times \left\{ \Xi_1^{3S_1^{(8)}} \mathcal{W}_{Y_2}(\mathbf{x}, \mathbf{y}; \mathbf{y}', \mathbf{x}') + \Xi_2^{3S_1^{(8)}} \mathcal{W}_{Y_2}(\mathbf{x}, \mathbf{y}; \mathbf{x}', \mathbf{x}') \right. \\
& \left. + \Xi_3^{3S_1^{(8)}} \mathcal{W}_{Y_2}(\mathbf{x}, \mathbf{x}; \mathbf{y}', \mathbf{x}') + \Xi_4^{3S_1^{(8)}} \mathcal{W}_{Y_2}(\mathbf{x}, \mathbf{x}; \mathbf{x}', \mathbf{x}') \right\}, \tag{7.29}
\end{aligned}$$

where we have used the  $\varphi$  in Eq. (3.38) and  $\mathbf{X}_{\perp}$  is the transverse coordinate in the proton which is the same as shown in Eq. (7.15) with assumption  $\mathbf{k}_{1\perp} \approx \mathbf{k}'_{1\perp}$ .  $Y_1$  ( $Y_2$ ) is a rapidity of the gluon coming from proton (nucleus). We have introduced new notation  $\mathcal{W}_Y$  which

reads

$$\mathcal{W}_Y(\mathbf{x}, \mathbf{y}; \mathbf{y}', \mathbf{x}') \equiv \langle \text{tr}[t^c \tilde{U}(\mathbf{x}_\perp) t^a \tilde{U}^\dagger(\mathbf{y}_\perp)] \text{tr}[\tilde{U}(\mathbf{y}'_\perp) t^a \tilde{U}^\dagger(\mathbf{x}'_\perp) t^c] \rangle_Y. \quad (7.30)$$

In contrast to the quark pair production in the color singlet state, four characteristic matrices are emerged in Eq. (7.29);

$$\begin{aligned} \Xi_1^{3S_1^{(8)}}(\mathbf{k}_1, \mathbf{k}_2, \mathbf{k}, \mathbf{k}') &= \sum_{S_z} \text{tr}_d[\mathcal{P}_{1S_z}(P; l=0) T_{q\bar{q}}(\mathbf{k}_{1\perp}, \mathbf{k}_\perp)] \text{tr}_d[T_{q\bar{q}}^\dagger(\mathbf{k}'_{1\perp}, \mathbf{k}'_\perp) \mathcal{P}_{1S_z}^\dagger(P; l'=0)], \\ \Xi_2^{3S_1^{(8)}}(\mathbf{k}_1, \mathbf{k}_2, \mathbf{k}) &= \sum_{S_z} \text{tr}_d[\mathcal{P}_{1S_z}(P; l=0) T_{q\bar{q}}(\mathbf{k}_{1\perp}, \mathbf{k}_\perp)] \text{tr}_d[T_g^\dagger(\mathbf{k}'_{1\perp}) \mathcal{P}_{1S_z}^\dagger(P; l'=0)], \\ \Xi_3^{3S_1^{(8)}}(\mathbf{k}_1, \mathbf{k}_2, \mathbf{k}') &= \sum_{S_z} \text{tr}_d[\mathcal{P}_{1S_z}(P; l=0) T_g(\mathbf{k}_{1\perp})] \text{tr}_d[T_{q\bar{q}}^\dagger(\mathbf{k}'_{1\perp}, \mathbf{k}'_\perp) \mathcal{P}_{1S_z}^\dagger(P; l'=0)], \\ \Xi_4^{3S_1^{(8)}}(\mathbf{k}_1, \mathbf{k}_2) &= \sum_{S_z} \text{tr}_d[\mathcal{P}_{1S_z}(P; l=0) T_g(\mathbf{k}_{1\perp})] \text{tr}_d[T_g^\dagger(\mathbf{k}'_{1\perp}) \mathcal{P}_{1S_z}^\dagger(P; l'=0)], \end{aligned} \quad (7.31)$$

which are shown as a graphical representations in Fig. 7.3.

Next, let us simplify Eq. (7.29) further. By the systematic use of Fierz identity, Eq. (7.30) can be rewritten as

$$\begin{aligned} &\mathcal{W}_Y(\mathbf{x}, \mathbf{y}; \mathbf{y}', \mathbf{x}') \\ &= \frac{1}{4} \langle \text{tr}[\tilde{U}(\mathbf{y}'_\perp) \tilde{U}^\dagger(\mathbf{y}_\perp)] \text{tr}[\tilde{U}(\mathbf{x}_\perp) \tilde{U}^\dagger(\mathbf{x}'_\perp)] \rangle_Y - \frac{1}{4N} \langle \text{tr}[\tilde{U}(\mathbf{x}_\perp) \tilde{U}^\dagger(\mathbf{y}_\perp) \tilde{U}(\mathbf{y}'_\perp) \tilde{U}^\dagger(\mathbf{x}'_\perp)] \rangle_Y \\ &\quad - \frac{1}{4N} \langle \text{tr}[\tilde{U}(\mathbf{x}_\perp) \tilde{U}^\dagger(\mathbf{x}'_\perp) \tilde{U}(\mathbf{y}_\perp) \tilde{U}^\dagger(\mathbf{y}'_\perp)] \rangle_Y + \frac{1}{4N^2} \langle \text{tr}[\tilde{U}(\mathbf{x}_\perp) \tilde{U}^\dagger(\mathbf{y}_\perp)] \text{tr}[\tilde{U}(\mathbf{y}'_\perp) \tilde{U}^\dagger(\mathbf{x}'_\perp)] \rangle_Y, \end{aligned} \quad (7.32)$$

where first term in the right hand side has a scale of order  $\mathcal{O}(N_c^2)$ , the second and third terms are  $\mathcal{O}(N_c)$ , and fourth term is  $\mathcal{O}(1)$ . Then we find Eq. (7.30) becomes with the large- $N_c$  limit

$$\mathcal{W}_Y(\mathbf{x}, \mathbf{y}; \mathbf{y}', \mathbf{x}') \stackrel{LN_c}{=} \frac{N_c^2}{4} S_Y(\mathbf{x}_\perp, \mathbf{x}'_\perp) S_Y(\mathbf{y}_\perp, \mathbf{y}'_\perp) \quad (7.33)$$

where we have assumed the relation in Eq. (2.48).

In order to obtain the cross section in the momentum space, we consider a Fourier

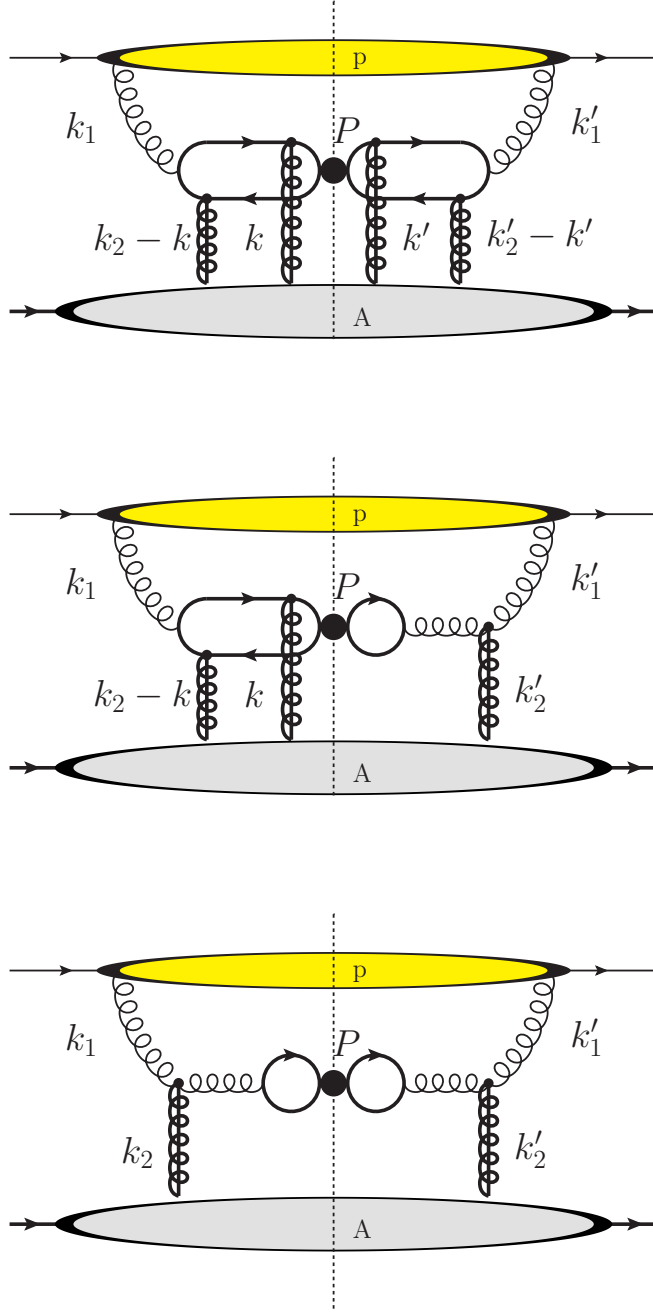


Figure 7.3: Specific diagrams of the production of the quark pair in  ${}^3S_1^{(8)}$ ; Upper figure is related to  $\Xi_1^{3S_1^{(8)}}$ , Middle is related to  $\Xi_2^{3S_1^{(8)}}$ , and Lower is related to  $\Xi_4^{3S_1^{(8)}}$ . Dash line at each diagram corresponds to final state cut. Black blob represents color octet state. The gluons coming from the nucleus provide eikonal phases to the quark propagators.  $\Xi_3^{3S_1^{(8)}}$  is a complex conjugate to  $\Xi_2^{3S_1^{(8)}}$ .

transform of the  $\mathcal{W}_Y(\mathbf{x}, \mathbf{y}; \mathbf{y}', \mathbf{x}')$  in the large- $N_c$  limit which is given by

$$\begin{aligned} & \int_{\mathbf{x}_\perp, \mathbf{y}_\perp, \mathbf{x}'_\perp, \mathbf{y}'_\perp} e^{i\mathbf{k}_\perp \cdot \mathbf{x}_\perp - i\mathbf{k}'_\perp \cdot \mathbf{x}'_\perp} e^{i(\mathbf{P}_\perp - \mathbf{k}_\perp - \mathbf{k}_{1\perp}) \cdot \mathbf{y}_\perp} e^{-i(\mathbf{P}_\perp - \mathbf{k}'_\perp - \mathbf{k}'_{1\perp}) \cdot \mathbf{y}'_\perp} \mathcal{W}_Y(\mathbf{x}, \mathbf{y}; \mathbf{y}', \mathbf{x}') \\ &= \int_{\mathbf{k}_{2\perp}} (2\pi)^2 \delta^{(2)}(\mathbf{P}_\perp - \mathbf{k}_{1\perp} - \mathbf{k}_{2\perp}) \int_{\mathbf{Y}_\perp} \frac{N_c^2}{4} (2\pi)^2 \delta^{(2)}(\mathbf{k}_\perp - \mathbf{k}'_\perp) \tilde{S}_Y(\mathbf{k}_\perp) \tilde{S}_Y(\mathbf{k}_{2\perp} - \mathbf{k}_\perp) \end{aligned} \quad (7.34)$$

where  $\tilde{S}_Y$  is the scattering matrix in the momentum representation. Here we have assumed the translational invariance in the heavy nucleus and  $\mathbf{k}_{1\perp} \approx \mathbf{k}'_{1\perp}$ . And we have integrated out  $\int_{\mathbf{y}_\perp}$ . By convoluting the hard matrix element  $\Xi_1^{3S_1^{(8)}}$  with Eq. (7.34), we obtain

$$\begin{aligned} & \int_{\mathbf{k}_\perp, \mathbf{k}'_\perp} \Xi_1^{3S_1^{(8)}}(\mathbf{k}_1, \mathbf{k}_2, \mathbf{k}, \mathbf{k}') \int_{\mathbf{x}_\perp, \mathbf{y}_\perp, \mathbf{x}'_\perp, \mathbf{y}'_\perp} e^{i\mathbf{k}_\perp \cdot \mathbf{x}_\perp - i\mathbf{k}'_\perp \cdot \mathbf{x}'_\perp} e^{i(\mathbf{P}_\perp - \mathbf{k}_\perp - \mathbf{k}_{1\perp}) \cdot \mathbf{y}_\perp} e^{-i(\mathbf{P}_\perp - \mathbf{k}'_\perp - \mathbf{k}'_{1\perp}) \cdot \mathbf{y}'_\perp} \mathcal{W}_Y(\mathbf{x}, \mathbf{y}; \mathbf{y}', \mathbf{x}') \\ &= \int_{\mathbf{k}_{2\perp}} (2\pi)^2 \delta^{(2)}(\mathbf{P}_\perp - \mathbf{k}_{1\perp} - \mathbf{k}_{2\perp}) \int_{\mathbf{Y}_\perp} \frac{N_c^2}{4} \int_{\mathbf{k}_\perp} \tilde{S}_Y(\mathbf{k}_\perp) \tilde{S}_Y(\mathbf{k}_{2\perp} - \mathbf{k}_\perp) \Xi_1^{3S_1^{(8)}}(\mathbf{k}_1, \mathbf{k}_2, \mathbf{k}, \mathbf{k}') \end{aligned} \quad (7.35)$$

with  $\mathbf{k}' = \mathbf{k}_\perp$  in the right hand side. In the similar way, by convoluting  $\Xi_2^{3S_1^{(8)}}$ ,  $\Xi_3^{3S_1^{(8)}}$ , and  $\Xi_4^{3S_1^{(8)}}$  with Eq. (7.34), the square amplitude at an impact parameter  $\mathbf{b}$  is given by

$$\begin{aligned} & \overline{\sum} \left| \mathcal{M}_{q\bar{q}} \left( {}^3S_1^{(8)}(S_z); P \right) \right|^2 \\ &= \frac{M^3}{4(2\pi)^7 l^0} \frac{g^4}{2C_F} \int_{\mathbf{k}'_{1\perp}, \mathbf{k}_{2\perp}, \mathbf{k}_\perp} \frac{\Xi^{3S_1^{(8)}}(\mathbf{k}_1, \mathbf{k}_2, \mathbf{k})}{k_{1\perp}^2 k_{2\perp}^2} \int_{\mathbf{X}_\perp} e^{i(\mathbf{k}_{1\perp} - \mathbf{k}'_{1\perp}) \cdot (\mathbf{X}_\perp + \mathbf{b})} \frac{d\varphi_p(\mathbf{k}_{1\perp} | \mathbf{X}_\perp)}{d^2 \mathbf{X}_\perp} \\ & \quad \times \phi_{A, Y_2}^{\text{CO}}(\mathbf{k}_{2\perp}, \mathbf{k}_\perp), \end{aligned} \quad (7.36)$$

where the hard matrix elements are gathered as

$$\Xi^{3S_1^{(8)}}(\mathbf{k}_1, \mathbf{k}_2, \mathbf{k}) \equiv \sum_{S_z} \left| \text{tr}_d[\mathcal{P}_{1S_z}(P; l=0) T_{q\bar{q}}(\mathbf{k}_{1\perp}, \mathbf{k}_\perp)] + \text{tr}_d[\mathcal{P}_{1S_z}(P; l=0) T_g(\mathbf{k}_{1\perp})] \right|^2, \quad (7.37)$$

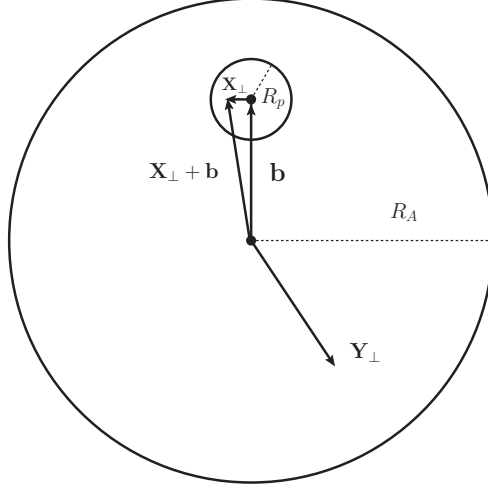


Figure 7.4: Transverse plane of the nucleus in pA collisions.  $\mathbf{X}_\perp(\mathbf{Y}_\perp)$  runs over the transverse plane of the proton (nucleus) having a radius  $R_p(R_A)$ .  $\mathbf{b}$  is an impact parameter characterized the distance from the center of nucleus to the center of proton.

and we have introduces the multi parton function which is defined as

$$\phi_{A,Y_2}^{\text{CO}}(\mathbf{k}_{2\perp}, \mathbf{k}_\perp) = \frac{\pi R_A^2 N_c k_{2\perp}^2}{4\alpha_s} \tilde{S}_{Y_2}(\mathbf{k}_\perp) \tilde{S}_{Y_2}(\mathbf{k}_{2\perp} - \mathbf{k}_\perp). \quad (7.38)$$

The factor  $\pi R_A^2$  is derived from the assumption of the translational invariance in the nucleus. In Eq. (7.36), we have shifted the the exponent as  $(\mathbf{k}_{1\perp} - \mathbf{k}'_{1\perp}) \cdot (\mathbf{X}_\perp + \mathbf{b})$  which represents that  $\mathbf{X}_\perp + \mathbf{b}$  becomes a relative transverse coordinate from the center of nucleus as is shown in Fig. (7.4). We have also assumed the translational invariance in the nucleus, namely, the saturation scale embedded in the multi parton function does not depend on the impact parameter. This multi parton function is the same as  $\phi_{A,Y}^{q\bar{q},g}$  in Eq. (3.46). The agreement between  $\phi_{A,Y}^{q\bar{q},g}$  and  $\phi_{A,Y}^{\text{CO}}$  is reasonable because of the use of the large- $N_c$  approximation.

Finally, in minimum bias event, the production cross section of the quark pair in the

color octet  $^3S_1$  state is given by

$$\begin{aligned} \frac{d\sigma_{q\bar{q}}^{^3S_1^{(8)}}}{d^2\mathbf{P}_\perp dy} &= \int_{\mathbf{b}} \frac{1}{2(2\pi)^3} \overline{\sum} \left| \mathcal{M}_{q\bar{q}} \left( ^3S_1^{(8)}(S_z); P \right) \right|^2 \\ &= \frac{M^3}{4(2\pi)^7 l^0} \frac{\alpha_s^2}{2\pi C_F} \int_{\mathbf{k}_{2\perp}, \mathbf{k}_\perp} \frac{\Xi^{^3S_1^{(8)}}(\mathbf{k}_1, \mathbf{k}_2, \mathbf{k})}{k_{1\perp}^2 k_{2\perp}^2} \varphi_{p, Y_1}(\mathbf{k}_{1\perp}) \phi_{A, Y_2}^{\text{CO}}(\mathbf{k}_{2\perp}, \mathbf{k}_\perp), \end{aligned} \quad (7.39)$$

and the short distance coefficient is determined by use of Eq. (C.21) in Appendix C as

$$C(q\bar{q}[^3S_1^{(8)}])_{\text{short}} = \frac{\alpha_s^2}{3(2\pi)^3 N_c C_F^2} \int_{\mathbf{k}_{2\perp}, \mathbf{k}_\perp} \frac{\Xi^{^3S_1^{(8)}}(\mathbf{k}_1, \mathbf{k}_2, \mathbf{k})}{k_{1\perp}^2 k_{2\perp}^2} \varphi_{p, Y_1}(\mathbf{k}_{1\perp}) \phi_{A, Y_2}^{\text{CO}}(\mathbf{k}_{2\perp}, \mathbf{k}_\perp). \quad (7.40)$$

The production cross section of the quarkonium from the quark pair in the color octet  $^3S_1$  state is given by

$$\frac{d\sigma_{\psi_Q}^{^3S_1^{(8)}}}{d^2\mathbf{P}_\perp dy} = \frac{2\alpha_s^2 \langle 0 | \mathcal{O}_8^{\psi_Q} (^3S_1) | 0 \rangle}{3(2\pi)^3 N_c C_F^2 M} \int_{\mathbf{k}_{2\perp}, \mathbf{k}_\perp} \frac{\Xi^{^3S_1^{(8)}}(\mathbf{k}_1, \mathbf{k}_2, \mathbf{k})}{k_{1\perp}^2 k_{2\perp}^2} \varphi_{p, Y_1}(\mathbf{k}_{1\perp}) \phi_{A, Y_2}^{\text{CO}}(\mathbf{k}_{2\perp}, \mathbf{k}_\perp) \quad (7.41)$$

with non-perturbative transition matrix element  $\langle 0 | \mathcal{O}_8^{\psi_Q} (^3S_1) | 0 \rangle$  which is determined by data fitting or lattice computations.

Here we comment on a computation of the production cross section of the quarkonium via a heavy quark pair in the color octet  $^1S_0$  state. In this channel, the main difference in a short distance coefficient from Eq. (7.40) is the hard matrix element which is given by

$$\Xi^{^1S_0^{(8)}}(\mathbf{k}_1, \mathbf{k}_2, \mathbf{k}) = \left| \text{tr}_d [\mathcal{P}_{00}(P; l=0) T_{q\bar{q}}(\mathbf{k}_{1\perp}, \mathbf{k}_\perp)] \right|^2. \quad (7.42)$$

Here  $\text{tr}_d [\mathcal{P}_{00}(P; l=0) T_g(\mathbf{k}_{1\perp}, \mathbf{k}_\perp)]$  is exactly zero because the quark pair which is created from gluon splitting never become a pseud scalar channel. Then, using Eq. (C.20) in Appendix C, the quarkonium production cross section from the heavy quark pair in the color octet  $^1S_0$  state is given by

$$\frac{d\sigma_{\psi_Q}^{^1S_0^{(8)}}}{d^2\mathbf{P}_\perp dy} = \frac{2\alpha_s^2 \langle 0 | \mathcal{O}_8^{\psi_Q} (^1S_0) | 0 \rangle}{(2\pi)^3 N_c C_F^2 M} \int_{\mathbf{k}_{2\perp}, \mathbf{k}_\perp} \frac{\Xi^{^1S_0^{(8)}}(\mathbf{k}_1, \mathbf{k}_2, \mathbf{k})}{k_{1\perp}^2 k_{2\perp}^2} \varphi_{p, Y_1}(\mathbf{k}_{1\perp}) \phi_{A, Y_2}^{\text{CO}}(\mathbf{k}_{2\perp}, \mathbf{k}_\perp). \quad (7.43)$$



Here the non-perturbative amplitude  $\langle 0 | \mathcal{O}_8^{\psi Q} (^1S_0) | 0 \rangle$  should also be determined by data fitting or lattice computations.

## 7.2 Color singlet model for quarkonium production with multi parton correlator

We have shown in Eq. (7.23) that the 4-point function is necessary to compute the direct  $J/\psi$  production cross section in the color singlet model. In general, the multiple  $n$ -point parton correlator which consists of  $n$  Wilson lines in the fundamental representation is a solution of the JIMWLK equation. Then it is difficult to express the analytic form of the 4-point function. However, if the color charge density of the nucleus has the Gaussian weight function, it is known that the 4-point correlation can reduce to very simple form as follows [60];

$$\begin{aligned} Q_Y(\mathbf{x}_\perp, \mathbf{y}_\perp; \mathbf{y}'_\perp, \mathbf{x}'_\perp) &\stackrel{LN_c}{=} S_Y(\mathbf{x}_\perp, \mathbf{x}'_\perp) S_Y(\mathbf{y}'_\perp, \mathbf{y}_\perp) \\ &\quad - \frac{\ln S_Y(\mathbf{x}_\perp, \mathbf{y}'_\perp) S_Y(\mathbf{x}'_\perp, \mathbf{y}_\perp) - \ln S_Y(\mathbf{x}_\perp, \mathbf{y}_\perp) S_Y(\mathbf{x}'_\perp, \mathbf{y}'_\perp)}{\ln S_Y(\mathbf{x}_\perp, \mathbf{x}'_\perp) S_Y(\mathbf{y}'_\perp, \mathbf{y}_\perp) - \ln S_Y(\mathbf{x}_\perp, \mathbf{y}_\perp) S_Y(\mathbf{x}'_\perp, \mathbf{y}'_\perp)} \\ &\quad \times [S_Y(\mathbf{x}_\perp, \mathbf{x}'_\perp) S_Y(\mathbf{y}'_\perp, \mathbf{y}_\perp) - S_Y(\mathbf{x}_\perp, \mathbf{y}_\perp) S_Y(\mathbf{x}'_\perp, \mathbf{y}'_\perp)] \end{aligned} \quad (7.44)$$

where we have used the large- $N_c$  approximation. We show in Appendix E the way to derive Eq. (7.44). Therefore, by using Eq. (7.44) in the large- $N_c$  limit, the color singlet expectation value in Eq. (7.23) is given by

$$\begin{aligned} &\frac{1}{N_c} \langle \text{tr}[\tilde{U}(\mathbf{x}_\perp) t^a \tilde{U}^\dagger(\mathbf{y}_\perp)] \text{tr}[\tilde{U}(\mathbf{y}'_\perp) t^a \tilde{U}^\dagger(\mathbf{x}'_\perp)] \rangle_Y \\ &\stackrel{LN_c}{=} \frac{1}{2} [Q_Y(\mathbf{x}_\perp, \mathbf{y}_\perp; \mathbf{y}'_\perp, \mathbf{x}'_\perp) - S_Y(\mathbf{x}_\perp, \mathbf{y}_\perp) S_Y(\mathbf{y}'_\perp, \mathbf{x}'_\perp)] \\ &= \frac{1}{2} [S_Y(\mathbf{x}_\perp, \mathbf{x}'_\perp) S_Y(\mathbf{y}'_\perp, \mathbf{y}_\perp) - S_Y(\mathbf{x}_\perp, \mathbf{y}_\perp) S_Y(\mathbf{y}'_\perp, \mathbf{x}'_\perp)] \left[ \frac{\ln \frac{S_Y(\mathbf{x}_\perp, \mathbf{x}'_\perp) S_Y(\mathbf{y}'_\perp, \mathbf{y}_\perp)}{S_Y(\mathbf{x}_\perp, \mathbf{y}'_\perp) S_Y(\mathbf{x}'_\perp, \mathbf{y}_\perp)}}{\ln \frac{S_Y(\mathbf{x}_\perp, \mathbf{x}'_\perp) S_Y(\mathbf{y}'_\perp, \mathbf{y}_\perp)}{S_Y(\mathbf{x}_\perp, \mathbf{y}_\perp) S_Y(\mathbf{x}'_\perp, \mathbf{y}'_\perp)}} \right]. \end{aligned} \quad (7.45)$$

Here we assume the gaussian form for  $S_Y$  in the nucleus as

$$S_Y(\mathbf{x}_\perp, \mathbf{y}_\perp) = \exp \left[ -\frac{Q_{sA}^2 (\mathbf{x}_\perp - \mathbf{y}_\perp)^2}{4} \right] \quad (7.46)$$

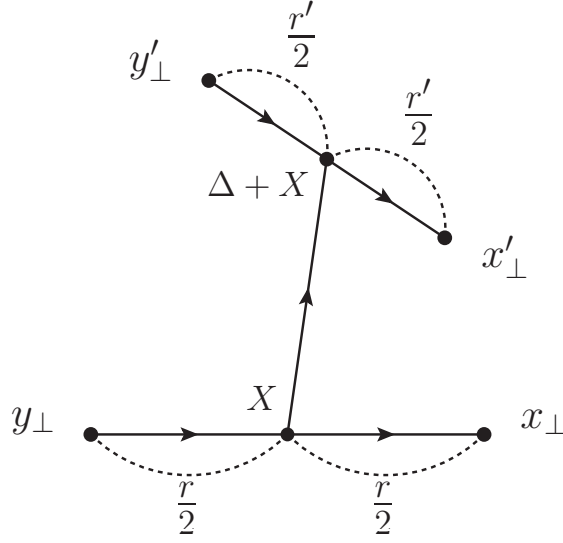


Figure 7.5: Transverse coordinates of the quarks in the quadrupole amplitude in Eq. (7.45).

and change the transverse coordinate as

$$\begin{aligned}
 \mathbf{x}_\perp &= \mathbf{X} + \frac{\mathbf{r}}{2} \rightarrow \frac{\mathbf{r}}{2}, \\
 \mathbf{y}_\perp &= \mathbf{X} - \frac{\mathbf{r}}{2} \rightarrow -\frac{\mathbf{r}}{2}, \\
 \mathbf{x}'_\perp &= \mathbf{\Delta} + \mathbf{X} + \frac{\mathbf{r}'}{2} \rightarrow \mathbf{\Delta} + \frac{\mathbf{r}'}{2}, \\
 \mathbf{y}'_\perp &= \mathbf{\Delta} + \mathbf{X} + \frac{\mathbf{r}'}{2} \rightarrow \mathbf{\Delta} - \frac{\mathbf{r}'}{2},
 \end{aligned} \tag{7.47}$$

which are shown in Fig. 7.5. The right arrows in Eq. (7.47) represent the use of the assumption of translational invariant in the nucleus. Then, we find the expectation value Eq. (7.45) as

$$\begin{aligned}
 &\frac{1}{N_c} \langle \text{tr}[\tilde{U}(\mathbf{x}_\perp) t^a \tilde{U}^\dagger(\mathbf{y}_\perp)] \text{tr}[\tilde{U}(\mathbf{y}'_\perp) t^a \tilde{U}^\dagger(\mathbf{x}'_\perp)] \rangle_Y \\
 &\stackrel{LN_c}{=} \frac{2\mathbf{r} \cdot \mathbf{r}'}{(\mathbf{r} + \mathbf{r}')^2 - 4\mathbf{\Delta}^2} [S_Y(\mathbf{x}_\perp, \mathbf{x}'_\perp) S_Y(\mathbf{y}'_\perp, \mathbf{y}_\perp) - S_Y(\mathbf{x}_\perp, \mathbf{y}_\perp) S_Y(\mathbf{y}'_\perp, \mathbf{x}'_\perp)]
 \end{aligned} \tag{7.48}$$

and thus the multi parton function Eq. (7.23) becomes

$$\begin{aligned} \phi_{A,Y}^{\text{CS}}(\mathbf{k}_{2\perp}; \mathbf{k}_\perp, \mathbf{k}'_\perp) &\stackrel{LN_c}{=} \frac{\pi R_A^2 \mathbf{k}_{2\perp}^2}{2\alpha_s} \int_{\mathbf{r}, \mathbf{r}', \Delta} e^{i\mathbf{l}_1 \cdot \mathbf{r}} e^{-i\mathbf{l}_2 \cdot \mathbf{r}'} e^{-i\mathbf{k}_{2\perp} \cdot \Delta} \frac{2\mathbf{r} \cdot \mathbf{r}'}{(\mathbf{r} + \mathbf{r}')^2 - 4\Delta^2} \\ &\times [S_Y(\mathbf{x}_\perp, \mathbf{x}'_\perp) S_Y(\mathbf{y}'_\perp, \mathbf{y}_\perp) - S_Y(\mathbf{x}_\perp, \mathbf{y}_\perp) S_Y(\mathbf{y}'_\perp, \mathbf{x}'_\perp)] \end{aligned} \quad (7.49)$$

where  $\mathbf{l}_1 = \mathbf{k}_\perp - \frac{\mathbf{k}_{2\perp}}{2}$  and  $\mathbf{l}_2 = \mathbf{k}'_\perp - \frac{\mathbf{k}_{2\perp}}{2}$ . Then we rewrite the direct  $J/\psi$  production cross section in Eq. (7.25) further by performing integral over  $\mathbf{k}_\perp$  and  $\mathbf{k}'_\perp$  as follows;

$$\frac{d\sigma_{\psi_Q}^{3S_1^{(1)}}}{d^2\mathbf{P}_\perp dy} = \frac{2\alpha_s^2 \langle 0 | \mathcal{O}_1^{\psi_Q}(^3S_1) | 0 \rangle}{3(2\pi)^3 N^2 C_F M} \int_{\mathbf{k}_{2\perp}} \frac{1}{k_{1\perp}^2 k_{2\perp}^2} \varphi_{p,Y_1}^{g,g}(\mathbf{k}_{1\perp}) \Omega_{A,Y_2}(\mathbf{k}_{2\perp}), \quad (7.50)$$

where  $\mathbf{k}_{1\perp} = \mathbf{P}_\perp - \mathbf{k}_{2\perp}$  and we have denoted  $\Omega_{A,Y_2}$  as

$$\Omega_{A,Y_2}(\mathbf{k}_{2\perp}) \equiv \int_{\mathbf{k}_\perp, \mathbf{k}'_\perp} \Xi^{3S_1^{(1)}}(\mathbf{k}_{2\perp}; \mathbf{k}_\perp, \mathbf{k}'_\perp) \phi_{A,Y_2}^{\text{CS}}(\mathbf{k}_{2\perp}; \mathbf{k}_\perp, \mathbf{k}'_\perp). \quad (7.51)$$

Here, by using the expression of the hard matrix element which is shown in Appendix B, we find <sup>4</sup>

$$\begin{aligned} \Omega_{A,Y_2}(\mathbf{k}_{2\perp}) &= \frac{\pi R_A^2 \mathbf{k}_{2\perp}^2}{\alpha_s} \int_{\mathbf{r}, \mathbf{r}', \Delta} e^{-i\mathbf{k}_{2\perp} \cdot \Delta} \frac{\mathbf{r} \cdot \mathbf{r}'}{(\mathbf{r} + \mathbf{r}')^2 - 4\Delta^2} K_0\left(\frac{\sqrt{\mathbf{k}_{1\perp}^2 + M^2}}{2} r\right) K_0\left(\frac{\sqrt{\mathbf{k}_{1\perp}^2 + M^2}}{2} r'\right) \\ &\times \frac{\mathbf{k}_{1\perp}^2 (\mathbf{k}_{1\perp}^2 + M^2)}{8\pi^2} [S_{Y_2}(\mathbf{x}_\perp, \mathbf{x}'_\perp) S_{Y_2}(\mathbf{y}'_\perp, \mathbf{y}_\perp) - S_{Y_2}(\mathbf{x}_\perp, \mathbf{y}_\perp) S_{Y_2}(\mathbf{y}'_\perp, \mathbf{x}'_\perp)] \\ &= \frac{\pi R_A^2 \mathbf{k}_{2\perp}^2}{\alpha_s} \frac{\mathbf{k}_{1\perp}^2 (\mathbf{k}_{1\perp}^2 + M^2)}{8\pi^2} \int_{\Delta} e^{-i\mathbf{k}_{2\perp} \cdot \Delta} F(\Delta), \end{aligned} \quad (7.53)$$

---

<sup>4</sup>The integration including the term which depends on  $L_1$  and  $L_2$  convert to the modified Bessel function as

$$\begin{aligned} \int_{\mathbf{k}_\perp} \frac{e^{i\mathbf{l}_1 \cdot \mathbf{r}}}{L_1} &= \frac{1}{8\pi} K_0\left(\frac{r}{2} \sqrt{\mathbf{k}_{1\perp}^2 + M^2}\right), \\ \int_{\mathbf{k}'_\perp} \frac{e^{i\mathbf{l}_2 \cdot \mathbf{r}'} }{L_2} &= \frac{1}{8\pi} K_0\left(\frac{r'}{2} \sqrt{\mathbf{k}_{1\perp}^2 + M^2}\right). \end{aligned} \quad (7.52)$$

Other integrations  $\int_{\mathbf{k}_\perp} e^{i\mathbf{l}_1 \cdot \mathbf{r}}$  and  $\int_{\mathbf{k}'_\perp} e^{i\mathbf{l}_2 \cdot \mathbf{r}'}$  necessarily produce  $\delta^{(2)}(\mathbf{r})$  or  $\delta^{(2)}(\mathbf{r}')$  which results in  $\mathbf{r} \delta^{(2)}(\mathbf{r}) = \mathbf{r}' \delta^{(2)}(\mathbf{r}') = 0$ . Therefore, we certainly pick up the term involving both  $L_1$  and  $L_2$  in the  $\mathbf{k}_{1\perp}$  and  $\mathbf{k}_{2\perp}$  integrations.

with compact notations  $L_1 = 4\mathbf{l}_{1\perp}^2 + \mathbf{k}_{1\perp}^2 + M^2$  and  $L_2 = 4\mathbf{l}_{2\perp}^2 + \mathbf{k}_{1\perp}^2 + M^2$  and the function  $F(\Delta)$  is defined as follows;

$$\begin{aligned}
F(\Delta) &\equiv \int_{\mathbf{r}, \mathbf{r}'} \frac{\mathbf{r} \cdot \mathbf{r}'}{(\mathbf{r} + \mathbf{r}')^2 - 4\Delta^2} K_0\left(\frac{\sqrt{\mathbf{k}_{1\perp}^2 + M^2}}{2} r\right) K_0\left(\frac{\sqrt{\mathbf{k}_{1\perp}^2 + M^2}}{2} r'\right) \\
&\quad \times e^{-\frac{Q_{sA}^2}{4}(r^2 + r'^2)} \left[ e^{\frac{Q_{sA}^2}{8}\{(r+\mathbf{r}')^2 - 4\Delta^2\}} - 1 \right] \\
&= \frac{Q_{sA}^2}{8} \int_{\mathbf{r}, \mathbf{r}'} (\mathbf{r} \cdot \mathbf{r}') K_0\left(\frac{\sqrt{\mathbf{k}_{1\perp}^2 + M^2}}{2} r\right) K_0\left(\frac{\sqrt{\mathbf{k}_{1\perp}^2 + M^2}}{2} r'\right) \\
&\quad \times e^{-\frac{Q_{sA}^2}{4}(r^2 + r'^2)} \int_0^1 d\xi e^{\frac{Q_{sA}^2}{8}\{(r+\mathbf{r}')^2 - 4\Delta^2\}\xi}. \tag{7.54}
\end{aligned}$$

In the second line in Eq. (7.54), as in Ref. [71, 72], we have used the following identity

$$e^{\frac{Q_{sA}^2}{8}\{(r+\mathbf{r}')^2 - 4\Delta^2\}} - 1 = \frac{Q_{sA}^2}{8} \{(\mathbf{r} + \mathbf{r}')^2 - 4\Delta^2\} \int_0^1 d\xi e^{\frac{Q_{sA}^2}{8}\{(r+\mathbf{r}')^2 - 4\Delta^2\}\xi}, \tag{7.55}$$

which makes the function  $F(\Delta)$  more manageable. Finally, we have expressed  $\Omega$  by use of the modified Bessel function in the second kind which is shown in the Appendix A. As shown in Ref. [71–73], the Bessel function should enter into the propagator of the heavy quark pair which is created from the gluon splitting. Finally, let us consider the  $F(\Delta)$  in the momentum representation. The Fourier transform of  $F(\Delta)$  is given by

$$\begin{aligned}
&\int_{\Delta} e^{-i\mathbf{k}_{2\perp} \cdot \Delta} F(\Delta) \\
&= \frac{Q_{sA}^2}{4} \int_0^1 d\xi \int_{\mathbf{r}, \mathbf{r}'} (\mathbf{r} \cdot \mathbf{r}') e^{\frac{Q_{sA}^2}{4}(\mathbf{r} \cdot \mathbf{r}')\xi} e^{-\frac{Q_{sA}^2}{8}(r^2 + r'^2)(2-\xi)} K_0\left(\frac{\sqrt{\mathbf{k}_{1\perp}^2 + M^2}}{2} r\right) K_0\left(\frac{\sqrt{\mathbf{k}_{1\perp}^2 + M^2}}{2} r'\right) \\
&\quad \times \int \Delta d\Delta \pi J_0(k_{2\perp} \Delta) e^{-\frac{Q_{sA}^2}{2}\Delta^2 \xi} \\
&= \frac{\pi^2}{2} \int_0^1 \frac{d\xi}{\xi} e^{-\frac{k_{2\perp}^2}{(2Q_{sA}^2 \xi)}} \int dr dr' r^2 r'^2 \int d\theta \cos \theta e^{\frac{Q_{sA}^2 r r' \xi}{4} \cos \theta} e^{-\frac{Q_{sA}^2}{8}(r^2 + r'^2)(2-\xi)} \\
&\quad \times K_0\left(\frac{\sqrt{\mathbf{k}_{1\perp}^2 + M^2}}{2} r\right) K_0\left(\frac{\sqrt{\mathbf{k}_{1\perp}^2 + M^2}}{2} r'\right) \tag{7.56}
\end{aligned}$$

where  $\theta$  is a polar angle between  $\mathbf{r}$  and  $\mathbf{r}'$ , and we have used Weber's formula Eq. (A.26). Eqs. (7.51–7.56) are the main result in this section.

Direct  $J/\psi$  and  $\Upsilon(1S)$  production in the color singlet model involve the characteristic factor  $\mathbf{r} \cdot \mathbf{r}'$ . The polar angular average of it leads to 0. Physical meaning of  $\mathbf{r} \cdot \mathbf{r}'$  is that both the heavy quark and the antiquark picks up external gluons to make the heavy quark pair  $P$ - and  $C$ -odd state<sup>5</sup>, and subsequently the heavy quark pair is bound into the quarkonium in  $^3S_1$  state such as  $J/\psi$  and  $\Upsilon(1S)$ . Expanding Eq. (7.54) at leading order in terms of  $Q_s^2$ , we find the finite contribution as

$$F(\Delta) \propto \int_{\mathbf{r}, \mathbf{r}'} Q_{sA}^4 (\mathbf{r} \cdot \mathbf{r}')^2. \quad (7.57)$$

The saturation momentum  $Q_{sA}^2$  scales as  $A^{1/3}Q_{sp}^2$  and the dipole size  $r, r'$  are changed to  $\sim 1/P_\perp$  by performing integral over  $\mathbf{r}$  and  $\mathbf{r}'$ , then the differential cross action of the quarkonium production in the color singlet model should fall off as  $\frac{d\sigma}{dP_\perp^2} \propto \frac{A^{2/3}Q_{sp}^4}{P_\perp^6}$ . On the other hand, the  $P_\perp$  dependence of the differential cross action of the quarkonium in the color evaporation model is differ from the one in the color singlet model because the heavy quark pair production from splitting of the gluon which propagates through the background gauge fields in the heavy nucleus is lacked as shown in Eq. (7.9). Then we expect the  $P_\perp$ -slope of the quarkonium cross section in our color singlet model is steeper than that of the color evaporation model at large  $P_\perp$  region.

Finally let us consider the  $A$  dependence of Eq. (7.50). As we have already shown,  $Q_{sA}^2$  is embedded in the exponent of the scattering matrix Eq. (7.46) and it can be estimated as  $\frac{\alpha_s^2 A^{1/3}}{\pi R_A^2} \left(\frac{1}{x}\right)^{0.3}$ . Here  $\alpha_s^2 A^{1/3}$  is a resummation parameter of the multiple scattering in the nucleus and order of unity;  $\alpha_s^2 A^{1/3} = \mathcal{O}(1)$ , even if the strong coupling constant is much

---

<sup>5</sup>In the spectroscopic representation, the quantum state of gluon is  $J^{PC} = 1^{--}$  then the eigenvalue with charge conjugation transform for the system involving  $n$  gluons is given by

$$C = (-1)^n.$$

$J/\psi$  is parity negative and also charge negative then the  $J/\psi$  production and decay involves the odd number of gluons,

$$J/\psi \longleftrightarrow (2n+1)g \quad (n = 0, 1, \dots).$$

Similarly, for  $\eta_c$  as pseudoscalar particle we find

$$\eta_c \longleftrightarrow (2n)g \quad (n = 1, 2, \dots).$$

This is the results by generalized selection rule called *Yang's theorem*.

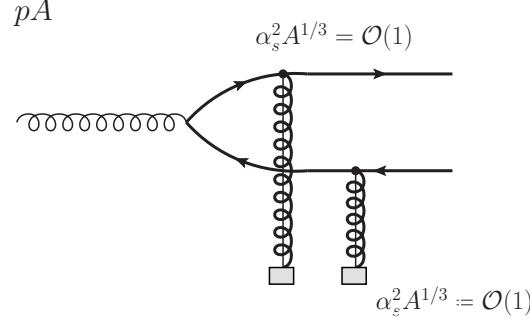


Figure 7.6: Direct  $J/\psi$  production in the color singlet model pA collisions. Grey box represents the multiple scattering in the nucleus. The direct  $J/\psi$  production cross section in pA collisions is order of  $\alpha_s$ .

smaller than unity. As a results, the quarkonium cross section in our color singlet model is proportional to  $A^{2/3}$  explicitly as we have shown the above. By taking a limit  $A \rightarrow 1$  (pp collisions), this  $J/\psi$  production amplitude contributes to higher order correction because the direct  $J/\psi$  production cross section in pp collisions at leading order in the coupling constant is order of  $\alpha_s^3$ . It means that two gluons fusion in initial collisions leads to color octet heavy quark pair and subsequently the heavy quark pair becomes color singlet state involving with additional recoil gluon in order to satisfy the parity and charge conditions. Then we might expect that the  $J/\psi$  production process which is shown in Fig. 7.6 does not contribute to the cross section in pp collisions but woks in pA collisions compared to pp collisions.

## 7.3 Numerical results

In the following calculations, we choose the proton size  $R_p = 0.9$  fm for heavy meson and quarkonium production. We cancel  $\alpha_s^2$  in front of the cross section Eq. (7.50) by  $\alpha_s$  appearing in the denominator in  $\phi_{A,y}^{\text{CS}}$  and in  $\varphi_{p,y}$ .

### 7.3.1 Transverse momentum spectrum of direct $J/\psi$ production

In this subsection, we show a numerical results of the direct  $J/\psi$  production cross section in pA collisions at mid rapidity in the RHIC energy by using the color singlet model Eq. (7.50). Here we do not consider the  $x$ -evolution of the dipole amplitude which is embedded in the cross section in our computations and limit ourselves to estimation of order of the  $J/\psi$  production cross section which is determined only by initial condition

of the dipole amplitude because we just focus on whether the  $J/\psi$  production in the color singlet model can contribute to the total cross section and can change the nuclear modification factor quantitatively. In addition, we have assumed that the quadrupole amplitude consists of only the dipole amplitude which is gaussian form. Then we must consider the kinematical region where the quantum evolution does not start yet and the gaussian form of it is preserved approximately. In order to prevent the quantum evolution of the dipole amplitude, we should consider only the quarkonium production involving the momentum fraction  $x$  of the gluon in the proton and nucleus is larger than an initial value of the beginning of the quantum evolution. In this paper, we set  $x_0 = 0.01$  and  $J/\psi$  production at mid rapidity in the RHIC energy is appropriate for numerical computations because the  $J/\psi$  production is relevant to  $x_0 < x$ . For  $x_0 \leq x \leq 1$ , we also apply the phenomenological Ansatz Eq. (3.64) as we have used in the computations within the color evaporation model.

Before we go to the results, let us first consider Eq. (7.56). Multiple scattering effect of the heavy quark pair off background gauge fields provides the exponential phase  $e^{\frac{Q_{sA}^2 rr' \xi}{4} \cos \theta}$ . Here we expanded it multiplied by  $\cos \theta$  in a series as follows;

$$\begin{aligned} & \cos \theta e^{\frac{Q_{sA}^2 rr' \xi}{4} \cos \theta} \\ &= \cos \theta \left( \sum_{k=0}^{k_{max} \rightarrow \infty} \frac{1}{(2k+1)!} \left( \frac{Q_{sA}^2 rr' \xi}{4} \cos \theta \right)^{2k+1} + \sum_{k=0}^{k_{max} \rightarrow \infty} \frac{1}{(2k)!} \left( \frac{Q_{sA}^2 rr' \xi}{4} \cos \theta \right)^{2k} \right). \end{aligned} \quad (7.58)$$

In fact, we found the second term in the bracket of the right hand side in Eq. (7.58) becomes 0 by performing integral over the angle  $\theta$ . We can check it out easily by use of Eqs. (A.24)(A.25).<sup>6</sup>

Now we show in Fig. 7.7 (Upper) the transverse momentum spectrum of the  $J/\psi$  production in di-electron channel in pp collisions at mid rapidity  $|y| < 0.35$  at  $\sqrt{s} = 200$  GeV. We have computed the cross section in Eq. (7.50) with the uGD set MV given in Table 3.1 in the proton, by substituting the saturation scale of proton into Eq. (7.56). We have chosen the charm quark mass as  $m_c = M_{J/\psi}/2 = 1.55$  GeV which corresponds to the static limit  $v \rightarrow 0$ , namely the relative momentum between the quark and the antiquark becomes 0. Non-perturbative transition probability, namely the BS amplitude is determined by use of a radial wave function of S-wave at origin. In this paper, we

---

<sup>6</sup>Here we set  $k_{max} = 4$  in this paper. Actually we have checked the numerical result with  $k_{max} = 2$  is differ from the one with  $k_{max} = 4$  by order of 1%.

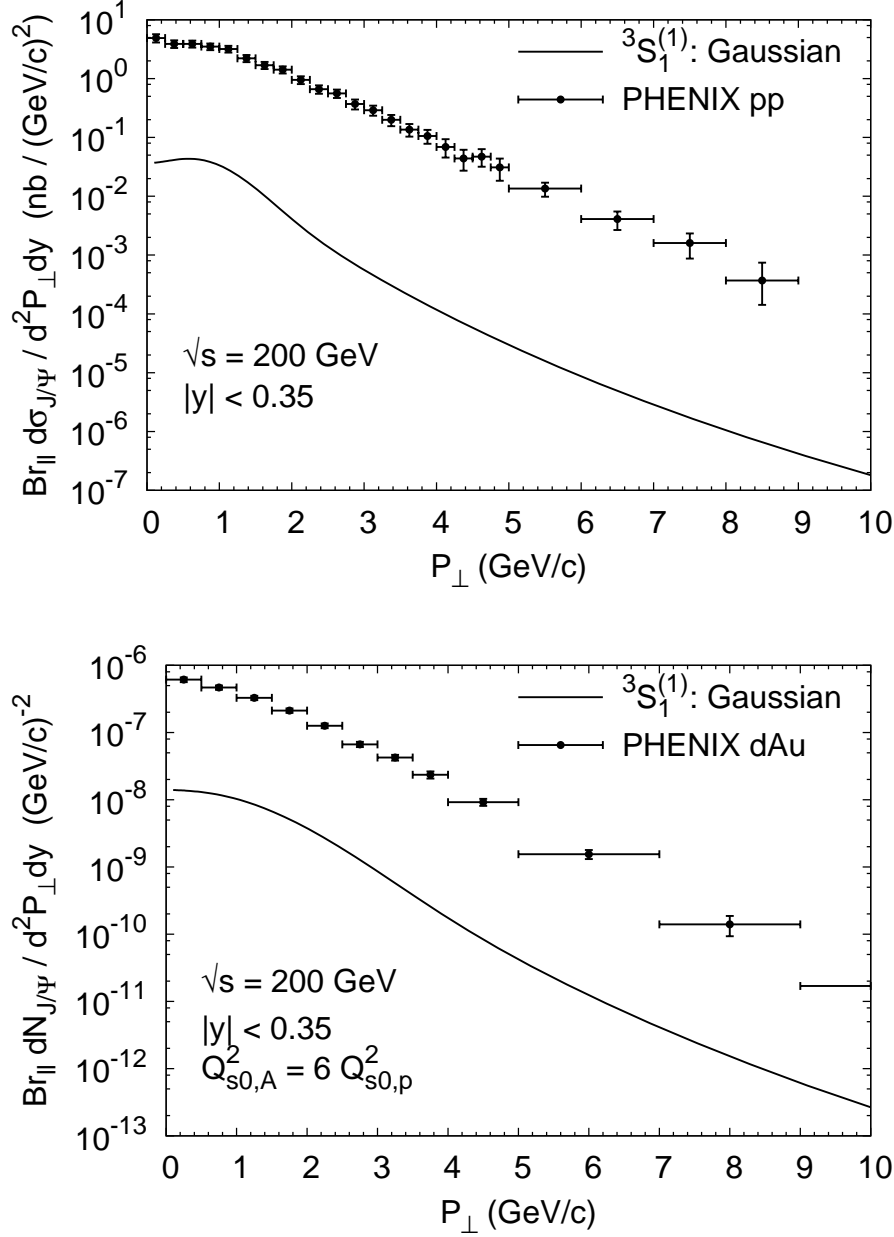


Figure 7.7: (Upper) Transverse momentum spectrum of direct  $^3S_1^{(1)}$   $J/\psi$  production cross section in di-lepton channel in pp collisions at  $\sqrt{s} = 200$  GeV for mid rapidity range  $|y| < 0.35$ . (Lower) Transverse momentum spectrum of direct  $^3S_1^{(1)}$   $J/\psi$  production multiplicity in di-lepton channel in pp collisions at  $\sqrt{s} = 200$  GeV for mid rapidity range  $|y| < 0.35$ .  $Br_{ll}$  is a branching ratio of the  $J/\psi$  decay into di-lepton channel and  $Br_{ll} = 0.0594$  for  $e^+e^-$  decay at mid rapidity. The results are obtained by using the production formula (7.25) with uGD set MV for the proton and Eq. (7.56). We fix  $Q_{s0,A}^2 = 6Q_{s0,p}^2$  with  $Q_{s0,p}^2 = 0.2$  GeV $^2$  and the charm quark mass is a half of  $J/\psi$  mass as  $2m_c = M_{J/\psi} = 3.1$  GeV. Data from [107, 110].



choose the LDME for  $^3S_1^{(1)}$  as  $\langle \mathcal{O}_1^{\psi Q} (^3S_1) \rangle = 1.16 \text{ GeV}^3$  which is cited from Ref. [100].

We found that the  $J/\psi$  production cross section in the color singlet model is approximately two orders of magnitude less than the data in pp collisions at RHIC. Although we have calculated the  $J/\psi$  production cross section by use of the dipole amplitude in the gaussian form which constructs the quadrupole amplitude in the large- $N_c$  limit, we conclude that the color singlet direct  $J/\psi$  production at leading order in coupling constant does not contribute to total  $J/\psi$  production cross section at mid rapidity in pp collisions at RHIC. And we expect this conclusion is not changed in the production at forward rapidity and at the LHC energy <sup>7</sup>.

When we compute the averaged multiplicity of the direct  $J/\psi$  production by use of Eq. (7.50), we should divide Eq. (7.50) by the inelastic cross section which estimated as  $\pi R_A^2$  and effectively it cancels out with the same factor in  $\phi_{A,y}^{\text{CS}}$  Eq. (7.49). Then the averaged multiplicity is proportional to the effective transverse area  $\pi R_p^2$  of the proton appearing in  $\varphi_{p,y}$ .

Fig. 7.7 (Lower) shows the averaged multiplicity of the  $J/\psi$  production in pA collisions at mid rapidity at RHIC by using Eq. (7.50) divided by total inelastic cross section which is approximated as  $\sigma_{\text{inel}}^{pA} \approx \pi R_A^2$ . We have also used the dipole scattering matrix in the gaussian form which consists of the quadrupole scattering matrix element in the large- $N_c$  limit Eq. (7.44). The initial saturation scale of the target nucleus is fixed as  $Q_{sA}^2 = 6Q_{sp}^2$ . It seems that our numerical result in pA collisions is close to the data than the case in pp collisions. We expect the  $J/\psi$  production cross section in pA collisions can be naively enhanced approximately fiftyfold than that in pp collisions because the  $J/\psi$  production cross section in the color singlet model is proportional to  $A^{2/3}$  which shown in Eq. (7.57).

### 7.3.2 Nuclear modification factor of direct $J/\psi$ production

Next, let us consider the nuclear modification factor of the  $J/\psi$  production in pA collisions, which has been defined in Eq. (5.7). We have already shown that direct the  $J/\psi$  production cross section computed in the color singlet model cannot reproduce the data both in pp collisions and pA collisions at RHIC. However we show the qualitative difference of the transverse momentum spectrum in pA collisions from that in pp collisions.

We show in Fig. 7.8 that  $R_{pA}$  of  $J/\psi$  (Upper) and  $\Upsilon(1S)$  (Lower) as a function of

---

<sup>7</sup>It has been known since early times that LO direct  $J/\psi$  production cross section in the color singlet model is smaller than the data in pp( $\bar{p}$ ) collisions at Tevatron in the context of collinear factorization framework.

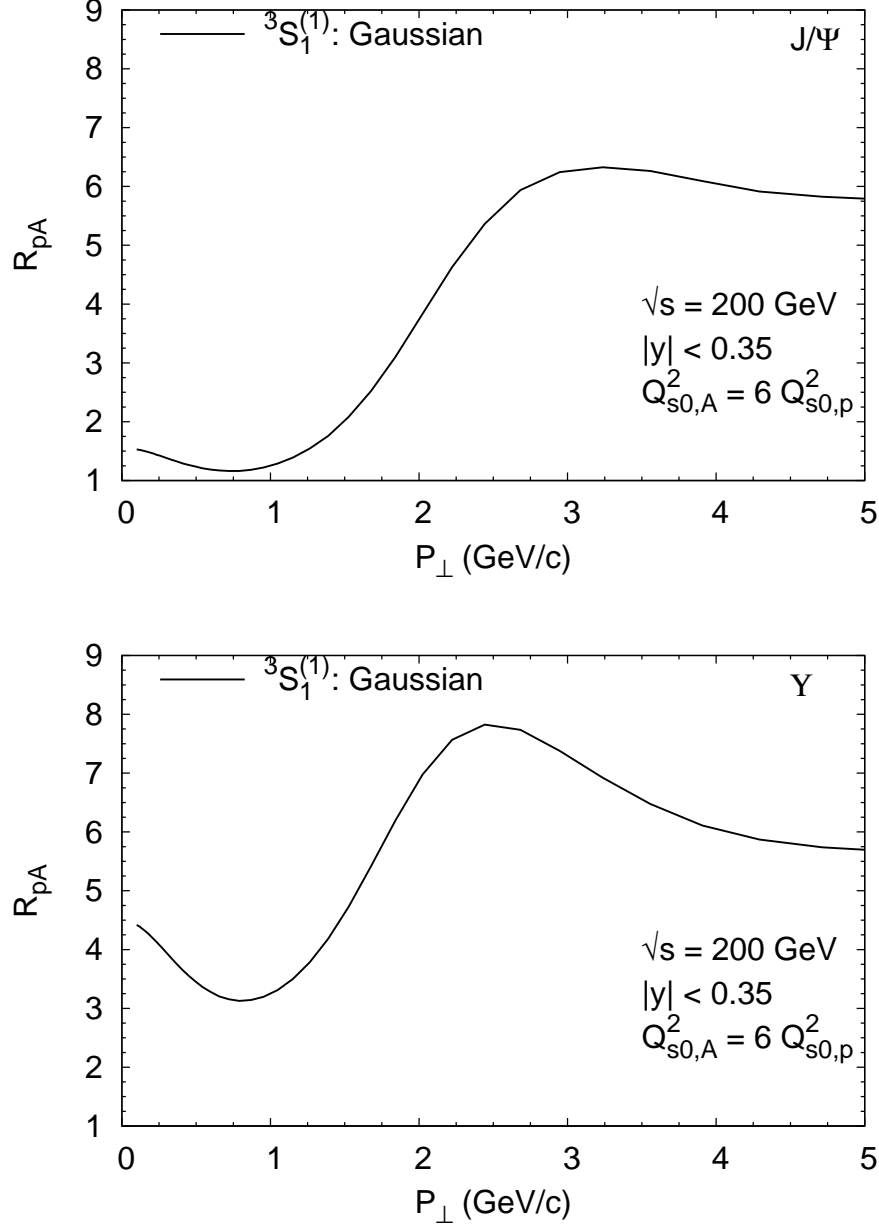


Figure 7.8: The ratio  $R_{pA}(P_{\perp})$  as a function of transverse momentum of  $J/\psi$  (Upper) and  $\Upsilon(1S)$  (Lower) productions in pA collisions at  $\sqrt{s} = 200$  GeV for  $|y| < 0.35$ . The charm quark mass is fixed as a half of the  $J/\psi$  mass  $2m_c = M_{J/\psi} = 3.1$  GeV, and similarly the bottom quark mass is  $2m_b = M_{\Upsilon(1S)} = 9.46$  GeV.

transverse momentum  $P_\perp$  at mid rapidity in the RHIC energy. The initial saturation scale of the target nucleus is fixed as  $Q_{sA}^2 = 6Q_{sp}^2$ . As stated above, the quarkonium cross section in pA collisions within the color singlet model is proportional to  $A^{2/3}$ , then the  $R_{pA}$  is expected to become larger than unity if no nuclear effect exists<sup>8</sup>.

In the lower momentum region ( $P_\perp \lesssim 2$  GeV), we found the  $R_{pA}$  is larger than unity but relatively suppressed than about  $A^{1/3} \sim 6$  and a small Cronin like peak around  $P_\perp = 3$  GeV because of the multiple scattering in the nucleus. At larger  $P_\perp$ , the  $R_{pA}$  becomes close to about  $A^{1/3} \sim 6$ . Similarly, we computed the  $\Upsilon(1S)$  production by use of Eq. (7.50) with  $2m_b = M_{\Upsilon(1S)} = 9.46$  GeV and found the  $R_{pA}$  of the  $\Upsilon(1S)$  is suppressed than about  $A^{1/3}$  but larger than unity. And a large Cronin like peak is also found at lower- $P_\perp$ , although the  $R_{pA}$  of  $\Upsilon(1S)$  is less suppressed than that of  $J/\psi$ .

### 7.3.3 $J/\psi$ production from heavy quark pair in color octet state

Finally, we consider only a qualitative behavior of  $R_{pA}$  of  $J/\psi$  production via color octet charm quark pair in order to check whether the suppression of  $R_{pA}$  is similar to that in the color evaporation model. As a simple example, we would consider color octet charm quark pair in  $^1S_0$  state by use of Eq. (7.43). We assume the  $^1S_0$  color octet charm quark pair becomes the  $J/\psi$  through a non-perturbative interaction at long distance. Here we do not go into the detail about the cross section of  $J/\psi$  from color octet  $c\bar{c}$  because the non-perturbative long distance matrix element to compute the cross section of  $J/\psi$  from color octet charm quark pair is not known precisely. To determine the non-perturbative long distance matrix element, we need to compute all the channels in which the charm quark pair is bound to  $J/\psi$  and must extract the long distance matrix element by fitting data. Then we will leave it in future work. As to computing the nuclear modification factor of the  $J/\psi$  via charm quark pair in the color octet state, the long distance matrix element of pA collisions could cancel out that in pp collisions if we assume the long distance matrix element in pp collisions is the same as in pA collisions. Then in this case we do not have to know the specific value of the long distance matrix element and we can also include the quantum evolution effects of the multi parti function Eq. (7.38) in the same way as shown in the  $J/\psi$  production in the color evaporation model.

We show In Fig. 7.9 the  $R_{pA}$  of the  $J/\psi$  production from the color octet charm quark

---

<sup>8</sup>In the  $R_{pA}$ , the numerator includes  $A^{2/3}$  in the averaged multiplicity  $dN/d^2P_\perp dy|_{pA}$ , while the number of binary collisions is proportional to approximately  $A^{1/3}$ . Then we naively expect  $R_{pA} \sim A^{1/3}$  at large  $P_\perp$ .

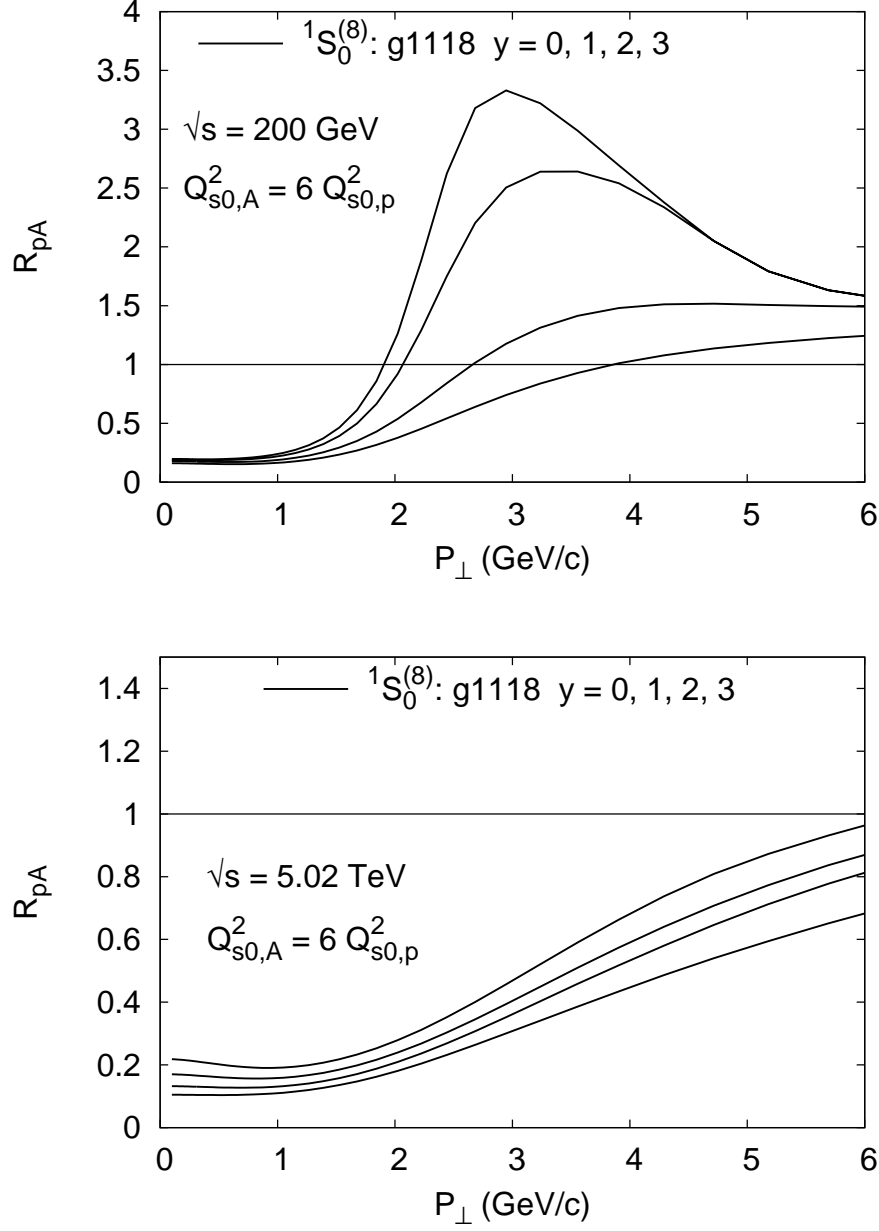


Figure 7.9:  $R_{pA}(P_{\perp})$  as a function of transverse momentum of  $J/\psi$  production in pA collisions at  $\sqrt{s} = 200$  GeV (Upper) and  $\sqrt{s} = 5.02$  TeV (Lower) at each rapidity  $y = 0, 1, 2, 3$ . We have assumed color octet  $c\bar{c}$  in  $^1S_0$  state becomes  $J/\psi$  with non-perturbative interaction. The charm quark mass is fixed as a half of the  $J/\psi$  mass  $2m_c = M_{J/\psi} = 3.1$  GeV.

pair in  $^1S_0$  at  $\sqrt{s} = 200$  GeV (Upper) and  $\sqrt{s} = 5.02$  TeV (Lower) at rapidity  $y = 0, 1, 2, 3$ . We have used the uGD set g1118 both in proton and nucleus and set  $Q_{s0,A}^2 = 6Q_{s0,p}^2$ . In the RHIC energy, we found a strong suppression of the  $R_{pA}$  at mid and forward rapidity in the low  $P_\perp \lesssim 2$  GeV region and large Cronin like peak around  $\sim 3$  GeV at  $y = 0$  and 1. As the rapidity increases, the Cronin like peak disappears and the  $R_{pA}$  at large  $P_\perp$  gets close to unity. On the other hand, the  $R_{pA}$  in the LHC energy is more suppressed even at mid rapidity because of the quantum evolution effect. We certainly checked these behaviors of the  $R_{pA}$  at RHIC and the LHC are qualitatively the same as we have shown in the CEM production.

## 7.4 Short summary

In this chapter, we have computed the  $J/\psi$  production cross section within the color singlet model Eq. (7.50) at mid rapidity in the RHIC energy and compared it with data. We have assumed the large- $N_c$  approximation and constructed the quadrupole scattering matrix only by the dipole scattering matrix which is assumed to be the gaussian form. We wondered initially whether the nuclear modification factor  $R_{pA}$  of the  $J/\psi$  production which is computed in the color evaporation model can be modified quantitatively by adding the contribution of direct  $J/\psi$  production from the color singlet heavy quark pair.

Concerning the  $R_{pA}$  of direct  $J/\psi$  production, we found in Fig. 7.8 the enhancement which means that the  $R_{pA}$  is larger than unity because of the  $A$ -dependence in the specific function Eq. (7.57) which appears in our color singlet model. However, the cross section of the direct  $J/\psi$  production can not reproduce the data both in pp collisions and dAu collisions at RHIC. From these results, although we do not consider the quantum evolution effect of dipole and quadrupole scattering matrices, we conclude that the direct  $J/\psi$  production from color singlet quark pair might not be dominant production process and does not change the nuclear modification factor quantitatively in itself. In this paper, while we just compared our numerical results with the RHIC data, we expect the direct  $J/\psi$  production from color singlet quark pair in itself is not dominant production process at the LHC too.

On the other hand, we never mean that the dynamics of bound state formation is not important for understanding the difference between our result of the  $R_{pA}$  of the  $J/\psi$  production in pA collisions at the LHC and the data. We have not included a contribution of the higher state feed-down and possibly the direct  $J/\psi$  production from the color singlet

heavy quark pair at next to leading order (NLO) in strong coupling constant with  $v = 0$  can contribute to the total cross section because the new production channel is opened at NLO. Then we will leave it in future study.

# Chapter 8

## Summary

### Approach

Our calculations in this paper are based on the framework of heavy quark pair production from the CGC in pA collisions where a pA collision is regarded as a dilute-dense system. The quark pair production cross section is evaluated at leading order in the strong coupling constant and the color charge density  $\rho_p$  in the proton, but in all orders in the nucleus color charge density (3.44). Single quark production cross-section is obtained by integrating the pair production cross-section over the anti-quark phase space.

Incoming gluon from the proton is produced by the unintegrated gluon distribution (uGD), while gluon coming from nucleus allows a multi parton function such as 3-point function (3.46). In the large- $N_c$  limit, the multi parton function is obtained by using the dipole amplitude which is defined as a product of two Wilson lines in the fundamental representation averaging all the configurations of the classical color charge density. The dipole amplitude also represents eikonal phase which include multiple scattering effect of valence partons in the nucleus. At small Bjorken's  $x$ ,  $\alpha_s \ln(1/x)$  correction becomes larger and important for the phenomenology. Nonlinear BK equation allows us to include quantum evolution effects at small  $x$  in the dipole amplitude. Then, the CGC formula systematically describes both classical multiple scattering effect of valence partons and the nonlinear QCD evolution effect on the quark pair production (3.22).

At initial point of evolution  $x_0 = 0.01$ , the BK equation with running coupling correction is constrained by global fitting of HERA data. We use the constrained initial condition of the BK equation and construct the unintegrated gluon distribution at small  $x \leq x_0$  in the proton. On the other hand, we change the initial saturation scale of the gluon distribution for the heavy nucleus, by assuming the translational invariance in the

nucleus and limiting the minimum bias event. For  $x_0 \leq x \leq 1$ , on the other hand, we apply the phenomenological Ansatz (3.64) where we extrapolate the uGD at  $x_0$ . This extrapolation implies that the saturation scale is frozen at large  $x$ . As for the central and peripheral collisions, we use the Glauber model to compute the number of collisions. We assume in this paper that a nuclear density is constant to simplify the discussion.

Physical quarkonium and heavy meson productions cross section are obtained by convoluting the quark pair cross section with non-perturbative hadronization model. We firstly studied the quarkonium production in the CEM where the hadronization dynamics is treated simply and later attempted to match the quark pair production cross section from the CGC with the NRQCD approach where the dynamics of hadronization is more complicated. We use the heavy quark fragmentation function for describing the heavy meson production.

## Results

We have shown the numerical results of quarkonium and heavy meson production in pA collisions compared to the available data at RHIC and the LHC.

The transverse momentum spectra of quarkonium and heavy meson production cross sections are accompanied by large uncertainties on input parameters. However, the uncertainties of the results are canceled in  $R_{pA}$  which quantifies the production and propagation of quarkonium/heavy meson in pA collisions. We have found that in the CEM  $R_{pA}$  of  $J/\psi$  and  $D$  meson in pA collisions at the LHC are suppressed than those at RHIC because of the non-linear QCD evolution effect in the small- $x$  region. As to the peripheral collisions at RHIC, our model fails to describe the data. Then the computations by the use of more realistic nuclear profile is needed. We comment that the  $D\bar{D}$  correlation in pA collisions can provide the valuable information of saturation effects in the heavy nucleus. However, we might need to consider the decay process of heavy meson (e.g.  $D \rightarrow e$ ) in order to compare our results to data because statistics of  $D\bar{D}$  production itself is small then the lepton from heavy quark decay is often used in experiments.

In order to clear the reason why the  $R_{pA}$  of  $J/\psi$  production at the LHC is comparable to that at RHIC, we investigated the hadronization dynamics by using the color singlet model. We found the color singlet model bring a possibility to enhance the cross section of quarkonium production in pA collisions than pp collisions. This is because the large number of atomic mass number  $A$  compensate for a suppression of higher order in coupling constant as  $\alpha_s^2 A^{1/3} \sim \mathcal{O}(1)$  which is encoded in multi parton correlator in the



nucleus. Although we have not included the quantum evolution effects, we have verified the enhancement of  $J/\psi$  and  $\Upsilon(1S)$  production cross section in pA collisions compared to normalized pp collisions. Multi parton function is observed characteristically in pA collisions, and then, it suggest that the multi parton function brings different feature in quarkonium production in pA collisions than pp collisions.

However, we found the color singlet model does not contribute the total inclusive  $J/\psi$  production at RHIC. This might mean we need to compute the contribution of color octet channel precisely or NLO hard process. If the heavy meson production experiments will be carried out precisely, the importance of dynamics of hadronization (bound state) can be expected to become more clear. In any case, our results in this paper are first quantitative theoretical results which can be comparable to the data and the important start point for the study of heavy quark pair production in the CGC framework.

## Outlook

Finally, we show outlook of this study.

### Completing NRQCD matching

We have matched the heavy quark pair production in S-wave from the CGC with NRQCD factorization approach. However, the P-wave production is also required in order to extract the Long Distance matrix Elements from the data of hadron collider such as Tevatron and the LHC. Hard matrix elements of P-wave production in the context of the CGC can be found in Ref. [70].

### Quantum evolution of multi parton function

Color singlet model for quarkonium production is relevant to quadrupole amplitude in the nucleus. When the distribution of the color charge density is gaussian, we have already known that the quadrupole amplitude consists of dipole amplitude only in the large  $N$  approximation. Then, in order to study the rapidity dependence of the production cross section, it is dispensable to include the evolution effect in the quadrupole amplitude though the dipole amplitude which obeys rcBK equation, or providing a numerical solution of JIMWLK equation directly.

### Higher order correction

Recently NRQCD framework has been extended to NLO systematically, which results in a significantly improved description of quarkonium production in pp collisions [97, 98]. The NLO extension of the CGC framework for hadron production in pA collisions is also elaborated recently [149]. As we have remarked in Chap. 3, the pair production formula (3.44) used in this study is derived at LO in  $\alpha_s$  and the color charge density in the proton, but includes full orders of dense target effects. Extension of the CGC framework from the LO to the NLO accuracy is seriously attempted nowadays for more accurate and robust study. For example, the near-side peak in azimuthal angle correlation between the quark pair can appear at NLO in collinear factorization framework, and comparison of these frameworks seems important.

### Soft parton resummation

As pointed out by the authors in Ref. [150, 151], improvement of soft gluon resummation needs in back-to-back kinematics of  $D\bar{D}$  (or  $B\bar{B}$ ) pair production and also in production of  $J/\psi$  at small  $P_\perp$  compared to invariant mass of the pair. We leave these for a future study.

### In nucleus-nucleus collisions

In the context of HICs, the extending our study to the AA collisions is important study. The CGC calculation at the present day describes the particle production at only low transverse momentum region because the typical saturation scale is semi hard but comparable to the heavy quark mass scale or larger a little. On the other hand, if we can verify that the heavy quark production in the larger transverse momentum region at pA collisions does not depend on the CNM effects, pA collisions can be regarded as a reference of AA collisions. In fact, the energy loss mechanism of heavy quark in hot medium expects strongly suppression of  $R_{AA}$  at larger transverse momentum. So the model extension in order to describe the cross section of heavy quark production ( $J/\psi$ ,  $D$ ) as a function of transverse momentum is important future work.

# Appendix A

## Notations and Identities

### A.1 Notation

We show the notations and the definitions used in this paper. When we meet a two expression with same Lorentz and color indices, we promise to contract them.

$$\begin{aligned} h = c = 1, \quad g^{\mu\nu} &= \text{diag}(1, -1, -1, -1), \\ x^\mu &= (t, \mathbf{x}), \quad p^\mu = (E, \mathbf{p}), \\ x^2 = g_{\mu\nu} x^\mu x^\nu &= t^2 - \mathbf{x}^2, \quad p^2 = g_{\mu\nu} p^\mu p^\nu = E^2 - \mathbf{p}^2, \\ p^\mu &= i \frac{\partial}{\partial x_\mu} = i \partial^\mu, \\ \square &= \partial_\mu \partial^\mu. \end{aligned} \tag{A.1}$$

Another important definition is a metric of light-cone frame. In particular, the Wilson line as the gauge link is defined in terms of the gauge field in the light-cone frame. in this paper, we take [133]

$$x^+ = \frac{1}{\sqrt{2}}(x^0 + x^3) \tag{A.2}$$

$$x^- = \frac{1}{\sqrt{2}}(x^0 - x^3), \tag{A.3}$$

and define the light cone momentum  $x^\mu = (x^+, x^-, \mathbf{x}_\perp)$  with light cone metric  $g_{+-} = g_{-+} = 1$ ,  $g_{11} = g_{22} = -1$  and the other zero.  $v^2 = 2v^+v^- - \mathbf{v}_\perp^2$  and  $u \cdot v = u^+v^- + u^-v^+ - \mathbf{u}_\perp \cdot \mathbf{v}_\perp$

## A.2 $\gamma$ -matrices

In 4 dimensional Clifford algebra,

$$\begin{aligned}\{\gamma^\mu, \gamma^\nu\} &= 2g^{\mu\nu}, \\ \sigma^{\mu\nu} &= \frac{i}{2}[\gamma^\mu, \gamma^\nu], \\ \text{tr}[\gamma^\mu \gamma^\nu] &= 4g^{\mu\nu}, \\ \text{tr}[\gamma^\mu \gamma^\nu \gamma^\rho \gamma^\sigma] &= 4(g^{\mu\nu} g^{\rho\sigma} - g^{\mu\rho} g^{\nu\sigma} + g^{\mu\sigma} g^{\nu\rho}).\end{aligned}\tag{A.4}$$

Dirac matrices  $\gamma^\mu$  in standard Dirac expression is,

$$\gamma^0 = \begin{pmatrix} \mathbf{1} & \mathbf{0} \\ \mathbf{0} & -\mathbf{1} \end{pmatrix}, \quad \gamma^i = \begin{pmatrix} 0 & \sigma^i \\ -\sigma^i & 0 \end{pmatrix}, \quad \gamma^5 = i\gamma^0\gamma^1\gamma^2\gamma^3 = \begin{pmatrix} \mathbf{0} & \mathbf{1} \\ \mathbf{1} & \mathbf{0} \end{pmatrix}.\tag{A.5}$$

Here  $\sigma^i$  is SU(2) Pauli matrices and

$$\sigma^1 = \begin{pmatrix} 0 & 1 \\ 1 & 0 \end{pmatrix}, \quad \sigma^2 = \begin{pmatrix} 0 & -i \\ i & 0 \end{pmatrix}, \quad \sigma^3 = \begin{pmatrix} 1 & 0 \\ 0 & -1 \end{pmatrix}.\tag{A.6}$$

## A.3 SU(3) algebra

$t^a$  is a generator of compact SU(3) Lie group and fill the property of Lie algebra.

$$\text{tr}[t^a] = 0,\tag{A.7}$$

$$[t^a, t^b] = if^{abc}t^c, f^{abc} = f_{abc}.\tag{A.8}$$

$t^a = \frac{\lambda^a}{2}$  in the fundamental representation and Gell-Mann matrices  $\lambda^a$  have a following value.

$$\begin{aligned}\lambda^i &= \begin{pmatrix} \sigma^i & 0 \\ 0 & 0 \end{pmatrix} \quad ; i = 1, 2, 3, \quad \lambda^4 = \begin{pmatrix} 0 & 0 & 1 \\ 0 & 0 & 0 \\ 1 & 0 & 0 \end{pmatrix}, \quad \lambda^5 = \begin{pmatrix} 0 & 0 & -i \\ 0 & 0 & 0 \\ i & 0 & 0 \end{pmatrix}, \\ \lambda^6 &= \begin{pmatrix} 1 & 0 \\ 0 & \sigma^1 \end{pmatrix}, \quad \lambda^7 = \begin{pmatrix} 0 & 0 \\ 0 & \sigma^2 \end{pmatrix}, \quad \lambda^8 = \frac{1}{\sqrt{3}} \begin{pmatrix} 1 & 0 & 0 \\ 0 & 1 & 0 \\ 0 & 0 & -2 \end{pmatrix}.\end{aligned}\tag{A.9}$$

$t^\alpha$  has a following anti-commutation relation,

$$\{t^a, t^b\} = \frac{1}{3}\delta^{ab}\mathbf{1} + d^{abc}t^c, d^{abc} = d_{abc}. \quad (\text{A.10})$$

This expression is completely symmetric with exchanging the indices  $a$ ,  $b$  and  $c$ . The coefficients for each relation are

$$\begin{aligned} 1 &= f_{123} = 2f_{147} = 2f_{246} = 2f_{257} = 2f_{345} = -2f_{156} = -2f_{367} = \frac{2f_{458}}{\sqrt{3}} = \frac{2f_{678}}{\sqrt{3}}, \\ \frac{1}{\sqrt{3}} &= d_{118} = d_{228} = d_{338} = -d_{888}, \\ -\frac{1}{2\sqrt{3}} &= d_{448} = d_{558} = d_{668} = d_{778}, \\ \frac{1}{2} &= d_{146} = d_{157} = d_{247} = d_{256} = d_{344} = d_{355} = -d_{366} = -d_{377}. \end{aligned} \quad (\text{A.11})$$

We also note the sum of these structure functions are given by

$$\begin{aligned} \sum_{abc} d^{abc} d^{abc} &= \frac{40}{3} \\ \sum_{abc} f^{abc} f^{abc} &= 24. \end{aligned} \quad (\text{A.12})$$

In addition to the above relations, there are some more relations as follows:

$$t^a t^b = \frac{1}{2}(d^{abn} + if^{abn})t^n + \frac{1}{6}\delta^{ab}, \quad (\text{A.13})$$

$$\text{tr}[t^a t^b] = \frac{1}{2}\delta^{ab}, \quad (\text{A.14})$$

$$t^a t^b t^c = \frac{1}{2}(d^{abn} + if^{abn})t^n t^c + \frac{1}{6}\delta^{ab}t^c, \quad (\text{A.15})$$

$$\text{tr}[t^a t^b t^c] = \frac{1}{4}(d^{abc} + if^{abc}). \quad (\text{A.16})$$

## A.4 Clebsh-Gordon coefficient

In general, Clebsh-Gordon coefficient is given by

$$\begin{aligned}
& \langle J_1, m_1; J_2, M_2 | J, M \rangle \\
&= \delta_{M, M_1+M_2} \sqrt{2J+1} \Delta(J_1 J_2 J) \\
&\times \sqrt{(J_1+M_1)!(J_1-M_1)!(J_2+M_2)!(J_2-M_2)!(J+M)!(J-M)!} \\
&\times \sum_z (-1)^z [z!(J_1+J_2-J-z)!(J_1-M_1-z)!(J_2+M_2-z)!(J-J_2+M_1+z)! \\
&\quad \times (J-J_1-M_2+z)!]^{-1},
\end{aligned} \tag{A.17}$$

where

$$\Delta(J_1 J_2 J) = \sqrt{\frac{(J_1+J_2-J)!(J+J_1-J_2)!(J+J_2-J_1)!}{(J_1+J_2+J+1)!}}. \tag{A.18}$$

We note  $0! = 1$ .

## A.5 Fierz identities

Along with the Fierz identities for  $SU(N)$  algebra

$$(t^a)_{ij}(t^a)_{kl} = \frac{1}{2} \left( \delta_{il}\delta_{jk} - \frac{1}{N}\delta_{ij}\delta_{kl} \right) \tag{A.19}$$

which imply

$$\text{tr}[t^a M_1 t^a M_2] = \frac{1}{2} \text{tr}[M_1] \text{tr}[M_2] - \frac{1}{2N} \text{tr}[M_1 M_2] \tag{A.20}$$

$$\text{tr}[t^a M_1] \text{tr}[t^a M_2] = \frac{1}{2} \text{tr}[M_1 M_2] - \frac{1}{2N} \text{tr}[M_1] \text{tr}[M_2] \tag{A.21}$$

for any  $(N \times N)$  matrices  $M_1$  and  $M_2$ .

## A.6 Formulae

We show some formulas used in our calculations.

- Bessel function of the first kind (Hansen's representation);

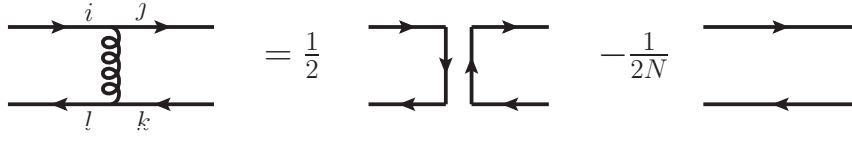


Figure A.1: Graphical representation of Fierz identities for  $SU(N)$  algebra.

$$J_n(z) = \frac{1}{\pi i n} \int_0^\pi e^{iz \cos \theta} \cos n\theta d\theta. \quad (\text{A.22})$$

- Modified Bessel function of the second kind;

$$K_0(m\mathbf{x}_\perp) = \frac{1}{2\pi} \int \frac{d^2\mathbf{k}_\perp}{\mathbf{k}_\perp^2 + m^2} e^{i\mathbf{k}_\perp \cdot \mathbf{x}_\perp}. \quad (\text{A.23})$$

- Trigonometric functions;

$$\cos^{2n} \theta = \frac{1}{2^{2n-1}} \left[ \sum_{r=0}^{n-1} \binom{2n}{r} \cos(2n-2r)\theta + \frac{1}{2} \binom{2n}{n} \right] \quad (\text{A.24})$$

$$\cos^{2n+1} \theta = \frac{1}{2^{2n}} \sum_{r=0}^n \binom{2n+1}{r} \cos(2n-2r+1)\theta. \quad (\text{A.25})$$

- Weber's Integration;

$$\int_0^\infty dx e^{-a^2 x^2} x J_0(bx) = e^{-b^2/(4a^2)} / (2a^2). \quad (\text{A.26})$$

# Appendix B

## Hard part of the cross section

In this chapter, we present the detail expression of the hard matrix part of the cross section which is used in Eq. (7.15). To see the detail results, let us introduce some projection momentum to treat light cone variables explicitly:

$$n_-^\mu = \frac{1}{\sqrt{2}}(1, 0, 0, 1) \tag{B.1}$$

$$n_+^\mu = \frac{1}{\sqrt{2}}(1, 0, 0, -1) \tag{B.2}$$

$$n_i^\mu = (0, 1, 1, 0) \qquad n_+^2 = n_-^2 = n_+ \cdot n_i = n_- \cdot n_i = 0 \tag{B.3}$$

$$n_+ \cdot n_- = 1 \tag{B.4}$$

$$n_i^2 = -2. \tag{B.5}$$



### $^3S_1^{(1)}$ channel

For color singlet  $^3S_1^{(1)}$  state, summing over the final spin components, an explicit expression of the hard part is given by

$$\begin{aligned}
& \Xi^{^3S_1^{(1)}}(\mathbf{k}_1, \mathbf{k}_2, \mathbf{k}, \mathbf{k}') \\
&= \sum_{S_z} \text{tr}_d[\mathcal{P}_{1S_z}(P; l=0) T_{q\bar{q}}(\mathbf{k}_{1\perp}, \mathbf{k}_{\perp})] \text{tr}_d[T_{q\bar{q}}^\dagger(\mathbf{k}_{1\perp}, \mathbf{k}'_{\perp}) \mathcal{P}_{1S_z}^\dagger(P; l=0)] \\
&= \left( -g^{\mu\nu} + \frac{P^\mu P^\nu}{M^2} \right) \frac{1}{2M^2} \frac{1}{2^4} \frac{1}{(P^+)^2} \\
&\times \frac{\text{tr}_d[(\not{P} - M) \gamma_\mu (\not{P} + M) \not{h}_+ (\not{P} - 2\not{k} + M) \not{h}_- (\not{P} - 2\not{k} - 2\not{k}_1 + M) \not{h}_+]}{[(\mathbf{P}_\perp - 2\mathbf{k}_\perp)^2 + (\mathbf{P}_\perp - 2\mathbf{k}_\perp - 2\mathbf{k}_{1\perp})^2 + 2M^2]} \\
&\times \frac{\text{tr}_d[\not{h}_+ (\not{P} - 2\not{k}' - 2\not{k}_1 + M) \not{h}_- (\not{P} - 2\not{k}' + M) \not{h}_+ (\not{P} + M) \gamma_\nu (\not{P} - M)]}{[(\mathbf{P}_\perp - 2\mathbf{k}'_\perp)^2 + (\mathbf{P}_\perp - 2\mathbf{k}'_\perp - 2\mathbf{k}_{1\perp})^2 + 2M^2]}, \quad (\text{B.6})
\end{aligned}$$

where the  $J/\psi$  mass is  $M = 2m$  in terms of  $v = 0$  limit. We have also used the following relation:

$$\sum_{i=T_1, T_2, L} \varepsilon_i^\mu \varepsilon_i^{\nu*} = -g^{\mu\nu} + \frac{P^\mu P^\nu}{M^2}. \quad (\text{B.7})$$

By the use of the mathematica package "*FeynCalc*" [135], we found

$$\Xi^{^3S_1^{(1)}}(\mathbf{k}_1, \mathbf{k}_2, \mathbf{k}, \mathbf{k}') = \frac{F^{(1)}}{D^{(1)}}, \quad (\text{B.8})$$

where the denominator of  $\Xi^{^3S_1^{(1)}}$  is given by

$$D^{(1)} = [4\mathbf{l}_{1\perp}^2 + \mathbf{k}_{1\perp}^2 + M^2][4\mathbf{l}_{2\perp}^2 + \mathbf{k}_{1\perp}^2 + M^2] = L_1 L_2, \quad (\text{B.9})$$

and the numerator is

$$F^{(1)} = 2(\mathbf{k}_{1\perp}^4 + 2\mathbf{k}_{1\perp}^2 M^2 + M^4 - 4\mathbf{k}_{1\perp}^2(\mathbf{l}_{1\perp}^2 + \mathbf{l}_{2\perp}^2) + 16(\mathbf{l}_{2\perp}^2)(\mathbf{l}_{1\perp}^2) + 4M^2(\mathbf{l}_{1\perp}^2 + \mathbf{l}_{2\perp}^2)), \quad (\text{B.10})$$

where

$$\mathbf{l}_{1\perp} = \mathbf{k}_{\perp} - \frac{\mathbf{k}_{2\perp}}{2} \quad (\text{B.11})$$

$$\mathbf{l}_{2\perp} = \mathbf{k}'_{\perp} - \frac{\mathbf{k}_{2\perp}}{2} \quad (\text{B.12})$$

with  $\mathbf{P}_{\perp} = \mathbf{k}_{1\perp} + \mathbf{k}_{2\perp}$  and compact notations defined as

$$\begin{aligned} L_1 &= 4\mathbf{l}_{1\perp}^2 + \mathbf{k}_{1\perp}^2 + M^2 \\ L_2 &= 4\mathbf{l}_{2\perp}^2 + \mathbf{k}_{1\perp}^2 + M^2. \end{aligned} \quad (\text{B.13})$$

Finally, we can obtain the following result

$$\Xi^{^3S_1^{(1)}}(\mathbf{k}_1, \mathbf{k}_2, \mathbf{k}, \mathbf{k}') = \frac{8\mathbf{k}_{1\perp}^2(\mathbf{k}_{1\perp}^2 + M^2)}{L_1 L_2} - 4\mathbf{k}_{1\perp}^2 \left( \frac{1}{L_1} + \frac{1}{L_2} \right) + 2. \quad (\text{B.14})$$

$^1S_0^{(8)}$  **channel**

For color octet  $^1S_0$  state, the square matrix element is just given by

$$\Xi^{^1S_0^{(8)}}(\mathbf{k}_1, \mathbf{k}_2, \mathbf{k}) = \frac{2^5(\mathbf{k}_{1\perp}^2 \mathbf{l}_{1\perp}^2 - (\mathbf{k}_{1\perp} \cdot \mathbf{l}_{1\perp})^2)}{L_1^2}. \quad (\text{B.15})$$

# Appendix C

## Quarkonium and Heavy meson

Quarkonium as a bound state of a quark and an antiquark is very similar to positronium which is a QED bound state. Spectroscopic classification of various quarkonium states is shown in Table C. QCD motivated potential consists of one gluon exchange part at short distance  $\propto -\alpha_s/r$ , and confining part at long distance  $\kappa r$  with  $r$  is the distance between the quark and the antiquark, and  $\kappa \sim 1$  GeV/fm.

Concerning the quarkonium production, there are two production sources. One is prompt production where the quarkonium is hadronized directly from the heavy quark which is created in initial gluon scattering, and there is also a contribution by feed-down of higher excited states which are produced primarily (e.g.  $\chi_c \rightarrow J/\psi + \gamma$ ). Another source is non-prompt production by a heavy meson decays via weak interaction (e.g.  $B^+ \rightarrow J/\psi + K^+$ ). Prompt production process largely contributes to a total production yield of quarkonia. We show in Table C.3 a ratios of the contribution source with respect to each state to total quarkonium yield in the prompt production.

$c\bar{c}$ mesons	$\eta_c(1S)$	$J/\psi(1S)$	$\chi_{c0}(1P)$	$\chi_{c1}(1P)$	$\chi_{c2}(1P)$	$\psi'(2S)$
Mass [GeV]	2.98	3.10	3.42	3.51	3.56	3.69
$J^{PC}$	$0^{-+}$	$1^{--}$	$0^{++}$	$1^{++}$	$2^{++}$	$1^{--}$
$b\bar{b}$ mesons	$\eta_b(1S)$	$\Upsilon(1S)$	$\chi_{b0}(1P)$	$\chi_{b1}(1P)$	$\chi_{b2}(1P)$	$\Upsilon(2S)$
Mass [GeV]	9.40	9.46	9.86	9.89	9.91	10.02
$J^{PC}$	$0^{-+}$	$1^{--}$	$0^{++}$	$1^{++}$	$2^{++}$	$1^{--}$

Table C.1: Spectroscopic classification of charmonium and bottomonium with respect to each quantum number. Cited from [153].

Charmed mesons	$D^\pm$	$D^0$	$D^{*\pm}$	$D^{*0}$	Bottom mesons	$B^\pm$	$B^0$
Mass [GeV]	1.87	1.86	2.01(0)	2.00(7)	Mass [GeV]	5.28	5.28
$I(J^P)$	$\frac{1}{2}(0^-)$	$\frac{1}{2}(0^-)$	$\frac{1}{2}(1^-)$	$\frac{1}{2}(1^-)$	$I(J^P)$	$\frac{1}{2}(0^-)$	$\frac{1}{2}(0^-)$

Table C.2: Spectroscopic classification of Charmed meson and Bottom meson with respect to each quantum number. Cited from [153].

$H$	$F_H$ (in %)	$H$	$F_H$ (in %)
$J/\psi$	$64 \pm 6$	$\Upsilon(1S)$	$50.9 \pm 8.2(\text{stat.}) \pm 9.0(\text{sys.})$
$\psi(2S)$	$7 \pm 2 \sim 15 \pm 5$	$\Upsilon(2S)$	$10.7 + 7.7 / - 4.8$
$\chi_c(1P)$	$29.7 \pm 1.7(\text{stat.}) \pm 5.7(\text{sys.})$	$\chi_b(1)$	$27.1 \pm 6.9(\text{stat.}) \pm 4.4(\text{sys.})$

Table C.3: The ratios of the contribution source to total  $J/\psi$  yield in the prompt production.  $F_{J/\psi}$  expresses the direct  $J/\psi$  production rate,  $F_{\psi(2S)}$  is the ratio of a contribution from the  $\psi(2S)$  feed down to the  $J/\psi$  yield, and  $F_{\chi_c}$  is the same as  $F_{\psi(2S)}$ .  $F_H$  for the  $\Upsilon$  production is the same as  $J/\psi$ . Cited from [77].

In contrast to quarkonium, a heavy meson involving specific flavor quantum number consists of a heavy quark and a light quark. The spectroscopic classification of heavy mesons is shown in Table C. The contribution sources to the heavy meson production Heavy meson production sources are also clarified by prompt and non-prompt production as explained in the quarkonium production.

In this Appendix, we present specific hadronization models of quarkonium (Color Singlet Model, Color Evaporation Model, and NRQCD approach) and fragmentation functions of open heavy flavor heavy meson. These models are used widely so far in phenomenological studies.

## C.1 Color Singlet Model

Color Singlet Model (CSM) for quarkonium production is based on the quarkonium potential model combined with the parton model calculation at short distance [80–82]. In the CSM, a factorization between a short distance matrix element describing the production of an on-shell heavy quark pair and a long distance matrix element describing the non-perturbative bound state is assumed. Once this factorization assumption is justified, large transverse momentum scale in addition to the heavy quark mass scale compared

with  $\Lambda_{\text{QCD}}$  allows us to calculate the short distance amplitude with the perturbation theory in terms of the strong coupling constant  $\alpha_s$ . In hadronic collisions, if the produced heavy quark pair is color octet state, an additional gluon is required to make the color octet quark pair become color singlet in the bound state. In regard to this point, we further assume that the color singlet quark pair production with the additional gluon is perturbatively calculated.

Based on these assumptions, production amplitude of a quarkonium  $H$  is expressed as

$$\mathcal{M}_H = \int d^4l \mathcal{M}_{q\bar{q}}(l) \psi_H(l), \quad (\text{C.1})$$

where  $\mathcal{M}_{q\bar{q}}$  is heavy quark pair production amplitude in the color singlet state and the Bethe-Salpeter amplitude ( $\psi_H$ ).  $l^\mu$  is a relative momentum between the composite quark and the antiquark. Here,  $\mathcal{M}_{q\bar{q}}$  includes all the hard scattering part of the amplitude. If all the components of  $l^\mu$  are smaller than the invariant mass  $M \simeq 2m_q$  of the pair in the quarkonium rest frame, then we can expand  $\mathcal{M}_{q\bar{q}}$  in terms of  $l^0/M$  and  $|\mathbf{l}|/M$  as follows;

$$\mathcal{M}_H \sim \mathcal{M}_{q\bar{q}}(0) \int d^4l \psi_H(l) + \left. \frac{\partial}{\partial l^\mu} \mathcal{M}_{q\bar{q}}(l) \right|_{l=0} \int l^\mu d^4l \psi_H(l) + \dots \quad (\text{C.2})$$

First term corresponds to the S-wave amplitude and the second term, which involves a derivative of the wave function at origin, corresponds to the P-wave amplitude. In principle, the amplitude is expressed as an infinite series in  $(l^\mu)^n$  ( $n = 0, 1, \dots$ ). However, it might be sufficient to compute only the low order terms in the expanded amplitude because the higher order terms are considered to be suppressed by factors of  $(l/M)^n$ <sup>1</sup>.

## C.2 Color Evaporation Model

Color Evaporation Model (CEM) assumes that a part of the produced heavy quark pairs bound into a color singlet quarkonium with soft gluon interaction<sup>2</sup> [77, 83], and the dynamics of this hadronization is not depend on the color state of the produced heavy quark pair. Production cross section of a quarkonium  $H$  from a  $q\bar{q}$  quark pair is computed

---

<sup>1</sup>Strict speaking, we must compute higher order corrections to confirm whether the perturbative expansion in terms of coupling constant converges or not.

<sup>2</sup>This color neutralization is called *evaporation*.

PDF	$m_c$ (GeV)	$\frac{\mu}{m_{c\perp}}$	$F_{c\bar{c}\rightarrow J/\psi}$	PDF	$m_b$ (GeV)	$\frac{\mu}{m_{b\perp}}$	$F_{b\bar{b}\rightarrow \Upsilon(1S)}$
MRST HO	1.2	2	0.0144	MRST HO	4.75	1	0.0276
MRST HO	1.4	1	0.0248	MRST HO	4.5	2	0.0201
CTEQ 5M	1.2	2	0.0155	MRST HO	5.0	0.5	0.0508
GRV 98 HO	1.3	1	0.0229	GRV 98 HO	4.75	1	0.0225

Table C.4: Parameters  $F_{c\bar{c}\rightarrow J/\psi}$  and  $F_{b\bar{b}\rightarrow \Upsilon}$  of inclusive production for various choices of parton distribution functions (PDFs) [84–87], quark masses ( $m$ ), and ratio of renormalization scales ( $\mu$ ).  $\mu$  is set to a constant times the transverse mass ( $m_{\perp} = \sqrt{m^2 + \mathbf{P}_{\perp}^2}$ ), where  $\mathbf{P}_{\perp}$  is the total momentum of the quark and antiquark. Cited from Ref. [77]. See also Ref. [88, 89].

$H$	$J/\psi$	$\psi'(2S)$	$\chi_{c1}$	$H$	$\Upsilon(1S)$	$\Upsilon(2S)$	$\chi_{b1}(1P)$
$F_{c\bar{c}\rightarrow J/\psi}^{\text{direct}}/F_{c\bar{c}\rightarrow J/\psi}^{\text{inclusive}}$	0.62	0.14	0.60	$F_{b\bar{b}\rightarrow \Upsilon}^{\text{direct}}/F_{b\bar{b}\rightarrow \Upsilon}^{\text{inclusive}}$	0.52	0.33	1.08

Table C.5: Ratio of the direct CEM parameters  $F_{c\bar{c}\rightarrow H}^{\text{direct}}$  and  $F_{b\bar{b}\rightarrow H}^{\text{direct}}$  to those of inclusive production. Cited from Ref. [77].

as follows;

$$d\sigma_H = F_{q\bar{q}\rightarrow H} \int_{(2m_q)^2}^{(2M_Q)^2} dM^2 \frac{d\sigma_{q\bar{q}}}{dM^2} \quad (\text{C.3})$$

where  $m_q$  is the quark mass and  $M_Q$  is a mass of the open heavy flavor meson and  $M$  is a invariant mass of the quark pair.  $F_{q\bar{q}\rightarrow H}$  is an empirical factor which controls the order of magnitude of the cross section. This formula represents that all the quark pairs within a certain invariant mass region from the quark mass up to the the decay threshold bound into a quarkonium with the transition probability  $F_{q\bar{q}\rightarrow H}$ . This empirical factor  $F_{q\bar{q}\rightarrow H}$  has been estimated in the collinear factorization framework by fitting the data, and we show the fitted values of  $F_{q\bar{q}\rightarrow H}$  for inclusive and direct production of charmonia and bottomonia in Table. C.4 and C.5. We should note that the CEM provides only unpolarized cross section in contrast to the CSM.

## C.3 Non-Relativistic QCD approach

### C.3.1 Factorization

Non-Relativistic QCD (NRQCD) effective field theory [90–92] is more sophisticated approach to compute a production and a decay of a quarkonium. The production cross section of a quarkonium  $H$  in the NRQCD reads

$$d\sigma_H = \sum_n C_{\text{short}}^n \langle 0 | \mathcal{O}_n^H | 0 \rangle \quad (\text{C.4})$$

where  $n$  is a arbitrary quantum state of the  $q\bar{q}$  binding into the  $H$ . The Eq. (C.4) is based on a assumption of factorization between the short distance coefficient  $C_{\text{short}}^n$  involving heavy quark mass scale  $m$  or larger, which is computed perturbatively in terms of strong coupling constant  $\alpha_s$ , and a long distance matrix element  $\langle 0 | \mathcal{O}_n^H | 0 \rangle$  involving the smaller scales  $mv$ ,  $mv^2$ , or  $\Lambda_{\text{QCD}}$  with small heavy quark relative velocity  $v$ . Of particular importance is that we should interpret the NRQCD calculations as the results in the quarkonium rest frame. Concerning a  $q\bar{q}$  bound state with color coulomb force,  $mv$  corresponds to a relative momentum of heavy quark and antiquark in the quarkonium rest frame and  $mv^2$  corresponds to a binding energy of the quarkonium. Thus, one can understand the validity of perturbation expansion in powers of  $v$  within the NRQCD framework, and both the  $\alpha_s$  and the  $v$  can be used as the small expansion parameters. The NRQCD operator of heavy quark pair is given by

$$\mathcal{O}_n^H = \psi^\dagger \mathcal{K}_n \chi \chi^\dagger \mathcal{K}_n' \psi \quad (\text{C.5})$$

where  $\psi_f$  ( $\chi_f$ ) is a two component Pauli spinor field which annihilates (produces) a heavy quark  $f$  (antiquark  $\bar{f}$ ) In fact, a four component Dirac field consists of these two component spinor as  $\Psi = \begin{pmatrix} \psi \\ \chi \end{pmatrix}$ , and off diagonal term in the Lagrangian allow the two spinor to couple each other.  $\mathcal{K}_n$  and  $\mathcal{K}_n'$  represent a products of a unit color matrix, a spin matrix, a polynomial in covariant derivative, and other fields.

By inserting a complete set with light hadronic states  $\sum_X \sum_{m_J} |H + X\rangle \langle H + X| = 1$  with  $m_J$  the total spin component of the quarkonium between  $\chi^\dagger$  and  $\chi$  in Eq. (C.5), we

find

$$\mathcal{O}_n^H = \psi^\dagger \mathcal{K}_n \chi \left( \sum_X \sum_{m_J} |H+X\rangle \langle H+X| \right) \chi^\dagger \mathcal{K}'_n \psi. \quad (\text{C.6})$$

Here we assume that the sum of the low energy state  $X$  is dominated by the QCD vacuum  $|0\rangle$  as the lowest energy state. We call the approximation of  $\sum_X |X\rangle \approx |0\rangle$  the vacuum saturation approximation. Therefore, we obtain the relation between a production matrix element and a decay matrix element of the quarkonium as follows ;

$$\begin{aligned} \langle 0 | \mathcal{O}_n^H | 0 \rangle &= \langle 0 | \psi^\dagger \mathcal{K}_n \chi \underbrace{\left( \sum_X \sum_{m_J} |H+X\rangle \langle H+X| \right)}_{\approx \sum_{m_J} |H+0\rangle \langle H+0|} \chi^\dagger \mathcal{K}'_n \psi | 0 \rangle \\ &\approx (2J+1) \langle H | \chi^\dagger \mathcal{K}'_n \psi | 0 \rangle \underbrace{\langle 0 | \psi^\dagger \mathcal{K}_n \chi | H \rangle}_{\approx 1} \approx (2J+1) \langle H | \mathcal{O}_n | H \rangle. \end{aligned} \quad (\text{C.7})$$

where new NRQCD operator is defined as  $\mathcal{O}_n \equiv \chi^\dagger \mathcal{K}'_n \psi \psi^\dagger \mathcal{K}_n \chi$ . In the second line, we have assumed the SU(2) spin rotational invariance of  $\chi^\dagger \mathcal{K}'_n \psi | 0 \rangle \langle 0 | \psi^\dagger \mathcal{K}_n \chi$ . In the heavy quark mass limits  $m \rightarrow \infty$ , the spin quantum number  $J$  of the heavy quark (and also the antiquark) is conserved.<sup>3</sup> Assuming this symmetry to simplify the discussion, the matrix element is identical for each of the  $\sum_{m_J} = (2J+1)$  spin state but differ in the spin component  $m_J$ . In the last expression, we have used the QCD vacuum saturation approximation again.

Let us show a simple example; the relation between the decay amplitude and the production amplitude of  $\eta_c$  which consists of  $c\bar{c}$  pair in the color singlet state. The decay matrix element of  $\eta_c$  is given by  $\langle \eta_c | \psi^\dagger \chi \chi^\dagger \psi | \eta_c \rangle$ . If  $|\eta_c\rangle$  exactly consists of only  $c\bar{c}$  with  $^1S_0$  quantum number in the Fock space, the vacuum saturation approximation is exactly justified since  $\chi^\dagger \psi | \eta_c \rangle = \chi^\dagger \psi | c\bar{c} \rangle = | 0 \rangle$ . However the  $\eta_c$  indeed involves various Fock components such as  $|c\bar{c}g\rangle$ ,  $|c\bar{c}gg\rangle$  involving the dynamical gluons. One dynamical gluon which is induced by operating a spacial covariant derivative on the quark field is of order  $v$  in coulomb gauge<sup>4</sup>. Therefore, the higher order corrections in the  $v$  for the vacuum saturation approximation to the intermediate state  $|X\rangle$  which is shown in Eq. (C.7) are

---

<sup>3</sup>Finite mass correction such as spin flip term in the QCD Lagrangian actually breaks the heavy quark spin symmetry.

<sup>4</sup>This order estimation in coulomb gauge was carried out in Ref. [93]. The coulomb gauge is very useful to compute the quarkonium production since no negative norm exists.



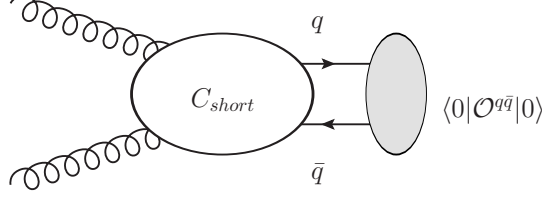


Figure C.1: Short distance coefficient is defined as a perturbative part by subtracting the matrix element  $\langle 0 | \mathcal{O}^{q\bar{q}} | 0 \rangle$  from the  $q\bar{q}$  production cross section.

covered with the dynamical gluons. Expanding the Fock state of  $\eta_c$  up to order  $v^2$  explicitly, we found

$$\begin{aligned}
& \langle \eta_c | \psi^\dagger \chi \chi^\dagger \psi | \eta_c \rangle \\
&= \underbrace{\langle \eta_c | \psi^\dagger \chi | 0 \rangle \langle 0 | \chi^\dagger \psi | \eta_c \rangle}_{\mathcal{O}(v^0)} + \underbrace{\langle \eta_c | \psi^\dagger \chi | g \rangle \langle g | \chi^\dagger \psi | \eta_c \rangle}_{\mathcal{O}(v^2)} + \underbrace{\langle \eta_c | \psi^\dagger \chi | gg \rangle \langle gg | \chi^\dagger \psi | \eta_c \rangle}_{\mathcal{O}(v^4)} + \mathcal{O}(v^6) \\
&\approx |\langle 0 | \chi^\dagger \psi | \eta_c(c\bar{c}) \rangle|^2 [1 + \mathcal{O}(v^4)].
\end{aligned} \tag{C.8}$$

In the third line, we have dropped the term of  $\mathcal{O}(v^2)$  because of color conservation which means that a color singlet  $\eta_c$  can't be converted into a color octet gluon and vice versa by interacting with background fields.  $\langle 0 | \chi^\dagger \psi | \eta_c(c\bar{c}) \rangle$  in Eq. (C.8) is the amplitude which represents that the  $c\bar{c}$  pair is created in far past by the operators  $\chi^\dagger \psi$  and then bound into the  $\eta_c$  in far future. This is just the Bethe-Salpeter amplitude whose expression is given in Appendix D.

In contrast to color singlet operators, the vacuum saturation approximation actually can not be applied to a NRQCD operators in the color octet state such as  $\psi^\dagger t^a \chi \chi^\dagger t^a \psi$  because the matrix element  $\langle H | \psi^\dagger t^a \chi | X \rangle$  vanishes when  $|X\rangle$  is the QCD vacuum  $|0\rangle$  or any color singlet state. Then, the matrix element for the color octet operator should be constrained by fitting the experimental data or computed by using the lattice gauge theory.

### C.3.2 Short distance coefficient

In this section, we show how to compute the short distance coefficient in Eq. (C.4) in terms of the NRQCD.

We firstly consider a production of the heavy quark pair in the  $^{2S+1}L_J^{(1,8)}$  state with the indices (1) and (8) which are color singlet and octet respectively. And  $S, L, J$  are

spin, angular momentum, and total spin (or angular momentum) of the heavy quark pair respectively. We note that this heavy quark pair is not bound yet. The production cross section of the heavy quark pair reads

$$d\sigma(q\bar{q}[{}^{2S+1}L_J^{(1,8)}]) = C(q\bar{q}[{}^{2S+1}L_J^{(1,8)}])_{\text{short}} \langle 0 | \mathcal{O}_{1,8}^{q\bar{q}}({}^{2S+1}L_J) | 0 \rangle, \quad (\text{C.9})$$

where the short distance coefficient  $C_{\text{short}}$  involves the heavy quark pair production and the NRQCD operator is

$$\mathcal{O}_{1,8}^{q\bar{q}}({}^{2S+1}L_J) = \chi^\dagger \mathcal{K} \psi \left( \sum_{J_z} |q\bar{q}[{}^{2S+1}L_J^{(1,8)}]\rangle \langle q\bar{q}[{}^{2S+1}L_J^{(1,8)}]| \right) \psi^\dagger \mathcal{K}' \chi \quad (\text{C.10})$$

where we have inserted a complete set with the heavy quark pair between  $\psi$  and  $\psi^\dagger$ . Eq. (C.9) is similar to Eq. (C.4) except for the long distance matrix element. Using the Clebsh-Gordon coefficient, the intermediate state in Eq. (C.10) is given by

$$\begin{aligned} & |q\bar{q}[{}^{2S+1}L_J^{(1,8)}]\rangle \\ &= \sum_{L_z, S_z} \sum_{s_1, s_2} \sum_{i, j} \int \frac{d^3 l}{(2\pi)^3 2l^0} \delta\left(l^0 - \frac{\mathbf{l}^2}{M}\right) Y_{LL_z}(\hat{\mathbf{l}}) \langle \tfrac{1}{2}, s_1; \tfrac{1}{2}, s_2 | S, S_z \rangle \langle L, L_z; S, S_z | J, J_z \rangle \\ & \times \langle 3i; \bar{3}j | 1, 8c \rangle |q_i(l; s_1) \bar{q}_j(-l; s_2)\rangle, \end{aligned} \quad (\text{C.11})$$

where  $l^\mu$  is the relative momentum between the quark and the antiquark and  $Y_{LL_z}$  is a spherical harmonics. The heavy quark  $q$  (antiquark  $\bar{q}$ ) has a spin component  $s_1$  ( $s_2$ ) and color  $i$  ( $j$ ). The color projection operators are given in Eq. (7.4). As discussed in Ref. [96], the  $\delta$ -function for the relative energy in Eq. (C.11) restricts the spacial relative momentum between the quark and the antiquark to  $|\mathbf{l}| = \sqrt{Ml^0}$  with  $M = 2m$ . Since the kinetic energy of the pair is estimated  $Mv^2$  in the rest frame, it is possible for us to assume  $l^0 \simeq Mv^2 \ll M = 2m$ . Then the relative velocity between the quark and the antiquark is given by  $|\mathbf{l}|/M \simeq v$  which is also assumed to be a small variable. Concerning the expectation value  $\langle 0 | \mathcal{O}_{1,8}^{q\bar{q}}({}^{2S+1}L_J) | 0 \rangle$ , the amplitude  $\langle 0 | \chi^\dagger \mathcal{K} \psi | q\bar{q}[{}^{2S+1}L_J^{(1,8)}] \rangle$  represents that the  $q\bar{q}$  pair in the  ${}^{2S+1}L_J^{(1,8)}$  state is created by the operators  $\chi^\dagger \mathcal{K} \psi$ .

Next, let us consider the quarkonium production cross section which is given by

$$d\sigma(q\bar{q}[{}^{2S+1}L_J^{(1,8)}] \rightarrow \psi_Q) = \frac{C(q\bar{q}[{}^{2S+1}L_J^{(1,8)}])_{\text{short}}}{m} \langle 0 | \mathcal{O}_{1,8}^{\psi_Q}({}^{2S+1}L_J) | 0 \rangle. \quad (\text{C.12})$$

The short distance coefficient  $C_{\text{short}}$  is the same as that of the heavy quark pair production which is shown in Eq. (C.9).  $\langle 0 | \mathcal{O}_{1,8}^{\psi_Q}(^{2S+1}L_J) | 0 \rangle$  is the nonperturbative long distance matrix element of the quarkonium  $\psi_Q$  production in the NRQCD and indices (1) and (8) represent the quarkonium in the color singlet state is produced from the color singlet quark pair or the color octet quark pair respectively. We note that the factor  $1/m$  in Eq. (C.12) adjusts a mass dimension of  $\langle 0 | \mathcal{O}_{1,8}^{\psi_Q}(^{2S+1}L_J) | 0 \rangle$  which differs by unity from  $\langle 0 | \mathcal{O}_{1,8}^{q\bar{q}}(^{2S+1}L_J) | 0 \rangle$  in Eq. (C.9). In fact, the quark field and the antiquark field are respectively given by [96]

$$\begin{aligned}\psi_i^\alpha(x) &= \sum_s \int \frac{d^3p}{(2\pi)^3} b_i(p, s) \xi^\alpha(p, s) e^{-ip \cdot x}, \\ \chi_i^\alpha(x) &= \sum_s \int \frac{d^3p}{(2\pi)^3} c_i^\dagger(p, s) \eta^\alpha(p, s) e^{ip \cdot x},\end{aligned}\tag{C.13}$$

where two component spinors  $\xi$  and  $\eta$  are normalized according to <sup>5</sup>

$$\sum_{s=1}^2 \xi_\alpha(p, s) \xi_\beta^\dagger(p, s) = \sum_{s=1}^2 \eta_\alpha(p, s) \eta_\beta^\dagger(p, s) = \delta_{\alpha\beta},\tag{C.15}$$

with the quark color  $i$ . The creation operator and the annihilation operator in Eq. (C.13) satisfy the anticommutation relation as follows;

$$\{b_i(p, s), b_j^\dagger(p', s')\} = \{c_i(p, s), c_j^\dagger(p', s')\} = (2\pi)^3 \delta_{ij} \delta_{ss'} \delta^{(3)}(p - p').\tag{C.16}$$

Then, we can understand that  $\langle 0 | \mathcal{O}_{1,8}^{q\bar{q}}(^{2S+1}L_J) | 0 \rangle$  certainly differs in the mass dimension from  $\langle 0 | \mathcal{O}_{1,8}^{\psi_Q}(^{2S+1}L_J) | 0 \rangle$  which is also normalized nonrelativistically. The normalization condition of the  $\langle 0 | \mathcal{O}_{1,8}^{\psi_Q}(^{2S+1}L_J) | 0 \rangle$  is given in Eq. (D.30) in Appendix D. Once we obtain the  $C_{\text{short}}$  in Eq. (C.9), we can compute the quarkonium production cross section by substituting the  $C_{\text{short}}$  for the heavy quark pair production at short distance into Eq. (C.12).

If we know the cross section of the heavy quark pair  $d\sigma(q\bar{q}[^{2S+1}L_J^{(1,8)}])$  which is shown

---

<sup>5</sup>Through this paper, we take

$$\xi(p, 1) = \begin{pmatrix} 1 \\ 0 \end{pmatrix}, \quad \xi(p, 2) = \begin{pmatrix} 0 \\ 1 \end{pmatrix}, \quad \eta(-p, 1) = \begin{pmatrix} 0 \\ -1 \end{pmatrix}, \quad \eta(-p, 2) = \begin{pmatrix} 1 \\ 0 \end{pmatrix}.\tag{C.14}$$

in the left hand side of Eq. (C.9), the short distance coefficient is given by

$$C(q\bar{q}[^{2S+1}L_J^{(1,8)}])_{\text{short}} = \frac{d\sigma(q\bar{q}[^{2S+1}L_J^{(1,8)}])}{\langle 0|\mathcal{O}_{1,8}^{q\bar{q}}(^{2S+1}L_J)|0\rangle} \quad (\text{C.17})$$

where the matrix element  $\langle 0|\mathcal{O}_{1,8}^{q\bar{q}}(^{2S+1}L_J)|0\rangle$  should be computed in the NRQCD. The expression of  $\langle 0|\mathcal{O}_{1,8}^{q\bar{q}}(^{2S+1}L_J)|0\rangle$  is computed easily by using Eq. (C.11) and Eq. (C.13). As for the heavy quark pair production in the color singlet and the S-wave, we find

$$\begin{aligned} \langle 0|\mathcal{O}_1^{q\bar{q}}(^1S_0)|0\rangle &= \langle 0|\chi^\dagger\psi|q\bar{q}[^1S_0^{(1)}]\rangle\langle q\bar{q}[^1S_0^{(1)}]|\psi^\dagger\chi|0\rangle \\ &= \frac{M^3}{2^2(2\pi)^5} \frac{N}{l^0} \end{aligned} \quad (\text{C.18})$$

$$\begin{aligned} \langle 0|\mathcal{O}_1^{q\bar{q}}(^3S_1)|0\rangle &= \langle 0|\chi^\dagger\sigma\psi\left(\sum_{S_z}|q\bar{q}[^3S_1^{(1)}]\rangle\langle q\bar{q}[^3S_1^{(1)}]|\right)\psi^\dagger\sigma\chi|0\rangle \\ &= \frac{3M^3}{2^2(2\pi)^5} \frac{N}{l^0}. \end{aligned} \quad (\text{C.19})$$

where  $M = 2m$  and  $N$  is the color. A very important feature is that the relative energy  $l^0 \sim Mv^2$  is given in the denominator in Eqs. (C.18)(C.19). In the static limit  $v \rightarrow 0$ , these amplitudes themselves diverge but the numerator in Eq. (C.17), which is computed in the NRQCD by using Eq. (C.11), also has the ill-factor  $1/l^0$ . Then actually the infrared divergence does not emerge. We note the amplitudes Eqs. (C.18)(C.19) does not depend on a process of the heavy quark pair production and are universal in the NRQCD factorization. As far, we have shown the amplitude in the color singlet state, while the heavy quark pair production in the color octet state provides the same relations except for the Casimir factor which are given by

$$\langle 0|\mathcal{O}_8^{q\bar{q}}(^1S_0)|0\rangle = C_F\langle 0|\mathcal{O}_1^{q\bar{q}}(^1S_0)|0\rangle \quad (\text{C.20})$$

$$\langle 0|\mathcal{O}_8^{q\bar{q}}(^3S_1)|0\rangle = C_F\langle 0|\mathcal{O}_1^{q\bar{q}}(^3S_1)|0\rangle \quad (\text{C.21})$$

with  $C_F = (N^2 - 1)/2N$ .

## C.4 Heavy meson fragmentation

Assuming that a heavy quark and an anti heavy quark which are produced in hard gluon scattering evolve into a heavy meson and an anti heavy meson individually, we can easily

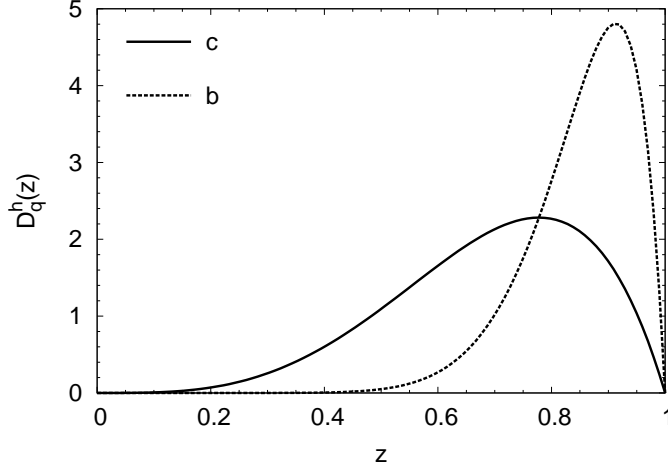


Figure C.2: Kartvelishvili fragmentation function [126]  $D_q^h(z)$  to find a current heavy quark  $q$  with longitudinal momentum fraction  $z$ . Non-perturbative parameter is 3.5 (13.5) for  $D$  ( $B$ ) [129, 130].

obtain the heavy meson pair production cross section. The production cross section of the heavy meson  $h$  is computed by using the heavy quark fragmentation function  $D_q^h(z)$  for final state hadronization process.  $q$  represents the heavy quark, which evolves into  $h$  with the momentum fraction  $z$  of the  $q$ .  $D_q^h(z)dz$  means a probability to find the heavy meson  $h$  produced in the momentum range  $[z, z+dz]$ , and is normalized as  $\int D_q^h(z)dz = 1$ . We usually assume that the fragmentation function of the antiquark is the same for the quark. Phenomenologically, the most popular parameterizations of the fragmentation function  $D_q^h(z)$  are listed as follows;

$$\text{Peterson [125]} : D_q^h(z) \propto \frac{1}{z} \left( 1 - \frac{1}{z} - \frac{\epsilon}{1-z} \right)^{-2} \quad (\text{C.22})$$

$$\text{Kartvelishvili [126]} : D_q^h(z) \propto z^\alpha (1-z) \quad (\text{C.23})$$

where  $\epsilon$  and  $\alpha$  are non-perturbative parameters which can be obtained by fitting a data of the heavy meson productions. For example, we show in Fig. C.2 the Kartvelishvili fragmentation function with an appropriate parameters for charm quark and bottom quark. The behavior of the fragmentation functions indicates that the momentum of the heavy quark is not so modified by a background field through the hadronization. Finally, we should note that the heavy quark fragmentation functions in Eq. (C.22)(C.23) are not Lorentz invariant.

# Appendix D

## Bethe-Salpeter amplitude

We consider Bethe-Salpeter (BS) amplitude [94] which describes a non-perturbative formation of  $J/\psi$  from  $c\bar{c}$ . In general, the BS equation is not closed equation then it is impossible to find a analytic solution. However if we regard a system in the non-relativistic limit, the solution can be expressed in terms of a wave function obeying the Schödinger equation. We will present a new way to construct the BS amplitude in this appendix.

### D.1 General definition of BS equation

First of all, we show a general expression of the BS equation. Homogeneous BS equation with interaction kernel  $K$  and propagators for free Dirac fields (quark and antiquark) is following convolution;

$$\left(\frac{1}{2}P + \not{l} - m\right) \psi_H(l; P) \left(\frac{1}{2}P - \not{l} + m\right) = \int d^4l' K(l, l'; P) \psi_H(l'; P). \quad (\text{D.1})$$

Here  $P = p_1 + p_2$  is the total momentum and  $l = (p_1 - p_2)/2$  is the relative momentum with  $p_1$  the momentum of quark and  $p_2$  the antiquark. The antiquark mass is the same as the quark ( $m$ ). Interaction kernel  $K$  is a function of relative momentum. Using the ladder approximation, the right hand side of the BS equation reduces a more simple form

$$\int d^4l' K(l, l'; P) \psi_H(l'; P) \equiv \int d^4l' K^{\mu\nu}(l, l'; P) \gamma_\mu \psi_H(l'; P) \gamma_\nu. \quad (\text{D.2})$$

In the following, we will show that if we separate a time component of the interaction kernel from the convolution in the non-relativistic approximation, the interaction kernel

reduces 3-dimension potential.

Non-local BS amplitude is generally defined as

$$\Psi_H(x_1, x_2; P) = \langle 0 | T [\psi(x_1) \bar{\psi}(x_2)] | H \rangle = \langle 0 | T [\psi(x_1) \bar{\psi}(x_2)] | \mathbf{P}; S, S_z \rangle, \quad (\text{D.3})$$

where  $T$  represents a time order products. in this paper, we consider a S-state (angular momentum  $L = 0$ ) only, therefore, the bound state is assigned by a momentum ( $\mathbf{P}$ ) and spin ( $S$  and  $S_z$ ). Since the translational symmetry of vacuum is assumed, the BS amplitude in the momentum space is given by

$$\psi_H(l; P) = e^{iP \cdot X} \int \frac{d^4 l}{(2\pi)^4} e^{il \cdot x} \Psi(x_1, x_2; P) \quad (\text{D.4})$$

where  $X = (x_1 + x_2)/2$  and  $x = x_1 - x_2$ . The center of mass coordinate is not relevant to the physical quantity because it just provides a phase factor. Then we neglect the  $X$  dependence of the BS amplitude.

Mass dimension of the BS amplitude is determined by the normalization condition. Relativistically, the normalization condition of one particle state is given by

$$\langle H | H \rangle = \langle \mathbf{P}'; S', S'_z | \mathbf{P}; S, S_z \rangle = (2\pi)^3 2P^0 \delta_{S, S'} \delta_{S_z, S'_z} \delta^{(3)}(\mathbf{P} - \mathbf{P}'). \quad (\text{D.5})$$

Then we found that the mass dimension of  $|H\rangle$  is  $-1$ .

## D.2 BS amplitude in the non-relativistic limit

In this section, we show a way to construct of the BS amplitude in the non-relativistic limit. We redefine the BS equation of  $J/\psi$  as follows <sup>1</sup>;

$$\left( \frac{1}{2} \not{P} + \not{l} - m \right) \psi_H(l^\mu; P) \left( \frac{1}{2} \not{P} - \not{l} + m \right) = - \int \frac{d^4 k}{2\pi i} K(\mathbf{k}) \psi_H(l^\mu - k^\mu; P). \quad (\text{D.6})$$

We can treat  $K(\mathbf{k})$  as a potential between composite particles.

Firstly, we decompose the BS amplitude with 16-component spinor as following  $4 \times 4$

---

<sup>1</sup>In the right hand side of this equation, the integral measure convolutes an extra factor,  $2\pi i$ .  $2\pi i$  takes an important role to reproduce the Schödinger equation .

matrix [95];

$$\psi_H(l^\mu; P^\mu) = \begin{pmatrix} \psi_H^{++}(l^\mu) & \psi_H^{+-}(l^\mu) \\ \psi_H^{-+}(l^\mu) & \psi_H^{--}(l^\mu) \end{pmatrix}. \quad (\text{D.7})$$

$\psi_H^{++}, \psi_H^{+-}, \psi_H^{-+}, \psi_H^{--}$  are  $2 \times 2$  matrices and  $+$  ( $-$ ) corresponds to upper (lower) 2-component of positive (negative) energy solution. We have abbreviated the label  $P$  in the right hand side of Eq. (D.7). This decomposition help us to find a solution of the BS amplitude easily. Then we can rewrite the BS equation

$$\begin{pmatrix} \frac{M}{2} + \omega - m & -\sigma \cdot \mathbf{l} \\ \sigma \cdot \mathbf{l} & -\frac{M}{2} - \omega - m \end{pmatrix} \begin{pmatrix} \psi_H^{++}(l) & \psi_H^{+-}(l) \\ \psi_H^{-+}(l) & \psi_H^{--}(l) \end{pmatrix} \begin{pmatrix} \frac{M}{2} - \omega + m & \sigma \cdot \mathbf{l} \\ -\sigma \cdot \mathbf{l} & -\frac{M}{2} + \omega + m \end{pmatrix} \\ = - \int \frac{d^4 k}{2\pi i} K(\mathbf{k}) \begin{pmatrix} \psi_H^{++}(l-k) & \psi_H^{+-}(l-k) \\ \psi_H^{-+}(l-k) & \psi_H^{--}(l-k) \end{pmatrix}. \quad (\text{D.8})$$

Here  $M$  is the mass of  $J/\psi$  and  $\omega$  is a *relative energy* between composite quark pair ( $c\bar{c}$ ).

Next, we consider the BS amplitude in the  $J/\psi$  rest frame and take a non-relativistic limit. In the non-relativistic limit, we assume particle number conservation and that additional  $c\bar{c}$  creation and annihilation never occurred. In this case,  $\psi_H^{+-}$ , which is constructed of the positive energy state of  $c$  and the negative energy state of  $\bar{c}$ , provides a dominant contribution. Expanding the matrix of Eq. (D.8), we obtain the following relation

$$\begin{aligned} \psi_H^{++}(l^\mu) &\approx \frac{1}{\frac{1}{2}E_0 + \epsilon} (\sigma \cdot \mathbf{l}) \psi_H^{-+}(l^\mu) + \frac{1}{2m - \epsilon} \psi_H^{+-}(l^\mu) (\sigma \cdot \mathbf{l}) \\ &- \frac{1}{(\frac{1}{2}E_0 + \epsilon)(2m - \epsilon)} (\sigma \cdot \mathbf{l}) \psi_H^{--}(l^\mu) (\sigma \cdot \mathbf{l}) + \frac{(-2\pi i)^{-1}}{(\frac{1}{2}E_0 + \epsilon)(2m - \epsilon)} \int d^4 k K(\mathbf{k}) \psi_H^{++}(l^\mu + k^\mu), \end{aligned} \quad (\text{D.9})$$

$$\begin{aligned} \psi_H^{+-}(l^\mu) &- \frac{1}{\frac{1}{2}E_0 - \epsilon} \psi_H^{++}(l^\mu) (\sigma \cdot \mathbf{l}) + \frac{1}{(\frac{1}{2}E_0)^2 - \epsilon^2} (\sigma \cdot \mathbf{l}) \psi_H^{-+}(l^\mu) (\sigma \cdot \mathbf{l}) \\ &- \frac{1}{\frac{1}{2}E_0 + \epsilon} (\sigma \cdot \mathbf{l}) \psi_H^{--}(l^\mu) = \frac{(2\pi i)^{-1}}{(\frac{1}{2}E_0)^2 - \epsilon^2} \int d^4 k K(\mathbf{k}) \psi_H^{+-}(l^\mu + k^\mu), \end{aligned} \quad (\text{D.10})$$

$$\begin{aligned} \psi_H^{-+}(l^\mu) &\approx \frac{1}{2m + \epsilon} (\sigma \cdot \mathbf{l}) \psi_H^{++}(l^\mu) - \frac{1}{(2m)^2 - \epsilon^2} (\sigma \cdot \mathbf{l}) \psi_H^{+-}(l^\mu) (\sigma \cdot \mathbf{l}) \\ &+ \frac{1}{2m - \epsilon} \psi_H^{--}(l^\mu) (\sigma \cdot \mathbf{l}) + \frac{(2\pi i)^{-1}}{(2m)^2 - \epsilon^2} \int d^4 k K(\mathbf{k}) \psi_H^{-+}(l^\mu + k^\mu), \end{aligned} \quad (\text{D.11})$$



$$\begin{aligned}\psi_H^{--}(l^\mu) &\approx \frac{1}{(\epsilon - \frac{1}{2}E_0)(\epsilon + 2m)}(\sigma \cdot \mathbf{l})\psi_H^{++}(l^\mu)(\sigma \cdot \mathbf{l}) + \frac{1}{\frac{1}{2}E_0 - \epsilon}\psi_H^{-+}(l^\mu)(\sigma \cdot \mathbf{l}) \\ &+ \frac{1}{2m + \epsilon}(\sigma \cdot \mathbf{l})\psi_H^{+-}(l^\mu) + \frac{(2\pi i)^{-1}}{(\epsilon - \frac{1}{2}E_0)(\epsilon + 2m)} \int d^4k K(\mathbf{k})\psi_H^{--}(l^\mu + k^\mu),\end{aligned}\quad (\text{D.12})$$

where a weak binding energy  $E_0 = M - 2m \ll m$  is introduced. For each above equations, assuming the  $\psi_H^{+-}$  term is dominant, we found

$$\psi_H^{++} \sim \frac{1}{2m - \omega}\psi_H^{+-}(\sigma \cdot \mathbf{l}), \quad (\text{D.13})$$

$$\psi_H^{-+} \sim \frac{1}{(2m + \omega)(2m - \omega)}(\sigma \cdot \mathbf{l})\psi_H^{+-}(\sigma \cdot \mathbf{l}), \quad (\text{D.14})$$

$$\psi_H^{--} \sim \frac{1}{2m + \omega}(\sigma \cdot \mathbf{l})\psi_H^{+-}. \quad (\text{D.15})$$

Furthermore, substituting the above approximate expression into Eq. (D.10) for  $\psi_H^{+-}$ , we can obtain the following equation:

$$\psi_H^{+-}(l^\mu) = \frac{1}{F(\omega)} \frac{1}{2\pi i} \int d^4k K(\mathbf{k})\psi_H^{+-}(l^\mu - k^\mu), \quad (\text{D.16})$$

where

$$F(\omega) = \frac{E_0^2}{4} - \omega^2 - \left(\frac{E_0}{2} - \omega\right) \frac{\mathbf{l}^2}{2m + \omega} - \left(\frac{E_0}{2} + \omega\right) \frac{\mathbf{l}^2}{2m - \omega} + \frac{\mathbf{l}^4}{(2m + \omega)(2m - \omega)}. \quad (\text{D.17})$$

It is not difficult to understand this expression encoded into the right hand side of Eq. (D.16) is the products of quark propagator and that of antiquark.

Let us introduce a non-relativistic BS wave function  $\varphi$  defined as

$$\varphi(\mathbf{l}) = \int_{-\infty}^{\infty} d\omega \psi_H^{+-}(l^\mu) = \int_{-\infty}^{\infty} d\omega \psi_H^{+-}(\omega, \mathbf{l}). \quad (\text{D.18})$$

Integrating the both hand sides of Eq. (D.16) results in

$$\begin{aligned}\varphi(\mathbf{l}) &= \int_{-\infty}^{\infty} d\omega \frac{1}{F(\omega)} \frac{1}{2\pi i} \int d^3k \int_{-\infty}^{\infty} dk^0 K(\mathbf{k})\psi_H^{+-}(l^0 - k^0, \mathbf{q} - \mathbf{k}) \\ &= \frac{1}{D(\mathbf{l})} \frac{1}{2\pi i} \int d^3k K(\mathbf{k})\varphi(\mathbf{l} - \mathbf{k}).\end{aligned}\quad (\text{D.19})$$

where

$$\frac{1}{D(\mathbf{l})} = \int_{-\infty}^{\infty} d\omega \frac{1}{F(\omega)} \sim \frac{2\pi i}{E_0 - \frac{\mathbf{l}^2}{m}}. \quad (\text{D.20})$$

As shown in the previous section, we have included  $2\pi i$  in the definition of the BS equation, however, in Eq. (D.20)  $2\pi i$  in the numerator and denominator cancel out each other. Rewriting Eq. (D.20), we find

$$\left(E_0 - \frac{\mathbf{l}^2}{m}\right) \varphi(\mathbf{l}) = \int d^3k K(\mathbf{k}) \varphi(\mathbf{l} - \mathbf{k}). \quad (\text{D.21})$$

We have already known that this is a convoluted Schrödinger equation in the momentum space.

In general, non-relativistic wave function  $\varphi(\mathbf{l})$  is given by

$$\varphi(\mathbf{l}) = 2\pi\sqrt{2M} \frac{1}{\sqrt{2}} \frac{\delta_{ij}}{\sqrt{N_c}} (\sigma \cdot \varepsilon) \phi(\mathbf{l}), \quad (\text{D.22})$$

where  $\sqrt{M}$  is the factor derived from the normalization condition Eq. (D.5)<sup>2</sup>.  $\delta_{ij}/\sqrt{N}$  and  $(\sigma \cdot \varepsilon)$  represent a color and spin projection respectively, which are found in Eq. (7.11) and Eq. (7.4)<sup>3</sup>. Normalized polarization vector  $\varepsilon^\mu$  in the centre of mass frame is given by

$$\epsilon^\mu = \begin{cases} \frac{1}{\sqrt{2}}(0, -1, \mp i, 0) & S_z = \pm 1 \\ (0, 0, 0, 1) & S_z = 0 \end{cases}. \quad (\text{D.23})$$

Here we set a spin quantization direction to  $z$ -axis in the rest frame of  $J/\psi$ .  $\phi(\mathbf{l})$  is the product of radial wave function in the momentum space and spherical harmonics.

Finally we consider a correspondence between the BS amplitude ( $\psi_H$ ) and non-relativistic BS wave function ( $\varphi$ ). For the  $\psi_B^{+-}(q^\mu)$  component, we find

$$\begin{aligned} \psi_H^{+-}(l^\mu) &= \frac{1}{F(\omega)} \frac{1}{2\pi i} \int d^4k K(\mathbf{k}) \psi_H^{+-}(l^\mu - k^\mu) \\ &= \frac{1}{F(\omega)} \frac{1}{2\pi i} \int d^3k K(\mathbf{k}) \varphi(\mathbf{l} - \mathbf{k}), \end{aligned} \quad (\text{D.24})$$

---

<sup>2</sup>The mass dimension of the BS amplitude is  $-1$  and that of the wave function  $\phi(\mathbf{l})$  is  $-3/2$ .

<sup>3</sup>In this context, we consider a vector meson production ( $J/\psi$ ). If we consider scalar meson production ( $\eta_c$ ), we manipulate  $\varepsilon \cdot \mathbf{l} \rightarrow \mathbf{1}$  in the BS amplitude  $\varphi(\mathbf{l})$ .

and in the non-relativistic limit,  $F(\omega)^{-1}$  is given by

$$\frac{1}{F(\omega)} = \frac{-1}{\left(\omega - \frac{E_0}{2} + \frac{\mathbf{l}^2}{2m} - i\delta\right) \left(\omega + \frac{E_0}{2} - \frac{\mathbf{l}^2}{2m} + i\delta\right)}. \quad (\text{D.25})$$

Here we write explicitly the infinitesimal imaginary part of  $F(\omega)$ . Therefore, we obtain

$$\psi_H^{+-}(\mathbf{l}^\mu) = -\frac{1}{2\pi i} \frac{1}{\left(\omega - \frac{E_0}{2} + \frac{\mathbf{l}^2}{2m}\right) \left(\omega + \frac{E_0}{2} - \frac{\mathbf{l}^2}{2m}\right)} \int d^3k K(\mathbf{k}) \varphi(\mathbf{l} - \mathbf{k}). \quad (\text{D.26})$$

Furthermore, comparing the Schödinger equation in which  $\varphi(\mathbf{q})$  obey, we find

$$\psi_H^{+-}(\mathbf{l}^\mu) = i \frac{\delta_{ij}}{\sqrt{N_c}} \frac{\sqrt{M} \left(E_0 - \frac{\mathbf{q}^2}{m}\right) \phi(\mathbf{l})}{\left(\omega - \frac{E_0}{2} + \frac{\mathbf{l}^2}{2m}\right) \left(\omega + \frac{E_0}{2} - \frac{\mathbf{l}^2}{2m}\right)} (\boldsymbol{\sigma} \cdot \boldsymbol{\varepsilon}). \quad (\text{D.27})$$

and obtain the other components  $\psi_H^{++}, \psi_H^{-+}$  and  $\psi_H^{--}$  by using  $\psi_H^{+-}$ . In the end, we find the BS amplitude in the center of mass system,

$$\begin{aligned} \psi_H(l; P) &= i \frac{\delta_{ij}}{\sqrt{N_c}} \frac{\sqrt{M} \left(E_0 - \frac{\mathbf{l}^2}{m}\right) \phi(\mathbf{l})}{\left(\omega + \frac{E_0}{2} - \frac{\mathbf{l}^2}{2m}\right) \left(\omega - \frac{E_0}{2} + \frac{\mathbf{l}^2}{2m}\right)} \begin{pmatrix} \frac{(\boldsymbol{\sigma} \cdot \boldsymbol{\varepsilon})(\boldsymbol{\sigma} \cdot \mathbf{l})}{2m - \omega} & \boldsymbol{\sigma} \cdot \boldsymbol{\varepsilon} \\ \frac{(\boldsymbol{\sigma} \cdot \mathbf{l})(\boldsymbol{\sigma} \cdot \boldsymbol{\varepsilon})(\boldsymbol{\sigma} \cdot \mathbf{l})}{(2m + \omega)(2m - \omega)} & \frac{(\boldsymbol{\sigma} \cdot \mathbf{l})(\boldsymbol{\sigma} \cdot \boldsymbol{\varepsilon})}{2m + \omega} \end{pmatrix} \\ &= -i \frac{\delta_{ij}}{\sqrt{N_c}} \frac{\sqrt{M} \left(E_0 - \frac{\mathbf{l}^2}{m}\right) \phi(\mathbf{l})}{\left(\omega + \frac{E_0}{2} - \frac{\mathbf{l}^2}{2m}\right) \left(\omega - \frac{E_0}{2} + \frac{\mathbf{l}^2}{2m}\right)} \left(\frac{1 + \not{n}}{2}\right) \not{\varepsilon}. \end{aligned} \quad (\text{D.28})$$

Here  $n^\mu = (1, 0, 0, 0)$  is a time like four vector.

### D.3 BS amplitude in the NRQCD

Non-Relativistic QCD effective field theory provides more rigorous description of heavy quarkonium transition at long distance, based on the double expansion in  $\alpha_s$  and  $v$ . The quark (antiquark) field corresponds to an independent two component Pauli field and is separated from the degree of freedom of light quarks. This treatment is valid in the non-relativistic limit since the number of quark and antiquark is conserved. Furthermore, no negative norm states exist in the coulomb gauge, then we can construct any Fock state by operating the creation operator on the QCD vacuum.

In this paper, we consider the case  $v \rightarrow 0$  limit, then we should consider only the BS

amplitude of the exact  $c\bar{c}$  production. The BS amplitude of  $\eta_c$  and that of  $J/\psi$  are related to each other with heavy quark spin symmetry. Therefore, in this section, we consider the  $\eta_c$  production. In the rest frame, we define the one particle state as

$$\begin{aligned}
|\eta_c\rangle &= |\mathbf{P}; 0, 0\rangle \\
&= \sum_{s_1, s_2} \langle 1/2, s_1; 1/2, s_2 | 0, 0 \rangle \sum_{i, j} \langle 3, i; \bar{3}, j | 1 \rangle \int \frac{d^3\mathbf{l}}{(2\pi)^3} \phi(\mathbf{l}) |\mathbf{p}_1(s_1), i; \mathbf{p}_2(s_2), j\rangle \\
&= \sum_{s_1, s_2} \frac{\delta_{s_1+s_2, 0}}{\sqrt{2}} \sum_{i, j} \frac{\delta_{i, j}}{\sqrt{N_c}} \int \frac{d^3\mathbf{l}}{(2\pi)^3} \phi(\mathbf{l}) |\mathbf{p}_1(s_1), i; \mathbf{p}_2(s_2), j\rangle
\end{aligned} \tag{D.29}$$

with nonrelativistic normalization condition

$$\langle \mathbf{P}'; 0, 0 | \mathbf{P}; 0, 0 \rangle = (2\pi)^3 \delta^{(3)}(\mathbf{P} - \mathbf{P}'). \tag{D.30}$$

Two particle state is defined as

$$|\mathbf{p}_1(s_1), i; \mathbf{p}_2(s_2), j\rangle = b_i^\dagger(p_1, s_1) c_j(p_2, s_2) |0\rangle \tag{D.31}$$

where creation and annihilation operator construct the Pauli fields which are shown in Eq. (C.13). In the non-relativistic limit ( $v = 0$ ), employing Eq. (C.16). we can find the BS amplitude of  $\eta_c$  production <sup>4</sup>,

$$\begin{aligned}
\langle 0 | \mathcal{O}_1^{\eta_c} (^1S_0) | 0 \rangle &\equiv \langle 0 | \psi \chi^\dagger | \mathbf{P}; S, S_z \rangle \\
&= 2N_c \frac{1}{\sqrt{2}} \frac{1}{\sqrt{N_c}} \int \frac{d^3\mathbf{l}}{(2\pi)^3} \tilde{R}(\mathbf{l}) \frac{1}{\sqrt{4\pi}} \\
&= \frac{N_c}{\sqrt{2\pi}} R(\mathbf{r} = 0)
\end{aligned} \tag{D.32}$$

The factor  $2N$  is derived from the sum of spin and color indices. We have assumed that the wave function of  $J/\psi$  is the same as  $\eta_c$  up to an correction  $\mathcal{O}(v^2)$  due to the heavy quark spin symmetry.

---

<sup>4</sup>This is the same as  $\psi^{+-}$  in the non-relativistic limit defined in the previous section.

# Appendix E

## Quadrupole amplitude in Gaussian approximation

In this appendix, we present the way to formulate the Quadrupole correlator with the gaussian distribution of the color charge density. The detail discussion is the same as Ref. [60, 63].

### E.1 Dipole amplitude

Firstly, we consider a tadpole correction on Wilson line in the fundamental representation [63]. This corrections play an important role to consider the interactions between the Wilson lines.

Let us define the Wilson line in the fundamental representation as

$$\tilde{U}(\mathbf{x}_\perp) = \mathcal{P} \exp \left[ -ig^2 \int_{-\infty}^{+\infty} dz^- \frac{1}{\nabla_\perp^2} \rho_a(z^-, \mathbf{x}_\perp) t^a \right], \quad (\text{E.1})$$

where  $t^a$  is a color matrix in the fundamental representation of  $SU(N_c)$ . Here we assume that a trajectory of the quark is  $z^-$  direction. Then we can regards  $z^-$  as a light cone time of the quark.  $\rho_a$  is a color charge density of valence quark in the hadron or nucleus. This color charge density at transverse coordinate  $\mathbf{x}_\perp$  is related to the following expression

$$\frac{1}{\nabla_\perp^2} \rho_a(z^-, \mathbf{x}_\perp) = \int d^2 \mathbf{z}_\perp G_0(\mathbf{x}_\perp - \mathbf{z}_\perp) \rho_a(z^-, \mathbf{z}_\perp) \quad (\text{E.2})$$

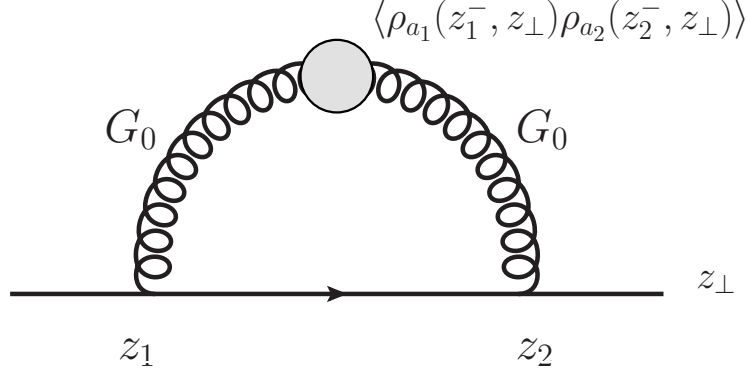


Figure E.1: Graphical representation of one loop quantum correction  $\varphi_1$  to the Wilson line in the fundamental representation. Two point correlation  $\langle \rho \rho \rangle$  with the gaussian distribution connects the index  $z_1^-$  and  $z_2^-$  and leads to the tadpole correction.

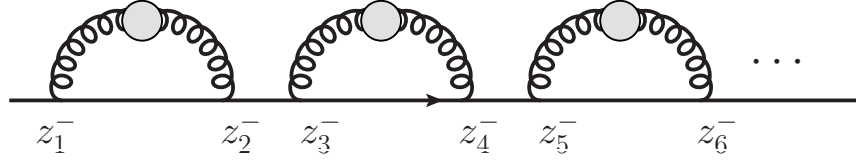


Figure E.2: Graphical representation of n-loop correction  $\varphi_n$  to the Wilson line in the fundamental representation. With gaussian distribution for the color charge density, each quantum correction becomes one tadpole diagram.

where  $G_0$  is free propagator which satisfies

$$G_0(\mathbf{x}_\perp - \mathbf{z}_\perp) = - \int \frac{d^2 \mathbf{k}_\perp}{(2\pi)^2} \frac{e^{i \mathbf{k}_\perp \cdot (\mathbf{x}_\perp - \mathbf{z}_\perp)}}{k_\perp^2}. \quad (\text{E.3})$$

Next, we define another Wilson line in the fundamental representation

$$\tilde{U}(a^-, b^- | \mathbf{x}_\perp) = \mathcal{P} \exp \left[ -ig^2 \int_{a^-}^{b^-} dz^- \frac{1}{\nabla_\perp^2} \rho_a(z^-, \mathbf{x}_\perp) t^a \right]. \quad (\text{E.4})$$

Here we consider the expectation value  $\langle \tilde{U}(a^-, b^- | \mathbf{x}_\perp) \rangle$ . By expanding the path ordered

exponent, we can find

$$\begin{aligned} \langle \tilde{U}(a^-, b^- | \mathbf{x}_\perp) \rangle &= \sum_n \frac{(-ig^2)^n}{n!} \int \Pi_{i=0}^n [d^2 \mathbf{z}_{i\perp} G_0(\mathbf{x}_\perp - \mathbf{z}_{i\perp})] \\ &\times \int_{a^-}^{b^-} dz_1^- \int_{a^-}^{b^-} dz_2^- \cdots \int_{a^-}^{b^-} dz_n^- \langle \rho_{a_1}(z_1^-, \mathbf{z}_\perp) \cdots \rho_{a_n}(z_n^-, \mathbf{z}_\perp) \rangle t^{a_1} \cdots t^{a_n}. \end{aligned} \quad (\text{E.5})$$

Here,  $\langle \rho_{a_1}(z_1^-, \mathbf{z}_\perp) \cdots \rho_{a_n}(z_n^-, \mathbf{z}_\perp) \rangle$  can be reduced to averages of products of two  $\rho$  due to the Wick's theorem. We consider a quantum correction  $\varphi_1$  on the fundamental Wilson line as depicted in Fig. E.1 and  $\varphi_1$  is given by

$$\varphi_1 \equiv G_0(\mathbf{x}_\perp - \mathbf{z}_{1\perp}) G_0(\mathbf{x}_\perp - \mathbf{z}_{2\perp}) \quad (\text{E.6})$$

By assuming the gaussian distribution for the color charge density (MV model), the two point correlation is simply given by

$$\langle \rho_{a_1}(z_1^-, \mathbf{z}_{1\perp}) \rho_{a_2}(z_2^-, \mathbf{z}_{2\perp}) \rangle = \mu^2(z_1^-) \delta_{a_1 a_2} \delta(z_1^- - z_2^-) \delta^{(2)}(\mathbf{z}_{1\perp} - \mathbf{z}_{2\perp}), \quad (\text{E.7})$$

then, we can regard the quantum correction  $\varphi_1$  as just a tadpole correction. Furthermore, the delta function of the light cone time  $z^-$  restricts the path ordering of one tadpole. Then we find that only the possible way for n-tadpole corrections  $\varphi_n$  is shown in Fig. E.2. When we use the identity  $\int_{z_1^-}^{b^-} dz_2^- \delta(z_1^- - z_2^-) = 1/2$ , we finally obtain

$$\begin{aligned} &\langle \tilde{U}(a^-, b^- | \mathbf{x}_\perp) \rangle \\ &= \sum_n \frac{(-ig^2)^n}{n!} \Pi_{i=1}^{n-1} \int d^2 \mathbf{z}_{i\perp} d^2 \mathbf{z}_{i+1\perp} G_0(\mathbf{x}_\perp - \mathbf{z}_{i\perp}) G_0(\mathbf{x}_\perp - \mathbf{z}_{i+1\perp}) \delta^{(2)}(\mathbf{z}_{i\perp} - \mathbf{z}_{i+1\perp}) \\ &\times \int_{a^-}^{b^-} dz_1^- \int_{a^-}^{b^-} dz_2^- \delta(z_1^- - z_2^-) \mu^2(z_1^-) \cdots \int_{a^-}^{b^-} dz_{2k-1}^- \int_{a^-}^{b^-} dz_{2k}^- \delta(z_{2k-1}^- - z_{2k}^-) \mu^2(z_{2k-1}^-) \\ &\times (t^{a_2} t^{a_2}) \cdots (t^{a_n} t^{a_n}) \\ &= \sum_k \frac{(-g^4)^k}{k!} \frac{1}{k!} \Pi_{i=1}^k \int d^2 \mathbf{z}_{i\perp} G_0^2(\mathbf{x}_\perp - \mathbf{z}_{i\perp}) (t^a t^a)^k \left( \int_{a^-}^{b^-} dz^- \mu^2(z^-) \right)^k \end{aligned} \quad (\text{E.8})$$

where  $n = 2k$ . In the limit as  $a^- \rightarrow -\infty$  and  $b^- \rightarrow +\infty$ , we find

$$\langle \tilde{U}(\mathbf{x}_\perp) \rangle = \exp \left[ -\frac{C_F}{2} \mu^2 L_{xx} \right], \quad (\text{E.9})$$

where  $\mu^2$  and  $L_{xy}$  are defined as

$$\mu^2 \equiv \int_{a^-}^{b^-} dz^- \mu^2(z^-), \quad (\text{E.10})$$

$$L_{xy} \equiv g^4 \int d^2 \mathbf{z}_\perp G_0(\mathbf{x}_\perp - \mathbf{z}_\perp) G_0(\mathbf{y}_\perp - \mathbf{z}_\perp). \quad (\text{E.11})$$

$dz^- \mu^2(z^-)$  is interpreted as a density of color charge squared per unit area in the slice between  $z^-$  and  $z^- + dz^-$ .

Next, we turn to the expectation value of the product  $\tilde{U}(\mathbf{x}_\perp) \tilde{U}^\dagger(\mathbf{y}_\perp)$ . We trace the similar way to consider the single Wilson line case in the above. By assuming the gaussian distribution of the color charge density, the Wilson line at the transverse coordinate  $\mathbf{x}_\perp$  includes the integration of the tadpole corrections at the slice between  $z^-$  and  $z^- + dz^-$  and the Wilson line at  $\mathbf{y}_\perp$  itself has also the tadpole corrections. Furthermore, the link gauge connecting between the two Wilson lines is depicted as a vertical gluon line in Fig. E.3 because the correlation between the two Wilson lines remains only when the interaction points coincide each other. The only permitted expression of the expectation value of  $\tilde{U}(\mathbf{x}_\perp) \tilde{U}^\dagger(\mathbf{y}_\perp)$  is given by

$$\begin{aligned} \langle \tilde{U}(a^-, b^- | \mathbf{x}_\perp) \tilde{U}^\dagger(a^-, b^- | \mathbf{y}_\perp) \rangle &= \sum_{n=0}^{\infty} 2^n \int_{a^-}^{b^-} dz_1^- \frac{\mu^2(z_1^-)}{2} \int_{z_1^-}^{b^-} dz_2^- \frac{\mu^2(z_2^-)}{2} \cdots \int_{z_{n-1}^-}^{b^-} dz_n^- \frac{\mu^2(z_n^-)}{2} \\ &\times \left[ g^4 (t^a t^a) \int d^2 \mathbf{z}_\perp G_0(\mathbf{x}_\perp - \mathbf{z}_\perp) G_0(\mathbf{y}_\perp - \mathbf{z}_\perp) \right]^n \\ &\times \underbrace{\langle \tilde{U}(a^-, z_1^- | \mathbf{x}_\perp) \rangle \langle \tilde{U}(z_1^-, z_2^- | \mathbf{x}_\perp) \rangle \cdots \langle \tilde{U}(z_n^-, b^- | \mathbf{x}_\perp) \rangle}_{\text{Tadpoles on } \mathbf{x}_\perp \text{ line}} \\ &\times \underbrace{\langle \tilde{U}(a^-, z_1^- | \mathbf{y}_\perp) \rangle \langle \tilde{U}(z_1^-, z_2^- | \mathbf{y}_\perp) \rangle \cdots \langle \tilde{U}(z_n^-, b^- | \mathbf{y}_\perp) \rangle}_{\text{Tadpoles on } \mathbf{y}_\perp \text{ line}}, \end{aligned} \quad (\text{E.12})$$

This expression includes a product of Tadpole corrections between  $a^-$  and  $b^-$  and the



product can be reduced to one Wilson line as

$$\langle \tilde{U}(a^-, b^- | \mathbf{x}_\perp) \rangle = \langle \tilde{U}(a^-, z_1^- | \mathbf{x}_\perp) \rangle \langle \tilde{U}(z_1^-, z_2^- | \mathbf{x}_\perp) \rangle \cdots \langle \tilde{U}(z_n^-, b^- | \mathbf{x}_\perp) \rangle, \quad (\text{E.13})$$

$$\langle \tilde{U}(a^-, b^- | \mathbf{y}_\perp) \rangle = \langle \tilde{U}(a^-, z_1^- | \mathbf{y}_\perp) \rangle \langle \tilde{U}(z_1^-, z_2^- | \mathbf{y}_\perp) \rangle \cdots \langle \tilde{U}(z_n^-, b^- | \mathbf{y}_\perp) \rangle. \quad (\text{E.14})$$

The bracket  $[\cdots]^n$  represents a sum over the number  $n$  of rungs in the ladder diagram. A factor  $2^n$  in Eq. (E.12) means no relative order between the  $z^-$  on the line at  $\mathbf{x}_\perp$  and one at  $\mathbf{y}_\perp$ . As a result,

$$\begin{aligned} & \langle \tilde{U}(a^-, b^- | \mathbf{x}_\perp) \tilde{U}^\dagger(a^-, b^- | \mathbf{y}_\perp) \rangle \\ &= \langle \tilde{U}(a^-, b^- | \mathbf{x}_\perp) \rangle \langle \tilde{U}(a^-, b^- | \mathbf{y}_\perp) \rangle \sum_{n=0}^{\infty} \frac{1}{n!} \int_{a^-}^{b^-} dz_1 \mu^2(z_1^-) \int_{a^-}^{b^-} dz_2 \mu^2(z_2^-) \cdots \int_{a^-}^{b^-} dz_n \mu^2(z_n^-) \\ & \quad \times \left[ g^4 (t^a t^a) \int d^2 \mathbf{z}_\perp G_0(\mathbf{x}_\perp - \mathbf{z}_\perp) G_0(\mathbf{y}_\perp - \mathbf{z}_\perp) \right]^n \\ &= \exp \left[ -\frac{g^4}{2} (t^a t^a) \left( \int_{a^-}^{b^-} dz \mu^2(z^-) \right) \int d^2 \mathbf{z}_\perp \{ G_0(\mathbf{x}_\perp - \mathbf{z}_\perp) - G_0(\mathbf{y}_\perp - \mathbf{z}_\perp) \}^2 \right], \quad (\text{E.15}) \end{aligned}$$

where we have rewritten the range of the integration and divided by  $n!$  in the second line and combined the results in Eq. E.8 at the third line. By taking  $a^- \rightarrow -\infty$  and  $b^- \rightarrow +\infty$ , we obtain

$$\langle \tilde{U}(\mathbf{x}_\perp) \tilde{U}^\dagger(\mathbf{y}_\perp) \rangle = \exp \left[ -\frac{1}{2} C_F \mu^2 \Gamma(\mathbf{x}_\perp - \mathbf{y}_\perp) \right] \quad (\text{E.16})$$

where we have introduced the function  $\Gamma(\mathbf{x}_\perp - \mathbf{y}_\perp)$  which is defined by

$$\begin{aligned} \Gamma(\mathbf{x}_\perp - \mathbf{y}_\perp) &\equiv g^4 \int d^2 \mathbf{z}_\perp (G_0(\mathbf{x}_\perp - \mathbf{z}_\perp) - G_0(\mathbf{y}_\perp - \mathbf{z}_\perp))^2 \\ &= L_{xx} + L_{yy} - 2L_{xy}. \end{aligned} \quad (\text{E.17})$$

Then, by averaging the color, we can immediately find the dipole amplitude as follows

$$S_Y(\mathbf{x}_\perp, \mathbf{y}_\perp) \equiv \frac{1}{N_c} \text{tr} \langle \tilde{U}(\mathbf{x}_\perp) \tilde{U}^\dagger(\mathbf{y}_\perp) \rangle_Y = \exp \left[ -\frac{1}{2} C_F \mu^2 \Gamma(\mathbf{x}_\perp - \mathbf{y}_\perp) \right]. \quad (\text{E.18})$$

Here  $Y$  is the rapidity.

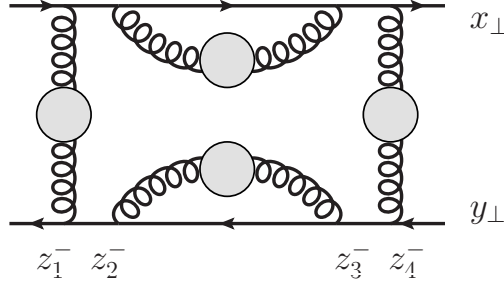


Figure E.3: Graphical representation of a typical interaction between the Wilson line at  $\mathbf{x}_\perp$  and the conjugate one at  $\mathbf{y}_\perp$ . Wilson line has tadpole corrections as self interactions in the each light cone time slice. There are additional interactions between two Wilson lines.

## E.2 Quadrupole amplitude

In this section, we consider a quadrupole amplitude in the Gaussian distribution of the color charge density. Quadrupole amplitude is defined as

$$Q_Y(\mathbf{x}_\perp, \mathbf{y}_\perp; \mathbf{u}_\perp, \mathbf{v}_\perp) \equiv \frac{1}{N_c} \text{tr} \langle \tilde{U}(\mathbf{x}_\perp) \tilde{U}^\dagger(\mathbf{v}_\perp) \tilde{U}(\mathbf{u}_\perp) \tilde{U}^\dagger(\mathbf{y}_\perp) \rangle_Y. \quad (\text{E.19})$$

In this case, we should consider both tadpole and non-tadpole ladder correction as well as the dipole amplitude. To separate these corrections, we define the expectation value as

$$\frac{1}{N_c} \text{tr} \langle \tilde{U}(\mathbf{x}_\perp) \tilde{U}^\dagger(\mathbf{v}_\perp) \tilde{U}(\mathbf{u}_\perp) \tilde{U}^\dagger(\mathbf{y}_\perp) \rangle \equiv \mathcal{T}\mathcal{N}, \quad (\text{E.20})$$

where  $\mathcal{T}$  includes only tadpole corrections in the four Wilson lines which is given by

$$\mathcal{T} = e^{-\frac{1}{2} C_F \mu^2 (L_{xx} + L_{yy} + L_{uu} + L_{vv})}. \quad (\text{E.21})$$

The factor  $1/2$  in the above exponent is required to reduce an overestimation for the case of  $\mathbf{x}_\perp = \mathbf{v}_\perp$  and so on. On the other hand  $\mathcal{N}$  is non-tadpole corrections.  $\mathcal{N}$  is the same as  $Q_Y$  but containing only links which connect different Wilson lines. A typical term in  $\mathcal{N}$  is shown in Fig. E.4 As stated above,  $\langle \rho \rho \rangle$  is local in  $z^-$ , then links must connect points at the same  $z^-$  and diagrams with the crossed links are not allowed. Generally,  $\mathcal{N}$  is defined

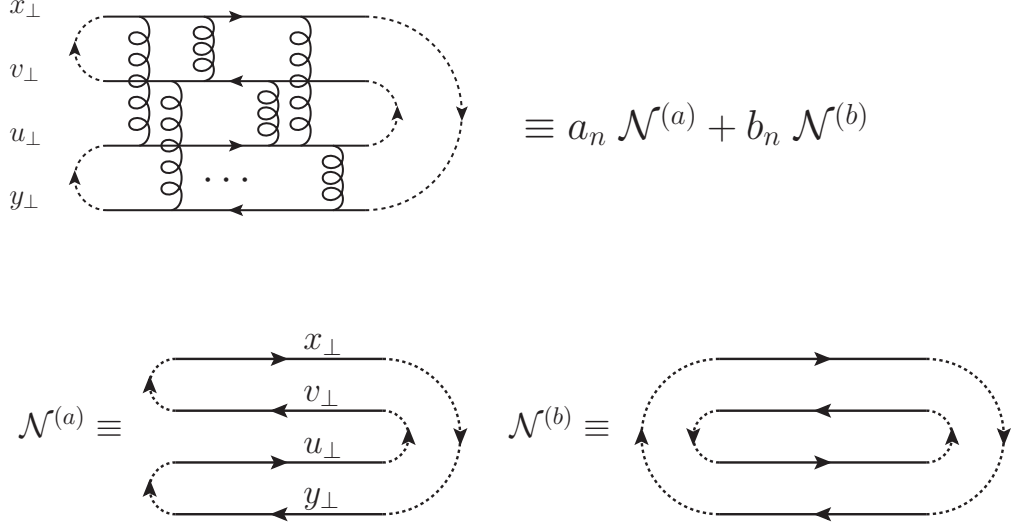


Figure E.4: Non-tadpole term  $\mathcal{N}_n$  with  $n$  rungs interactions in the ladder which divided as two topological types. The arrow represents a direction of the path ordering of Wilson line.

by

$$\mathcal{N} = \sum_{n=0}^{\infty} \int_{z_1^- < \dots < z_n^-} \mathcal{N}_n(z_1^-, \dots, z_n^-), \quad (\text{E.22})$$

where  $\mathcal{N}_n(z_1^-, \dots, z_n^-)$  includes the number of  $n$  links with the ordering of times  $z^-$  as  $z_1^- < \dots < z_n^-$ . By the systematic use of the Fierz identity, we can find that non-tadpole  $\mathcal{N}$  consists of two terms  $\mathcal{N}^{(a)}$  and  $\mathcal{N}^{(b)}$  as follows

$$\mathcal{N}_n = a_n \mathcal{N}^{(a)} + b_n \mathcal{N}^{(b)} \quad (\text{E.23})$$

with coefficient  $a_n, b_n$ . Graphical representation of this expression is shown in Fig. E.4. If there is 0 link in  $\mathcal{N}$ , then we find  $\mathcal{N} = \mathcal{N}^{(a)}$  exactly<sup>1</sup>. The coefficients are given by

$$a_0 = 1, \quad b_0 = 0. \quad (\text{E.24})$$

Once we can obtain the expression of  $\mathcal{N}_{n-1}$ , then in order to find  $\mathcal{N}_n$ , it is only necessary

<sup>1</sup>This is because finite links lead to  $\mathcal{N}^{(b)}$ .

to add one link to  $\mathcal{N}_{n-1}$  for every conceivable case. By the use of the Fierz identity again, we can find the additional six rungs in the ladder are given by

$$\mathbf{x}_\perp \mathbf{v}_\perp : \mu^2(z_n^-) C_F L_{xv} \mathcal{N}^{(a)}, \quad (\text{E.25})$$

$$\mathbf{x}_\perp \mathbf{u}_\perp : -\mu^2(z_n^-) L_{xu} \left( \frac{1}{2} \mathcal{N}^{(b)} - \frac{1}{2N_c} \mathcal{N}^{(a)} \right), \quad (\text{E.26})$$

$$\mathbf{x}_\perp \mathbf{y}_\perp : \mu^2(z_n^-) L_{xy} \left( \frac{1}{2} \mathcal{N}^{(b)} - \frac{1}{2N_c} \mathcal{N}^{(a)} \right), \quad (\text{E.27})$$

$$\mathbf{v}_\perp \mathbf{u}_\perp : \mu^2(z_n^-) L_{vu} \left( \frac{1}{2} \mathcal{N}^{(b)} - \frac{1}{2N_c} \mathcal{N}^{(a)} \right), \quad (\text{E.28})$$

$$\mathbf{v}_\perp \mathbf{y}_\perp : -\mu^2(z_n^-) L_{vy} \left( \frac{1}{2} \mathcal{N}^{(b)} - \frac{1}{2N_c} \mathcal{N}^{(a)} \right), \quad (\text{E.29})$$

$$\mathbf{u}_\perp \mathbf{y}_\perp : \mu^2(z_n^-) C_F L_{uy} \mathcal{N}^{(a)}, \quad (\text{E.30})$$

for the coefficient of  $a_{n-1}$  and

$$\mathbf{x}_\perp \mathbf{v}_\perp : \mu^2(z_n^-) L_{xv} \left( \frac{1}{2} \mathcal{N}^{(a)} - \frac{1}{2N_c} \mathcal{N}^{(b)} \right), \quad (\text{E.31})$$

$$\mathbf{x}_\perp \mathbf{u}_\perp : -\mu^2(z_n^-) L_{xu} \left( \frac{1}{2} \mathcal{N}^{(a)} - \frac{1}{2N_c} \mathcal{N}^{(b)} \right), \quad (\text{E.32})$$

$$\mathbf{x}_\perp \mathbf{y}_\perp : \mu^2(z_n^-) C_F L_{xy} \mathcal{N}^{(b)}, \quad (\text{E.33})$$

$$\mathbf{v}_\perp \mathbf{u}_\perp : \mu^2(z_n^-) C_F L_{vu} \mathcal{N}^{(b)}, \quad (\text{E.34})$$

$$\mathbf{v}_\perp \mathbf{y}_\perp : -\mu^2(z_n^-) L_{vy} \left( \frac{1}{2} \mathcal{N}^{(a)} - \frac{1}{2N_c} \mathcal{N}^{(b)} \right), \quad (\text{E.35})$$

$$\mathbf{u}_\perp \mathbf{y}_\perp : \mu^2(z_n^-) L_{uy} \left( \frac{1}{2} \mathcal{N}^{(a)} - \frac{1}{2N_c} \mathcal{N}^{(b)} \right), \quad (\text{E.36})$$

for the coefficient of  $b_{n-1}$ . Minus sign in the front of  $\mu^2(z_n^-)$  is derived from the contribution of the link which connects between the Wilson lines with the same direction in the path ordering exponent. Therefore, the identities for  $\mathcal{N}^{(a)}$  and  $\mathcal{N}^{(b)}$  form the following matrix

$$\begin{pmatrix} a_n \\ b_n \end{pmatrix} = \mu^2(z_n^-) \mathcal{U} \begin{pmatrix} a_{n-1} \\ b_{n-1} \end{pmatrix}, \quad (\text{E.37})$$

where  $\mathcal{U}$  is given by

$$\mathcal{U} = \begin{pmatrix} C_F(L_{xv} + L_{uy}) + \frac{1}{2N_c}F(x, v; u, y) & -\frac{1}{2}F(x, y; u, v) \\ -\frac{1}{2}F(x, y; u, y) & C_F(L_{xy} + L_{uv} + \frac{1}{2N_c}F(x, y; u, v)) \end{pmatrix}. \quad (\text{E.38})$$

We have used the notation  $F(x, y, u, v) = L_{xu} - L_{xv} + L_{yv} - L_{yu}$ . Matrix  $\mathcal{U}$  does not depend on the light cone time  $z^-$ , then we can find the recursion relation as follows

$$\begin{pmatrix} a_n \\ b_n \end{pmatrix} = [\Pi_{i=1}^n \mu^2(z_i^-)] \mathcal{U}^n \begin{pmatrix} a_0 \\ b_0 \end{pmatrix} = [\Pi_{i=1}^n \mu^2(z_i^-)] \mathcal{U}^n \begin{pmatrix} 1 \\ 0 \end{pmatrix}. \quad (\text{E.39})$$

Next, we compute

$$\begin{aligned} \int_{z_1^+ < \dots < z_n^-} \begin{pmatrix} a_n \\ b_n \end{pmatrix} &= \int_{z_1^+ < \dots < z_n^-} [\Pi_{i=1}^n \mu^2(z_i^-)] \mathcal{U}^n \begin{pmatrix} 1 \\ 0 \end{pmatrix} \\ &= \frac{1}{n!} \mu^{2n} \mathcal{U}^n \begin{pmatrix} 1 \\ 0 \end{pmatrix}. \end{aligned} \quad (\text{E.40})$$

If we can know the eigenvalues of  $\mathcal{U}$  in the right hand side of the above equation, we immediately obtain  $a_n$  and  $b_n$ . A characteristic equation provides two independent eigenvalues which are given by

$$\begin{aligned} \lambda_{\pm} &= \frac{1}{2} C_F(L_{xx} + L_{uu} + L_{yy} + L_{vv}) - \frac{1}{4N_c} [\Gamma(x - u) + \Gamma(v - y)] \\ &\quad - \left( \frac{N_c}{8} - \frac{1}{4N_c} \right) [\Gamma(x - v) + \Gamma(u - y) + \Gamma(x - y) + \Gamma(u - v)] \pm \frac{N_c}{4} \sqrt{\Delta} \end{aligned} \quad (\text{E.41})$$

where  $\Delta \equiv (\alpha - \gamma)^2 + \frac{4}{N_c^2}(\alpha - \beta)(\gamma - \beta)$ . General solution can be written by the use of a linear combination of two eigenvalues as follows;

$$\begin{aligned} \sum_{n=0}^{\infty} \int_{z_1^+ < \dots < z_n^-} \begin{pmatrix} a_n \\ b_n \end{pmatrix} &= \sum_{n=0}^{\infty} \frac{1}{n!} \mu^{2n} \begin{pmatrix} a_+ \lambda_+^n + a_- \lambda_-^n \\ b_+ \lambda_+^n + b_- \lambda_-^n \end{pmatrix} \\ &= \begin{pmatrix} a_+ e^{\mu^2 \lambda_+} + a_- e^{\mu^2 \lambda_-} \\ b_+ e^{\mu^2 \lambda_+} + b_- e^{\mu^2 \lambda_-} \end{pmatrix}, \end{aligned} \quad (\text{E.42})$$

where

$$a_{\pm} = \frac{\sqrt{\Delta} \pm (\alpha - \gamma)}{2\sqrt{\Delta}} \quad (\text{E.43})$$

$$b_{\pm} = \pm \frac{\Gamma(x-u) + \Gamma(v-y) - \Gamma(x-y) - \Gamma(v-u)}{2N_c\sqrt{\Delta}} \quad (\text{E.44})$$

with  $a_+ + a_- = a_0 = 1$  and  $b_+ + b_- = b_0 = 0$ . Here we have introduced the notations defined as

$$\alpha \equiv L_{xv} + L_{uy} \quad (\text{E.45})$$

$$\beta \equiv L_{xu} + L_{vy} \quad (\text{E.46})$$

$$\gamma \equiv L_{xy} + L_{vu}. \quad (\text{E.47})$$

Inserting  $\mathcal{N}^{(a)} = 1$  and  $\mathcal{N}^{(b)} = N_c$  into Eq. (E.44), we obtain

$$\mathcal{N} = (a_+ + N_c b_+) e^{\mu^2 \lambda_+} + (a_- + N_c b_-) e^{\mu^2 \lambda_-}. \quad (\text{E.48})$$

Therefore, as a result, we can find the quadrupole amplitude as follows;

$$\begin{aligned} & Q_Y(\mathbf{x}_{\perp}, \mathbf{y}_{\perp}; \mathbf{u}_{\perp}, \mathbf{v}_{\perp}) \\ &= e^{-\frac{\mu^2}{4N_c}(\Gamma(x-u)+\Gamma(v-y))} \left[ \left( \frac{\sqrt{\Delta} + \alpha - \gamma}{2\sqrt{\Delta}} + \frac{\gamma - \beta}{\sqrt{\Delta}} \right) e^{\frac{N_c}{4}\mu^2\sqrt{\Delta}} + \left( \frac{\sqrt{\Delta} - \alpha + \gamma}{2\sqrt{\Delta}} - \frac{\gamma - \beta}{\sqrt{\Delta}} \right) e^{-\frac{N_c}{4}\mu^2\sqrt{\Delta}} \right] \\ & \times e^{-\left(\frac{N_c}{8} - \frac{1}{N_c}\right)\mu^2(\Gamma(x-v)+\Gamma(u-y)+\Gamma(x-y)+\Gamma(v-u))}. \end{aligned} \quad (\text{E.49})$$

Finally, we present the approximated result in large- $N_c$  limit,

$$\begin{aligned} & Q_Y(\mathbf{x}_{\perp}, \mathbf{y}_{\perp}; \mathbf{u}_{\perp}, \mathbf{v}_{\perp}) \\ & \stackrel{LN_c}{=} e^{-\frac{N_c}{4}\mu^2(\Gamma(x-v)+\Gamma(u-y))} + \frac{\gamma - \beta}{\alpha - \gamma} \left[ e^{-\frac{N_c}{4}\mu^2(\Gamma(x-v)+\Gamma(u-y))} - e^{-\frac{N_c}{4}\mu^2(\Gamma(x-y)+\Gamma(y-u))} \right] \end{aligned} \quad (\text{E.50})$$

and furthermore using the function  $\Gamma$  in the large- $N_c$  limit given by

$$\Gamma(x-y) = -\frac{2}{\mu^2 C_F} \ln S_Y(x, y) \stackrel{LN_c}{=} -\frac{4}{\mu^2 N_c} \ln S_Y(x, y), \quad (\text{E.51})$$

we can rewrite the quadrupole amplitude in terms of only dipole amplitude as

$$\begin{aligned}
Q_Y(\mathbf{x}_\perp, \mathbf{y}_\perp; \mathbf{u}_\perp, \mathbf{v}_\perp) &\stackrel{LN_c}{=} S_Y(\mathbf{x}_\perp, \mathbf{v}_\perp) S_Y(\mathbf{u}_\perp, \mathbf{y}_\perp) \\
&- \frac{\ln S_Y(\mathbf{x}_\perp, \mathbf{u}_\perp) S_Y(\mathbf{v}_\perp, \mathbf{y}_\perp) - \ln S_Y(\mathbf{x}_\perp, \mathbf{y}_\perp) S_Y(\mathbf{u}_\perp, \mathbf{v}_\perp)}{\ln S_Y(\mathbf{x}_\perp, \mathbf{v}_\perp) S_Y(\mathbf{u}_\perp, \mathbf{y}_\perp) - \ln S_Y(\mathbf{x}_\perp, \mathbf{y}_\perp) S_Y(\mathbf{u}_\perp, \mathbf{v}_\perp)} \\
&\quad \times [S_Y(\mathbf{x}_\perp, \mathbf{v}_\perp) S_Y(\mathbf{u}_\perp, \mathbf{y}_\perp) - S_Y(\mathbf{x}_\perp, \mathbf{y}_\perp) S_Y(\mathbf{u}_\perp, \mathbf{v}_\perp)].
\end{aligned} \tag{E.52}$$

This is simple and useful for numerical computations.

# Bibliography

- [1] S. Pokorski, *Gauge Field Theories*, Cambridge University Press, Cambridge (2000).
- [2] Y. Kovchegov and E. Levin, *QUANTUM CHROMODYNAMICS AT HIGH ENERGY*, Cambridge University Press, Cambridge (2012).
- [3] J.R. Forshaw and D.A. Ross, *Quantum Chromodynamics and the Pomeron*, Cambridge University Press, Cambridge (1997).
- [4] F. Halzen and A. D. Martin, *Quarks and Leptons: An Introductory Course in Modern Particle Physics*, Wiley, New York (1984).
- [5] J. C. Collins and M. J. Perry, Phys. Rev. Lett. **34** (1975) 1353.
- [6] N. Cabibbo and G. Parisi, Phys. Lett. **B 59** (1975) 67.
- [7] S. Borsányi et al., JHEP **1011** (2010) 077 [arXiv:1007.2580 [hep-lat]].
- [8] P. Romatschke and U. Romatschke, Phys. Rev. Lett. **99** (2007) 172301.
- [9] M. Luzum and P. Romatschke, Phys. Rev. C **78** (2008) 034915 [Erratum-ibid. **C79** (2009) 039903].
- [10] D. Kharzeev and M. Nardi, Phys. Lett. **B 507** (2001) 121, [arXiv: nucl-th/0012025].  
D. Kharzeev, E. Levin, and M. Nardi, Nucl. Phys. **A 730** (2004) 448, Erratum-ibid. **A 743** (2004) 329, [arXiv: hep-ph/0212316].
- [11] T. Matsui and H. Satz, Phys. Lett. **B178** (1986) 416.
- [12] A. Adare et al. (**PHENIX** Collaboration), Phys. Rev. Lett. **104** (2010) 132301 [arXiv:0804.4168 [nucl-ex]].



- [13] J.L.Albacete *et al.*, Int. J. Mod. Phys. E **22** (2013) 1330007 [arXiv:1301.3395 [hep-ph]].
- [14] J. L. Albacete, A. Dumitru, H. Fujii, and Y. Nara, Nucl. Phys. **A 897**, 1 (2013), [arXiv:1209.2001 [hep-ph]].
- [15] <http://www-h1.desy.de/publications/htmlsplit/H1prelim-10-142.long.html>
- [16] V. Radescu, (**H1** and **ZEUS** collaborations), [arXiv:1308.0374 [hep-ex]]
- [17] F. Arleo and S. Peigne, JHEP 1303 (2013) 122, [arXiv:1212.0434 [hep-ph]].
- [18] F. Arleo, R. Kolevatov, S. Peigne, and M. Rustamova, [arXiv:1304.0901 [hep-ph]].
- [19] V.N. Gribov and L.N. Lipatov, Sov.J.Nucl.Phys. **15** (1972) 438-450, Yad.Fiz. 15 (1972) 781-807.
- [20] G. Altarelli and G. Parisi, Nucl. Phys. **B126** (1977) 298.
- [21] Y. L. Dokshitzer, Sov.Phys.JETP **46** (1977) 641-653, Zh.Eksp.Teor.Fiz. 73 (1977) 1216-1240
- [22] E.A. Kuraev, L.N. Lipatov, and V. S. Fadin, Sov.Phys.JETP **45** (1977) 199-204, Zh.Eksp.Teor.Fiz. 72 (1977) 377-389.
- [23] I.I. Balitsky and L.N. Lipatov, Sov.J.Nucl.Phys. **28** (1978) 822-829, Yad.Fiz. 28 (1978) 1597-1611.
- [24] Al. H. Mueller, Nucl. Phys. **B415** (1994) 373-385.
- [25] Al. H. Mueller, Nucl. Phys. **B437** (1995) 107-126.
- [26] Al. H. Mueller and B. Patel, Nucl. Phys. **B425** (1994) 471-488.
- [27] M. Froissart, Phys. Rev. **123** (1961) 1053-1057.
- [28] L. V. Gribov, E. M. Levin and M. G. Ryskin, Phys. Rept. **100**, 1 (1983).
- [29] A. H. Mueller and J. -w. Qiu, Nucl. Phys. B **268**, 427 (1986).
- [30] K. J. Golec-Biernat, M. Wusthoff, Phys. Rev. **D 59** (1998) 014017, [arXiv: hep-ph/9807513]

- [31] A.M. Stasto, K. Golec-Biernat, J. Kwiecinski, Phys. Rev. Lett. **86**, 596 (2001).
- [32] F. Gelis, R. Peschanski, G. Soyez, L. Schoeffel, Phys. Lett. **B 647**, 376 (2007) [arXiv:hep-ph/0610435].
- [33] L. McLerran and R. Venugopalan, Phys. Rev. **D 49**, 2233 (1994).
- [34] L. McLerran and R. Venugopalan, Phys. Rev. **D 49**, 3352 (1994).
- [35] L. McLerran and R. Venugopalan, Phys. Rev. **D 50**, 2225 (1994).
- [36] E. Iancu, A. Leonidov, and L. McLerran, [arXiv:hep-ph/0202270].
- [37] E. Iancu and R. Venugopalan, [arXiv:hep-ph/0303204].
- [38] F. Gelis, E. Iancu, J. Jalilian-Marian, and R. Venugopalan, Ann. Rev. Nucl. Part. Sci. **60**, (2010) 463 [arXiv:1002.0333[hep-ph]].
- [39] J. Jalilian-Marian, A. Kovner, A. Leonidov, and H. Weigert, Nucl. Phys. **B 504** (1997) 415 [arXiv:hep-ph/9701284].
- [40] J. Jalilian-Marian, A. Kovner, A. Leonidov, and H. Weigert, Phys. Rev. **D 59** (1998) 014014 [arXiv:hep-ph/9706377].
- [41] J. Jalilian-Marian, A. Kovner, and H. Weigert, Phys. Rev. **D 59** (1998) 014015 [arXiv:hep-ph/9709432].
- [42] A. Kovner, J. G. Milhano, and H. Weigert, Phys. Rev. **D 62** (2000) 114005 [arXiv:hep-ph/0004014].
- [43] H. Weigert, Nucl. Phys. **A 703** (2002) 823 [arXiv:hep-ph/0004044].
- [44] E. Iancu, A. Leonidov, and L. McLerran, Nucl. Phys. **A 692** (2001) 583 [arXiv:hep-ph/0011241].
- [45] E. Iancu, A. Leonidov, and L. McLerran, Phys. Lett. **B 510** (2001) 133 [arXiv:hep-ph/0102009].
- [46] E. Ferreiro, E. Iancu, A. Leonidov, and L. McLerran, Nucl. Phys. **A 703** (2002) 489 [arXiv:hep-ph/0109115].
- [47] I. Balitsky, Nucl. Phys. **B 463**, 99 (1996).

- [48] Yu.V. Kovchegov, Phys. Rev. **D 54**, 5463 (1996).
- [49] I. Balitsky, Phys. Rev. D **75**, 014001 (2007).
- [50] J.L. Albacete, Yuri V. Kovchegov, Phys. Rev. **D 75**, 125021 (2007), [arXiv:0704.0612[hep-ph]].
- [51] J.L. Albacete, Phys. Rev. Lett. **99**, 262301 (2007), [arXiv:0707.2545 [hep-ph]].
- [52] I. Balitsky and G. A. Chirilli, Phys. Rev. **D77**, 014019 (2008), [arXiv:0710.4330 [hep-ph]].
- [53] J.L. Albacete, Nestor Armesto, J.G. Milhano, C.A. Salgado, Phys. Rev. D **80**, 034031 (2009) [arXiv:0902.1112[hep-ph]].
- [54] J.L. Albacete, N. Armesto, J.G. Milhano, P. Quiroga-Arias, and C.A. Salgado, Eur. Phys. J. C **71**, 1705 (2011) [arXiv:1012.4408[hep-ph]].
- [55] J.L. Albacete and C. Marquet, Phys. Rev. Lett.**105** (2010) 162301 [arXiv:1005.4065 [hep-ph] ].
- [56] J. L. ALbacete and A. Dumitru, [arXiv:1011.5161 [hep-ph]].
- [57] H. Fujii, K. Itakura, Y. Kitadono and Y. Nara, J. Phys. G **38**, 124125 (2011) [arXiv:1107.1333 [hep-ph]].
- [58] J. L. Albacete, A. Dumitru, H. Fujii and Y. Nara, Nucl. Phys. A **897**, 1 (2013) [arXiv:1209.2001 [hep-ph]].
- [59] A. Dumitru, A. Hayashigaki, and J. Jalilian-Marian, Nucl. Phys. **A 765** (2006) 464, [arXiv:hep-ph/0506308]
- [60] F. Dominguez, C. Marquet, A. M. Stasto, and B.-W. Xiao, Phys. Rev. **D 87** (2013) 034007 [arXiv:1210.1141 [hep-ph]]
- [61] J. Pumplin, D. R. Stump, J. Huston, H. L. Lai, P. Nadolsky, K. Tung, JHEP 0207 (2002) 012.
- [62] A. J. Baltz, F. Gelis, L. McLerran, and A. Peshier, Nucl. Phys. **A 695** (2001) 395, [nucl-th/0101024].
- [63] F. Gelis and A. Peshier, Nucl. Phys. **A 697** (2002) 879 [arXiv:hep-ph/0107142].

- [64] J.P. Blaizot, F. Gelis, R. Venugopalan, Nucl. Phys. **A 743**, 13 (2004).
- [65] J.P. Blaizot, F. Gelis, R. Venugopalan, Nucl. Phys. **A 743**, 57 (2004).
- [66] H. Fujii, F. Gelis, R. Venugopalan, Phys. Rev. Lett. **95**, 162002 (2005)
- [67] H. Fujii, F. Gelis, R. Venugopalan, Nucl. Phys. **A 780**, 146 (2006).
- [68] H. Fujii and K. Watanabe, Nucl. Phys. **A 915**, 1 (2013), [arXiv:1304.2221 [hep-ph]].
- [69] H. Fujii and K. Watanabe, Nucl. Phys. **A 920**, 78 (2013), [arXiv:1308.1258 [hep-ph]].
- [70] Z.-B. Kang, Y.-Q. Ma, and R. Venugopalan, [arXiv:1309.7337 [hep-ph]].
- [71] F. Dominguez, D. E. Kharzeev, E. M. Levin, A. H. Mueller, K. Tuchin, Phys. Lett. **B 710** (2012) 182 [arXiv:1109.1250 [hep-ph]].
- [72] D. E. Kharzeev, E. M. Levin, K. Tuchin, Nucl. Phys. **A 924** (2014) 47 [arXiv:1205.1554 [hep-ph]].
- [73] D. Kharzeev and K. Tuchin, Nucl. Phys. **A 770**, 40 (2006).
- [74] J. H. Kühn, J. Kaplan, and E. G. O. Safiani, Nucl. Phys. **B 157** (1979) 125.
- [75] B. Guberina, J. H. Kühn, R. D. Peccei, and R. Rückl, Nucl. Phys. **B 174** (1980) 317.
- [76] M. Bedjidian et al, [arXiv:hep-ph/0311048].
- [77] N. Brambilla et al, (Quarkonium Working Group), [arXiv:hep-ph/0412158[hep-ph]] (2004).
- [78] N. Brambilla et al, Eur. Phys. J. **C 71** (2011) 1534 [arXiv:1010.5827 [hep-ph]].
- [79] Z. Conesa del Valle, et al., [arXiv:1105.4545 [hep-ph]], and references therein.
- [80] G. A. Schuler, arXiv:hep-ph/9403387.
- [81] C.-H. Chang, Nucl. Phys. **B 172** (1980) 425.
- [82] R. Baier and R. Rückl, Phys. Lett. **B 102** (1981) 364.
- [83] H. Fritzsch, Phys. Lett. **B 67** (1977) 217.

- [84] A. D. Martin, R. G. Roberts, W. J. Stirling, and R. S. Thorne, Eur. Phys. J. **C 4** (1998) 463 [hep-ph/9803445].
- [85] A. D. Martin, R. G. Roberts, W. J. Stirling, and R. S. Thorne, Phys. Lett. **B443** (1998) 301[hep-ph/9808371]. Phys. Lett. **B 531** (2002) 216.
- [86] H. L. Lai et al, (**CTEQ** Collaboration), Eur. Phys. J. **C12** (2000) 375 [hep-ph/9903282].
- [87] M. Gluck, E. Reya, and A. Vogt, Eur. Phys. J. **C5** (1998) 461 [hep-ph/9806404].
- [88] R. Vogt, [hep-ph/0203151].
- [89] A. D. Frawley, T. Ullrich, R. Vogt, Phys. Rep. **462** (2008) 125.
- [90] W. E. Caswell and G. P. Lepage, Phys. Lett. **B 167** (1986) 437.
- [91] B. A. Thacker and G. P. Lepage, Phys. Rev. **D 43** (1991) 196.
- [92] G. T. Bodwin, E. Braaten, and G. P. Lepage, Phys. Rev. **D 51** (1995) 1125, [Erratum-ibid. **D 55** (1997) 5853].
- [93] G. P. Lepage, L. Magnea, C. Nakhleh, U. Magnea, and K. Hornbostel, Phys. Rev. **D 46** (1992) 4052.
- [94] E. E. Salpeter and H. A. Bethe, Phys. Rev. **84** (1951) 1232, E. E. Salpeter, Phys. Rev. **87** (1952) 328. N. Nakanishi, Prog. Theor. Phys. Suppl. **43** (1969) 614.
- [95] This derivation is based on T. Matsui's unpublished note.
- [96] P. Cho and A. K. Leibovich, Phys. Rev. **D 53** 6203 (1996).
- [97] M. Butenschön and B. Kniehl, Phys. Rev. Lett. **106** (2011) 022003.
- [98] Y.-Q. Ma, K. Wang, and K.-Ta. Chao, Phys. Rev. Lett. **106** (2011) 042002.
- [99] W. Buchmüller and S.-H.H. Tye, Phys. Rev. **D 24** (1981)132.
- [100] E. J. Eichten and C. Quigg, *Quarkonium wave functions at the origin*, Phys. Rev. **D 52** (1995) 1726.
- [101] H. Fujii and T. Matsui, Phys. Lett. **B 545**, 82 (2002); H. Fujii, Nucl. Phys. **A 709**, 236 (2002).

- [102] H. Fujii, Phys. Rev. **C 67** 031901 (2003).
- [103] R. Arnaldi et al. (**NA60** Collaboration), Phys. Lett. **B 706** (2012) 263, [arXiv:1004.5523 [nucl-ex]]
- [104] A. Adare et al. (**PHENIX** Collaboration), Phys. Rev. Lett. **98** (2007) 232301 [nucl-ex/0611020].
- [105] B. Abelev et al.), (**ALICE** Collaboration) Phys. Rev. Lett. **109** (2012) 072301, [arXiv:1202.1383 [hep-ex]]
- [106] A. Adare et al. (**PHENIX** Collaboration), Phys. Rev. Lett. **107** (2011) 142301 [arXiv:1010.1246 [nucl-ex]].
- [107] A. Adare et al. (**PHENIX** Collaboration), Phys. Rev. **C 87** (2013) 034904, [arXiv:1204.0777[nucl-ex]].
- [108] B. Abelev et al. (**ALICE** Collaboration), [arXiv:1308.6726 [nucl-ex]].
- [109] R. Aaij et al. (**LHCb** Collaboration), [arXiv:1308.6729 [nucl-ex]].
- [110] A. Adare et al. (**PHENIX** collaboration), Phys. Rev. **D 85** (2012) 092004 [arXiv:1105.1966 [hep-ex]].
- [111] G. Aad et al. (**ATLAS** Collaboration), Phys. Rev. **D 87** (2013) 052004 [arXiv:1211.7255 [hep-ex]].
- [112] R. Aaij et al. (**LHCb** Collaboration), Eur. Phys. J. **C 72** (2012) 2025 [arXiv:1202.6579[hep-ex]].
- [113] K. Aamodt et al. (**ALICE** Collaboration), Phys. Lett. **B 704** (2011) 442 [arXiv:1105.0380 [hep-ex]].
- [114] B. Abelev et al. (**ALICE** Collaboration), JHEP 1209 (2012) 112 [arXiv:1203.2160 [nucl-ex]].
- [115] B. Abelev et al. (**ALICE** Collaboration), Phys. Rev. Lett. **109** (2012) 112301 [arXiv:1205.6443 [hep-ex]].
- [116] B. Abelev, *et al.* (**ALICE** Collaboration), JHEP 1201 (2012) 128, [arXiv:1111.1553 [hep-ex]].

- [117] J. Adams et al. (**STAR** Collaboration), Phys. Rev. Lett.**94** (2005) 062301 [arXiv:nucl-ex/0407006].
- [118] G. Luparello for ALICE Collaboration, [arXiv:1310.1714 [nucl-ex]].
- [119] R. Aaij et al. (**LHCb** Collaboration), JHEP 1206 (2012) 141 [arXiv:1205.0975 [hep-ex]].
- [120] L. Adamczyk et al. (**STAR** Collaboration), Phys. Rev. D **86** (2012) 072013 [arXiv:1204.4244 [nucl-ex]].
- [121] R. Aaij *et al.* (**LHCb** Collaboration), [arXiv:1306.3663 [hep-ex]].
- [122] K. Dusling and R. Venugopalan, Phys. Rev. D**87** (2013) 094034, [arXiv:1302.7018 [hep-ph]].
- [123] R.Maciula and A.Szczurek, Phys. Rev. D **87** (2013) 094022 [arXiv:1301.3033 [hep-ph]].
- [124] M. Nahrgang, J. Aichelin, P.B. Gossiaux and K. Werner, arXiv:1305.3823 [hep-ph].
- [125] C. Peterson, D. Schlatter, I. Schmitt, and P. M. Zerwas, Phys. Rev. D **27**, 105 (1983).
- [126] V.G. Kartvelishvili, A.K. Likhoded and V.A. Petrov, Phys. Lett. B **78**, 615 (1978).
- [127] B. A. Kniehl, G. Kramer, I. Schienbein, H. Spiesberger, Phys. Rev. D **77**, 014011 (2008), [arXiv:0705.4392 [hep-ph]].
- [128] T. Kneesch, B. A. Kniehl, G. Kramer, I. Schienbein, Nucl. Phys. B **799**, 34 (2008), [arXiv:0712.0481 [hep-ph]] .
- [129] F.D. Aaron *et al.* (H1 Collaboration), Eur. Phys. J. C**59**, 589 (2009).
- [130] J.Abdallah *et al.* (DELPHI Collaboration), Eur. Phys. J. C **71**, 1557 (2011) [arXiv:1102.4748 [hep-ex]].
- [131] See Particle Data Group (<http://pdg.lbl.gov/2008/reviews/rpp2008-rev-frag-functions.pdf>).
- [132] J.Abdallah et al. (DELPHI Collaboration), [hep-ex/0311005].

- [133] S. J. Brodsky, H.-C. Pauli, and S. S. Pinsky, Phys. Rep. **301** (1998) 299.
- [134] Eskola, Paukkunen, Salgado, JHEP **04** (2009) 065.
- [135] See "<http://www.feyncalc.org/>" for detail use of mathematica package.
- [136] Y.L. Dokshitzer and D.E. Kharzeev, Phys. Lett. B **519**, 199 (2001).
- [137] M. Djordjevic and M. Gyulassy, Nucl. Phys. A **733**, 265 (2004), [arXiv:0310.076 [nucl-th]].
- [138] Y. Akamatsu, T. Hatsuda and T. Hirano, Phys. Rev. C **79**, 054907 (2009) [arXiv:0809.1499 [hep-ph]].
- [139] V. Topor Pop, M. Gyulassy, J. Barrette, C. Gale, and M. Petrovici, [arXiv:1306.0885 [hep-ph]]
- [140] R. Rapp and H. van Hees, R. C. Hwa, X.-N. Wang (Ed.) Quark Gluon Plasma 4, World Scientific, 111 (2010) [arXiv:0903.1096 [hep-ph]].
- [141] H. van Hees and R. Rapp, Phys. Rev. C **71**, 034907 (2005) [arXiv:nucl-th/0412015],
- [142] R. L. Thews, M. Schroedter, and J. Rafelski, Phys. Rev. C **63**, 054905 (2001) [arXiv:hep-ph/0007323].
- [143] P. Braun-Munzinger and J. Stachel, Nucl. Phys. A **690**, 119 (2001), [arXiv:nucl-th/0007059].
- [144] R. Rapp, D. Blaschke, and P. Crochet, Prog. Part. Nucl. Phys. **65** (2010) 209, [arXiv:0807.2470 [hep-ph]].
- [145] K. Tuchin, Nucl. Phys. A **899**, 44 (2013), [arXiv:1209.0799 [hep-ph]].
- [146] Z. Kang and J.-W. Qiu, Phys. Lett. B **721** (2013) 277, [arXiv:1212.6541 [hep-ph]].
- [147] E.G. Ferreira, F. Fleuret, J.P. Lansberg, and A. Rakotozafindrabe, Phys. Lett. B **680**, 50 (2009);
- [148] E.G. Ferreira, F. Fleuret, J.P. Lansberg, N. Matagne and A. Rakotozafindrabe, Few Body Syst. **53**, 27 (2012).



- [149] G. A. Chirilli, B. -W. Xiao, and F. Yuan, Phys. Rev. Lett. **108**, 122301 (2012), [arXiv:1112.1061 [hep-ph]].
- [150] A. H. Mueller, B.-W. Xiao and F. Yuan, Phys. Rev. Lett. **110** (2013) 082301, [arXiv:1210.5792 [hep-ph]].
- [151] A. H. Mueller, Bo-Wen Xiao, and Feng Yuan, [arXiv:1308.2993 [hep-ph]]
- [152] L. Gladilin, [arXiv:hep-ex/9912064]
- [153] J. Beringer et al., (Particle Data Group), Phys. Rev. **D86** (2012) 010001.
- [154] M. Winna for the **ALICE** Collaboration, [arXiv:1404.1615 [hep-ex]].
- [155] J. Wilkinson for the **ALICE** Collaboration, [arXiv:1402.3124 [hep-ex]].
- [156] A. Dumitru and E. Petreska, Nucl. Phys. **A 879** 59 (2012), [arXiv:1112.4760 [hep-ph]].
- [157] T. Lappi and H. Mäntysaari, Phys. Rev. **D88** 114020 (2013), [arXiv:1309.6963 [hep-ph]].
- [158] J. Breitweg et al. (**ZEUS** Collaboration), Eur. Phys. **J. C7** (1999) 609, [hep-ex/9809005].
- [159] Francois Arleo and Stephane Peigne, JHEP 1303 (2013) 122 ,[arXiv:1212.0434 [hep-ph]],  
JHEP 1305 (2013) 155 ,[arXiv:1304.0901 [hep-ph]].